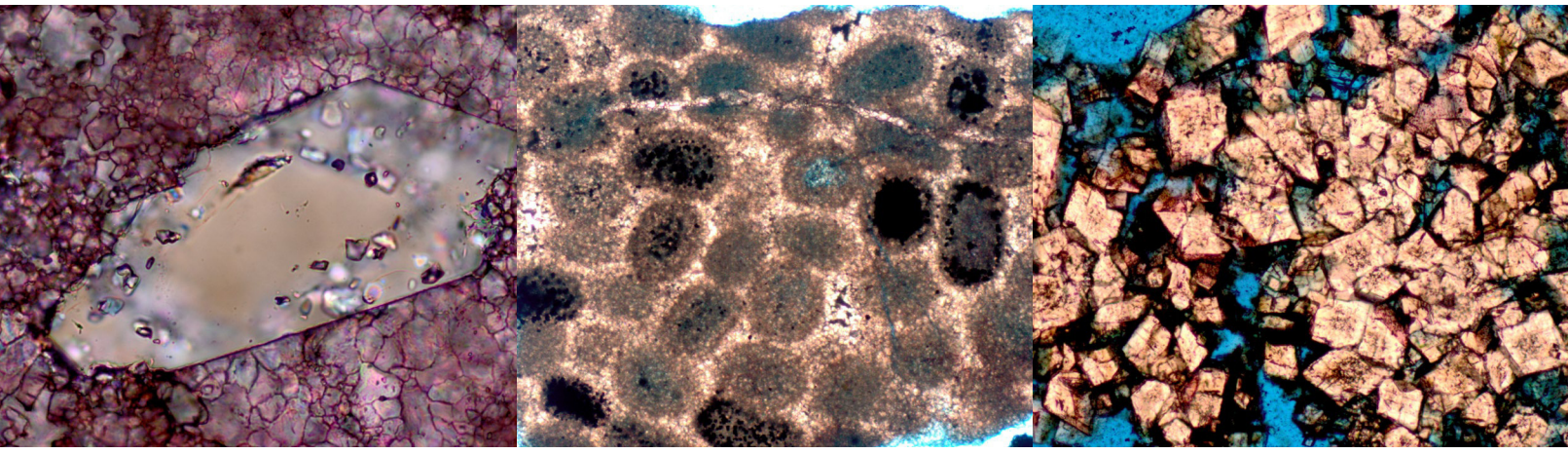

# Reservoir Characterization to Improve Exploration Concepts of the Upper Jurassic in the Southern Bavarian Molasse Basin

Elena Mraz

TECHNISCHE UNIVERSITÄT MÜNCHEN
Ingenieurfakultät Bau Geo Umwelt
Lehrstuhl für Ingenieurgeologie

# Reservoir Characterization to Improve Exploration Concepts of the Upper Jurassic in the Southern Bavarian Molasse Basin

**Elena Mraz**

Vollständiger Abdruck der von der Ingenieurfakultät Bau Geo Umwelt der Technischen Universität München zur Erlangung des akademischen Grades eines

**Doktor-Ingenieurs (Dr.-Ing.)**

genehmigten Dissertation.

| | |
|---|---|
| Vorsitzender: | Prof. Dr. Michael Krautblatter |
| Prüfer der Dissertation: | 1. Prof. Dr. Kurosch Thuro |
| | 2. Prof. Dr. Inga Moeck |
| | 3. Prof. Dr. Thomas Hamacher |

Die Dissertation wurde am 27.11.2018 bei der Technischen Universität München eingereicht und durch die Ingenieurfakultät Bau Geo Umwelt am 16.04.2019 angenommen.

# Abstract

The South German Upper Jurassic reservoir is part of the North Alpine Foreland Basin, which extends from France and Switzerland to Germany, Austria, and Slovenia. In the 1960-1980s, the Upper Jurassic reservoir as a carbonate play was explored for hydrocarbons, and since 2000 for geothermal energy, resulting in 22 geothermal plants cumulating in the area around Munich today. The Upper Jurassic strata is exposed at the karstified Franconian and Swabian Alb with a southward dip. Due to the wedge-shaped geometry of the foreland basin, referred to as Molasse Basin, the Upper Jurassic rocks are buried south of the Danube River and deepen to 2-3 km in the area around Munich and more than 5 km toward the Alpine frontal fault. Effectively, the Upper Jurassic reservoir temperature increases with depth to the south.

While most of the geothermal wells are economically productive with flow rates higher than 60 L/s, few wells exhibit a low productivity especially south and west of the Munich area. Moreover, at some wells, which are spatially very close, a remarkable variety of well productivity exists, indicating a permeability heterogeneity of the reservoir. Faults and facies are debated to cause the reservoir permeability heterogeneity, however, the geologic controls on reservoir productivity were not systematically investigated through scientific reservoir characterization so far. Carbonate rocks are controlled and influenced either by deposition, diagenesis, fractures or karst structures. This study aims therefore to characterize the Upper Jurassic carbonate reservoir by microfacies analysis and lithological investigations on borehole cuttings, cores and outcrop analogues to better understand processes leading to today's porosity and permeability.

For the investigation of the deep Upper Jurassic reservoir (> 3 km), drill cuttings and drill cores of 17 deep wells were selected which intersect the Upper Jurassic carbonate rocks across the whole Molasse Basin. To evaluate the influencing geological processes which might have caused the low reservoir productivity, rock samples were described and characterized by petrography and microfacies analysis (depositional environment) using optical microscopy. The diagenetic fluid evolution was analyzed by fluid inclusions studies and stable isotope data. Cathodoluminescence, scanning electron microscopy (SEM) and X-ray diffraction (XRD) measurements were used to describe secondary diagenetic processes.

In contrast to earlier studies, the microfacies analysis showed that the lowly permeable Helvetian facies is not present in the southern part of the North Alpine Foreland Basin, which was assumed to cause the low reservoir productivity by previous researchers. However, a new transitional facies is now described, which developed in the southern part of the Molasse Basin during the Oxfordian. The transition zone facies is characterized by dense, dark, micritic carbonate rocks, which contain abundant planktonic organisms such as radiolaria, foraminifera, and echinoderms (e.g. *Saccocoma* sp.). The microfossil content and petrography of the deep (>3 km) Kimmeridgian and Tithonian rocks is similar to the carbonate rocks (Franconian facies) in the area around Munich, however they show a higher compaction

degree (stylolites) and hence less pore space. The fluid evolution was characterized in the Upper Jurassic carbonate rocks and cement phases. The diagenetic sequence and fluid evolution (temperature and chemistry) was determined using geochemical data and cathodoluminescence microscopy. The fluid evolution showed a continuous dilution of the former Upper Jurassic sea water with a meteoric fluid, which was determined using fluid inclusions and stable isotopes. The present reservoir fluid is diluted in a higher grade by a meteoric fluid in the eastern part than in the western part of the Bavarian Molasse basin. Furthermore, the fluid evolution analysis indicated an increase in reservoir temperature during the foreland basin formation up to 200°C, and a following subsequent cooling of the fluid to the present reservoir temperature of max. 150 °C. In this study, the fluid temperature evolution of the eastern North Alpine Foreland Basin showed that the lower temperature anomaly of the aquifer possibly exists since the maximum burial depth was reached in the area around Lake Chiemsee. By comparing the fluid evolution (temperature and chemistry) and the diagenetic sequence, a dolomitization during the burial diagenesis can be assumed. The late Tithonian (Purbeckian) carbonate rocks showed a dolomite genesis probably in line with the evaporitic reflux dolomitization. A burial seawater dolomitization during the burial diagenesis was suggested for the Kimmeridgian carbonate rocks, which were affected by tectonics contemporaneously. The dolomitization processes formed different dolomite types in the Upper Jurassic, with planar-e dolostones providing the highest matrix permeability, and planar-a dolostones the lowest matrix permeability. Therefore, the decreasing well productivity to the south can be explained by the observed lower amount and thickness of planar-e dolostones, and the occurrence of planar-a dolostones at greater depths causing presumably a declining permeability.

Consequently, the productivity decline of Upper Jurassic carbonate rocks in the southern deep basin part (>3 km) cannot be caused by the Helvetian facies, as the facies of the Kimmeridgian and Tithonian carbonates is comparable to the productive rocks at Munich. Possible causes can be (I) the dense, micritic transition zone facies of the Oxfordian, (II) a greater compaction originating from the greater overburden pressure, and (III) by a different diagenesis with the occurrence of planar-a dolostone. Because of the higher reservoir temperatures, the diagenesis developed in a different degree, and was possibly not forming highly permeable planar-e dolostones, found in the high productivity zones of the Upper Jurassic geothermal play today.

# Zusammenfassung

Das süddeutsche, oberjurassische Reservoir ist Teil des Nordalpinen Vorlandbeckens, welches sich von Frankreich und der Schweiz nach Deutschland, Österreich und Slowenien erstreckt. In den 1960-1980er Jahren wurde das oberjurassische Reservoir als Karbonatlagerstätte nach Kohlenwasserstoffen und seit 2000 für eine geothermale Energiegewinnung exploriert, welches heute zu 22 Geothermieanlagen im Raum München geführt hat. Die Oberjura Schichtenfolge ist in der verkarsteten Fränkischen und Schwäbischen Alb nach Süden einfallend aufgeschlossen. Durch die keilförmige Geometrie des Vorlandbeckens, auch Molassebecken genannt, sind die Oberjura Karbonatgesteine im Süden der Donau überdeckt und vertiefen sich auf 2-3 km im Raum München und mehr als 5 km am nordalpinen Alpenrand. Nach Süden nehmen die Reservoirtemperaturen mit einer höheren Tiefenlage zu.

Obwohl die meisten geothermalen Bohrungen ökonomische, produktive Fließraten von mehr als 60 L/s besitzen, gibt es einige Bohrungen mit einer geringen Produktivität vor allem im Süden und Westen von München. Zum Teil zeigen auch räumlich eng zusammenliegende Bohrungen einen deutlichen Unterschied in der Produktivität, was auf eine heterogene Verteilung der Permeabilität im Reservoir hinweist. Störungen und die Fazies sind vermutlich für die heterogene Permeabilitätsverteilung verantwortlich, jedoch ist bislang der geologische Einfluss auf die Reservoirproduktivität nicht systematisch durch eine wissenschaftliche Reservoircharakterisierung untersucht worden. Karbonatgesteine werden durch den Ablagerungsraum, Diagenese, Klüfte und Karststrukturen beeinflusst. Diese Studie hat daher das Ziel das oberjurassische Karbonatreservoir durch die Mikrofazies-Analyse und der Lithologie der Karbonatgesteine an Hand von Bohrklein, Bohrkernen und Analogproben von Aufschlüssen zu charakterisieren, um ein besseres Verständnis über die Prozesse zu erhalten, welche zur heutigen Porosität und Permeabilität geführt haben.

Für die Untersuchung der geringen Produktivität des tieferen, oberjurassischen Reservoirs (> 3 km) wurden Bohrklein und Bohrkerne von 17 Tiefbohrungen ausgewählt, welche den Oberjura im Vorlandbecken durchteufen. Um die beeinflussenden Faktoren zu untersuchen, die die geringere Produktivität hervorrufen wurden Gesteinsproben nach Petrographie und Mikrofazies (Ablagerungsraum) mittels optischer Mikroskopie beschrieben und charakterisiert. Die diagenetische Fluidevolution ist durch Flüssigkeitseinschlussstudien und stabilen Isotopendaten analysiert worden. Messungen der Kathodolumineszenz, Rasterelektronenmikroskopie (REM) und Röntgendiffraktometrie wurden verwendet, um sekundäre diagenetische Prozesse zu beschreiben.

Im Vergleich zu früheren Studien, zeigen die mikrofaziellen Analysen, dass die gering permeable Helvetische Fazies im südlichen Teil des nordalpinen Vorlandbeckens nicht vorhanden ist, was bisher als Ursache für die geringere Reservoirproduktivität von Wissenschaftlern angenommen wurde. Jedoch konnte nun eine neue Übergangsfazies charakterisiert werden, welche sich im Oxfordium im südlichen Teil des Molassebeckens entwickelte. Die Übergangsfazies ist charakterisiert durch dichte, dunkle, mikritische Karbonatgesteine, welche einen hohen Anteil an planktonischen Organismen wie Radiolarien, Foraminiferen und Echinodermen (z. Bsp. *Saccocoma* sp.) enthält. Im Mikrofossilgehalt

und in der Petrographie zeigen die tiefliegenden (> 3 km) Kimmeridgium- und Tithonium-Gesteine Ähnlichkeiten zu den Karbonatgesteinen (Fränkische Fazies) in der Gegend um München, jedoch eine Zunahme der Kompaktion (Stylolithe) und dadurch einen geringeren Porenraum. Die Fluidevolution wurde an Hand der oberjurassischen Karbonatgesteine und Zemente charakterisiert. Die diagenetische und Fluid- Entwicklung (Temperatur und Chemie) wurden mittels geochemischer Daten und Kathodolumineszenzmikroskopie untersucht. Die Fluidevolution zeigte eine kontinuierliche Verdünnung des früheren oberjurassischen Meerwassers durch ein meteorisches Fluid, welches über Flüssigkeitseinschlüsse und stabile Isotope bestimmt wurde. Das heutige Reservoirfluid ist im östlichen Bereich stärker ausgesüßt als im westlichen Bereich des bayerischen Molassebeckens. Weiterhin konnte bei der Fluidevolution eine Zunahme der Reservoirtemperatur während der Vorlandbeckenentwicklung mit bis zu 200°C und einer anschließenden Abkühlung des Fluids auf die heutige Reservoirtemperatur von max. 150°C ermittelt werden. In dieser Studie hat die Fluidtemperaturevolution im östlichen Nordalpinen Vorlandbecken gezeigt, dass die negative Temperaturanomalie des Aquifers möglicherweise existiert seit die maximale Versenkungstiefe im Gebiet des Chiemsees erreicht wurde. Durch den Vergleich der Fluidevolution (Temperatur und Chemie) und der diagenetischen Entwicklung kann eine Dolomitisierung während der Versenkungsdiagenese angenommen werden. Die (Purbeck) Karbonatgesteine des oberen Tithonium zeigen wahrscheinlich eine Dolomitentstehung wie bei der evaporitischen Reflux-Dolomitisierung an. Eine buriale Salzwasserdolomitisierung ist für die Karbonatgesteine des Kimmeridgium während der Versenkungsdiagenese wahrscheinlich, welche zeitgleich von Tektonik beeinflusst wurde. Durch die Dolomitisierungsprozesse wurden verschiedene Dolomittypen im Oberjura gebildet, einmal planar-e Dolomitstein mit der höchsten Matrixpermeabilität und planar-a Dolomitstein mit der geringsten Matrixpermeabilität. Daher kann die Produktivität im Süden durch die beobachtete geringere Existenz und die geringere Mächtigkeit der planar-e Dolomitsteinen und durch das Vorkommen von planar-a Dolomitsteinen in größeren Tiefen begründet sein, welche wahrscheinlich eine Abnahme der Permeabilität verursacht hat.

Somit kann die geringere Produktivität der oberjurassischen Karbonatgesteine im südlichen Beckenteil (> 3 km) nicht durch die Helvetische Fazies begründet werden, da die Fazies der Kimmeridgium- und Tithonium-Karbonate ähnlich sind zu den produktiven Gesteinen in München. Mögliche Ursachen können (I) die dichte mikritische Übergangsfazies des Oxfordium, (II) die stärkere Kompaktion durch den höheren Überlagerungsdruck und (III) durch die veränderte Diagenese mit dem Vorkommen von planar-a Dolomitsteinen sein. Durch die höheren Reservoirtemperaturen entwickelte sich die Diagenese in einem anderen Grad und formte nicht die hochpermeablen planar-e Dolomitsteine, welche in den hochproduktiven Zonen des Oberjura heute gefunden werden.

# Acknowledgements

This study would have never been possible without the support of many people. Therefore, I would like to express my thanks to those, who accompanied me on this journey.

First, I would like to thank my supervisors Prof. Dr. I. Moeck and Prof. Dr. K. Thuro for the opportunity to investigate the Upper Jurassic carbonate reservoir, as well as for the inspiration, valuable advice and most importantly for the support and encouragement. Especially, I want to thank my mentor Dr. M. Wolfgramm for all the long and intense discussions, support and unending source of encouragement. Moreover, I also want to thank Prof. Dr. Hamacher for his participation as examiner.

I would also like to acknowledge the German Federal Ministry for Economic Affairs and Energy (BMWi) for financial support. The borehole data and rock samples used in this research were kindly provided by ExxonMobil Productions Germany GmbH, DEA Deutsche Erdoel AG, St.Galler Stadtwerke, Geothermieprojekt Geretsried Nord GmbH & Co. KG, Geothermie Unterhaching Produktions-GmbH & Co KG, SWM Services GmbH, Geothermische Kraftwerksgesellschaft Traunreut mbH, Clariant Produkte (Deutschland) GmbH, Exorka GmbH, and Erdwerk GmbH. The hydrochemistry data from the Traunreut well during production was kindly provided by Florian Heine, TUM Chair of Hydrogeology. Furthermore, I would like to thank Karen Helm-Knapp and Vladimir Ruttner for their patience in thin and thick section preparation. Special thanks go to my colleagues at the Chair of Engineering Geology, for their help, support, and discussions. I'm very grateful for the support and critical reviews by Dr. G. Lehrberger, Florian Heine, and Dr. J. Schneider.

Last but not least, I would like to thank my family and friends for their constant support, encouragement, and patience over the last three years.

# Contents

# Index of figures

# Index of tables

# 1 Introduction

## 1.1 Geothermal exploration and production

### 1.1.1 Global perspective and geothermal play type

Natural, geothermal heat is stored in the Earth crust and is used where this heat reaches the surfaces since thousands of years, e.g. at hot springs. Geothermal heat is either transported predominately by conduction, forming the conduction dominated geothermal play types with average geothermal gradients as in intra-cratonal basins, or in foreland basins with adjacent orogenic belts or in basement terrains; or heat is transported predominantly by convection or advection, forming the convection dominated geothermal play types with elevated geothermal gradients as in magmatic, plutonic or non-magmatic extensional terrain play provinces (Moeck, 2014). The geothermal heat is generated in the uppermost Earth crust by radiogenic decay of minerals as uranium, thorium, or potassium, and a small amount is still stored from the formation of the planet Earth (Stober and Bucher, 2012).

Due to the low thermal conductivity of rocks, a very slow heat transport is assumed, and the geothermal heat is therefore stored in the Earth crust. The time scale of geothermal heat production and heat transport is steady but slow in convection dominated play provinces and accelerated in conduction dominated play provinces (Moeck, 2014). This naturally generated heat can be accessed and utilized for geothermal energy production, and hence belongs to the renewable energies.

Worldwide, the geothermal energy market is growing by producing energy from convective and conductive systems over the last thirty years (Bertani, 2016). The advantage of geothermal energy is that it can be used for base load operation, and among the renewable energies only geothermal does not fluctuate with weather and seasonal conditions. As the geothermal energy source is always available, it can stabilize the national grid, and it is a renewable decarbonized energy form. Moreover, geothermal energy is manageable and scalable, depending on the heat demand (Bauer et al., 2014; Stober and Bucher, 2012). Using ground source heat pumps in single homes, large buildings, campuses, quartiers or districts, they can be heated by geothermal energy (domestic heating) (Fig. 1) (Weber and Moeck, 2018). Hydrothermal wells arranged in a doublet system can support geothermal energy for district heating grids or can be utilized for power production. Globally, most geothermal projects generate power and are installed in volcanic or tectonically active areas (Moeck, 2014). Only a minority of geothermal projects is installed at conduction dominated play provinces, and Germany is one of the pioneer in developing hydrothermal technologies to utilize - compared to the worldwide installed geothermal capacity - unconventional geothermal systems. Therefore, the North Alpine Foreland Basin in southern Germany is hitherto an outstanding geothermal technology area in comparison to these thermally active convection dominated areas (Moeck, 2014).

In general, geothermal energy production is possible by a hydrothermal or by a petrothermal system. Hydrothermal systems utilize hydrothermal technologies where large drilling diameters allow high flow

rates. The categorization of “high” versus “low” flow rates depends on the play type, e.g. 60 L/s is “high” in a sandstone reservoir at intra-cratonal basins, whereas it is “moderate” in carbonate reservoirs (Moeck and Zimmer, 2014). A hydrothermal technology can only be applied when a sufficient amount of producible fluids is present in a sufficient permeable reservoir. Hydrothermal systems use directly a reservoir fluid which is stored in a permeable and porous sedimentary layer. For spa applications, a single well is sufficient to cover the heat demand, whereas district heating requires a higher energy demand, which is covered by hydrothermal well doublet systems (Bauer et al., 2014). In a hydrothermal well doublet, the natural occurring reservoir fluid flows in a production well to the surface and is cooled at a heat exchanger at the geothermal power plant. Afterward, the cooled reservoir fluid is usually injected in a second well into the reservoir in a closed system.

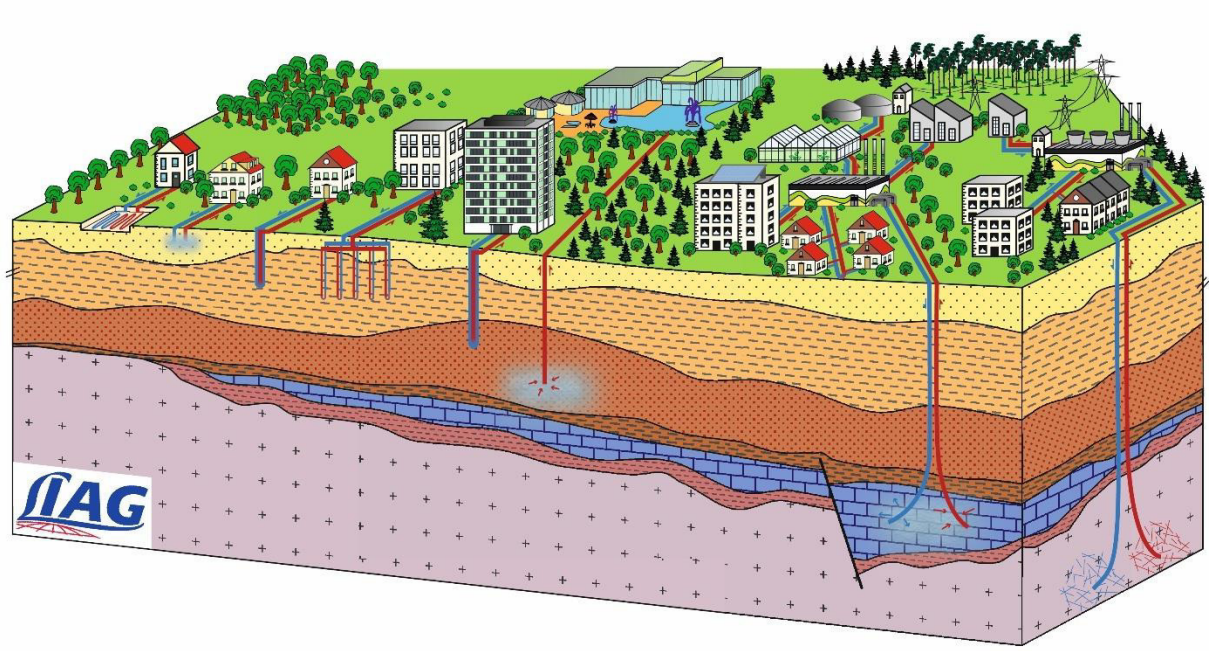


Fig. 1: Possible uses of geothermal energy, depending on the depth and an average geothermal gradient, which is characteristic for a conductive dominated heat transport (Weber and Moeck, 2018). The different illustrated technologies show that a geothermal utilization is possible depending on depth and temperature (scalable) and manageable to the energy demand at the surface.

In contrast to the hydrothermal technology, the petrothermal technology is applied when an insufficient volume of reservoir fluids is present to afford the high flow rates of more than 50 L/s. According to Moeck (2014), petrothermal reservoirs have a permeability of less than $10^{-15}$ m² and a porosity of less than 10 %. In petrothermal systems, an artificial fluid is pumped through an injection well into a hot, brittle reservoir rock where fractures systems and fault are used as a natural heat exchanger, completed by a production well. Such petrothermal well doublets require generally a hydraulic stimulation, which can induce seismicity. Although petrothermal technology was tested the first time in the 1970’s (Moeck, 2014), it still requires research efforts to increase the efficiency and sustainability.

### 1.1.2 Local perspective – The Bavarian Molasse Basin

The North Alpine Foreland Basin, the so-called Molasse Basin, provides a geothermal system, which is dominated by a conductive heat flow and controlled by faults and fractures as well as by litho- and biofacies (Moeck, 2014). The most important area for geothermal utilization is the 300-650 m thick Upper Jurassic reservoir which hosts a warm fluid (65-130°C) in fractured, karstified and dolomitized carbonate rocks in depths of around 2-3 km (Agemar et al., 2014b). Over the last past decades, the Upper Jurassic carbonate rocks have been explored by geothermal, thermal, hydrocarbon, and water wells in southern Germany. Due to the special significance of the Upper Jurassic reservoir in reaching the climate protection goals of the COP 21 summit and the German Renewable Energy Source Act (EEG) goals (Verbraucherschutz, 2018), further geothermal plants need to be planned, also in southern Germany. Up to now, the Upper Jurassic reservoir is used for district heating and at some sites to generate power. The heat demand is specifically increasing, because the "Energiewende" focus on renewable power generation, even though the major demand in primary energy is heat in Germany (Faltlhauser and Geiß, 2018; Weber and Moeck, 2018). In Germany, the future energy development referring to climate protection need therefore to focus on the "Wärmewende", generating renewable heat, especially by geothermal heat from the Upper Jurassic reservoir in Bavaria.

The development of geothermal projects in the Molasse Basin started when the fluid-rich hydrocarbon well Erding was drilled in 1983 (Agemar et al., 2014a), which is used as a geothermal well today. In 2006, the first geothermal well Unterhaching was drilled with the aim of a geothermal application, which started the main phase for geothermal exploration in the area around Munich. This main exploration phase was interrupted by the unsuccessful geothermal well Geretsried GEN-1 in 2012 and is increasing since 2017 again. In general, the thermal performance of a geothermal plant is defined by the density of the fluid, specific heat capacity, flow rate, and temperature of the fluid (Schulz et al., 2007). Today, the fluid salinity is constant below 1 g/L (Mayrhofer et al., 2014) and the specific heat capacity can be assumed constant, the remaining significant parameters are flow rate and temperature of the fluid. In the Upper Jurassic reservoir, geothermal wells usually have fluid temperatures in the range between 65-130°C and show flow rates higher than 60 L/s. Both parameters are controlled by the depth of the reservoir and by the permeability of the Upper Jurassic carbonate rocks. While, the depth of the Upper Jurassic reservoir in the Molasse Basin can be determined by a seismic campaign, however, the permeability remains the only unknown parameter in the carbonate reservoir exploration. Consequently, to find high-permeability areas in the Upper Jurassic carbonate rocks knowledge of the influencing factors such as porosity, rock strength, depositional environment (facies), diagenesis (e.g. pressure solution, recrystallization, dolomitization, karstification), and tectonic structures is necessary.

In the area around Munich, the Upper Jurassic reservoir is explored by seismic campaigns and well data in depths of 2.5-3.5 km, because of the accumulation of successful geothermal wells in the last 20 years. Hitherto, reservoir exploration in the south German Molasse Basin has still not reached an industrial maturity, due to the still small number of wells and a varying permeability of the Upper Jurassic carbonate rocks (22 projects over around 23.000 km²). In southern Germany, geothermal energy

production is further found in eastern Bavaria, but not in the southern part of the Molasse Basin. As the requirements for a geothermal plant producing energy for domestic heating are temperatures above 60°C and flow rates higher than 35 L/s (Agemar et al., 2014b), it is applicable at areas with an intermediate permeability of the Upper Jurassic carbonate rocks. In contrast, to produce power from the Upper Jurassic warm fluid, temperatures above 110°C are essential as well as high flow rates (Agemar et al., 2014b). As geothermal power is higher profitable and favored, the exploration of the Upper Jurassic reservoir was expanded to the southern part of the Molasse Basin, because the reservoir temperature increases to the south (Agemar et al., 2012).

This increase in temperature is due to the wedge-shape of the foreland basin, with the Upper Jurassic strata (previously called Malm) covered by sedimentary rocks with up to 5 km near the north Alpine boundary (Kuhlemann and Kempf, 2002). The geothermal projects Geretsried and Mauerstetten for example tried to target the hotter reservoir fluid in the southern basin part. These wells were placed within fault zones and build-up structures, visible in seismic data (Mraz et al., 2018a), and encountered the Upper Jurassic reservoir at depths of around 4-5 km (ca. 130-150°C). However, these two wells did not reach an economic level for a geothermal application, as the Upper Jurassic carbonate rocks did not provide sufficient flow pathways. Up to now, in the south of Munich projects were not successful for a geothermal application, because of a too low permeability.

## 1.2 Carbonate reservoirs

This permeability decline of the Upper Jurassic reservoir to the south (Birner, 2013) has not been investigated in detail and only hypothesis were discussed. As an example, based on the dark rock color and the appearance of dense, micritic limestones in the Upper Jurassic reservoir, prior researchers suggested that the dense, dark, micritic limestones of the Helvetian facies (Quinten-Fm.) occur in the southern basin part of the South German Molasse Basin (Birner, 2013; Schneider, 1962). Another hypothesis is the lower degree of karstification of the Upper Jurassic rocks in the southern basin, as the subaerial exposure during the Cretaceous happened for a shorter period (Koschel, 1991; Strasser, 1988; Villinger, 1988). However, this hypothesis is not supported by the recent seismic interpretations indicating a karst morphology on the reservoir top in the area around Munich (von Hartmann et al., 2018). A third hypothesis refers to the different well productivity due to differences in diagenesis (e.g. dolomitization), faults and fractures of the Upper Jurassic strata which might be influenced by the increasing depth and temperature of the reservoir rocks to the south. Thereby, the massive facies is considered to provide the best geothermal play supporting high flow rates in the area around Munich (Birner et al., 2012).

In general, carbonate reservoirs are well explored for their facies, porosity, permeability and diagenesis for example, as they host the main reservoirs for hydrocarbons (e.g. Saudi Arabia, Alberta Basin (Canada), Mississippi, Gulf Coast (USA)). However, carbonate rocks are controlled by many different parameters such as the primary depositional environment, and by secondary processes such as dolomitization, karstification, recrystallization and compaction which can change within meters in a

reservoir (Flügel, 2010; Ahr, 2008; Lucia, 2007). In contrast, sandstone reservoirs are relative homogenous, and the porosity versus permeability shows a linear decrease with depth (Moeck, 2014). Carbonate reservoir do not show a relationship of permeability/porosity with depth, and a reservoir with low matrix porosity can provide sufficient permeability due to fractures and karst structures (Moeck, 2014). Hence, the four main controlling parameters are (1) depositional environment, (2) diagenesis, (3) fractures, and (4) karstification and dissolution and are explained in detail below and in chapter 5.

(1) depositional environment

The depositional environment and depositional setting describe where the sediments are formed. The depositional environment is characterized by the carbonate-producing organisms, which strongly depends on light, water temperature and sedimentary influx (Flügel, 2010). The microfacies analysis is used to recognize and interpret the depositional environment, e.g. by using the paleontological data (Flügel, 2010). Moreover, the carbonate rocks are classified by Dunham (1962) and Folk (1962); (1959) according to their amount of components, fossils, and their composition of carbonate sands and muds.

(2) diagenesis

The diagenesis in a carbonate setting describes the processes which form carbonate sediments into carbonate sedimentary rocks. These include cementation (precipitation of minerals in pore spaces) and recrystallization (Flügel, 2010). Besides, secondary processes (dolomitization, recrystallization, silification) can occur during different stages of diagenesis which depend on the tectonic setting. In carbonate rocks the main secondary processes are compaction (stylolites), recrystallization and cementation, which can increase or decrease the primary pore space (Machel, 2004). The diagenesis is analyzed by cement phases which can be distinguished by a different geochemistry, crystal morphology, fluid inclusions and growth zonation (Flügel, 2010).

(3) fractures

In carbonate rocks, either limestones or dolostones, fractures can occur due to differential stresses resulting in a brittle or ductile behavior depending on the depth (Wong and Baud, 2012). The Upper Jurassic carbonate reservoir in the North Alpine Foreland Basin was strongly affected by tectonics during the Alpine orogeny, which resulted in fractures and fault systems (Mraz et al., 2018a; Budach et al., 2017). The occurrence of fractures and fault systems can lead to an increase in the reservoir porosity and permeability (Bense et al., 2013; Cacace et al., 2013; Billi et al., 2003; Knott et al., 1996).

(4) karstification and dissolution

The carbonate rocks can be affected by dissolution or precipitation of calcite minerals, for example resulting in an increase or decrease of porosity and permeability, respectively. Karst is a phenomena which is characterized by fissures, sinkholes, underground streams and caverns at the surface where dissolution of rocks was induced by rain, fresh or ground water during period of subaerial exposure (Klimchouk et al., 2017). In some carbonate reservoirs a hypogene dissolution by hydrothermal fluids can further occur (Klimchouk et al., 2017), often linked to fractures and fault zones. Hence, karstification and dissolution can form and produce flow pathways within the carbonate rock mass. A possible period

of subaerial exposure of the Upper Jurassic carbonate rocks is during the early Lower Cretaceous (Villinger, 1988).

## 1.3 Scientific questions and methods

In this study, possible hypotheses for the low productivity in the Upper Jurassic reservoir are (I) a change in facies and depositional environment and/or (II) a different diagenesis and dolomitization. A change in facies and depositional environment can cause dense, low-porous limestones, which can result in a low-permeability. So far, the transitions between the facies realms are unclear, especially descriptions of the occurring facies in the southern part of the Molasse Basin. Another aspect is that the lithostratigraphy of the Franconian and Swabian facies is not applicable to drill cuttings which are always produced by geothermal wells in the southern part of the North Alpine Foreland Basin. Differences in diagenesis of the carbonate rocks are assumed to occur due to higher reservoir temperatures and fluid pressures, and higher overburden pressures due to the greater depth in the south of the Molasse Basin.

For this new characterization of the geothermal, carbonate Upper Jurassic reservoir, a comparison of the limestones, cements, dolomite crystals, and dolomite types which occur in the Molasse Basin and at outcrop areas is performed. In this research, a large study area is selected, from Lake Constance in the west to Lake Chiemsee in the east and from the outcrop areas of the Franconian and Swabian Alb to the southern part of the North Alpine Foreland Basin, which is the first basin-wide comparison of the Upper Jurassic carbonate rocks in a geothermal context. The Upper Jurassic carbonate rocks are studied for facies types (Meyer, 1994; Meyer and Schmidt-Kaler, 1989), hydraulic and hydrochemical properties (Stober, 2014; Birner et al., 2012), diagenesis and dolomitization (Reinhold, 1996; Liedmann, 1992), particularly in outcrops of the Franconian and Swabian Alb. But still very limited data exists of the buried Upper Jurassic strata in the Molasse Basin.

The present study characterizes the Upper Jurassic carbonate reservoir rocks by lithology, microfacies depositional environment, optical porosity, recrystallization and/or calcification, dolomitization, and diagenesis. Besides, the relationship between the facies, diagenesis, dolomite types, and porosity is analyzed, as well as occurring dolomite types are compared between the shallow (< 1 km) and the deep (1-5 km) reservoir. In this study, the dolomitization is of special interest, as good target areas are generally found within the dolomitized massive facies of the Upper Jurassic (Birner et al., 2012; Böhm et al., 2011). In addition, influences of fracture zones and fault systems on the well productivity are investigated by the well production data and geophysical borehole measurements. By this, the knowledge of the Upper Jurassic reservoir and the distribution of high-permeability areas is extended southward. The focus is, however, on a general characterization of the depositional environment and diagenesis in the southern, deeper Upper Jurassic reservoir. Therefore, this study does not want to take all regional and local phenomena into account.

The key questions of this study are reflected in three research papers, and hence the results of this study are structured by these papers. The three following research papers were written during this study:

- Chapter 5.1: Elena Mraz, Inga Moeck, Markus Wolfgramm, and Kurosch Thuro (submitted) Microfacies Analysis in Upper Jurassic Carbonates with Implications for Reservoir Quality in the Molasse Basin. Facies.
- Chapter 5.2: Elena Mraz, Markus Wolfgramm, Inga Moeck, and Kurosch Thuro (2019) Detailed Fluid Inclusion and Stable Isotope Analysis on Deep Carbonates from the North Alpine Foreland Basin to Constrain Paleofluid Evolution. *Geofluids,* p. 23.
- Chapter 5.3: Elena Mraz, Markus Wolfgramm, Inga Moeck, and Kurosch Thuro (in prep.) Dolomitization of Upper Jurassic carbonate platform rocks: A case study from the North Alpine Foreland Basin.

# 2 Study area and sample points

The focus area of this study was on the deeper carbonate Upper Jurassic reservoir (> 3 km) in the southern part of the Molasse Basin (Fig. 2). The Upper Jurassic reservoir was sampled over a wide depth range (0-5 km) to determine possible changes in lithology, fluid composition, diagenesis and pore space with increasing depth, and from east to west. For the basin-wide study, 17 deep wells (2-5 km) which can be subdivided into ten non-productive wells, in the context of geothermal exploration, and seven productive wells intersecting the Upper Jurassic reservoir were selected, in addition to 40 outcrops (Fig. 2). The wells are St. Gallen (STG), hydrocarbon well A1, hydrocarbon well B1, hydrocarbon well C1, Bad Woerishofen (BWO), Mauerstetten (MST: GT1 and GT1a), Schongau (SCH), Geretsried (GEN: GEN-1 and GEN-1ST-A1), Unterhaching (UHA: UHA1 and UHA2), Taufkirchen (TFK), Sauerlach (SAU), Kirchstockach (KIR), Traunreut (TRN: TRN1 and TRN2), Freiham (FRH: FRH1 and FRH2), and Moosburg (MOS: SC3). In the following, the doublet and sidetrack wells as Traunreut 1 and 2 for example are combined and named as a single site like TRN.

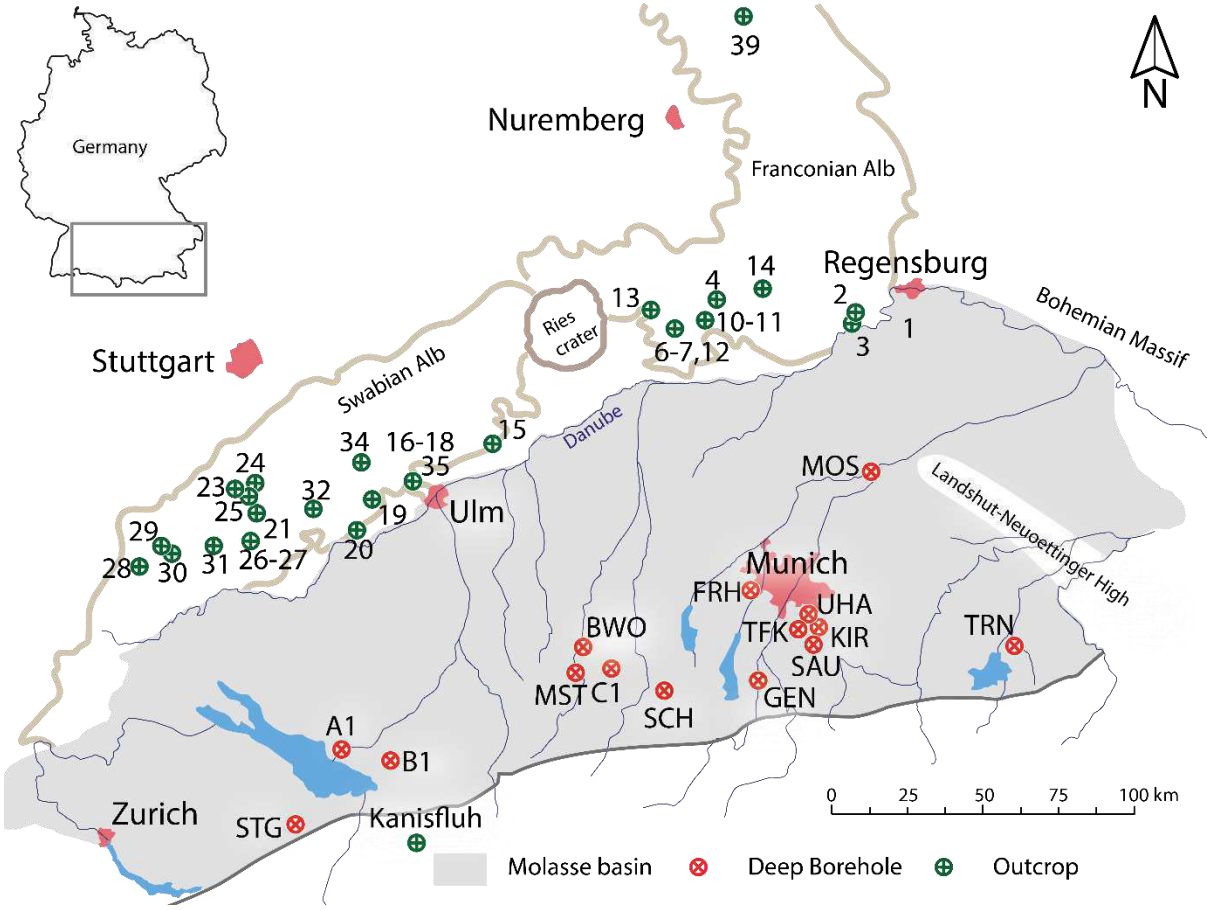


Fig. 2: Overview of the rock samples of the deep wells and outcrops in the Molasse Basin, southern Germany.

Overall, 1400 rock samples, 117 m drill cores, 650 cuttings and 824 thin sections were available from the 17 wells in the southern Molasse Basin. The sediment thickness of the Upper Jurassic carbonate rocks varies around 400-600 m in the study area. Some of the selected wells only reach at their final

depth the sediments of the Lower Kimmeridgian (previously called Malm gamma), and therefore do not encounter the complete Upper Jurassic. Hence, most carbonate rock samples (limestones and dolostones) of this study belong to the Kimmeridgian (previously Malm delta-epsilon) and Tithonian. The Kimmeridgian and Tithonian rocks represent the part of the Upper Jurassic aquifer, which is mainly dolomitized and highly permeable.

The Upper Jurassic reservoir is intersected at depths of around 4.3 km at GEN and at 2.9 km at UHA. The geothermal borehole MST reached the top reservoir at around 3.4 km depth. The three hydrocarbon boreholes C 1 (top reservoir: 3.2 km), B 1 (top reservoir: 3.6 km) and A 1 (top reservoir: 2.6 km) were drilled during the 1950s to 1960s. The geothermal borehole STG in Switzerland, south of Lake Constance reach the Upper Jurassic reservoir top at a depth of 3.8 km. In general, the Upper Jurassic reservoir is encountered at around 3.6 km in the western part and at 4.4 in the eastern part of the Molasse Basin. The investigated outcrop area for the Helvetian facies is located in the Vorarlberg (Austria) north of the city Au, at the Kanisfluh (Fig. 2). Furthermore, rock samples from the 39 outcrops (74 samples) originating from the Franconian Alb and Swabian Alb (Fig. 2) were analyzed. The outcrop samples are carbonate rocks, generally of the Kimmeridgian, and can show dedolomitization and karst phenomena due to the comparable longer surface influences. Drill cutting samples were limestones (light gray to dark gray, matrix to component-rich), dolostones (light beige to dark brown), and vein calcite crystals (white to transparent). A reddish to brown but regularly white calcite and dedolomite samples were limited to surface outcrops (karst zones).

# 3 Geology and Paleogeography

## 3.1 Paleogeography and tectonics

The Upper Jurassic carbonate reservoir is situated in the North Alpine Foreland Basin, overlaying Permo-Carboniferous sediments and a crystalline basement (Kuhlemann and Kempf, 2002). During the Late Jurassic, the passive Tethys margin was occupied by an extensive carbonate-dominated platform that extended northward, the so-called Franconian platform (Ziegler, 1990) (Fig. 3). In the late Kimmeridgian to Tithonian, sea level gradually dropped and a sea level low stand was reached at the Jurassic-Cretaceous transition (Ziegler, 1990). The Tethys transgressed and regressed from the south on the platform during the Cretaceous, causing erosional phases of the Upper Jurassic rocks. In the Paleogene, the Central European Alps developed as the Adriatic and European plates collided (Lemcke, 1988), which caused a southward subduction of the Penninic Ocean. This convergence resulted in a northward thrusting of the European passive margin area and a downward flexing of the European plate. This entailed the formation of the North Alpine Foreland Basin (Molasse Basin) (Bachmann and Müller, 1996). As the Foreland Basin evolved, the Upper Jurassic carbonate rocks were deformed and fault and fracture systems develop in the Eocene to Miocene parallel to the Alps (Mraz et al., 2018a; Budach et al., 2017; Kuhlemann and Kempf, 2002; Lemcke, 1988) (Fig. 4). The subsequent deposition of two regressive cycles of marine and fresh water sediments occurred during the Paleogene (Kuhlemann and

Kempf, 2002; Lemcke, 1988). Afterward, Quaternary sediments were deposited on top. The Molasse Basin can be subdivided into a western and an eastern part with the transition zone west of Munich. Due to the wedge-shape of the Molasse Basin, the Upper Jurassic sedimentary rocks crop out at the Franconian and Swabian Alb and are situated at around 5 km depth at the Alpine deformation front today (Fig. 4).

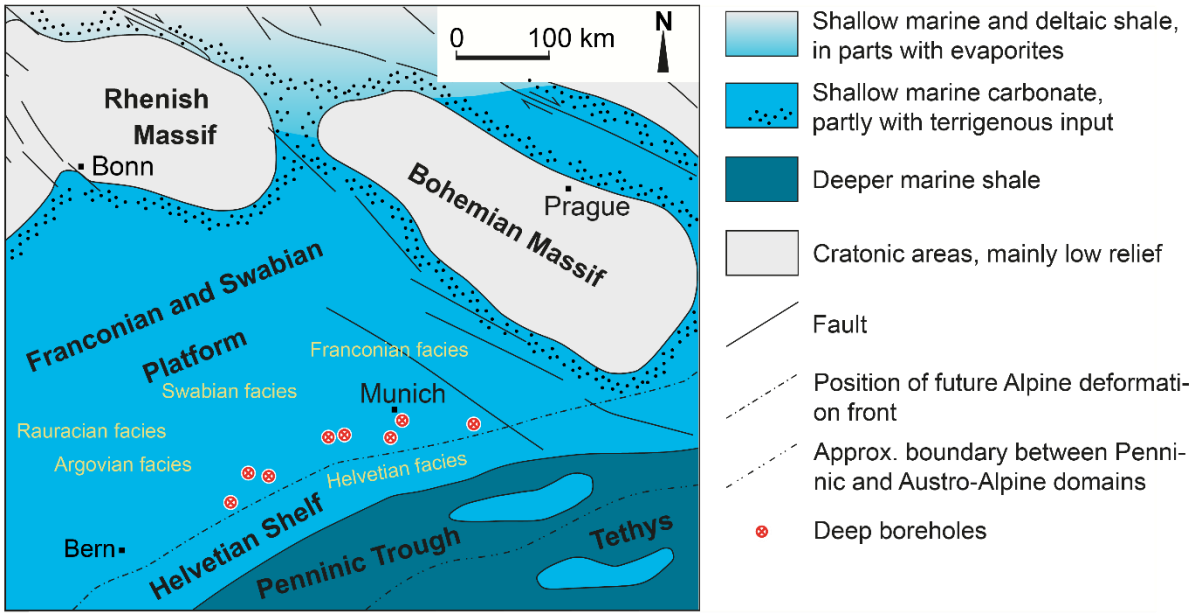


Fig. 3: Paleogeographic overview of the study area, modified from Ziegler (1990).

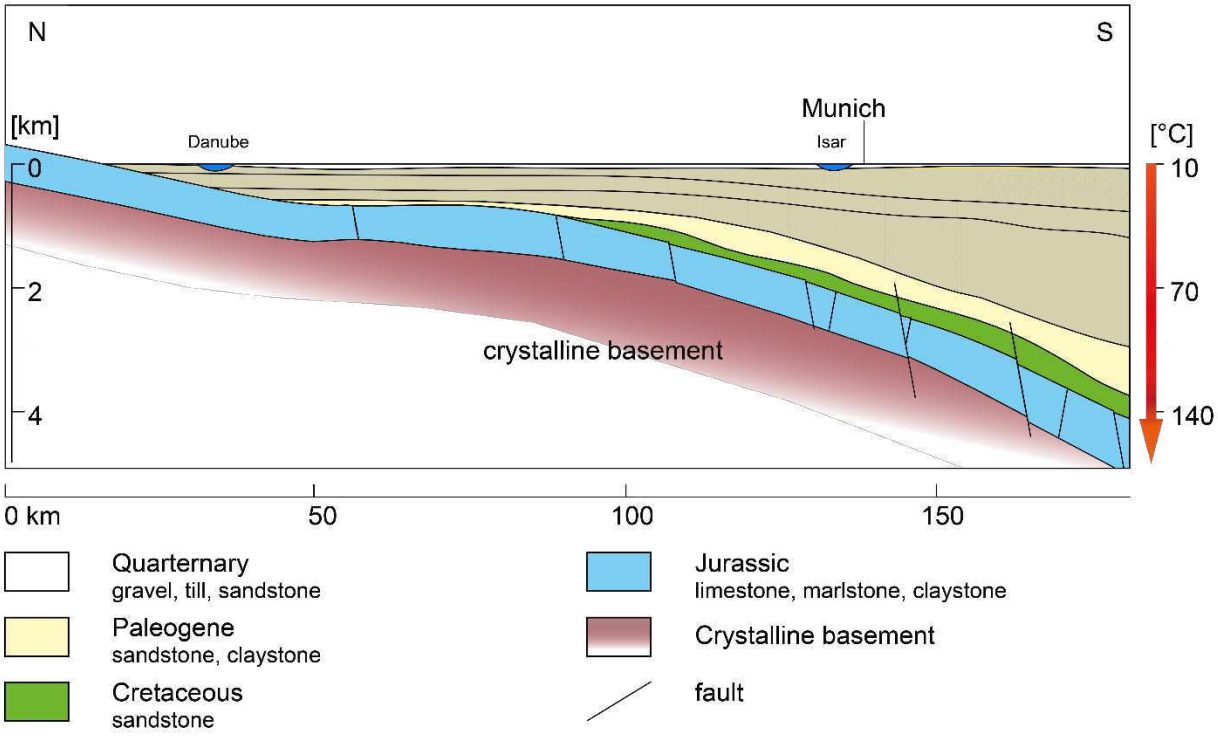


Fig. 4: Cross-section of the North Alpine Foreland Basin, with the main Upper Jurassic aquifer, after Lemcke (1988) and temperature.

During the Upper Jurassic, the northern passive continental margin of the Tethys was composed from north to south of the Rhenish-Bohemian Massif (continent, separated by the Hessian Seaway), which merges into the Franconian platform (synonym Swiss plateau), Helvetian shelf, slope (Ultrahelvetikum), Penninic trough and the Tethys basin (Mohr and Funk, 1995; Ziegler, 1990; Wildi et al., 1989) (Fig. 3). In southern Germany, the dominant depositional environment was on the Franconian platform. On the Franconian platform, an epicontinental sea (Meyer and Schmidt-Kaler 1989; Ziegler 1990) with a shallow marine ecosystem and a water depth of 50-150 m was developed (Gygi, 1992; Selg and Wagenplast, 1990) (Fig. 3).

## 3.2 Geology of the Upper Jurassic

The evolution of the Upper Jurassic reservoir in the Molasse Basin started with the deposition of carbonate rocks, limestones and dolostones on a carbonate platform in an epicontinental sea (Niebuhr and Pürner, 2014; Meyer and Schmidt-Kaler, 1989). The lithology, stratigraphy, and microfacies of the Upper Jurassic carbonate rocks of the Molasse Basin are further described in detail in chapter 5.1 and by Wolfgramm et al. (2017); Beichel et al. (2014); Lüschen et al. (2014); Wolfgramm et al. (2012); (2011); Reinhold (1996); Liedmann (1992); Geyer and Gwinner (1991); Meyer and Schmidt-Kaler (1989), and others.

.

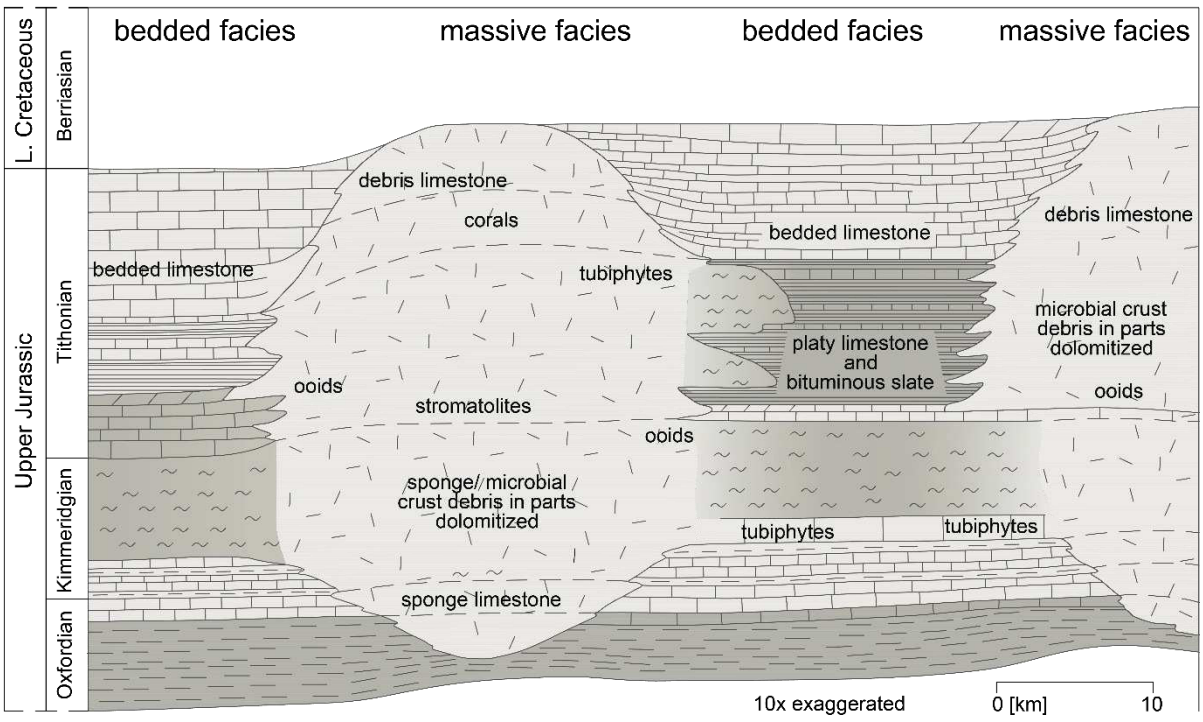


Fig. 5: Bedded and massive facies in line with Meyer and Schmidt-Kaler (1989) and Pawellek and Aigner (2003).

The Upper Jurassic carbonate rocks can be subdivided by the main and dominating organisms and by the depositional environment into a massive facies and a bedded facies in the Swabian and Franconian

facies (Meyer and Schmidt-Kaler, 1989) (Fig. 5). The massive facies, or sometimes so-called reef facies, is composed of siliceous sponges, microbial mats, tubiphytes, ooids, and peloids, which are sometimes reworked (Pawellek and Aigner, 2003; Meyer, 1994). In contrast, the bedded facies was deposited within basins and contains transported bioclasts of the surrounding massive facies in micritic, marly limestones (Meyer, 1994). To the late Upper Jurassic (upper Tithonian), the carbonate rocks grade into a brackish, evaporitic facies, the so-called Purbeck facies (Joachimski, 1994; Strasser, 1988; Barthel, 1969). The Upper Jurassic carbonates are classified in southern Germany as the Weißjura-group, with a lithostratigraphy based on the index regions in the Franconian and Swabian Alb (Niebuhr and Pürner, 2014; Meyer and Schmidt-Kaler, 1989). Previously used terms and traditional subdivisions for the Upper Jurassic in southern Germany are the ‘Malm’ by Oppel (1858) and ‘Weisser Jura’ by Quenstedt (1858)

Massive dolostones (highly permeable) are usually distributed within the Kimmeridgian, have developed from the massive facies, and build up the main high-permeability section in the reservoir (Wolfgramm et al., 2011; Böhm et al., 2010). The carbonate rocks of the Tithonian and Purbeckian showed slightly different dolomite types (Liedmann, 1992), which sometimes form a second highly permeable area in the Upper Jurassic reservoir (Wolfgramm et al., 2011; Böhm et al., 2010).

In periods of subaerial exposure, probable during the Cretaceous, and by the presence of meteoric waters, the Upper Jurassic carbonate rocks were dissolved, became karstified and in parts dedolomitized, especially the shallow reservoir rocks and at the outcrop areas (Koch, 2011; Reinhold, 1996). During the diagenesis, the carbonate rocks of the Upper Jurassic were affected by recrystallization and dolomitization processes (Liedmann, 1992), by a hydrocarbon emplacement, and migration of silicate rich fluids.

## 3.3 Facies realms of the Upper Jurassic

The Upper Jurassic is divided into five facies realms in the North Alpine Foreland Basin (Fig. 3): the Franconian facies, Swabian facies, Argovian facies (Geyer and Gwinner, 1991; Aldinger, 1968; Oppel, 1858), Rauracien facies (Gygi, 2012; Gressly, 1864), and Helvetian facies (Gygi, 2013; Meyer and Schmidt-Kaler, 1989).

### 3.3.1 Franconian facies

The massive facies of the Franconian facies is classified as the Frankenalb-Fm. (> 500 m thickness) and is not further subdivided (Niebuhr and Pürner, 2014; Meyer and Schmidt-Kaler, 1989). The bedded facies encompasses ten formations in the southern Franconian Alb (Niebuhr and Pürner, 2014). The bedded facies differs slightly from the southern to the middle Franconian Alb, and the northern Franconian Alb (Niebuhr and Pürner, 2014; Schlegelmilch, 2012; von Freyberg, 1966). The transition between the Swabian to the Franconian facies is around 30 km east of the Ries crater (Niebuhr and Pürner, 2014; von Freyberg, 1966; Schmidt-Kaler, 1962). The Franconian facies extends to the Bohemian Massif in the east, where it is preserved in outcrop relicts in the area between Straubing and

Passau (Niebuhr, 2014; von Freyberg, 1966), and is covered to the south by Molasse sediments of the Cenozoic (von Freyberg, 1966). Furthermore, only the southwestern Franconian facies is described, as it is assumed that this facies type prolongs to the Molasse subsurface in the south.

The Middle to Upper Jurassic border is characterized by a green ammonite layer, gray marlstones, dark to black claystone layers, and by a glauconitic limestone layer (thickness around 20 cm) (Niebuhr, 2014; Schlegelmilch, 2012; von Freyberg, 1966; Schmidt-Kaler, 1962; Quenstedt, 1858). The Oxfordian is defined as the Dietfurt-Fm. (previous Malm alpha and beta or Untere Mergelkalke and Werkkalk; 45-55 m) (Niebuhr and Pürner, 2014; Schlegelmilch, 2012). During the early Dietfurt-Fm. a strong change between marlstones and limestones, and afterward (former Malm beta) limestones are deposited (von Freyberg, 1966; Schmidt-Kaler, 1962). The former border of Malm alpha to Malm beta is indicated by the Planula zone (Meyer and Schmidt-Kaler, 1989). Furthermore, while the sedimentation of the Dietfurt-Fm. submarine or subaquatic erosion occurred, as condensed sequence (like a placer) with abundant ammonites of different biozones are described (von Freyberg, 1966; Schmidt-Kaler, 1962). A submarine erosion, a reworking of sediment without bigger clasts or consolidated sediment, occurs only in the Oxfordian and not later again. There are further only curved layers due to submarine landslides in consolidated sediment in the Altmühltal-Fm. (von Freyberg, 1966). The submarine erosion caused suspension currents which were also deposited on the algae build-ups in a minor degree (von Freyberg, 1966). Erosional discontinuities are only described for the early Dietfurt-Fm. (von Freyberg, 1966).

The Kimmeridgian is subdivided into the Arzberg-Fm., Treuchtlingen-Fm., and Torleite-Fm. (Niebuhr and Pürner, 2014; Schlegelmilch, 2012). The Arzberg-Fm. (previously Malm gamma or Obere Mergelkalke; 25-40 m) begins with a regression phase (erosional discontinuity) and an marlstone deposition with a condensed sequence of abundant ammonites (Platynota zone, around 5 m) (Meyer and Schmidt-Kaler, 1989; von Freyberg, 1966; Schmidt-Kaler, 1962). The Treuchtlingen-Fm. (previously Malm delta, Treuchtlinger Marmor, Dickbankkalke mit Schwämmen, Schwammrasen-Fazies, tafelbankige Kalke und Dolomite; 40 m) encompasses thick bedded limestones with siliceous sponges, algae crusts, tuberoids, and tubiphytes (Meyer and Schmidt-Kaler, 1989). The Torleite-Fm. (previous Malm epsilon, Torleite Bankkalke; 20-30 m) is a thinly bedded limestone with abundant ammonites and cherts (Meyer and Schmidt-Kaler, 1989).

The Tithonian encompasses seven formations, the Geisental-Fm., Altmühltal-Fm., Mörnsheim-Fm., Usseltal-Fm., Rennertshofen-Fm., and the Neuburg-Fm. (Niebuhr and Pürner, 2014; Schlegelmilch, 2012). The Geisental-Fm. (previously Malm zeta 1 or Bankkalke; max. 50 m) begins at some areas with a red marlstone layer (around 20 cm) and contains gray bedded limestones (Meyer and Schmidt-Kaler, 1989). To the Altmühltal-Fm. (previously Malm zeta 2 or Solnhofener Schichten; 40-50 m) the limestones become more divers, with the deposition of lithographic limestones in small basins (platy limestone). The Mörnsheim-Fm. (previously Malm zeta 3 or Mörsheimer Schichten; 45-65 m) is composed of siliceous thinly bedded platy limestones, and reef-debris limestones with thin marly limestone layers. The Usseltal-Fm. (previously Malm zeta 4 or Usseltal – Schichten; max. 70 m) is an alternating sequence of limestones with platy limestones. The Rennertshofen-Fm. (previously Malm

zeta 5 or Rennertshofener Schichten; max. 110 m) has limestones alternating with marlstone layers. The youngest deposited formation is the Neuburg-Fm. (previously Malm zeta 5 or Neuburger Bankkalke; 53 m), containing limestones with intersecting marlstone layers (Meyer and Schmidt-Kaler, 1989). On top are the sediments of the Purbeckian and the Lower Cretaceous.

For the Tithonian, a special bituminous shale facies is described within the bedded facies with radiolarians, dinoflagellates (tasmanacea) and a high bitumen content (Meyer and Schmidt-Kaler, 1993). The tasmanaceas indicate euxinian conditions and were deposited in high amounts (algal bloom) in cyclic sedimentation within an anoxic high-saline environment (Meyer and Schmidt-Kaler, 1993). Due to erosion and karstification during the Cretaceous the anoxic bituminous shales were oxidized and became white in color (Meyer and Schmidt-Kaler, 1993).

### 3.3.2 Swabian facies & Argovian facies

The Swabian facies extends from north-east Switzerland to the Swabian Alb (Niebuhr and Pürner, 2014), as well as below the Molasse Basin from the Swabian Alb to the south next to Lake Constance, where the transition to the Quinten-Fm. (Helvetian facies) in the south is described by Aldinger (1968) and to the Argovian facies in the west by Gygi (2012).

The Swabian facies begins with the Impressamergel-Fm. and the Wohlgeschichtete-Kalke-Fm. in the Oxfordian. The Impressamergel-Fm. (previously Oxford-Mergel, Untere Weißjuramergel, Malm alpha; 50-80 m) is composed of marlstones with limestones at the bottom and top (Meyer and Schmidt-Kaler, 1989). The Wohlgeschichtete-Kalke-Fm. (previously Oxford-Kalke, Wohlgeschichtete Kalke, Malm beta; late Oxfordian to early Kimmeridgian; 20-30 m) is build up by light gray limestones (Geyer and Gwinner, 1991; Meyer and Schmidt-Kaler, 1989). Afterward, the Lacunosamergel-Fm., Untere-Felsenkalke-Fm., Obere-Felsenkalke-Fm., Liegende-Bankkalke-Fm., Zementmergel-Fm. and the Mergelstetten-Fm. are deposited during the Kimmeridgian (Geyer and Gwinner, 1991). The Lacunosamergel-Fm. (previous Kimmeridge-Mergel, Mittlerer Weißjuramergel, Ataxioceraten-Schichten; Malm gamma; 20-70 m) starts with the Platynota zone and with a marly sedimentation (Meyer and Schmidt-Kaler, 1989). Untere-Felsenkalke-Fm. (previously Untere Felsenkalke, untere Kimmeridge-Kalke, Malm delta; 20-50 m) begins with thinly bedded limestones alternating with marly limestones followed by pure limestones (Meyer and Schmidt-Kaler, 1989). Subsequently, the Obere-Felsenkalk-Fm. (previously Malm epsilon; 20-25 m) was deposited on limestones.

With a glauconitic, dark marlstone layer (Glaukonitbank), in parts with mica and lithoclasts, starts the Upper Jurassic sedimentation of the Weißjura-Group (Niebuhr and Pürner, 2014; Schlegelmilch, 2012; von Freyberg, 1966). The thickness of the glauconite layer is between 0,3-3 m and contains sometimes a gravel debris rock at the basis (Schlegelmilch, 2012). The border between the Impressamergel-Fm. and the Wohlgeschichtete-Kalke-Fm. is described with a bioturbated fucoids layer (Schmidt-Kaler, 1962; Quenstedt, 1858). Fucoids are further described for the Lacunosamergel-Fm. (Schmidt-Kaler, 1962). The Lochenschichten (Lochenfazies) is a fossil-rich layer at the boundary Impressamergel-Fm.

to Wohlgeschichtete-Kalke-Fm. Coarse-grained Lochfels belongs to the Obere-Felsenkalke-Fm. and is a recrystallized calcite (Schlegelmilch, 2012; Schneider, 1958).

The Liegende-Bankkalke-Fm. (previously Liegende Bankkalke, obere Kimmeridge-Kalke, Malm zeta 1; 10-100 m) is composed of gray limestones alternating with thin marlstones. The Zementmergel-Fm. (previously Obere Weißjuramergel, Zementmergel, Malm zeta 2; 1-100 m) contains mainly marlstones, which are alternating with limestones (Meyer and Schmidt-Kaler, 1989). The Liegende-Bankkalke-Fm. and the Zementmergel-Fm. intersect with the Mergelstetten-Fm. The Mergelstetten-Fm. (120 m) is an alternating sequence of marlstones with marly limestones, and further show bioturbation and autochthonous breccias.

In the Swabian facies, the Liegende-Bankkalke-Fm. and Zementmergel-Fm. still belong to the Kimmeridgian, whereas the carbonates of the Geisental-Fm. (previously Malm zeta 1) of the Franconian facies were deposited during the Tithonian (Geyer and Gwinner, 1991). Therefore, the boundary between the Kimmeridgian and Tithonian are different between the Swabian and Franconian facies. Moreover, the Hangende-Bankkalke-Fm. (previously Hangende Bankkalke, Malm zeta 3; 50-150 m) is discordant deposited and younger carbonates of Tithonian age are eroded (Geyer and Gwinner, 1991). During the Tithonian there is a regression of the Tethys causing restricted lagoons, where finely laminated lime slates with Saccocoma were deposited (Keupp and Matyszkiewicz, 1997; Aldinger, 1968). The massive facies of the Swabian facies is separated by a basinal structure, the Swabian Marl Basin, from the massive facies of the Franconian facies (Meyer and Schmidt-Kaler, 1989).

The word Argovian comes from the Swiss Canton Aargau and was originally used for a sponge-rich limestone layer which is directly deposited on the Middle Jurassic near Andelot in France (Gygi, 2012; Oppel, 1858; Marcou, 1848). In recent literature, the Argovian facies is used and described similar to the Swabian facies for northeast Switzerland (Geyer and Gwinner, 1991; Aldinger, 1968; Oppel, 1858). The Argovian facies intersects to the northwest-west with the Rauracien facies (Gygi, 2012). After Aldinger (1968), the Argovian facies extends near to Lake Constance, whereas Büchi et al. (1965) describe the Argovian facies west of Zurich. Further, Büchi et al. (1965) and Gygi (2012) characterize the Argovian facies compared to the Swabian facies with a higher clay and marl content.

The Argovian facies is described and classified within the Canton Aargau (Aarau) and Schaffhausen by Gygi (2013, 2012). The Argovian facies starts on top of the late Middle Jurassic with the Ifenthal-Fm. (synonym Herznach-Fm.), a fossiliferous iron-oolithic rich marlstone layer which is often reduced or developed as a condensed sequence (Gygi, 2012). The Argovian facies is composed of the Wildegg-Fm., Villigen-Fm., and the Schwarzbach-Fm. (Gygi, 2012). The Wildegg-Formation is equivalent to the Impressamergel-Fm. (Transversarium to Bimammatum-Zone) of the Swabian facies and was deposited during the middle to late Oxfordian. Moreover, it encompasses the Birmenstorf-Member and Effingen-Member. The Birmenstorf-Member (3-5 m) is a micritic glauconitic limestone with a low marl content and contains siliceous sponges and ammonites. The main part of the Wildegg-Fm. is represented by the Effinger-Member (210-260 m, synonym Impressa-Mergel), a gray calcareous marlstone with a high quartz and a low feldspar content to argillaceous limestone with few fossils. The Effingen-Member has

a high detrital quartz content concentrated by turbidites and storms (Gygi, 2013). The Villigen-Fm. is a layered, micritic, in parts nodular and glauconitic limestone with abundant fossils (ammonites, bivalves, sponges), and was deposited in late Oxfordian to early Kimmeridgian in a distal environment. During the Kimmeridgian, the Schwarzbach-Fm. (equivalent to the Lacunosamergel-Fm.) was deposited, which is overlain by the Obere-Felsenkalke-Fm. (Planular zone) and further by the typical Swabian facies (Gygi, 2012).

### 3.3.3 Rauracien facies

The term Rauracien was originally used as a facies description for the coralline limestones of the Swiss Jurassic and of the Upper Rhine valley region after Gressly (1864). The coralline limestones at the beginning of the Oxfordian are not developed in the Franconian or Swabian facies. The Rauracien facies encompasses the St-Ursanne Fm. of the Swiss Jura and the Korallenkalk-Fm. of the Upper Rhine in Germany (Gygi, 2013). The Rauracien facies of the Upper Rhine valley merges to south and south-west into Argovian facies (Pichoux-Fm.) of the Swiss Jurassic (Gygi, 2012; Heim, 1919). The Swiss Jurassic reef complex is 20 km wide and 80km long. Water depths for the Oxfordian reef limestone of the northern and central Jura mountains (Rauracien facies) are described to be around 0 to 30 m (Wildi et al., 1989).

### 3.3.4 Helvetian facies

The Helvetian facies is usually described at allochthon formations in the Vorarlberg (Austria) and Walensee region (Switzerland) with marly Schilt-Fm. (Schiltschichten and Ueberschiltschichten) of the Oxfordian and the Quinten-Fm. as the youngest formation. The Helvetian facies is further described autochthonous for the area around Lake Constance (Aldinger, 1968; Schneider, 1958). Up to now, there is no classification of the Helvetian facies and the Quinten-Fm. at a type region (CH, 2017).

At the Vorarlberg, the Helveticum is the eastern extension of the Swiss Säntis-nappe, which belongs to the southern Helveticum and is not divided in the Sänits-nappe (Cretaceous) and Gonzen-nappe (Jurassic), as it is described for eastern Switzerland (Felber and Wyssling, 1979). The term ‘Helveticum’ is used in this research for the tectonic unit and ‘Helvetian facies’ for the sediments deposited on the Helvetian shelf during the Jurassic (Bögel and Schmidt, 1976). Due to the alpine tectonics, there are palinspastic reconstructions of the Helvetic realm (Wildi et al., 1989). In former research, the term ‘Helvetian basin’ is used numerously, which is problematic, as the Franconian platform merges into the Helvetian shelf.

The Quinten-Fm. (previously Hochgebirgskalk, Quintnerkalk, Malmkalk, or Tithonkalk) is described as a micritic limestone with pelagic microfauna encompassing radiolarians, planktonic shells (filaments), echinoderms (*Saccocoma* sp.), fragments of benthic organisms, gastropods, and ostracods (Felber and Wyssling, 1979). In the upper Quinten-Fm. tintinnids are abundant (Felber and Wyssling, 1979), which can be used as an indicator for the shelf region (Mohr, 1992). Felber and Wyssling (1979) describe the depositional environment as deep marine, a still water milieu below the euphotic zone, and with low

euxinian conditions due to a stagnating sedimentation. Rarely there are arenitic wackestones with allochthone, shallow marine organisms (miliolids, shells) within a pelagic microfauna (tintinnids, radiolaria, filaments) (Felber and Wyssling, 1979). The eastern Helvetic nappes can be classified by a calpionellid biostratigraphy (Mohr, 1992). Calpionellids are only abundant in the distal facies zone (Mohr, 1992), and are characteristic for the hemipelagic and pelagic sedimentation of the Tethys (Mohr and Funk, 1995). Calpionellids show a crystalline outer wall with a micritic filling, and no sparite in the inside (Flügel, 1982).

### 3.3.5 Upper Jurassic Facies of the Molasse Basin

The hydrocarbon wells, drilled in the 1950-60s, were evaluated after the hydrocarbons, oil and gas, and the macrofauna. The macrofauna such as ammonites were used to classify the carbonate rocks by lithostratigraphy connected to biostratigraphy of the Weißjura-Group type regions at outcrops. The depositional environment was not further analyzed, and the knowledge of the type regions was tried to adapt on the southern deposits of the Upper Jurassic. Therefore, carbonate rocks within the southern part of the North Alpine Foreland Basin were classified with the lithostratigraphy by Quenstedt (1858), even when a bedding or stratification was not visible (Anonymous, 1960). The microfacies content as well as the porosity of the carbonate rocks was not analyzed. Consequently, the description of the lithological profile was examined critically. To distinguish the Helvetian facies from the Franconian and Swabian facies, a rock color criterion was applied by previous researchers, as it was assumed that the dark gray to black carbonates belong to the Quinten-Fm. Furthermore, only the Franconian and Swabian facies should possess light gray to whitish rock colors (Lemcke, 1988). Hence, the facies transition of the Franconian-Swabian facies to the Helvetian facies was described by previous researchers along the line Wangen-Legau-Kaufbeuren-Ammersee (Lemcke, 1988).

For the boreholes Opfenbach, Tettnang, Hindelang (Schwerd and Huber, 1995), Maderhalm, Kierwang, Gaisbeuren, Ravensburg, and Sulzberg, in the east of Lake Constance, the Helvetian facies was described by Lemcke (1988) and Schneider (1962). Furthermore, Schneider (1962) described that the Upper Jurassic carbonate rocks of these boreholes are similar to the Quintner limestone (Quinten-Fm.) of the Kanisfluh. The Helvetian facies of the boreholes Opfenbach and Tettnang was classified due to only a related faunistic and lithologic content to the Swabian facies, and a clear difference of a higher bitumen content and a missing of marl layers in the late Upper Jurassic (Schneider, 1962). After Schneider (1962), the boreholes Gaisbeuren 1, Saulgau 1, Pfulendorf 1 intersect the Upper Jurassic in the bedded Swabian facies, whereas the boreholes Wurzach 1, Heimertingen 1, Scherstetten 1 are developed in the massive Swabian facies. As the Upper Jurassic carbonate rocks of the boreholes in the Molasse Basin subsurface are developed similar to the Swabian facies, a transition zone was assumed for the Kimmeridgian and Oxfordian in the southern part of the North Alpine Foreland Basin (Büchi et al., 1965; Schneider, 1962).

# 4 Methodology

Depositional facies and lithology of the veins and carbonate rocks were studied using optical and scanning microscopy on alizarin stained thin sections. The stable isotopes $\delta^{18}O$ and $\delta^{13}C$ were measured from drill cuttings. For the microthermometry and cathodoluminescence measurements, a new sample approach with cuttings of around 1 mm was developed by using the unprepared and unpolished drill cuttings. This multidisciplinary study is composed of petrographic, geochemical, fluid inclusion analyses as illustrated in Fig. 6 and is explained in the following.

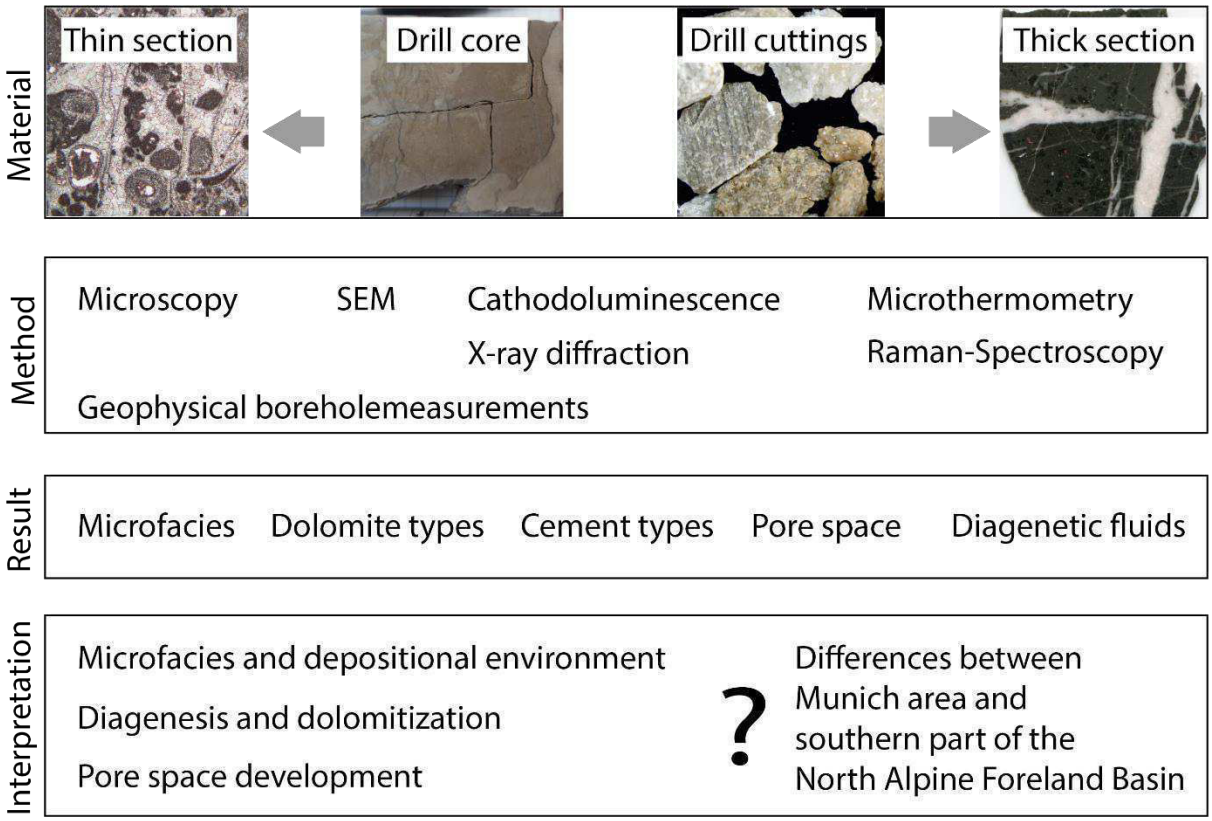


Fig. 6: Overview of the multidisciplinary methods used in this study. The rock material was prepared to thin and/or thick section.

## 4.1 Rock samples from wells

The Upper Jurassic wells were selected to investigate an east-west and north-south oriented profile in the Molasse Basin. On the east-west line the following wells are situated: TRN, GEN, SCH, MST, BWO, hydrocarbon wells A, B, C, and STG. From north to south the wells MOS, FRH, UHA and GEN were sampled. Both profile lines cross at the central well GEN. In general, 117 m bore cores and over 650 cutting samples were measured and evaluated. From most wells were drilling reports, geophysical measurements (logs), and rock samples of either drill cores or drill cuttings available.

## 4.2 Rock samples from outcrops

The use of outcrop analogues was emphasized as a tool in understanding subsurface reservoirs in order to reduce some of the main uncertainties associated with many reservoir studies. The main advantage in using outcrop analogues is the potential for nearly unlimited access to the rocks, and the opportunity to describe and characterize units in three dimensions. Besides, the studies by previous researchers could be extended to greater depths by the evaluation of outcrops in addition the wells. Therefore, rock samples from 40 outcrops (74 samples) were analyzed originating from the Franconian and Swabian Alb, as well as from the Kanisfluh.

## 4.3 Thin sections and Thick sections

Around 1400 rock samples including hand specimens, drill cores, and drill cuttings from boreholes and outcrops were used in this study to determine the lithology, microfacies and diagenesis. The Upper Jurassic samples of the 40 outcrops were hand specimens, whereas the samples of the 17 deep wells were either drill cores or drill cuttings. From the 40 outcrop samples, 10 were made into double-sided thick sections. The drill cutting material (around 650) was made into 349 thin sections with blue dyed resin or were measured unprepared as they were produced by drilling. The drill cuttings had generally a size of around 1 mm. The drill core samples of the Upper Jurassic were made into 648 thin and 15 thick sections. Overall, 824 thin sections, 15 thick sections and around 400 unprepared drill cuttings were analyzed.

Standard petrographic thin sections were prepared, with each samples vacuum impregnated with a blue dye epoxy prior to thin section preparation. The thick and thin sections were polished with ceroxid, which was sometimes visible in the SEM. Furthermore, the thin sections were half-stained by a low acid alizarin red solution.

## 4.4 Petrology and Microscopy

Mineralogy of carbonate rocks, microfossil content and pore types were analyzed by optical microscopy. The carbonate rocks were further classified by Folk (1959) and Dunham (1962). The pore types were classified in line with Choquette and Pray (1970), and the dolostone textures were classified according to Machel (2004); Sibley and Gregg (1987). Carbonate rocks with the amount of dolomite crystals above 75 % were called dolostones in the present study. The microfacies and compaction by the occurrence of stylolites were described. The different cement phases were determined by their morphology and dissolution of the crystals was determined. With the transmitted and polarized light microscopy, first information about the mineral- and fossil content, and texture were gained. The documentation was made with a coupled digital camera in combination with the Stream Motion Software from Olympus.

## 4.5 SEM and XRD

The scanning electron microscopy (SEM) and energy dispersive X-ray (EDX) analyses were carried out at thin sections and drill cuttings to determine the composition of the cement phases in the limestones and dolostones. The SEM measurements were conducted at the Zentrum für Wekstoffanalytik (ZWL) in Lauf an der Pegnitz. All 12 samples (Tab. 1), either drill cuttings or thin sections, were sputtered with a thin layer of carbon. In addition, a conductive material was fixed to the drill cutting samples to prevent a charging by the electron beam.

The SEM images are gathered by a focused electron beam on the sample surface under vacuum. Thereby, the electron beam interacts with the sample atoms and signals are produced which are measured at a detector. Due to the electron beam scanning in a raster, a high-resolution image (max. 2 nm) is produced. Furthermore, back-scattered electrons were measured at another detector to produce a back-scatter image, which related to the atomic number of the sample. The back-scattered electrons are secondary emitted electrons due to the excitation of the sample atoms by the focused electron beam. Due to the further interchange between sample and electron beam, X-rays are generated, which can be determined by energy dispersive X-ray spectrometer (EDX), to gain punctual and space-oriented analysis of the element distribution. In addition, quantitative element analyses were determined by EDX mapping of a predefined area.

Tab. 1: Table of SEM measurements.

| Sample | Description |
|---|---|
| GEN-1 | (1) calcite, (2) dolomite with idiomorphic crystals and bitumen, (3) matrix dolomite, (4) micritic limestone, (5) peloidal, ooidal grainstone, (6) matrix dolomite with stylolites |
| TRN-4610 | 2 cuttings: planar-s (1) and planar-e (2) dolostone |
| TRN-4350 | 2 cuttings: vein dolomite (1) und planar-a dolostone (2) |
| GEN-4540 (2), GEN-5605 (1) | Planar-a dolostone (2), dolostone with clay minerals (1) |
| GEN-6010 | Planar-a dolostone |
| FRH-2300 | 2 cuttings: vein calcite cement with pyrite (1) and glauconitic calcareous sandstone (2) |
| FRH-2910 | Matrix dolomite in limestone |
| FRH-2325 | 2 cuttings: peloidal grainstone (1), etched peloidal grainstone dolostone (2) |
| FRH-2885 | 2 cuttings: transparent, planar-s dolostone (1), dolostone with pyrite (2) |
| FRH-2325 | Planar-e dolostone |
| FRH-2910 | 3 cuttings: crust (1), layered dolostone (2), matrix dolomite (3) |
| GEN-1 | 2 cuttings: dolostone (1), contact dolomite to calcite cements (2) |
| TET-2744.7 | Stylolites |
| GEN-1ST-5018.2 | Limestone with oncoids, stylolites, algae |
| GEN-1ST-5018.6 | Cement generations, dolostone |

| Sample | Description |
|---|---|
| GEN-1ST-5036 | Stylolites |
| GEN-1ST-5205 | Dolomite crystals along stylolite |
| GEN-1ST-5386.9 | Dolomite breccia |
| GEN-1ST-5089.5 | Dolomite breccia |
| GEN-1ST-5010 | Matrix dolomite |
| GEN-1ST-5605 | Planar-e dolostone |
| GEN-1ST-5605 | Dark brown planar-a dolostone |
| GEN-1ST-5010 | Matrix dolomite |
| GEN-1ST-5605 | Dolostone |

In addition, XRD measurements (Tab. 2) were further conducted in line with DIN EN 13925-1, 2, 3; DIN EN 1330-11 on four Upper Jurassic bore core samples, which were selected from dark gray, micritic limestones (2942-4709 m TVD), at the Chair of Engineering Geology.

Tab. 2: Table of XRD measurements.

| Sample | Description |
|---|---|
| A1 | 91% Calcite, 4% Dolomite, 3% Quartz, 2% Muscovite |
| GEN-1ST-5019 | 94% Calcite, 6% Dolomite, small amount of quartz and pyrite |
| GEN-1ST-5205 | 97% Calcite, 3% Dolomite, small amount of quartz |
| GEN-1ST-5382 | 100% Calcite, small amount of quartz and dolomite |

The X-ray diffraction determined the mineral phases of a sample. The measurement is based on monochromatic diffraction of X-rays at the mineral lattice and on the resulting X-ray reflection. For each mineral a characteristic lattice distance, and the Bragg angle (Bragg equation) forms a mineral specific reflex pattern. Both quantitative analyses helped to further investigate the cements, microfabrics, and diagenetic sequence of the Upper Jurassic carbonate rocks.

## 4.6 Raman Spectroscopy

To identify the aqueous fluid system and mineral phases, micro-Raman spectroscopy was performed, using a Horiba Jobin Yvon XploRA PLUS confocal Raman microscope. The spectrometer was equipped with a frequency-doubled Nd:YAG laser (532 nm, with a maximum power of 22.5 mW) and an Olympus 100× long working distance objective with a numerical aperture of 0.9. The operation conditions had a confocal hole of 300, a spectral slit of 100, and a grating of 1800 T. However, the high fluorescence of the calcite host mineral in the range of 2500-4000 cm-1 led to an insufficient spectrum. Consequently, the aqueous 2-phase fluid inclusions could not be specifically identified using the micro-Raman spectroscopy.

## 4.7 Fluid inclusion studies

For the around 450 microthermometry measurements, mainly fluid inclusions in vein calcite and in planar-e dolostone were analyzed, which were linked to fracture zones. The microthermometry study of fluid inclusions was performed on double-polished thick sections from drill cores as well as on drill cuttings of vein calcites and dolomite crystals. For the microthermometry measurements, a new sample approach with cuttings of around 1 mm was developed by using the unprepared and unpolished drill cuttings. In addition, conventional thick sections were measured with microthermometry. At the Geretsried well, drill cuttings and conventional double-side polished thick sections of bore cores were measured using the microthermometry to compare the results and confirm the drill cutting measurements. To measure drill cuttings with microthermometry, the drill cuttings are usually embedded in an epoxy resin, polished on both sides, and used as thick sections with the drill cuttings still embedded in the resin. However, the epoxy resin is not stable in the temperature range between -110°C and 200°C, which was necessary for this study. Silicone or Teflon are stable polymers for this temperature range, but they are soft at room temperature, and the cuttings lose their bond to the polymers during polishing and fall off the resin. As a consequence, the cuttings in this study were cleaned with water and measured in the form in which they were produced.

The drill cuttings generally showed a smooth surface at former cleavage planes or at fresh fracture surfaces. However, not every cutting sample showed good visibility and a flat surface, and therefore they could not be measured in this fluid inclusion study. In the heating-freezing stage, the cuttings were always placed with the flat and largest surface on the silver block, and they were measured at very slow heating and cooling rates to prevent a high temperature gradient in the sample and to determine the exact temperature. Furthermore, the drill cuttings were directly measured at least 2-3 times to exclude a high temperature gradient in the sample. The microthermometry measurements were performed on a heating-cooling stage, a Linkam stage apparatus mounted on an Olympus microscope with a precision of 0.1 K. For the aqueous one-phase and two-phase fluid inclusions (liquid and vapor), the shape, size, texture, genesis, phase type, host mineral, and phase volume ratio were documented in line with Van den Kerkhof and Hein (2001). When a nucleation of a bubble was not possible in one-phase fluid inclusions at around 4°C, the sample was then further cooled to -110°C to check for possible phase transitions. In contrast, two-phase fluid inclusions were first heated in increasing order to homogenization in the liquid phase and afterward cooled to -110°C to minimize the possibility of inclusion deformation. The homogenization temperature ($T_h$) was measured in small inclusions by temperature cycling. Afterward, the eutectic temperature ($T_e$) and last melting and/or ice melting ($T_m$) temperature were measured. If possible, fluid inclusions in an assemblage (FIA) were investigated. In the present study, data from fluid inclusion assemblages (FIA) were used preferentially before single fluid inclusion measurements. However, when a constant liquid-vapor ratio in comparison to the FIA was given, some single $T_h$ measurements of one- and two-phase fluid inclusions were used in this study. Leakage of a fluid inclusion was sometimes not observable, but it was determined by an increase in $T_m$ and gas bubble size

during the measurement. Sometimes, a positive $T_m$ and a change in $T_m$ was observed in small fluid inclusions, which can be caused by metastability or by clathrate melting.

Tab. 3: FI-Fluid inclusions, CL-cathodoluminescence, X-thick section, Y-thin section, Z-cutting sample.

| Sample Well | Stratigraphy Upper Jurassic | depth [mTVD] | Method FI | n | Method CL | Sample n | Meas. n | Sample type |
|---|---|---|---|---|---|---|---|---|
| A6.1 | dolostone, Treuchtlingen-Fm. | | x | 1 | x | 1 | 1 | X |
| A6.3 | dolostone, Treuchtlingen-Fm. | | | | x | 1 | 4 | X |
| A10.18 | dolostone, Treuchtlingen-Fm. | | x | 2 | x | 1 | 4 | X |
| A10.7 | dolostone, Treuchtlingen-Fm. | | x | 1 | x | 1 | 1 | X |
| A10.9 | dolostone, Treuchtlingen-Fm. | | x | 1 | x | 1 | 2 | X |
| A11.1 | limestone, Altmühltal-Fm. | | x | 8 | x | 1 | 2 | X |
| A12.1 | dedolostone, Treuchtlingen-Fm. | | x | 4 | x | 1 | 3 | X |
| A13.2 | dedolostone, Treuchtlingen-Fm. | | x | 4 | x | 1 | 1 | X |
| A14.1 | limestone, Treuchtlingen-Fm. | | x | 1 | x | 1 | 4 | X |
| A21.4 | dolostone, Treuchtlingen-Fm. | | x | 2 | x | 1 | 5 | X |
| A25.1 | limestone, Treuchtlingen-Fm. | | x | 1 | x | 1 | 2 | X |
| A27.1 | limestone, Treuchtlingen-Fm. | | x | 1 | x | 1 | 6 | X |
| A32.2 | limestone, Arzberg-Fm. | | x | 1 | x | 1 | 2 | X |
| A34.1 | dolostone, Frankenalb-Fm. | | x | 1 | x | 1 | 1 | X |
| A39.1 | dolostone, Frankenalb-Fm. | 400 | x | 4 | | | | X |
| **sum** | | | | **32** | | **14** | **38** | |
| FRH-1 | Kimmeridgian | | x | 17 | x | 12 | 27 | Y, Z |
| GEN-1 | Kimmeridgian | 4365-4722 | x | 73 | | 15 | 8 | Z |
| GEN-1ST-A1 | Kimmeridgian | 4602-4722 | x | 29 | x | 1 | 2 | Z |
| C1 | Tithonian | 3303,2 | x | 15 | x | 1 | 1 | X |

| Sample Well | Stratigraphy Upper Jurassic | depth [mTVD] | Method FI | n | Method CL | Sample n | Meas. n | Sample type |
|---|---|---|---|---|---|---|---|---|
| MOS | Tithonian-Kimmeridgian | 1288-1449 | x | 40 | x | 2 | 4 | X |
| SCH | Tithonian | 4375-4378 | x | 84 | x | 4 | 9 | X |
| STG | Oxfordian-Kimmeridgian | 3910-4156 | x | 28 | x | 3 | 6 | X |
| A1 | Kimmeridgian | 2646-2739 | x | 18 | x | 2 | 2 | X |
| TRN-1 | Tithonian-Kimmeridgian | | x | 24 | x | 49 | 35 | Y, Z |
| TRN-2 | Tithonian-Kimmeridgian | 4336-4509 | x | 9 | x | 30 | 8 | Z |
| UHA-1 | Kimmeridgian | 3067,5 | x | 28 | x | 2 | 1 | Z |
| UHA-2 | Kimmeridgian | 3289,5 | x | 12 | x | 2 | 2 | Z |
| BWO | Tithonian-Kimmeridgian | 2370-2565 | x | 12 | x | 5 | 5 | Y, Z |
| **sum** | | | | **389** | | **128** | **110** | |

With the $T_m$, the bulk salinity was interpreted using the computer program SoWat (Sodium chloride Water), which is a model of almost equation of state for fluid inclusions in the $H_2O$-NaCl system (Driesner, 2007; Driesner and Heinrich, 2007; Goldstein and Reynolds, 1994). The measured $T_h$ using microthermometry should represent the minimal formation or trapping temperatures of the fluid inclusions (Roedder, 1984). For the fluid and temperature evolution, the formation (entrapment) temperature was calculated with a pressure correction (hydrostatic and lithostatic) using the assumed depth during crystal growth. For the maximum formation temperature, todays sample depth was used as the input parameter for the pressure correction, because it was assumed that the maximum depth has been reached today.

## 4.8 Cathodoluminescence microscopy

The cathodoluminescence (CL) was measured conventional at thin and thick sections, and in addition at unprepared and unpolished drill cuttings. Thereby, a cold cathode system from CITL (Cambridge Image Technology Ltd.) coupled to an Olympus microscope and a digital Olympus DP25 camera was used. Operating conditions were in the range of 260-365 µA/mm² and 15-20 keV gun current with a vacuum during the measurement below 0.06 mbar. The camera was adjusted to ISO 200 with a constant exposure time of 5 s for all photos. A problem was that the exposure time of the camera could not be extended to 5s or more, as usually an exposure time of 45s is used.

It was possible to measure drill cuttings in CL, if they had a smooth and flat surface. However, sometimes in contact with the electron beam the cuttings moved outside the visible field. Thus, it was necessary to check for a minimal space between the particles to prevent a shadow of the electron beam by neighboring cuttings, due to the thickness of the drill cuttings. In general, CL in carbonate rocks is, especially in calcite and dolomite crystals, due a doping of foreign atoms (impurities) and subordinating

by lattice defects (Götze, 2002; Amieux, 1982). Therefore, CL provides information on the growth textures in the crystals, which are indicative of the forming conditions and diagenesis. In addition, the CL color and intensity depends on activators, sensitizers, quenchers in the crystal lattice, and fluctuations in redox-potential, as well as in growth rates, temperature, crystal surface structure, fluid chemistry, and chemical species in solution (Boggs and Krinsley, 2006; Pagel, 2000). The CL in diagenetic carbonate rocks is usually visual detectable by the activator of manganese ($Mn^{2+}$), which can exchange the $Ca^{2+}$ and/or $Mg^{2+}$ position in the crystal lattice and can be further quenched by $Fe^{2+}$, $Co^{2+}$, $Ni^{2+}$ and $Fe^{3+}$ (Richter et al., 2003; Pagel, 2000). A intrinsic luminescence occurs, as the CL color is emitted of a carbonate crystals from the inside without any influence from surrounding effects or changes (Amieux, 1982). If there is no lattice contaminations or foreign atoms in stoichiometric calcite crystals, the CL color is dark blue to violet (Amieux, 1982). The $Mn^{2+}$ activated luminescence in calcite and dolomite crystals, change the CL from the intrinsic blue-violet color to an extrinsic orange-red color (Boggs and Krinsley, 2006). Hence, in this study different cement phases based on CL and fluid inclusion data were characterized. However, using a cold cathode, only qualitative measurements were possible. In the samples, sometime dust particles were visible by a bluish CL on the sample surface. An intrinsic, blue to violet CL was not visible in all executed CL measurements on calcite cements. Furthermore, the CL intensity was increased at uneven fracture surfaces at the drill cutting samples. The CL colors of the Upper Jurassic carbonate rocks were red, non-luminescent, red with non-luminescent concentric zonation, orange, yellow with non-luminescent sector zonation, and dull yellow.

## 4.9 Stable isotopes

For the stable isotope measurements, the Upper Jurassic carbonate samples were finely ground and examined in line with Hoefs (1997) in the mass spectrometer of the University of Kiel. Approximately 10 mg of a sample was dissolved in pure phosphoric acid. The calcite samples were completely dissolved after 4 min, the dolomite samples after 18 min. Subsequently, the resulting $CO_2$ was measured at temperatures between 850 - 1000°C under vacuum. The $^{12}C/^{13}C$ ratios were specified in δ notation with reference to the international standard PDB, the measurement error of the double determination was ± 0.5 ‰. The oxygen isotopes were given in accordance with the SMOW (water) or PDB (minerals) standard.

# 5 Results

In the following chapter, the three key questions of this study are addressed in three independent papers. The key questions for the low productivity in the Upper Jurassic reservoir to the south of the Molasse Basin are (I) a change in facies and depositional environment and/or (II) a different diagenesis and (III) different dolomitization. The independent papers are composed of an introduction, methodology, results, discussion, and conclusion. In the main synoptic discussion (chapter 6), all three key questions are further described, interpreted and examined critically in an overall context. Following, there is a brief description of the content of each paper.

In the first paper (chapter 5.1), the decrease in well productivity of the Upper Jurassic carbonate rocks is discussed by the possibly occurrence of the Helvetian facies in the southern part of the Molasse Basin. Furthermore, the lower degree in karstification of the Upper Jurassic rocks is investigated. Therefore, the carbonate rocks of the investigated wells are described and analyzed by lithology and microfacies. The aim of the paper is the description of a change in facies and depositional environment to the south which could coincides with a decline in permeability.

In the second paper (chapter 5.2), the paleo-fluid evolution is reconstructed by fluid inclusion studies and by stable isotope data. By this reconstruction, the diagenetic processes of the carbonate rocks are described, and a basin-wide characterization of the different cement phases is made. The focus was on the high- and low-permeability areas, which were analyzed by means of examined cements. The examined cements are formed after deposition and are used to reconstruct the reservoir evolution by composition and temperature of the paleo-fluids. The cements were sampled at different hydrocarbon and geothermal wells in the North Alpine Foreland Basin, as well as from outcrops in the Franconian and Swabian Alb. The aim was to describe changes in fluid evolution during diagenesis, which might have caused a decline in pore space and well productivity.

In the third paper (chapter 5.3), the focus is on dolomitization of the Upper Jurassic carbonate rocks, which are distributed at high productive well in the Molasse Basin. Up to now, the dolomitization is not completely understood, as well as the relevance of dolostones for fluid flow in geothermal wells. Previous studies of dolomitization focused on the shallow reservoir (< 1 km) and on outcrops of the Upper Jurassic carbonate rocks in the Swabian and Franconian Alb. In this study, three types of the Upper Jurassic dolomite and calcite cements were analyzed which have formed during diagenesis at depths greater than 3 km, at the Munich area, and at the outcrop areas. Hence, this study extended the investigations of the diagenetic processes to greater depths and higher temperatures. It was assumed that the diagenetic process of dolomitization happened in a different grade due to a higher temperature and pressure in the southern part of the Molasse Basin. The aim was to understand the dolomitization and formation of cement in the southern part of the Molasse Basin, which might have caused the decline in well productivity.

## 5.1 Microfacies Analysis in Upper Jurassic Carbonates with Implications for Reservoir Quality in the Molasse Basin

### 5.1.1 Introduction

The North Alpine Foreland Basin, referred to as the Molasse Basin, hosts a geothermal reservoir in Upper Jurassic carbonate rocks, which has already been explored and developed as a low-enthalpy hydrothermal resource (Agemar et al., 2014b). This Upper Jurassic carbonate aquifer is a reservoir for thermal water, stored in fractures and pore spaces (Birner, 2013). In the Munich area in southern Germany, the Upper Jurassic reservoir is encountered by more than 40 geothermal wells at depths of 2,500 m to 3,500 m with fluid temperatures of up to 150 °C. The Upper Jurassic carbonate rocks were deposited (in today's areas of Europe) within an epicontinental sea of the northern Tethys, which consists of the carbonate platform (Franconian platform) and the Helvetian shelf as a fringing shelf to the south (Ziegler, 1990; Meyer and Schmidt-Kaler, 1989). The Upper Jurassic strata crop out at the Franconian and Swabian Alb, dip to the south and are covered by Molasse sediments of Cenozoic age (Lemcke, 1988). With increasing depth of the Upper Jurassic reservoir southward, the fluid and rock temperatures increase. However, permeability of the carbonate rocks decline toward the Alps. Hence, for successful geothermal projects in the southern deep Molasse Basin, pore space development needs to be analyzed and characterized. The pore space of carbonate rocks is influenced by primary porosity (depositional environment) and diagenesis. This paper aims to analyze and characterize the depositional environment of the Upper Jurassic carbonate rocks by microfacies evaluation of rock sample from drill cores and cuttings to understand the permeability distribution in the southern part of the foreland basin.

Up to now, the permeability decline has been assumed to be caused by the following: The planktonic micritic Helvetian facies, described within hydrocarbon boreholes in the southern Molasse Basin, is the cause of the low reservoir permeability in the southern Molasse Basin (Schneider, 1962), due to the dense carbonates prior to diagenesis. The lower degree of karstification in hydrocarbon and balneological wells within the southwestern part of the basin may be another cause of this permeability decline (Koschel, 1991). The southern part is less affected by karstification, as surface erosion was only possible in a short period during the early Cretaceous (Strasser, 1988; Villinger, 1988). Hitherto, the transitions or locations of the facies types, the depositional environments, and diagenesis have still not been sufficiently described for the North Alpine Foreland Basin. The knowledge about the Upper Jurassic strata is mainly based on outcrops at the Franconian and Swabian Alb in Germany and the Helvetian and Argovian facies in northeastern Switzerland and western Austria (Lemcke, 1988). The Upper Jurassic rocks have been investigated since 1856, mainly at surface outcrops, and intensive during the hydrocarbon exploration in the 1950s-1980s within the Molasse Basin. With the geothermal exploration since 2000, the interest in this Upper Jurassic carbonate reservoir has been rejuvenated and requires further investigation of permeability and the commodity of producible thermal water. Borehole data show not only a basin-wide permeability decline to the south but also a darker carbonate rock color. Therefore, it is necessary to investigate the distribution of the facies types, especially the Helvetian

facies, to understand the causes of the low permeability of the Upper Jurassic in the southern deeper Molasse Basin. The facies type and thereby the depositional environment control the primary porosity, just like a higher primary porosity exists at reef structures compared to the micritic bedded facies with small bioclasts and low primary porosity. In this study, we used rock samples from seven deep boreholes, which were drilled for thermal, hydrocarbon and drinking water applications in the Upper Jurassic, from the west in Switzerland to the east in South Germany in the area around Lake Chiemsee. We studied the samples in detail for lithology, facies type and depositional environment. To understand the distribution of the facies types and the depositional environment on the Franconian platform and the transition to the Helvetian shelf, we first explain the common knowledge and interpretation, followed by the newly conducted borehole analysis of the facies types.

### 5.1.2 The Upper Jurassic geology of the Molasse Basin

Besides southern Germany, the Upper Jurassic in Europe is distributed in England, France, Switzerland, northern Germany, Poland, Greece, Italy, Croatia and Austria (Pieńkowski et al., 2008). At least three different marine facies realms in the Upper Jurassic have been described for those regions: the sub-Mediterranean, the Mediterranean (tethyal), and the subboreal provinces (Schlegelmilch, 2012). In southern Germany, the predominant faunistic province is the sub-Mediterranean of the Tethys with a minor influence of the northern and southern faunistic provinces (Schlegelmilch, 2012).

The northern passive continental margin of the Tethys is composed from north to south of the Rhenish-Bohemian Massif (continent, divided by the Hessian Seaway), which merges into the Franconian platform (synonym Swiss plateau), Helvetian shelf, slope (Ultrahelvetikum), Penninic trough and the Tethys basin (Mohr and Funk, 1995; Ziegler, 1990; Wildi et al., 1989) (Fig. 7). In Southern Germany, the dominant depositional environment is the Franconian platform and the Helvetian shelf. A shallow marginal epicontinental sea with a shallow marine ecosystem and a water depth of 50-150 m developed on the Franconian platform (Gygi, 1992; Selg and Wagenplast, 1990), which merged into the deeper Helvetian shelf. In Switzerland, Aldinger (1968) divided the platform and the shelf further from north to south with the neritic Rauracien facies, the Argovian facies and the bathyal Helvetian facies (Gygi, 2012) (Fig. 7). For the Jurassic and Cretaceous sediments located in the Alps and Apennines, many research studies have described the transition of the carbonate platform to the continental margin radiolarites (Bernoulli and Jenkyns, 2009); and references therein). However, the description and interpretation are limited to the Alpine nappes and is not attributed to the Helvetian shelf or Franconian platform in the north (Bernoulli and Jenkyns, 2009). Up to now, five facies realms of the Upper Jurassic have been classified within the North Alpine Foreland Basin: the Franconian facies, Swabian facies, Argovian facies (Geyer and Gwinner, 1991; Aldinger, 1968; Oppel, 1858), Rauracien facies (Gygi, 2012; Gressly, 1864), and Helvetian facies (Gygi, 2013; Meyer and Schmidt-Kaler, 1989).

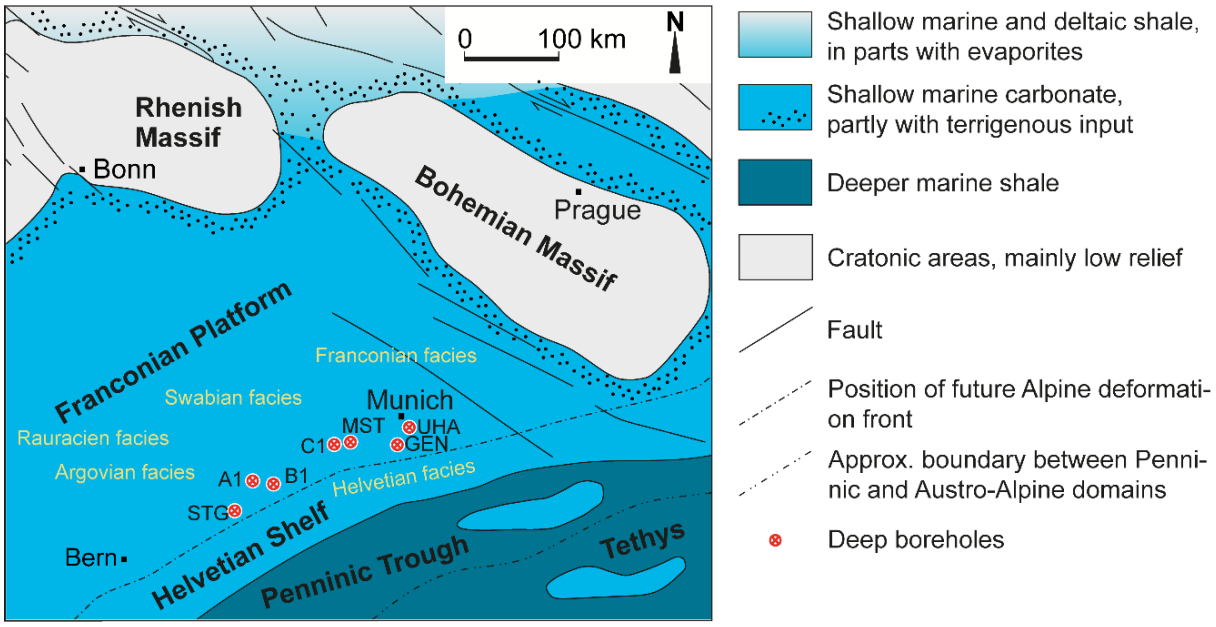


Fig. 7: The paleogeography of the northern Tethys margin in southern Germany, eastern Switzerland, and western Austria after Ziegler (1990); STG= St. Gallen 1, MST= Mauerstetten, GEN= Geretsried, UHA= Unterhaching; A 1, B 1, C 1 hydrocarbon boreholes.

The Franconian and Swabian facies were deposited on the Franconian platform, the Rauracien and Argovian facies on the Swiss part of the Franconian platform (so-called Swiss plateau), and the Helvetian facies on the shelf (Fig. 7). The Helvetian facies (Quinten-Fm.) is usually described at allochthonous outcrops in the Vorarlberg, western Austria, and at the Walensee region, eastern Switzerland. Up to now, there has not been a standard classification of the Helvetian facies and the Quinten-Fm. at a type region (CH, 2017), and the classifications by Felber and Wyssling (1979), Colins et al. (1989), and Lupu (1972) were used in this study. Due to the Alpine tectonics and the building of nappes, there have been palinspastic restorations of the Helvetic realm, which was originally deposited around 20 km further south (Wildi et al., 1989; Wyssling, 1985). The Helvetian facies, in addition, is defined to be autochthonous to the area around Lake Constance (Aldinger, 1968; Schneider, 1958).

The Upper Jurassic carbonates are classified in southern Germany as the Weißjura-group (Fig. 8), with a lithostratigraphy based on the index regions in the Franconian and Swabian Alb (Niebuhr and Pürner, 2014). Previously used terms and traditional subdivisions for the Upper Jurassic in southern Germany are the ‘Malm’ by Oppel (1858) and ‘Weisser Jura’ by Quenstedt (1858). Some researchers in Switzerland and southwestern Germany have used the sequence stratigraphy connected by ammonite biostratigraphy to classify the Argovian, Rauracien, Swabian, and Franconian facies of the Upper Jurassic (Pieńkowski et al., 2008; Ruf et al., 2005; Gygi, 1992; von Freyberg, 1966).

The Upper Jurassic deposits are further subdivided into a bedded and a massive reef facies in Germany (Fig. 8) (Meyer and Schmidt-Kaler, 1989). The reef facies is composed of reefs, patch reefs, and mud mound-building organisms such as dominant siliceous sponges, corals, bryozoans, tubiphytes, algae and stromatolites, as well as ooids and oncoids (Koch et al., 1994; Meyer, 1994). The bedded facies encompass limestone with alternating layers of marlstone. Both facies types can also be dolomitized, silicified, and karstified.

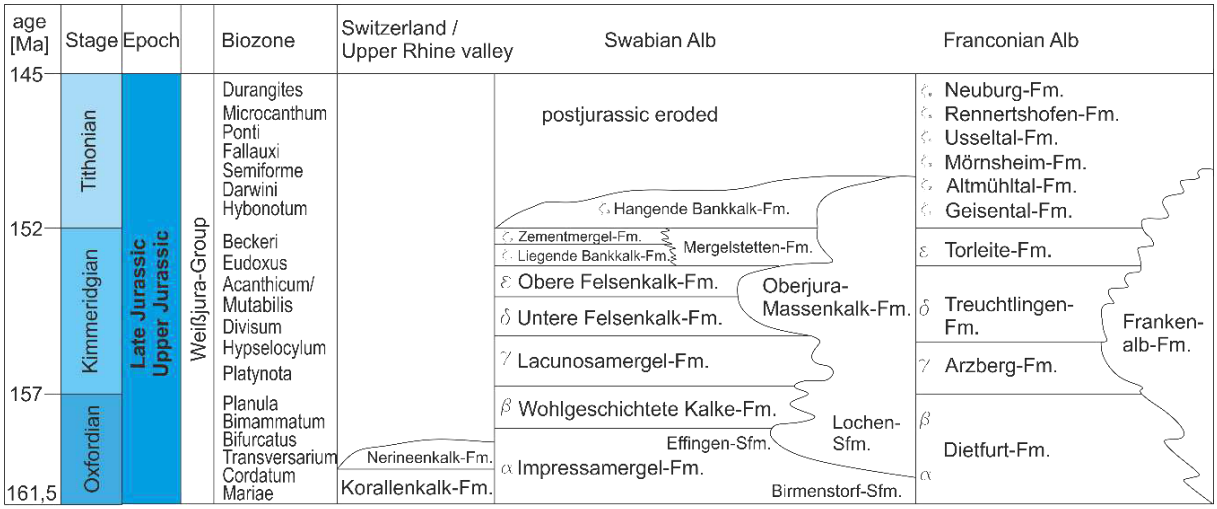


Fig. 8: Lithostratigraphic classification of the Upper Rhine valley (Rauracien facies), Swabian Alb (Swabian facies) and Franconian Alb (Franconian facies) type regions in Germany (Menning and Hendrich, 2016). The Greek letters stand for the formerly used classification of the Upper Jurassic (so-called Malm) according to (Oppel, 1858). Biozones after Schweigert (2015); Gygi (2013); Hardenbol et al. (1998).

The sedimentation of the Upper Jurassic carbonates on the Franconian platform began with the deposition of a glauconitic sandstone horizon in all five facies types (Schneider, 1962). The boundary of the Middle to Upper Jurassic is a condensed layer or a hiatus over a large part of the European landmass (Hardenbol et al., 1998), and a possible indication of eustatic control (Allenbach, 2001). With the beginning of the Upper Jurassic, the Tethys started to transgress eastward to the Regensburger Seaway and the Bohemian Massif in the north (Niebuhr and Pürner, 2014; von Freyberg, 1966). Limestones and marlstones were deposited in the Oxfordian. During the Kimmeridgian, the marly layers diminished and pure limestones with reef organisms were accumulated. In the Tithonian, the depositional environment became more diverse with restricted lagoons between reef structures due to basin-wide regression within the epicontinental sea (Hardenbol et al., 1998; Meyer and Schmidt-Kaler, 1989; Lemcke, 1988). The sedimentation of the Upper Jurassic ended with a maximum regression surface and the so-called Purbeck facies (Meyer, 1994; Lemcke, 1988; Strasser, 1988), brackish limestones with a terrigenous input. During the Cretaceous, there were phases of transgression and regression on the Franconian platform with the Tethys coming from the northern to the southern Alpine region and through the Regensburger Seaway from the east (Lemcke, 1988). During those sea level changes, the Upper Jurassic carbonate rocks were affected by surface erosion, and the carbonates became karstified. During the Late Cretaceous, the Tethys transgressed northward again, and the surface influence diminished. Consequently, the Cretaceous sediments are preliminarily found in the vicinity of the Alpine border (Lemcke, 1988). The deposited and eroded Cretaceous sediments are further covered by upper Eocene to upper Miocene and Quaternary deposits within the Molasse Basin (Lemcke, 1988).

**Transitions and distribution of the facies types**

The Franconian facies extends from the Bohemian Massif in the east to the area around 30 km east of the Ries crater (meteoric crater), where it intersects the Swabian facies (Niebuhr and Pürner, 2014; von Freyberg, 1966; Schmidt-Kaler, 1962). The Franconian Alb can be further subdivided by reef barriers into the northern, middle and southern Franconian Alb (Niebuhr and Pürner, 2014; Liedmann, 1992). The Franconian and Swabian facies dip to the south and are covered by Molasse sediments of the Cenozoic in the North Alpine Foreland Basin (Lemcke, 1988; von Freyberg, 1966). The Swabian facies extends from northeast Switzerland to the Swabian Alb and the westernmost Franconian Alb (Niebuhr and Pürner, 2014). In addition, the reef facies of the Swabian facies is separated from the reef facies of the Franconian facies by a basinal structure, the Swabian Marl Basin (Meyer and Schmidt-Kaler, 1989) (Fig. 9).

The marl content decreases from the Swabian to the Franconian facies and is still decreasing within the Franconian facies eastward (von Freyberg, 1966; Schmidt-Kaler, 1962) due to a shallower depositional environment (Liedmann, 1992). In the Swabian facies, reef-building started in the early Oxfordian, but massive sponge reef structures developed in all of southern Germany during the late Oxfordian (Schlegelmilch, 2012; Aldinger, 1968). At the beginning of the Kimmeridgian, reef-building briefly decreased and then increased to the main algae-sponge reef-building phase (Schlegelmilch, 2012; Koch et al., 1994; Aldinger, 1968). Additionally, the total carbonate thickness increases westward from the southern Franconian Alb to the Swabian Alb (von Freyberg, 1966) but can fluctuate due to synsedimentary uplifts and downlifts (Wildi et al., 1989; Schmidt-Kaler, 1962). The early to middle Kimmeridgian boundary (previously Malm gamma/delta boundary) is indicated in the Swabian and the Franconian facies by a strong faunistic change and a discordance, as light-colored limestones are on top of darker marly layers (Schmidt-Kaler, 1962).

According to Menning and Hendrich (2016), the transition of the Swabian and Franconian facies to the Helvetian facies in the submolasse is along a line Sipplingen-Memmingen-Füssen (Fig. 9). At Memmingen, the Swabian facies intersects the Franconian facies in the Molasse Basin (Menning and Hendrich, 2016). The Quinten-Fm. (Helvetian facies) should intercalate in the northwest with the Wohlgeschichtete-Kalke-Fm. of the Swabian facies (late Oxfordian, Swabian facies) and in the northeast with the Frankenalb-Fm. of the Franconian facies (Menning and Hendrich, 2016). In earlier research, a rock color criterion was used to distinguish the Helvetian facies from the Franconian and Swabian facies, as it was assumed that the dark gray to black carbonates belong to the Quinten-Fm. (Lemcke, 1988). In contrast, light gray to whitish rock colors should exist only in the Franconian and Swabian facies (Lemcke, 1988). Hence, the facies transition of the Franconian and Swabian facies to the Helvetian facies was described by previous researchers along the line Wangen-Legau-Kaufbeuren-Ammersee (Fig. 9) (Lemcke, 1988; Aldinger, 1968; Büchi et al., 1965). In the area of Lake Constance, the Helvetian and Swabian facies should intercalate according to Gygi (2012) and Aldinger (1968) with the Argovian facies in the west. In contrast, Büchi et al. (1965) described the westward extent of the Argovian facies around Zurich. The transition zone between the Swabian and Helvetian facies according

to Schneider (1958) should be indicated by the absence of the Ataxioceraten-Perisphincten fauna (lower Kimmeridgian, indicative of the Lacunosamergel-Fm.) in the southern part of the North Alpine Foreland Basin. The Helvetian facies, the transition between the epicontinental and geosynclinal (Alpine) Jurassic, is characterized by the lack of bigger marlstone layers and sponge complexes according to Liedmann (1992). To the northwest-west along the Rhenish Lineament, the Argovian facies (Pichoux-Fm.) of the Swiss Jurassic intersects the Rauracien facies (Gygi, 2012; Allenbach, 2001) or shows a transition east of the Rhine river and west of the Black forest according to Heim (1919). Based on the fauna distribution, a submarine barrier must have existed between the Alpine depositional area and the Franconian platform (von Freyberg, 1966). The submarine barrier could have been either the Helvetian shelf and Penninic trough or an elevated area like the Vindelician High.

All those theories and interpretations show a lack of a clear and sufficiently described characterization of the facies transition in the North Alpine Foreland Basin. To understand the primary porosity of the Upper Jurassic carbonate rocks, the controlling distribution of depositional environments and facies must be investigated.

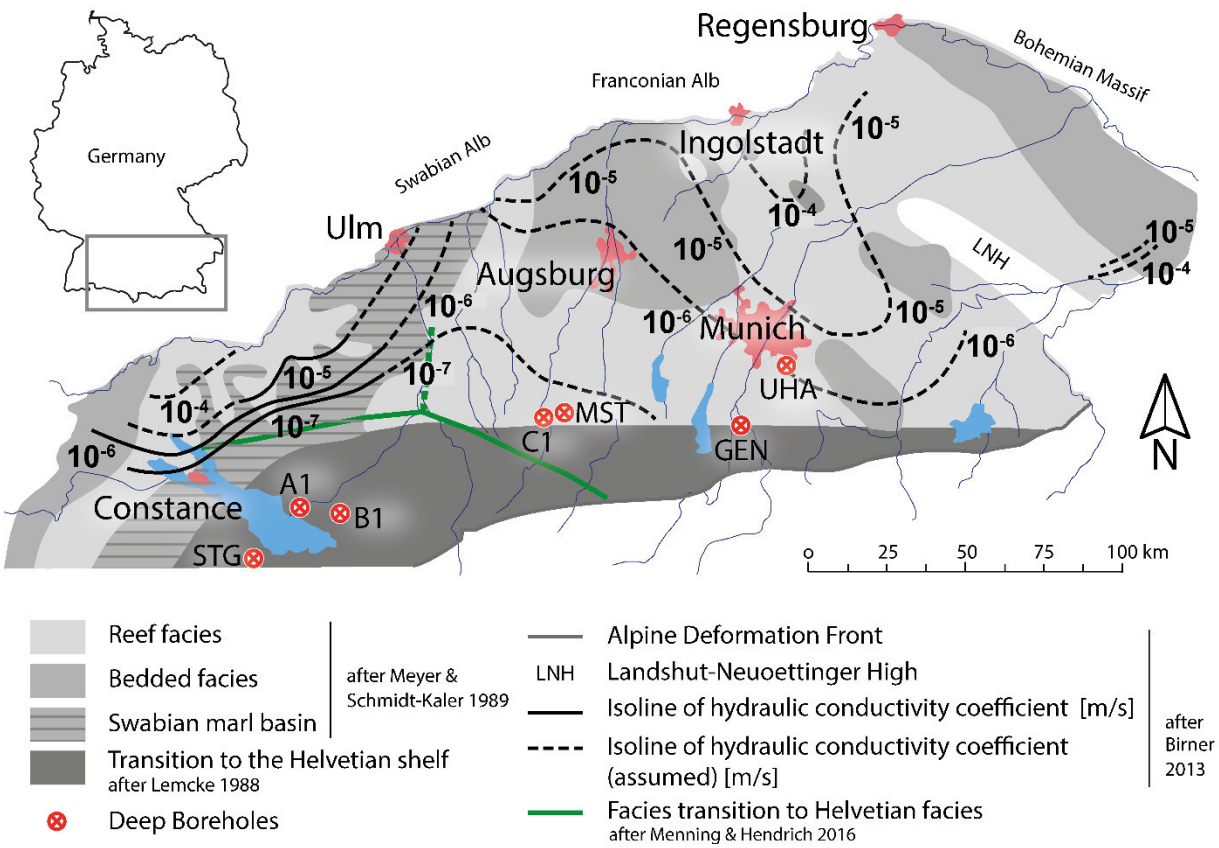


Fig. 9: Distribution of the depositional environments and coefficient of hydraulic conductivity for the Upper Jurassic after Menning and Hendrich (2016); Birner (2013); Meyer and Schmidt-Kaler (1989); Lemcke (1988); Schneider (1962) during the middle Kimmeridgian (previous Delta 1-2) (STG= St. Gallen 1, MST= Mauerstetten, GEN= Geretsried, UHA= Unterhaching, A 1, B 1, C 1 hydrocarbon boreholes).

Today, microfacies is used to classify the Upper Jurassic strata and depositional environment within boreholes (Beichel et al., 2014; Böhm et al., 2010; Koch et al., 2010; Koch, 1991; Pomoni-Papaioannou et al., 1989). The microfacies encompass different characteristics, which can be described in drill cores, cuttings or hand specimens and thin sections, so they are consequently applicable to every sample size (Flügel, 1982). The use of the biostratigraphy requires ammonites and macrofossils, which are generally not included and visible in rock samples from deep boreholes. Therefore, the use of microorganisms (microfacies) is a new classification approach in geothermal exploration (Steiger et al., 2015; Flügel, 2010) to determine lithology and depositional environment and is applied in this study.

### 5.1.3 Geological setting and study area

The study area is situated in the southern part of the Molasse Basin and represents the deeper down-lifted Upper Jurassic reservoir (> 3,500 m). Up to now, the seven investigated boreholes (Fig. 9), except Unterhaching, have not been used for geothermal energy production. There was a hydrocarbon drilling campaign during the 1950s-1980s in the Molasse Basin, so old hydrocarbon boreholes in addition to newly drilled geothermal boreholes have been used in the last decade. The easternmost borehole used in this research was Unterhaching, the westernmost was St. Gallen 1. The deep geothermal borehole Geretsried GEN-1 is located south of Munich, and the borehole Unterhaching is southeast of Munich (Fig. 9). The Upper Jurassic reservoir is intersected at depths of around 4.3 km at Geretsried and at Unterhaching at a depth of around 3 km. The geothermal borehole Mauerstetten 1 reached the top reservoir at around 3.4 km depth. The three hydrocarbon boreholes C 1 (top reservoir: 3,2 km), B 1 (top reservoir: 3.6 km) and A 1 (top reservoir: 2.6 km) were drilled during the 1950s to 1960s. The last and sixth borehole is the geothermal borehole St. Gallen 1 in Switzerland, south of Lake Constance, which reached the Upper Jurassic reservoir top at a depth of 3.8 km. The investigated outcrop area for the Helvetian facies is located in the Vorarlberg (Austria), at the Kanisfluh, which is an anticline overtilted to the north that belongs to the Säntis nappe (Rölz, 1966). Boreholes A 1, B 1, and C 1 (Fig. 9) should intersect the Quinten-Fm. (Helvetian facies) according to Lemcke (1988) and Schneider (1962), because the carbonate rocks possess only a related faunistic and lithologic content compared to the Swabian facies. In addition, the bitumen content is higher and marl and sponge layers are missing within those boreholes in the late Upper Jurassic. Schneider (1962) described the similarity of the Helvetian facies within boreholes of the southwestern Molasse Basin with the Quintner limestone (Quinten-Fm.) at the Kanisfluh (Vorarlberg, Austria). Other researchers have described a development similar to the Swabian facies in deep boreholes of the Molasse Basin for the lower Upper Jurassic (Büchi et al., 1965). Hence, researchers have previously assumed but not described a transition zone from the Helvetian facies to the Swabian and Franconian facies in the southern part of the North Alpine Foreland Basin during the Oxfordian and Kimmeridgian (Schneider, 1962). Prior research investigated the drill cores of deep boreholes in the context of hydrocarbon exploration and used the macrofauna to classify the lithology. Recent deep boreholes were classified by rock color and by microfacies, as only cuttings were available. In earlier research, it was further assumed that the Helvetian facies was intersected at the geothermal boreholes Geretsried and Mauerstetten due to the black rock color.

### 5.1.4 Methodology

Rock samples such as drill cores, cuttings, and thin sections, as well as the unpublished drilling reports, were available from the three hydrocarbon boreholes A 1, B 1 and C 1 (Anonymous, 1960, 1958, 1957). An unpublished drilling report, thin sections and cuttings were available from the boreholes Mauerstetten 1 and Geretsried 1. The cuttings were used to make additional thin sections. Thin sections from the cuttings and a report from the borehole Unterhaching (Beichel et al., 2014) were available for this study. At St. Gallen, thin sections from three side cores (double-polished) and the unpublished microfacies report GeotecConsult (2014) were accessible. We made ten thin sections from seven hand specimens from the Kanisfluh anticline in Vorarlberg, where the outcrops of the Helvetian facies are located. Carbonate rocks of the hydrocarbon drill cores were classified in the drilling reports using the lithostratigraphy by Quenstedt (1858), even when bedding or stratification was not visible (Anonymous, 1960). The microfacies content as well as the porosity of those carbonate rocks were not analyzed. Therefore, the description of the lithological profile at the hydrocarbon drill sites was examined very carefully.

Petrographic studies were conducted with cuttings and drill cores samples using reflected light microscopy, and on thin sections by transmitted light microscopy. Thin sections were made of either cuttings, hand specimens or drill core material from all seven boreholes and the outcrop, and they were further dyed with Alizarin Red S as well as blue resin to show open pore spaces. Rock samples of cuttings and 34 drill cores (around 85 m) from seven deep boreholes, drilled for hydrocarbons or geothermal application, were analyzed petrographically. The petrography of over 650 thin sections was determined describing the composition, rock color, microfacies content, depositional environment, primary porosity, compaction (stylolite), and they were classified according to Dunham (1962) and Folk (1962, 1959). If dolomite crystals were present as single crystals, they were described as matrix dolomite or replacement dolomite according to Machel (2004). If they were developed massive, they were described as dolostones. In some cases, cuttings were the only rock samples of the reservoir. The advantage of using cuttings is that they are always produced during drilling with sizes around 1 mm. Drill cores are necessary for investigating sedimentary structures, as cuttings are only small sections of those structures. Cuttings are sometimes strongly affected by the drilling process, and characteristic layers of clay- to siltstone are not preserved due to possible dissolution in contact with the drilling fluid. The microfacies of cuttings and thin sections were used in this study to analyze the facies and depositional environment. In addition, biostratigraphy based on ammonites as index fossils or macrofauna was not applicable to cuttings, because the rock samples were too small to classify a complete organism. In this study, all visible fossils within the micro- or macrofacies were described.

### 5.1.5 Lithology of the Upper Jurassic boreholes

The southernmost evaluated boreholes are boreholes A 1 and B 1 in Germany and borehole St. Gallen 1 in Switzerland. The boreholes Mauerstetten 1, C 1, and Geretsried 1 are further to the north along a west-east striking line, and Unterhaching is the north easternmost borehole. All seven boreholes

(Fig. 13) and the Helvetian facies outcrop (Kanisfluh) have a dark gray to black rock color in common. The deepest top reservoir is intersected in the Geretsried 1 borehole, the shallowest top reservoir at A 1, which is one of the southernmost boreholes today. All the boreholes are described from the oldest to the youngest, from the borehole bottom to the top in vertical depth (TVD).

### 5.1.5.1 Stratigraphy of the Upper Jurassic boreholes

We used stratigraphy based on biostratigraphy with ammonites as index fossils. However, ammonites were not found in the cuttings but only in one drill core at A 1. There, the ammonite *Taramelliceras argoviens* was described (Anonymous, 1957), which is a characteristic ammonite for the Cordatum biozone (Jeannet, 1951) (Fig. 13). In addition, the crustacean coprolite *Favreina salevensis* according to Brönnimann (1976), the planktonic crinoid *Saccocoma* sp. according to Keupp and Matyszkiewicz (1997), and filaments (Flügel, 2010) were visible within the analyzed boreholes (Fig. 13, Tab. 4). Filaments are thin, curved and around 5 mm long calcitic microstructures, possibly pelagic bivalve shells of Bositra sp. (Flügel, 2010).

Tab. 4: Index fossils of the microfacies, classified for the Upper Jurassic in southern Germany, and distribution in the analyzed boreholes (UHA: Unterhaching, GEN: Geretsried, MST: Mauerstetten, C 1, B 1, A 1).

| **Organisms** | **Index fossil** | **Environment** | **Borehole** | **Description** |
|---|---|---|---|---|
| *Favreina salevensis* | Purbeck facies, upper Tithonian | Restricted lagoons | B 1, C 1 | Brönnimann (1976) |
| Calpionellids | Quinten-Fm., Tithonian | Pelagic | Quinten-Fm. | (Mohr, 1992) |
| *Campbelliella striata* (previously *Bankia striata*) | Tithonian-Berriasian | Shallow water | UHA | (Flügel, 2010) |
| *Clypeina jurassica* | Tithonian | Inner platform | - | (Flügel, 2010, 1978) |
| *Saccocoma* sp. | Kimmeridgian - Tithonian | Pelagic | GEN, B 1, C 1, A 1, MST | (Flügel, 2010; Keupp and Matyszkiewicz, 1997) |
| Filaments (*Bositra* sp.) | Toarcian - Oxfordian | Subtidal to bathyal | UHA, GEN, A 1, MST | (Flügel, 1978) |

The planktonic crinoid *Saccocoma* sp., present in the analyzed boreholes, is possibly not restricted to the Kimmeridgian (Fig. 13). The coprolite *Favreina salevensis* is visible in the latest Upper Jurassic carbonates of C 1, and B 1, indicating a shallow marine influence (Fig. 13, Tab. 1). According to Flügel (2010), the biozonation of the Jurassic to Cretaceous tethyal shallow marine carbonates can be based on microfossils, such as abundant dasyclad associations, like *Salpingoporella* sp., *Campbelliella striata*, and *Clypeina jurassica* (Flügel, 2010) (Tab. 1). Hence, an extended biostratigraphy of microfossils to macrofossils of ammonites was available, which was applied in this study. Furthermore, all boreholes in the Upper Jurassic are covered by a glauconitic calcareous sandstone. If the investigated boreholes

intersected the Middle to Upper Jurassic boundary, an iron oolitic glauconitic sandstone layer was visible. Facies, depositional environment and porosity

**Borehole A 1**

At borehole A 1, the Upper Jurassic was developed over a thickness of 442 m (18 drill cores) with an alternating sequence of dark gray bioclastic wackestones with calcitic sandstones or extraclast-rich wackestones as intermediated layers (Fig. 10 C, D, F). There, the complete Upper Jurassic deposits are intersected, and the final depth is situated in the Middle Jurassic. The fractures within the Upper Jurassic limestone are filled by black coatings and calcite crystals, and stylolites are visible. Furthermore, the borehole intersects a fault zone within the lower third of the Upper Jurassic. The microfacies of the wackestones shows no calpionellids, but it contains bioclasts of echinoderms, ostracods, foraminifera, siliceous sponges and shell fragments with sizes up to 2 mm (Fig. 10 A, E). The former siliceous sponges are recrystallized to calcite.

At A 1, the Upper Jurassic sedimentation begins above a glauconitic horizon with a mudstone to bioclastic wackestone. The bioclastic wackestone shows planktonic organisms and fossil-rich layers. Toward the top, the wackestone becomes a peloidal to oncoidal floatstone with bigger bioclasts of serpulids and echinoids. The first dolomite rhombs are visible simultaneously as matrix or replacive dolomite. At the fault zone, the depositional environment becomes more proximal with an increase in organism content and size, as there are lithoclasts within the fault breccia. The fault breccia below the fault zone contains three different clasts of limestones. Firstly, a mudstone with dolomite and filaments, secondly, a fine-grained dolostone, and thirdly a peloidal grainstone to floatstone with dolomitized areas. Toward the top, dolomite crystals occur only in the middle of the upper wackestone along a stylolite and within limestone lithoclasts of the sandstone layer (Fig. 13). The wackestone below the fault zone contains dolomite rhombs within the matrix in addition to nodules and bioclasts. In the hanging wall of the fault zone, a mudstone is intersected, followed by a bioturbated wackestone. Subsequently, the approximately two-meter-thick sandstone layer was deposited on top of the bioturbated wackestone. The sandstone contains glauconite, mica, feldspars, and lithoclasts of quartz and limestone (Fig. 10 C).

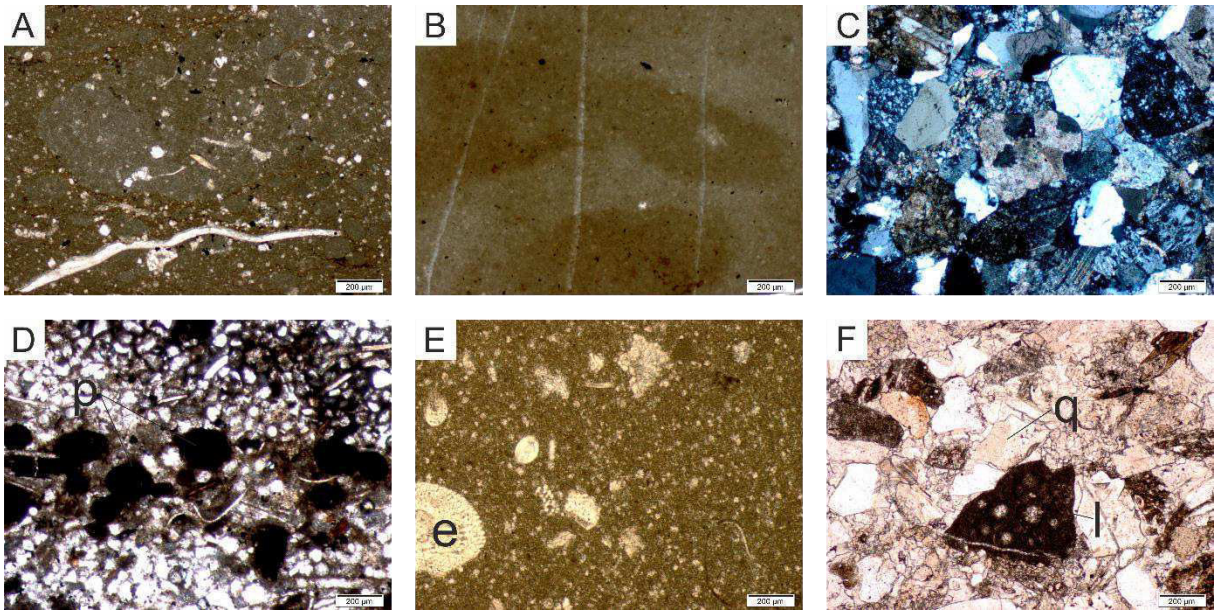


Fig. 10: Thin section photos of drill cores at A 1 (A to F decreasing depth) in transmitted light. A: nodular wackestone with bioclasts; B: nodular, bioturbated wackestone to mudstone; C: quarzitic sandstone in polarized light; D: gradation within the sandstone by bioclasts and peloids (p); E: wackestone with bigger bioclasts like echinoderms (e); F: sandstone with quartz clasts (q) and limestone lithoclasts (l).

The sandstone is graded by bigger and smaller clasts of quartz and bioclasts (shell fragments), as well as within the fine-grained sections by a change in bitumen content. In addition, the sandstone contains peloids within the graded material (Fig. 10 D). Some of the limestone lithoclasts contain matrix dolomite. Afterward, a bioturbated wackestone (Fig. 10 A, B) to bioclastic floatstone is intersected with abundant organisms, such as foraminifera, bivalves, echinoids, serpulids, and possibly algae (Fig. 10 E). The top of the Upper Jurassic is developed as a breccia to a calcareous sandstone with lithoclasts of limestone (Fig. 10 F), and clasts of quartz, glauconite, and mica, as well as a low content of iron oxides and hydroxides. The carbonate lithoclasts are likely to be clasts of reworked Upper Jurassic limestone.

The depositional environment at A 1, near Lake Constance, shows a distal to a later more proximal reefal input with clastic intermediate layers. The lower Upper Jurassic depositional environment is dominated by planktonic organisms, which merge into a more proximal development with bigger bioclasts during the late Upper Jurassic. The Upper Jurassic at the borehole cannot be classified by the lithostratigraphy of the Swabian or Franconian facies, as marker horizons are not visible, except for one characteristic ammonite.

**Borehole B 1**

At borehole B 1, the complete Upper Jurassic was developed with bioclastic-rich limestones over a thickness of 578 m (9 drill cores). The Middle to Upper Jurassic boundary was developed with a glauconitic sandstone containing coated lithoclasts and grains (Fig. 11 A). All the Upper Jurassic limestones contain vertical stylolites (nearly parallel to bedding), which are highly abundant in one wackestone layer and show a gray to dark gray rock color. In addition, the lower early wackestone

contains abundant planktonic organisms, and the later wackestone contains an intermediate layer of bioturbation and visible dolomite crystals within the matrix.

The glauconitic sandstone is covered by a bioclastic wackestone with planktonic organisms (Fig. 11 B). The planktonic organisms are crinoids, radiolarians, calcispheres, and pyritized fossils like bivalve and echinoderm fragments. In the hanging wall, the bioclastic wackestone becomes a bioclastic rudstone with abundant tubiphytes (Fig. 11 C), transported reef-building organisms, which show a chaotic structure. In the lower part of the rudstone sequence, there are further peloids and bioclasts of brachiopods (Fig. 11 D), which are replaced by bioclasts of bivalves and serpulids as well as sponge spiculae at the top. Then, the sedimentation changes and again a bioclastic wackestone was deposited, dominated in the lower part by stylolites. There is further bioturbation within the wackestone, and bioclasts with sizes around 1 mm are present (Fig. 11 E).

Above the bioturbated layers, there are bioclasts of crinoids (*Saccocoma* sp.), serpulids, foraminifera, and sponge spiculae (Fig. 11 F). Around 50 m above the bioturbated layers, dolomite crystals occur within the wackestone as matrix dolomite. Toward the top, the bioclastic wackestone becomes a bioclastic floatstone with echinoderms, foraminifera, algae, serpulids and sponges. The bioclastic floatstone encompasses the crustacean coprolite *Favreina salevensis* (Meyer, 1994; Brönnimann, 1976). The Upper Jurassic deposition ends with a bioclastic-rich breccia, overlain by a Lower Cretaceous calcareous sandstone.

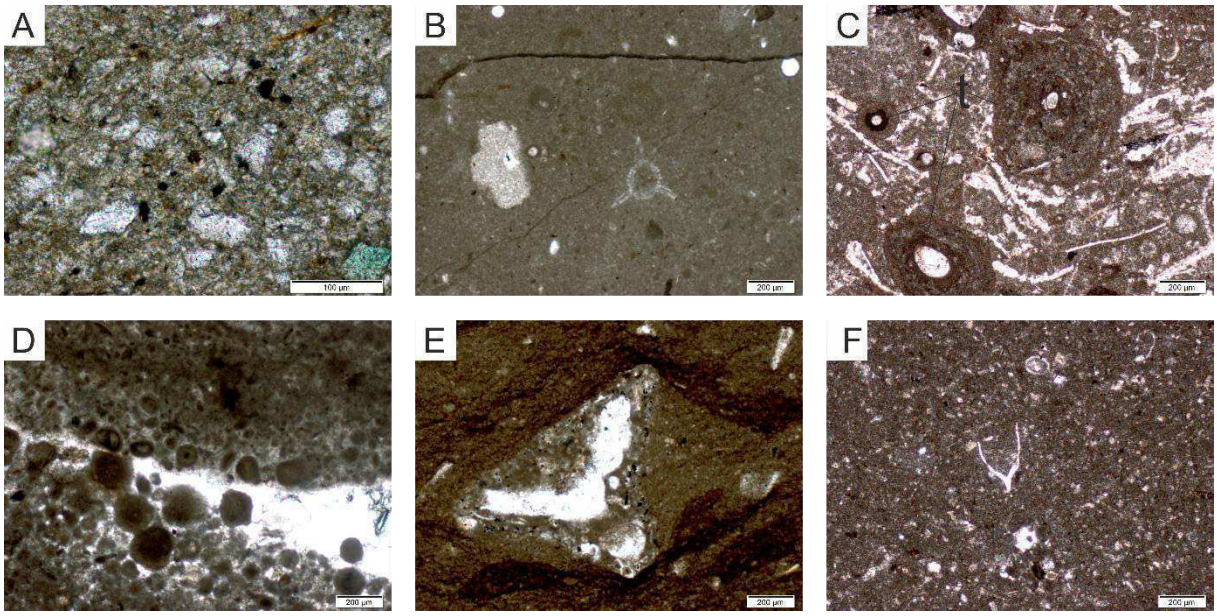


Fig. 11: Thin section photos of drill cores at B 1 (A to F decreasing depth) in transmitted light. A: glauconitic sandstone; B: wackestone with planktonic organisms; C: packstone with bioclasts (tubiphytes (t)); D: peloidal to ooidal packstone merging to a grainstone; E: wackestone with bigger allochthonous bioclasts; F: bioclastic wackestone with planktonic organisms and *Saccocoma* sp.

The depositional environment at B 1 changes twice from a calmer environment of bioclastic wackestones to a proximal environment with bioclastic rudstones and floatstones containing reworked

reef-building organisms. The early lower bioclastic wackestone shows a background sedimentation of planktonic organisms, which is not described for the Franconian and Swabian facies in the Oxfordian. The Upper Jurassic at B 1 cannot be analyzed by the Franconian or Swabian facies classification, as stratigraphic layers are absent, and the reef organisms are allochthonous.

**Borehole C 1**

Borehole C 1 intersects the late Upper Jurassic, which has a thickness of around 70 m (7 drill cores) and is a gray to light gray, bioclastic-rich limestone. No bioturbation is visible in the Upper Jurassic carbonate rocks, but reworked layers and an abundance of components and organisms can be seen. One mudstone layer shows an increased occurrence of stylolites.

The earliest intersected layer is a bioclastic wackestone, overlain by an extraclast-rich intermediate sandstone layer. A mudstone with very small organisms was deposited in the hanging wall (Fig. 12 A). Toward the top of the mudstone, the number of extraclasts such as quartz and glauconite grains increases with interbedded thin layers of reworked bioclasts and components. Furthermore, the extraclast-rich wackestone contains calcite druses and shows a slight lamination. Then, there is an abrupt change in deposition, and grainstones intercalate with thin packstone and bioclastic wackestone layers (~ 1 m) (Fig. 12 B).

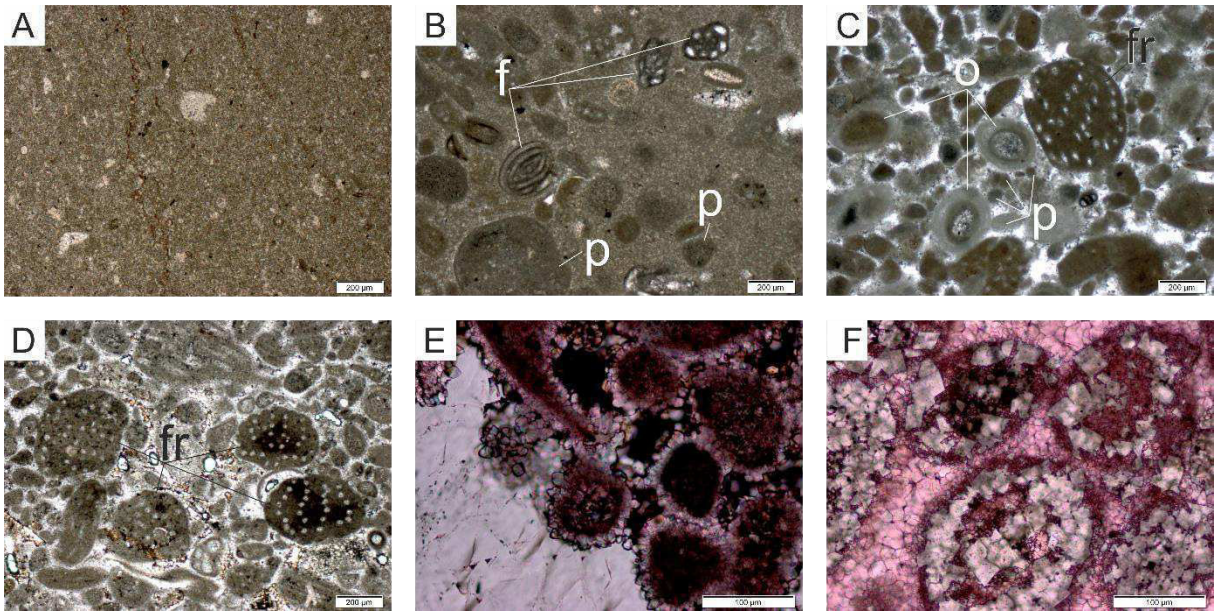


Fig. 12: Thin section photos of drill cores at C 1 (A to F decreasing depth) in transmitted light. A: bioclastic mudstone to wackestone; B: bioclastic wackestone with peloids (p) and foraminifera (f); C: grainstone with peloids (p), ooids (o) and *Favreina salevensis* (fr); D: peloidal grainstone with accumulated *Favreina salevensis* (fr); E: peloidal to ooidal grainstone with secondary pore space (calcite crystals); F: peloidal to ooidal grainstone with dolomitized ooids. E and F are dyed with alizarin S.

In the upper third of the intersected Upper Jurassic, the crustacean coprolite *Favreina salevensis* is abundant. The light gray peloidal to ooidal grainstone layers encompass bioclasts of bivalves, foraminifera, ostracods, and echinoderms (Fig. 12 C). Within the bioclastic wackestones, there is a

dominance of planktonic organisms, whereas in the peloidal to ooidal grainstones the fauna changes to proximal. The peloidal to ooidal grainstone appears with a slight gradation, where elongated clasts are oriented parallel to bedding (Fig. 12 C, D). The grainstone and the latest Upper Jurassic carbonates are further dolomitized (Fig. 12 F) and show some calcitic pore spaces (vugs) (Fig. 12 E). Finally, the latest Upper Jurassic is a bioclastic, peloidal floatstone with limestone lithoclasts and quartz crystals. The Upper Jurassic is overbedded by a Lower Cretaceous calcareous sandstone.

At C 1, the Upper Jurassic is similar to the Swabian and Franconian reef facies in the upper part, as the typical development of the Purbeck facies and *Favreina salevensis* fossils is intersected (Böhm et al., 2010). However, the depositional environment shows recurring intermediate layers and, therefore, a strongly influenced environment with different input areas.

**Mauerstetten 1 and 1a**

The borehole Mauerstetten 1 and the sidetrack Mauerstetten 1a show a very similar geology. Because of this, only the borehole Mauerstetten 1 is described and differences compared to Mauerstetten 1a are explained. The main borehole intersects the Upper Jurassic carbonates over a thickness of around 530 m (cuttings at least every 5 m measured depth) with the final depth in the late Middle Jurassic. The limestones of the Upper Jurassic are gray to dark gray and encompass bioclastic wackestones to grainstones with reef-building organisms. The main borehole intersects the fractured damage zone of a fault zone with calcite-filled fractures, whereas the sidetrack is placed within the unaffected hanging wall of the fault zone. At some fractures, bituminous crusts and dolomite crystals are visible.

At the boundary between the Middle and Upper Jurassic, there is a glauconitic sandstone with coated lithoclasts, grains, and iron ooids. The overlying early Upper Jurassic carbonates are composed of a bioclastic wackestone with radiolarians and planktonic organisms (Fig. 13 E), followed by a peloidal to ooidal grainstone, as well as silicified areas. The wackestone and grainstone contain dolomite rhombs within the matrix and dolostones as intermediate layers. The peloidal to ooidal grainstone is covered by a bioclastic wackestone, containing the crinoid *Saccocoma* sp., filaments, tubiphytes, sponge spiculae, and black crusts. Above, a peloidal, ooidal, bioclastic grainstone with a bioclastic packstone as an intermediate layer is developed. Toward the top of the peloidal to ooidal grainstone, dolomite is visible again and stylolites are abundant. The bioclastic grainstone encompasses mollusks, foraminifera, tubiphytes, algae mats, echinoderms, and bryozoa. With the beginning of the grainstone, oncoids develop until the dolomite crystals are visible. At the top, the peloidal to ooidal grainstone is again developed in parts like a packstone and merges into a bioclastic wackestone with dolomite crystals as matrix dolomite and sponge spiculae. Toward the hanging wall, there is again a development of a peloidal, ooidal, bioclastic grainstone with microbial and algae mats. The latest Upper Jurassic is represented by a breccia containing reworked lithoclasts and dolomite crystals, which is overlain by a calcareous sandstone of the Lower Cretaceous.

In the Upper Jurassic at Mauerstetten, the depositional environment developed from pelagic (planktonic organisms) to neritic with a sequence of smaller mud mounds, tubiphytes and peloidal to ooidal

grainstone layers. The late Upper Jurassic breccia shows similarities to the above-described Purbeck facies in a very shallow depositional environment. The sidetrack is located closer to a reef complex than the main borehole, as more reef-building organisms and bindstones are visible in the late Upper Jurassic. The classification of the Franconian or Swabian facies is applicable, as small reef-like buildups are described. Therefore, the upper part of the intersected facies at Mauerstetten might be classified as the massive facies of the Frankenalb-Fm.

**Geretsried GEN-1**

The borehole Geretsried GEN-1 intersects the Upper Jurassic carbonates over a vertical thickness of 525 m and is documented by cuttings. The Upper Jurassic limestones are composed of bioclastic wackestones intercalated with peloidal to ooidal grainstones to packstones. The carbonate rocks in the lower and upper part of the borehole are dolomitized, and bitumen and pyrite are present within former pore spaces. The boundary to the Middle Jurassic is not intersected at the borehole, which is situated in the vicinity of fault zones. Stylolites are cumulated within all wackestone layers.

The deepest layer of the borehole intersects a dolomitized mudstone to bioclastic wackestone with planktonic organisms, as well as sponge spiculae, tubiphytes, and peloids (Fig. 13 F). Toward the top, the dolomitized bioclastic wackestone becomes a dolostone, with no indications of the former texture. The dolostone is overlain by a mudstone to bioclastic wackestone, showing matrix dolomite again, as well as foraminifera and sponge spiculae. The following bioclastic packstone contains ostracods, bivalve fragments, and areas with sparite, coarse-grained calcite crystals. In the hanging wall of the bioclastic packstone, a nodular mudstone to wackestone is intersected, and the nodular structures are darker than the limestone matrix. The overlying bioclastic, ooidal grainstone contains matrix dolomite and miliolid foraminifera. Additional zoned dolostone cuttings are visible, which must originate from this area, as a dolostone is not intersected above. The grainstone is again overlain by a bioclastic wackestone to floatstone with serpulids and shows a cumulation of stylolites. Toward the top, the bioclastic wackestone becomes a peloidal packstone, which is composed of black pebbles and reworked lithoclasts. The latest Upper Jurassic is covered by a Lower Cretaceous calcareous sandstone.

The depositional environment at Geretsried shows a calm planktonic background sedimentation with reworked intermediate layers of bioclasts, which originated from reef complexes in the vicinity, possibly in the north. The depositional environment gets closer to a reef and reef debris sedimentation as the bioclasts become bigger during the Upper Jurassic. The lower part of the Upper Jurassic at Geretsried is developed similar to Mauerstetten with planktonic organisms (Fig. 13 E, F) but shows no calpionellids within the dark micritic limestone. The typical classification of the Franconian facies is not applicable due to the absence of marker horizons. Due to reworked reef organisms, such as tubiphytes and peloidal to ooidal grainstones, it is possible that the Franconian facies was developed in the vicinity of Geretsried during the Upper Jurassic.

**Unterhaching 1 and 2**

At the geothermal wells Unterhaching 1 and Unterhaching 2, the Upper Jurassic is intersected over a minimum vertical thickness of around 400 m, with cuttings as the only rock samples. The second borehole encounters a fault zone. In the following description, the first borehole is described, and differences compared to the second borehole are highlighted. The Upper Jurassic encompasses bioclastic-rich limestones with reef-building organisms. Both boreholes show coarse-grained dolostones in between packstone to grainstone layers. The boundary to the Middle Jurassic is not intersected within either borehole.

At Unterhaching, the lowest intersected Upper Jurassic carbonate is a bioclastic, peloidal, ooidal packstone to grainstone with sponges. Toward the top, the bioclastic, peloidal, ooidal packstone to grainstone becomes a dolostone with medium to coarse-grained dolomite crystals. The occurrence of dolomite is linked to the fault zone in the second borehole. Above the dolostone, a bioclastic, peloidal packstone, which merges into a bioclastic, peloidal grainstone, is intersected, encompassing foraminifera, echinoderms, bivalves, tubiphytes, and bryozoa. At the top of the bioclastic, peloidal grainstone, an intermediate layer with extraclasts is encountered. In the hanging wall of the bioclastic, peloidal grainstone, a bioclastic wackestone with packstone layers is visible and shows a mudstone layer on top. The mudstone is developed as a dolostone at the other borehole. The mudstone merges further into a bioclastic wackestone with foraminifera, and then into a peloidal packstone to grainstone toward the top. The peloidal grainstone is overlain by a dolostone in both boreholes. Above the dolostone layer, a bioclastic, peloidal grainstone with intermediate layers of a bindstone and peloidal packstone is intersected. The bioclastic, peloidal grainstone is composed of foraminifera, sponges, bioclasts, and echinoderms. The latest Upper Jurassic is built by a bioclastic wackestone, which is dolomitized in the upper part. The bioclastic wackestone contains foraminifera and calcispheres. The Upper Jurassic deposits are covered by a Lower Cretaceous calcareous sandstone.

At Unterhaching, the depositional environment is dominated by filaments and the crinoid *Saccocoma* sp. in the lower part, and it is distal to reef complexes but gets closer during the Upper Jurassic, as reef debris followed by reef-building organisms are visible. The lithostratigraphy of the type regions is not applicable to either borehole due to a lack of marker horizons.

**St. Gallen 1**

The borehole St. Gallen 1 intersects the Upper Jurassic sediments over a vertical thickness of around 340 m and intersects the Middle Jurassic deposits at the bottom. The Upper Jurassic sedimentation changes from a planktonic to a reef-dominated environment. In the lower part, dolomite and dedolomite crystals are found along stylolites. In the upper part, only dedolomite (calcite) and calcite-filled fractures have been described (GeotecConsult, 2014). The earliest part of the Upper Jurassic is composed of bioclastic silty sandstones (GeotecConsult, 2014). Toward the late Upper Jurassic, the influence of planktonic organisms decreases and the limestone becomes light gray instead of dark gray to black with abundant sponges. The Upper Jurassic contains a siliceous sponge reef facies typical of the Franconian

facies (GeotecConsult, 2014). The siliceous sponges have built small mud mounds with surrounding lagoonal layered sediments and biogenic detritus (GeotecConsult, 2014). A classification based on the index regions of the Upper Jurassic is not possible in this study due to the few samples.

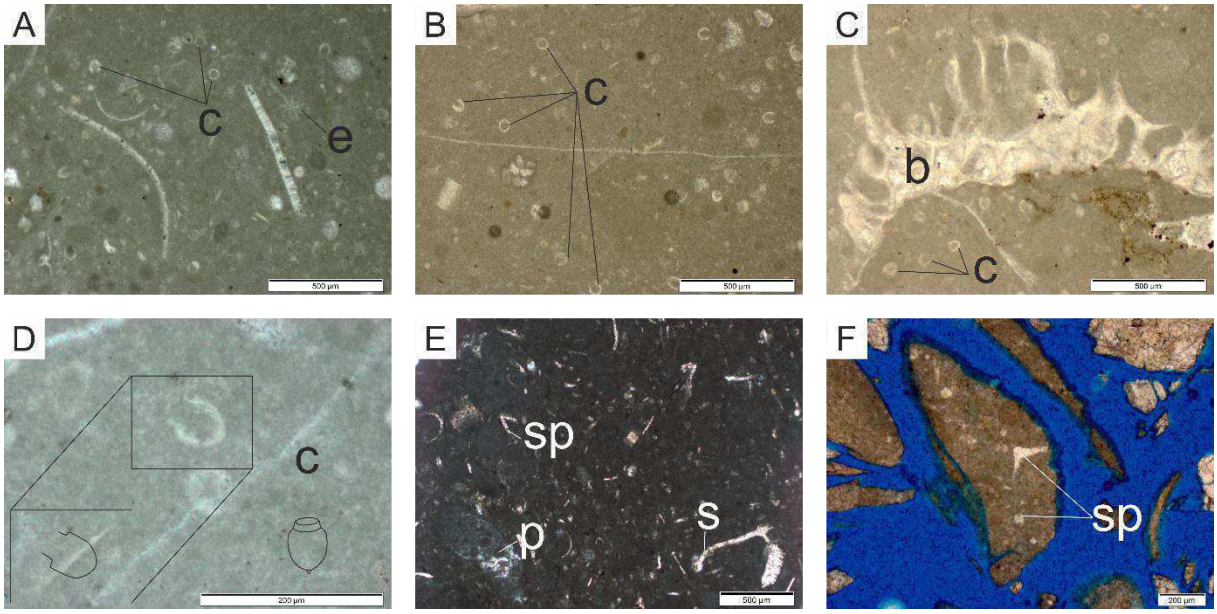


Fig. 13: Thin section photos of cuttings and hand samples in transmitted light. A: Quinten-Fm.: bioclastic wackestone (c: calpionellids, e: echinoid); B: Quinten-Fm.: bioclastic wackestone with echinoids, foraminifera, and calpionellids (=c); C: Quinten-Fm.: bioclastic wackestone with bryozoa (b) and calpionellids (c); D: Quinten-Fm.: bioclastic wackestone with calpionellid (c); E: Mauerstetten: bioclastic, peloidal (p) wackestone with sponge spiculae (sp), echinoid fragments and *Saccocoma* sp. (s) (early Upper Jurassic); F: Geretsried: bioclastic wackestone cutting of the earlier Upper Jurassic with sponge spiculae (sp).

**Kanisfluh – Helvetian facies**

The Helvetian facies was sampled within the Quinten-Fm. at the Kanisfluh anticline, near the city of Mellau in Austria. The sampled Quinten-Fm. (late Upper Jurassic) is a dark gray, dense wackestone with allochthonous bioclasts and abundant calpionellids (tintinnids) (Fig. 13 A, B, C, D). The bioclasts are bryozoa, echinoderms, sponge spiculae, shells and foraminifera, and they are not macroscopically visible in the hand specimens. In some samples, the limestone of the Quinten-Fm. shows a nodular texture due to bioturbation. The limestone shows additional calcite-filled fractures and druses filled with calcite and pyrite crystals. The fresh fracture surface shows conchoidal fractures due to brittle fracturing and smells at a fresh fracture surface like hydrogen sulfide and hydrocarbons.

The facies types from the investigated boreholes (Fig. 14) are summarized in Tab. 5. The bioclastic wackestone is the main component in all investigated boreholes with dark rocks. At Unterhaching, the proportion of bioclastic, peloidal, ooidal packstones and grainstones as well as reef debris is increased.

Tab. 5: Facies types of the analyzed boreholes St. Gallen (STG), A 1, B 1, C 1, Mauerstetten (MST), Geretsried (GEN), and Unterhaching (UHA) in the southern part of the Molasse Basin.

| **Type** | **STG [%]** | **A 1 [%]** | **B 1 [%]** | **C 1 [%]** | **MST [%]** | **GEN [%]** | **UHA [%]** |
|---|---|---|---|---|---|---|---|
| Mudstone | 5 | 15 | 0 | 47 | 0 | Min. 2 | Max. 3 |
| Wackestone | Max. 12 | 71 | 78 | Max. 10 | 40 | 44 | 10 |
| Packstone | 40 | 10 | 0 | 1 | Max. 10 | 28 | 20 |
| Grainstone | 35 | 0 | 20 | 32 | Max. 40 | 13 | Max. 22 |
| Dolomite | 5-10 | 4 | 2 | Max. 10 | 10 | 13 | 45 |
| | | | | | | | |
| Black rock color | 80 | 100 | 100 | 80 | 60 | 80 | 0 |

### 5.1.5.2 Matrix porosity versus fracture porosity

A visible porosity is present in a few rock samples (Tab. 6) and can be assumed in the visible calcite-filled fractures and fissures. The presence of sparite or calcite-filled druses, as described before (Fig. 14), indicates further previously open pore spaces. All analyzed boreholes, except Unterhaching, show zones of low inflow within the reservoir. Therefore, a permeability lower than 10 L/s is assumed at those wells. Tab. 6 shows the analyzed wells in comparison to the currently used and developed geothermal wells Pullach (Böhm et al., 2010), Kirchstockach (Wolfgramm et al., 2011), and Taufkirchen (Fisch et al., 2015b), which are further north, near Munich.

## 5.1.6 Discussion

The evaluated seven boreholes in the southern Molasse Basin show the same transition from the Middle Jurassic to the Upper Jurassic, with a glauconitic iron ooid-containing sandstone layer, if it was intersected. All the evaluated boreholes are covered by a calcareous sandstone, possibly deposited during the Lower Cretaceous. Hence, the subsidence and uplift as well as the global sea water level (Hardenbol et al., 1998) affected the depositional environment of the boreholes in the same pattern, and the boreholes are parallel to each other (Fig. 14).

Tab. 6: Distribution of porosity and permeability of the analyzed wells (UHA according to Beichel et al. (2014)) in comparison to the geothermal wells Pullach (PUL) (Böhm et al., 2010), Kirchstockach (KIR) (Wolfgramm et al., 2011), and Taufkirchen (TFK) (Fisch et al., 2015a) using the Upper Jurassic reservoir in Munich. (- no data available; **source: according to unpublished drilling report).

| **Well** | **Stage / feature** | **Description** | **Visible porosity** | | **Realized flow rate [L/s]** |
|---|---|---|---|---|---|
| | | | previous porosity [%] | Porosity [%] | |
| STG | - | - | - | <3 | <<10** |
| A1 | Fault zone | Fissures, druses, sparite | <3 | <3 | <<10** |
| B1 | Oxfordian | Rudstone to grainstone | 5 | <3 | <<10** |
| C1 | Tithonian | dolomitic grainstone | 5-15 | <3 | <<10** |
| MST | Tithonian - Kimmeridgian | Fractures, grainstone | 5-15 | <3 | <<10** |
| GEN | Tithonian - Kimmeridgian | dolomitic grainstone | 5-10 | 0-5 | <<10** |
| UHA | Tithonian - Kimmeridgian | dolostone | 9-15 | 9-15 | 130 |
| TFK | Tithonian - Kimmeridgian | dolostone | 9-15 | 9-15 | 120 |
| KIR | Tithonian- Kimmeridgian | dolostone | 5-15 | 5-15 | 145 |
| PUL | Tithonian | dolostone | - | 5-10 | 45 |

**Stratigraphy**

The distribution of the index microfossils (Tab. 4, Fig. 14) shows irregularities in the appearance of the planktonic crinoid *Saccocoma* sp. The planktonic crinoid is visible in the investigated sedimentary rocks, possibly deposited during the Oxfordian, Kimmeridgian to Tithonian. To be consistent with the literature (Keupp and Matyszkiewicz, 1997), either the described Oxfordian sediments were deposited in a shorter time period or *Saccocoma* sp. was abundant earlier in the southern part of the Molasse Basin. The coprolite *Favreina salevensis* is further visible in the latest Upper Jurassic carbonates of C 1 and B 1, indicating a shallow marine influence. Summarizing, the stratigraphy based on the macrofossils or microfossils is not applicable in detail. Hence, further studies of the microfossils within the southern Molasse Basin are needed.

**Facies and depositional environment**

The results of the borehole analysis determined changes and similarities between the depositional environments. Therefore, we first interpreted the paleogeography of the Franconian platform and the Helvetian shelf according to the possible location of the platform rim and patch reefs parallel to the platform rim. The platform rim of the Franconian Platform during the Upper Jurassic was described by

Mohr and Funk (1995) to be east-west oriented and by Büchi et al. (1965) and Heim (1919) to be northeast-southwest oriented. This study confirmed a northeast to southwest orientation of the platform rim due to a decreasing thickness from west to east and an increase in thickness from northwest to southeast. The platform rim of the Franconian Platform could be oriented parallel to the former Vindelician High, which subsided during the Upper Jurassic. The Vindelician High is described as an island within the Helvetian shelf and Franconian platform during the Lower and Middle Jurassic (Ziegler, 1990; Lemcke, 1988; Aldinger, 1968; Schneider, 1962; Roll, 1952). The Vindelician High extended from the northeastern Bohemian Massif to the west of Scherstetten, to the city of Augsburg, and then further to the southwest to east of Lausanne during the Lower Jurassic (Aldinger, 1968; Schneider, 1962; Trümpy, 1952). In the Middle Jurassic, the Vindelician High became separated from the Bohemian Massif by the Regensburger seaway (Lemcke, 1988), and the coast was located east of Scherstetten and west of Memmingen (Schneider, 1962). By this separation, the Tethys could transgress on the Franconian platform. The Vindelician High separated the Alpine from the south German depositional area by a possible submarine elevation (Roll, 1952). Trümpy (1952) described the last influence of the Vindelician High in Switzerland during the Oxfordian. It was assumed by Lemcke (1988) that an influence of the Vindelician High was not present during the Upper Jurassic. This study confirmed that during the Upper Jurassic, a tectonic influence was still present, as there is synsedimentary-caused variation in sediment thickness and synsedimentary fault zones at the continental margin which were specified by Cacace et al. (2013) and Wildi et al. (1989). The rim of the Franconian platform to the Helvetian shelf can be oriented parallel to the Vindelician High structure, which diminishes at the Middle to Upper Jurassic boundary but might still be tectonically active in fault zones. This parallel orientation of the platform rim can, therefore, help reconstruct the distribution of the depositional environment.

Palinspastic reconstruction maps of the European margin and the Alpine Tethys from north to south are described in Switzerland as follows: Tabular Jura, Folded Jura, Swiss Plateau, Helvetic Shelf, and Tethys (Wildi et al., 1989). The transition of the Franconian platform (Swiss Plateau) to the Helvetian shelf is characterized by patch reefs, with stabilizing and framework-building organisms (corals, sponges) at the outer rim of the platform in Switzerland (Mohr and Funk, 1995). Hence, the location of the platform rim can be confirmed by the occurrence of patch reefs. The sequence from the Franconian platform to the Helvetian shelf thus developed as follows: reefs and bedded facies, patch reefs parallel to the rim, transition zone, and shelf (Fig. 15).

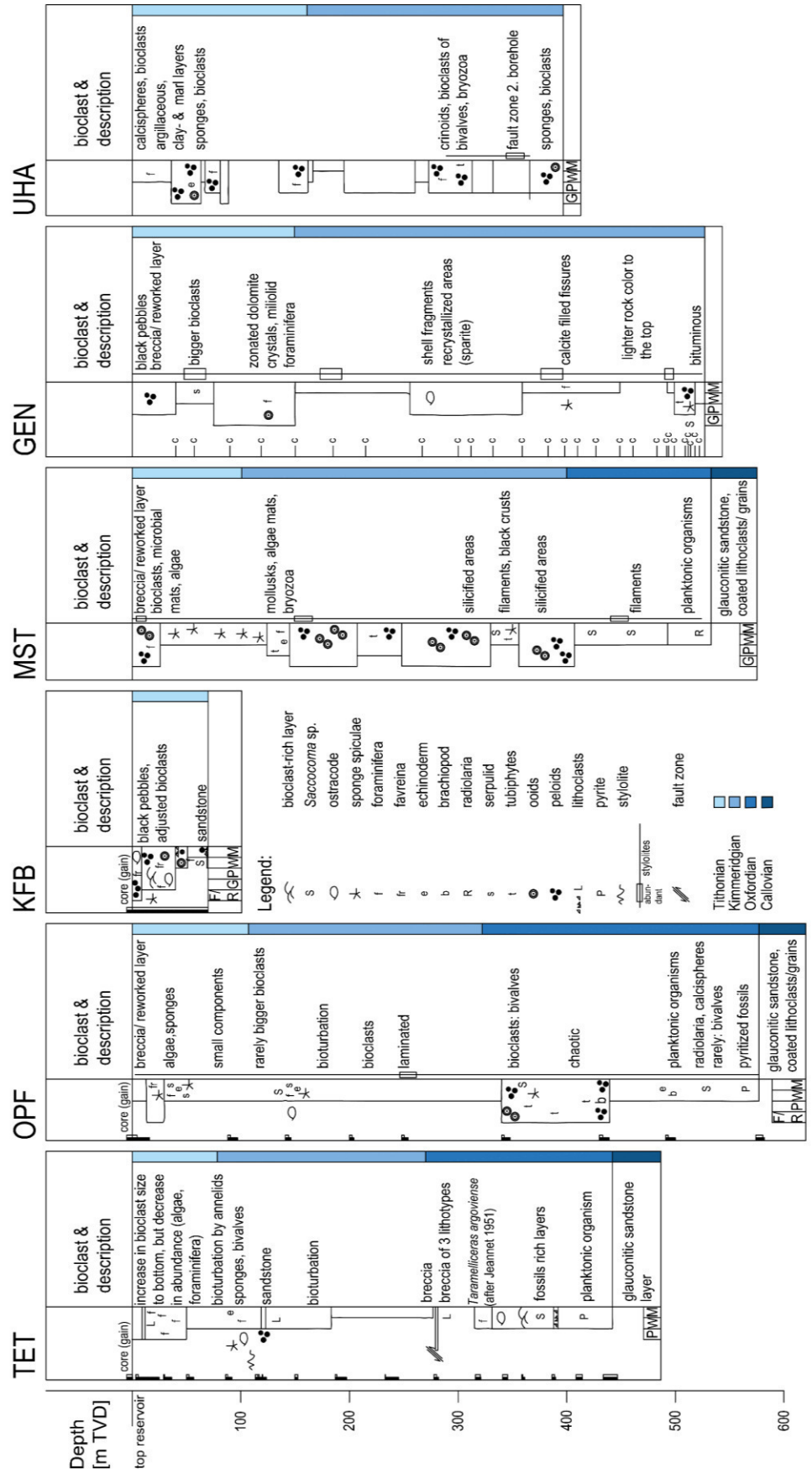


Fig. 14: Geology and microfacies of the investigated boreholes. A 1, B 1, C 1, MST, GEN, and UHA, profile line as illustrated in Fig. 9 and Fig. 16 by borehole location.

Hitherto, the occurrence of patch reefs has not been described in the literature for the south German Molasse Basin. The investigated boreholes show intermediate layers of reef and clastic detritus, possibly coming from nearby reef complexes and clastic transport currents. Reef complexes producing a bioclastic reef input on the Franconian platform can be located at the Swabian reef complex or to the south at the Zurich or Swiss 'reef complex' (Meyer and Schmidt-Kaler, 1989) (Fig. 16). The boundary of the Swiss reef complex to the Swabian reef complex is unknown in the northeast. A small seaway can be assumed, as the Argovian facies was deposited in between the two reef complexes. The term Alemannic High is used as a synonym for the Vindelician High by Trümpy (1952), but Ziegler (1990) and Aldinger (1968) differentiated between the Alemannic High in the west and the Vindelician High in the east during the early Middle Jurassic. Therefore, an exchange, visible by the Argovian facies, between the northern part (the later Franconian Platform) and the Tethys (Alpine and Helvetian facies) in the south was possible (Lemcke, 1988). Büchi et al. (1965) described an elevated area with Swabian facies, possibly the Swiss reef complex (Birmenstorf-Member), between Lake Constance and Zurich during the Oxfordian, which was also active in the Triassic and Middle Jurassic, with the Argovian facies to the southwest. Consequently, a reef complex existed on the former Alemannic High in the area around Zurich. Another consideration is a possible reef complex on the Vindelician High. There is no description in the literature of whether the Vindelician High diminished during the Middle Jurassic completely and was still not developed as a small submarine island. If so, a reef complex could have existed there as well. A further known reef input may originate from the Franconian to south Bavarian ooidal reef complex (South Franconian-Bavarian sponge platform) in the east, located in the area around Munich (Meyer and Schmidt-Kaler, 1989). The terrigenous input within the boreholes is composed of detritus such as quartz grains and small amounts of glauconite and mica. The landmasses affected by erosion are the Rhenish Massif and the Bohemian Massif north of the Franconian platform (Meyer and Schmidt-Kaler, 1989). The terrigenous input could be transported and deposited within the Swabian Marl Basin east of the Swabian reef complex (Meyer and Schmidt-Kaler, 1989) and further in the depositional area of the Argovian facies (Wildegg-Fm.), where the clastic input has been described as originating from the north-northwest (Gygi, 2013). The transport direction of detritus can be oriented parallel to the continental margin, as no areas of upwelling have been described (Mohr and Funk, 1995).

The deposition of borehole A 1 is possibly interrupted by clastic material from gravity flows or turbiditic suspension loads, because of the alternating sequences of limestone and silty sandstone. The bioclastic input within the limestone could come from platform edge reefs in the east or southwest. The quartz detritus could originate from the north or northwest, as it has been described for boreholes in Switzerland and the Argovian facies (Effingen-Member) (Gygi, 2012; Allenbach, 2001) or from the Rhenish Massif and the Swabian Marl Basin (Meyer and Schmidt-Kaler, 1989). The Effingen-Member of the Wildegg-Fm. (Argovian facies) is composed of clastic layers, which were transported by turbidites and storms (CH, 2017; Gygi, 2013). Considering the water currents flowing parallel to the southwest-northeast oriented platform rim, the clastic material of the Effingen-Member turbidites could have been transported eastward to A 1 in the form of a suspension load. Another possibility could be a channeling of turbidites to the east due to sea bottom relief. North of A 1, the typical Swabian facies was developed

(Schneider, 1962), therefore, the clastic input must have come from the northwest to west. At St. Gallen 1, southwest of A 1, no clastic input was deposited, consequently, the clastic input was not transported to the south or from the south, and reef-like growth was possible. Accordingly, the reef structure in southern Switzerland, in the area east of Zurich and at St. Gallen 1 (GeotecConsult, 2014), has no extension to the Swabian reef facies north of Lake Constance, as described above. As there are no descriptions of the Upper Jurassic south of the Alpine deformation front in the autochthonous in southern Germany, the further development of the Swiss reef facies to the south is unclear. Consequently, there is no continuous reef complex between the Swabian reef complex and the reef complex in the area around Zurich (Fig. 15). It is possible that the reef debris from the Zurich reef complex was transported to A 1 in the northeast. At B 1, no clastic input is visible and there is an increase in bioclasts, especially in tubiphytes, which indicates a vicinity to reef-building organisms, maybe from the Swabian reef complex or patch reefs parallel to the rim.

The number of transported reef organisms within the bioclastic wackestones is similar between the depositional area around Lake Constance (A 1 and B 1) and the Quinten-Fm. at the Kanisfluh. However, for the Quinten-Fm., the bioclastic input is described for the late Upper Jurassic and the Tros-Kalk-Member (Gygi, 2013). The bioclasts could have been transported by single turbidite-like flows into the Kanisfluh depositional environment (Felber and Wyssling, 1979) as described above.

Bioturbation is present in the two investigated boreholes, A 1 and B 1, indicating a calm and stagnant sedimentation. In the literature, bioturbated fucoid layers have been described for the Lacunosamergel-Fm. (Schmidt-Kaler, 1962; Quenstedt, 1858), and Mergelstetten-Fm. at the index regions. In addition, the coated grains with dark opaque minerals, possibly ore minerals, like at A 1, could indicate stagnant conditions as well. The black rock color is another piece of evidence for this, and it increases in thickness to the south. Due to the absence of upwelling areas, the inner shelf was restricted in nutrient supply and only minor circulation can be assumed with oligotrophic conditions (Mohr and Funk, 1995). This would indicate a position of the boreholes Mauerstetten, B 1 and Geretsried at the beginning of the Upper Jurassic, at the shelf to platform transition dominated by euxinic, stagnant conditions with a calm sedimentation. Because of the Upper Jurassic regression, the depositional area subsequently became dominated by platform sedimentation with reef complexes nearby and a patch reef development (Fig. 15).

Compared to the investigated boreholes, the Helvetian facies accumulated in a deep marine depositional environment, a calm water environment below the euphotic zone, with low Euxinian conditions due to a stagnant sedimentation according to Felber and Wyssling (1979). There are rare arenitic wackestones with allochthonous, shallow marine organisms (miliolids, shells) within a pelagic microfauna (tintinnids, radiolaria, filaments) (Felber and Wyssling, 1979; Lupu, 1972). The origin of the shallow marine organisms has been interpreted as single turbidite-like flows of organism-rich shallow water detritus (Felber and Wyssling, 1979). The eastern Helvetic nappes can be classified by a calpionellid biostratigraphy (Mohr, 1992). Calpionellids are only abundant in the pelagic facies zone (Mohr, 1992) and are characteristic of the hemipelagic and pelagic sedimentation of the Tethys (Mohr and Funk, 1995)

(Tab. 4). The lack of calpionellids is indicative of the platform (Mohr and Funk, 1995). Calpionellids show a crystalline outer wall with a micritic filling and no sparite inside (Flügel, 1982). As no calpionellids have been described within the analyzed boreholes of the Molasse Basin, the Helvetian facies is not present, and the sedimentation was on the platform. However, if calpionellids had been living in the hemipelagic to pelagic, they should be found in storm deposits on the shelf and platform.

In prior research, the dark gray to black rock color was used as an indicator of the Quinten-Fm. (Helvetian facies) (Lemcke, 1988), and therefore, the Helvetian facies was considered to be distributed in the southern German Molasse Basin (Schneider, 1962). In addition, due to this consideration, the Helvetian facies was assumed to be the cause of the low permeability, when the first deep geothermal wells were drilled. The thin section analysis of this research revealed that rock color can no longer be used as a main criterion for the Helvetian facies. Hitherto, the microfacies in the autochthonous and allochthonous Helvetian facies was only described at the Jurassic-Cretaceous boundary (Mohr, 1992). Therefore, the description of the Helvetian facies at the Kanisfluh, defined in this paper, is used as the typical upper Quinten-Fm.

The dark gray to black rock color and bitumen content could be caused by a high nutrient rate and an accelerated marine organic carbon burial (Bernoulli and Jenkyns, 2009; Allenbach, 2001) in a euxinic environment. In addition, the dark rock color may be caused by a high pyrite and clay content. The pyrite is still visible within the carbonate rocks of the Upper Jurassic. For the sedimentation of the Swabian bituminous layers (Lower and Middle Jurassic), Aldinger (1968) described a halocline, which caused a low and insufficient mass exchange of the bottom water. Therefore, hydrogen sulfide was concentrated as pyrite, like in former calcitic organisms at boreholes A 1 and B 1. Hence, the dark rock color cannot be caused by the development of the Helvetian facies but maybe by the transition zone facies (Fig. 16).

The newly defined transition zone facies can be described by the occurrence of dark gray to black rock colors with transported bioclasts within a dense pelagic mudstone to wackestone. The carbonate rocks of the transition zone facies can be intersected in the southern part of the North Alpine Foreland Basin and show a low primary porosity (Tab. 6). Due to the great depths, the carbonate rocks show a high compaction and a high occurrence of stylolites. In addition, fractures and fault zones become more dominant, as there are tectonic movements, like the subsidence of the Vindelician High, which are also visible by calcite-filled fractures. In the seven analyzed boreholes, dolomite crystals are visible either as matrix dolomite or as dolostones, possibly linked to fault zones.

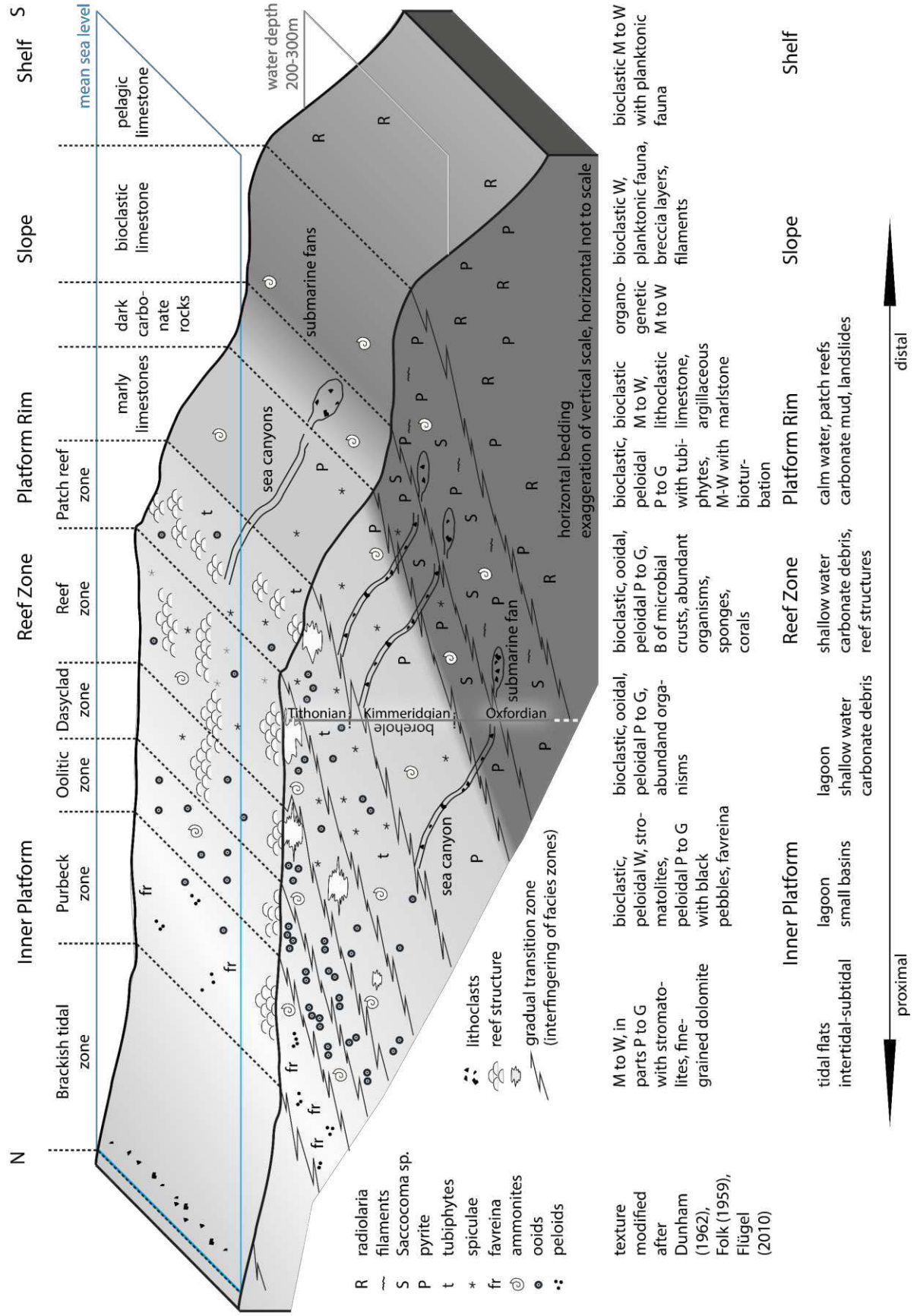


Fig. 15: Block diagram of possible marine depositional environments for the southern Molasse Basin during the late Upper Jurassic after Wolfgramm et al. (2011). The same legend is used as in Fig. 14 and Fig. 16, gray color – light gray to whitish carbonate rocks, brown color – dark gray carbonate rocks of the transition zone.

Reasons indicating a gradual transition zone of the Franconian platform to the Helvetian shelf include that the facies belts merged to the south during the Upper Jurassic (Fig. 15). Due to a regression in the lower to middle Upper Jurassic (Meyer and Schmidt-Kaler, 1989), the planktonic influence decreased and reef growth was possible. The early Upper Jurassic in Mauerstetten 1, C 1 and Geretsried 1 shows a development like the Dietfurt-Fm. and Impressamergel-Fm. but with a higher content of planktonic organisms such as foraminifers, radiolarians and crinoids like *Saccocoma* sp. and the black rock color. The planktonic character of the earliest Upper Jurassic carbonates appears in dark, micritic, organic-rich and pyrite-containing limestones, which are not described for the type regions but for other deep boreholes within the Molasse Basin (Wolfgramm et al., 2012). At Mauerstetten and C 1, and maybe at B 1, the patch reef accompanying the platform rim might be intersected within the late Upper Jurassic, as bioclastic packstones, grainstones, and bindstones (mud mounds) are visible (Fig. 15). The easternmost borehole Unterhaching is situated next to a reef complex based on reef debris and bioclasts and shows no patch reefs. Reef building and the vicinity to reef complexes are pointed out by small-scale changes in reef growth. Only reef debris was transported to Geretsried 1 and deposited in intermediate layers. In contrast, the depositional environment at Unterhaching shows no dark rock colors or planktonic organisms, therefore, it is always located on the Franconian platform. Furthermore, the lack of calpionellids indicates a depositional environment still on the platform or near the platform rim for boreholes St. Gallen 1, A 1, B 1, C 1, Mauerstetten 1, and Geretsried 1. In the lower Upper Jurassic, pelagic limestones with no pore spaces were deposited, indicative of the transition zone, which merged into reef debris-rich packstones to grainstones and bindstones, indicative of the platform rim and patch reefs. Those bioclastic-rich grainstones to bindstones show a former primary porosity, which is now filled by blocky calcite crystals. That describes a change in the typical Franconian and Swabian facies to the south, with a transition zone facies to the Helvetian shelf at the platform rim. For the detailed description of the depositional environment (passive continental margin structure), the bathymetry and relief of the sea ground are needed, and they are still the focus of research.

Consequently, the Helvetian facies is not intersected within Germany and the transition zone could be located between B 1 in the north, and the former depositional area of the Kanisfluh, the Quinten-Fm., in the south (Fig. 16). This microfacies approach showed that the previously assumed sharp transition and location of the Helvetian facies are not within the south German Molasse Basin. Therefore, the sediments of the analyzed boreholes were all deposited on the Franconian platform and upper platform transition. Consequently, the Helvetian facies is located further to the south than assumed and could not be the cause of the low permeability in the southern Molasse Basin.

Nevertheless, the limestones of the investigated boreholes do not show pore spaces but fractures and druses, which are filled with solid hydrocarbons or calcite crystals. Therefore, the hydrocarbons must have migrated through the carbonate rocks over a period to accumulate at fractures because of limited pore space. In the context of geothermal research, the formations composed of pelagic limestones do not provide a high matrix porosity or sufficient flow pathways for fluids today (Fig. 16). The thin section analysis showed that the primary porosity is linked to the facies, depositional environments, and to

dolomite crystal habitus. The calcite-filled fractures or druses and even dolomite crystals indicate flow pathways, which have been active since deposition. The former pore spaces in the grainstones and bindstones are filled by sparite.

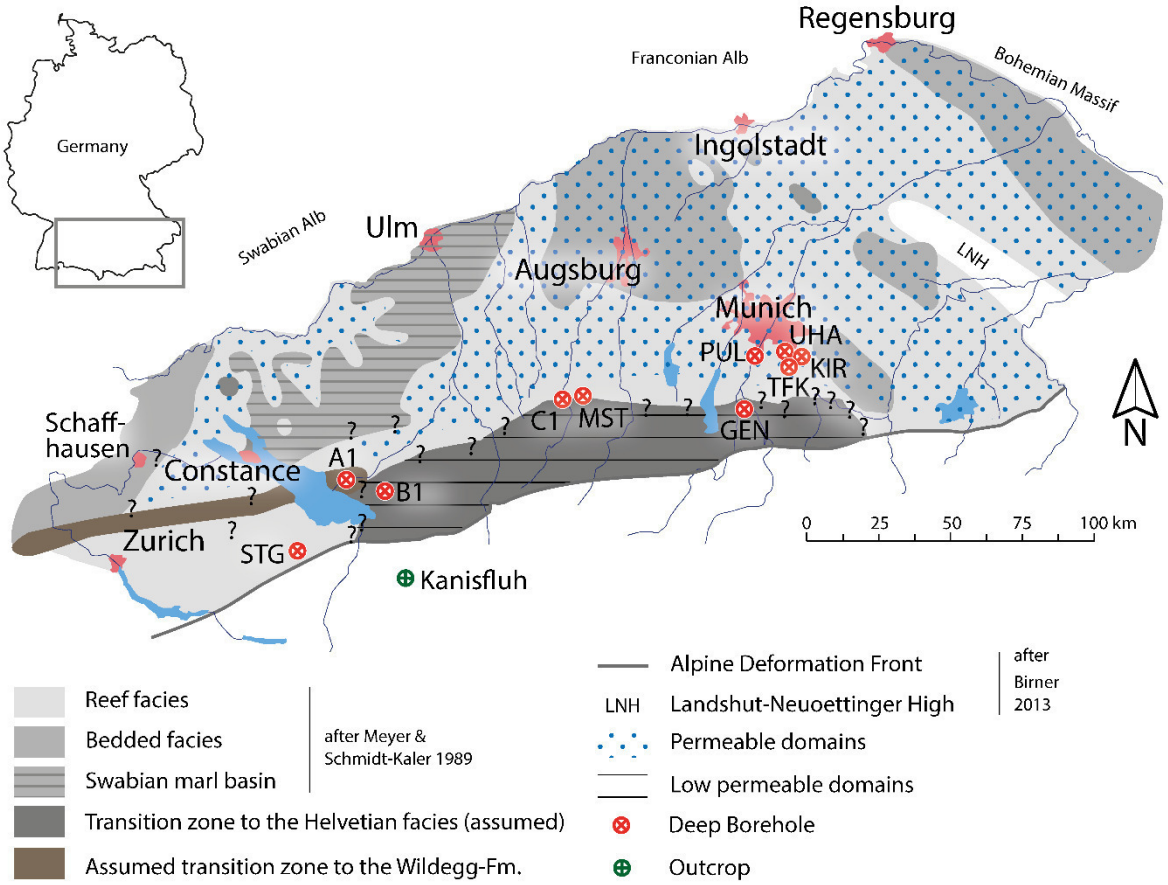


Fig. 16: Distribution of the permeability domains and the newly defined transition zone from the Franconian platform to the Helvetian shelf according to Birner (2013); Gygi (2013); Meyer and Schmidt-Kaler (1989) during the late Oxfordian (STG= St. Gallen 1, MST= Mauerstetten, GEN= Geretsried, UHA= Unterhaching; A 1, B 1, C 1 hydrocarbon boreholes).

A correlation between facies and porosity at the transition zones shows a low porosity within the black, pelagic wackestones (Fig. 16), evidenced by thin section analysis and well productivity. Suchi et al. (2013) specified high porosity values of 20 % for the southern Molasse Basin area, which contradicts our results. High-productivity wells are located further north (Fig. 16), on the Franconian platform. There, dolomite crystals grow in pure and less argillaceous limestones better and generate well-connected pore systems compared to dark, marly limestones (Machel, 2004). Therefore, the occurrence of idiomorphic, planar-e dolomites is favored. The quantitative determination of the porosity can be evaluated, in a second step, with geophysical borehole measurements, which was not the goal of this study. According to this research, fractures provide the main flow pathways at the evaluated low-permeability boreholes in the southern Upper Jurassic aquifer.

### 5.1.7 Conclusion

The results indicate a strong correlation between the facies, depositional environment, porosity and productivity of the Upper Jurassic carbonate rocks in the North Alpine Foreland Basin. The transition zone facies, analyzed in six boreholes, is characterized by black, pelagic wackestones to mudstones, with a low primary porosity and low productivity. The thin section analysis showed that the low permeability is caused by mudstone to wackestone with planktonic organisms in the southern Molasse Basin area. In addition, the typical Swabian and Franconian facies change to the south and show a higher content of planktonic organisms in the earlier carbonate rocks of the Upper Jurassic. However, the Helvetian facies does not occur in the southern part of the North Alpine Foreland Basin and must be located further south, as calpionellids are absent. A gradual transition zone of the Franconian platform to the Helvetian shelf can be assumed, which might be influenced by syn-tectonics and eustatic sea level changes. In addition, the diverse sedimentation environment shows changes in thickness possibly due to synsedimentary tectonics. In the area around Lake Constance, the depositional environment changes within a small area between Schaffhausen (Argovian facies), St. Gallen (Swiss reef complex), A 1 (possibly Argovian facies) and B 1 (transition zone). In the east, however, like at Mauerstetten, C 1 and Geretsried, the depositional environments are related to each other, with pelagic mudstones to bioclastic wackestones at the beginning followed by patch reefs with packstones, grainstones, and bindstones. However, the transition of the Franconian platform to the Helvetian shelf does continue within the North Alpine Foreland Basin.

The lithostratigraphy is not applicable to boreholes in the Molasse Basin, especially because only cuttings are available as rock samples. A new approach in this study was the use of microfacies to describe and interpret the depositional environment. For future research, we suggest using an extended biostratigraphy, where the zones are not only based on ammonites but also on microfossils, which are abundant in the limestones. Another approach are facies profiles, as introduced by Wolfgramm et al. (2012) and Koch and Clauser (2011), with additional geophysical measurements like a gamma ray or sonic type curve (resistivity log).

This research raised new scientific issues about the location and structure of the transition zone from the Franconian platform to the Helvetian shelf, which is located at the continental passive margin of the Tethys. However, a platform rim is indicated around boreholes B 1, C 1, Mauerstetten, and Geretsried, with an orientation from southwest to northeast. This rim is the northern extent of the transition zone, from the Franconian platform to the Helvetian shelf. At Mauerstetten and C 1, patch reefs were developed, whereas at B 1 and Geretsried, reef debris of those patch reefs was deposited in the late Upper Jurassic. In the lower Upper Jurassic, all investigated boreholes, besides Unterhaching, show planktonic organisms, indicative of the transition zone facies. The cause of the dark gray to black rock colors and the paleogeographic position of this anaerobic environment with a high organic content at the transition zone are still unclear. In the area where carbonate rocks were deposited as grainstone and bindstone, an initially high primary porosity can be assumed. Consequently, the diagenesis of the Upper Jurassic carbonates may have affected rock porosity to a higher degree. In addition, the facies and the

subsidence history of the Upper Jurassic carbonate rocks show a low primary porosity for the transition zone facies. Summarizing, the structure and paleogeography of the continental passive margin during the Upper Jurassic and the influence of diagenesis are important for understanding the permeability distribution in the North Alpine Foreland Basin. The results from microfacies analysis are relevant for locating successful reservoir production, indicating low-permeability domains in carbonate reservoir rock and should be considered for future geothermal exploration of the Upper Jurassic reservoir.

## 5.2 A Reconstruction of the Paleo-Fluid Evolution in the North Alpine Foreland Basin

### 5.2.1 Introduction

Processes which influence the porosity and permeability of a potential reservoir can be characterized when we know the diagenetic history. During the 1960-80s, the North Alpine Foreland Basin was explored for oil and gas, which were found primarily in Cenozoic sandstones, and to a minor degree in Upper Jurassic carbonate rocks (Landesamt für Bergbau, 2018; Véron, 2005; Wehner and Kuckelkorn, 1995; Bachmann et al., 1987; Büchi et al., 1965). Previous studies focused on the maturation of organic matter in the Cenozoic sedimentary rocks and to a minor degree on the burial history and paleo-geothermal gradient of the Mesozoic strata (Hiltmann et al., 1999; Schegg, 1992; Teichmüller and Teichmüller, 1986; Vollmayr, 1983; Jacob and Kuckelkorn, 1977). Our knowledge of the burial history, paleo-geothermal regime and the processes which control the Upper Jurassic reservoir is therefore quite incomplete. However, for the North Alpine Foreland Basin, the so-called Molasse Basin, the following basin developments have been described in previous studies:

- The Upper Jurassic reservoir serves as a source rock and/or as a reservoir rock (Wehner and Kuckelkorn, 1995; Meyer and Schmidt-Kaler, 1993; Jacob and Kuckelkorn, 1977). The main part of the hydrocarbons from the Paleogene originated from the Fish shale, lower Oligocene (Gross et al., 2018; Pytlak et al., 2017; Wehner and Kuckelkorn, 1995). In the Austrian part of the Molasse Basin, a probable source of the hydrocarbons has been located under the Alpine nappes, which had migrated into the Paleogene strata of the Molasse Basin (Gross et al., 2018). Up to now, the flow pathways and source area of the hydrocarbons are unclear for the Molasse Basin.
- Previous researchers described decreasing coalification gradients in Cenozoic sediments southward, which is caused by a decrease in the geothermal gradient, possibly due to an increased crustal thickness toward the Alpine body (Bachmann and Müller, 1996; Teichmüller and Teichmüller, 1986).
- A relatively low geothermal gradient is described in the eastern Molasse Basin of Germany, due to a lower maturity of the oil (Wehner and Kuckelkorn, 1995) and low Upper Jurassic reservoir temperatures (Agemar et al., 2012). In addition, indications of paleo-geothermal anomalies were reported from the Western Molasse Basin in Switzerland, probably linked to a paleo-hydrological regime (Schegg, 1992; Vollmayr, 1983). According to Wehner and Kuckelkorn (1995) this low-temperature anomaly is caused by an intensive karstification since the deposition of the Purbeck sediments, which has cooled down the.
- Vitrinite reflectance was used to determine the thermal maturity of sediments of the Cenozoic sedimentary rocks in the Molasse Basin and to reconstruct the thermal history during the Cenozoic (Zerlauth et al., 2016; Hiltmann et al., 1999; Schegg, 1992). However, vitrinite reflectance was not calibrated with fluid inclusion microthermometry in the Molasse Basin

(Mullis et al., 2017). In various hydrocarbon exploration areas, fluid inclusions were used to understand hydrocarbon migration and to reconstruct the thermal and burial history (Feely et al., 2016; Beaudoin et al., 2014; Parnell, 2010; Goldstein, 2001; McLimans, 1987; Burruss et al., 1985).

- According to Liedmann (1992), a paleo-temperature of around 100°C for late diagenetic cements and low saline fluid compositions (< 33 g/L NaCl) have been measured in shallow wells, with a maximum depth of 930 m.

The geothermal use of the Upper Jurassic reservoir in the Molasse Basin and the stored water has been of special interest since 2000 (Birner, 2013; Prestel, 1990). Previous researchers described the origin of the present reservoir water to be Pleistocene meteoric waters (Birner, 2013; Weise et al., 1991; Prestel, 1988; Stichler et al., 1987), which have migrated into the deep Upper Jurassic aquifer. Thereby, the former saline sea water became diluted and less saline. Studies about the dilution and fluid development, however, were conducted by Reinhold (1996); Liedmann (1992); Prestel et al. (1991) for the shallow Upper Jurassic and for outcrops of the Swabian and Franconian Alb in the north. In general, the diagenetic development of temperatures and pressures and e.g. dolomitization have been successfully described for the shallow Upper Jurassic strata with maximum depths of 1200 m (Reinhold, 1996; Liedmann, 1992; Prestel, 1990), but they have not been determined for the deeper aquifer (>1.000 m), which is used for geothermal energy production today.

The main aim of this paper is to reconstruct the paleo-fluid and paleo-temperature evolution of the Upper Jurassic reservoir. As physical and chemical conditions of diagenetic processes are preserved in fluid inclusions and cement phases, the focus of this study is on the fluid evolution stored in different cement phases of the carbonate rocks. The fluid inclusions and cement phases from geothermal wells and hydrocarbon boreholes of the Upper Jurassic reservoir were measured to increase the study area and knowledge to greater depths (up to 4,500 m). The fluid composition and paleo-temperatures were analyzed using microthermometry and calculated from stable isotope data, which were then employed to reconstruct the Upper Jurassic reservoir evolution. In addition, the lithology of the carbonate rocks was characterized (Mraz et al., 2018b). As only drill cuttings were produced from most geothermal wells, the rock samples of those wells were only subdivided into limestone, dolostone, dolomitic limestone, and vein calcites. Diagenesis, as well as dolomitization, are still the focus of research, and could not be investigated in detail in this study. In the present study, we were further able to understand the occurrence of temperature anomalies by looking at the evolution of the fluids, compositions, and temperatures.

### 5.2.2 Study area and samples points

Rock samples, drill cores and cuttings were available from 13 wells (252 samples) in the southern Molasse Basin (Tab. 7, Fig. 17). The wells are St. Gallen (STG), hydrocarbon well A1, hydrocarbon well C1, Bad Woerishofen (BWO), Schongau (SCH), Geretsried (GEN-1 and GEN-1ST-A1), Unterhaching (UHA1 and UHA2), Taufkirchen (TFK), Sauerlach (SAU), Kirchstockach (KIR),

Traunreut (TRN), Freiham (FRH), and Moosburg (MOS). The sediment thickness of the Upper Jurassic carbonate rocks varies around 400-600 m in the study area. Most carbonate rock samples (limestones and dolostones) of this study belong to the middle to upper Kimmeridgian (previously Malm delta-epsilon). The Kimmeridgian rocks represent the part of the Upper Jurassic aquifer, which is mainly dolomitized and highly permeable. The wells often consisted of transparent euhedral calcite crystals of veins associated with sucrosic dolomite crystals (planar-e dolostone; upper part of the Upper Jurassic). In some wells, almost white vein calcites were observed (lower part of the Upper Jurassic) together with gray to dark micritic limestones or strongly toothed massive dolostones (planar-a dolostone).

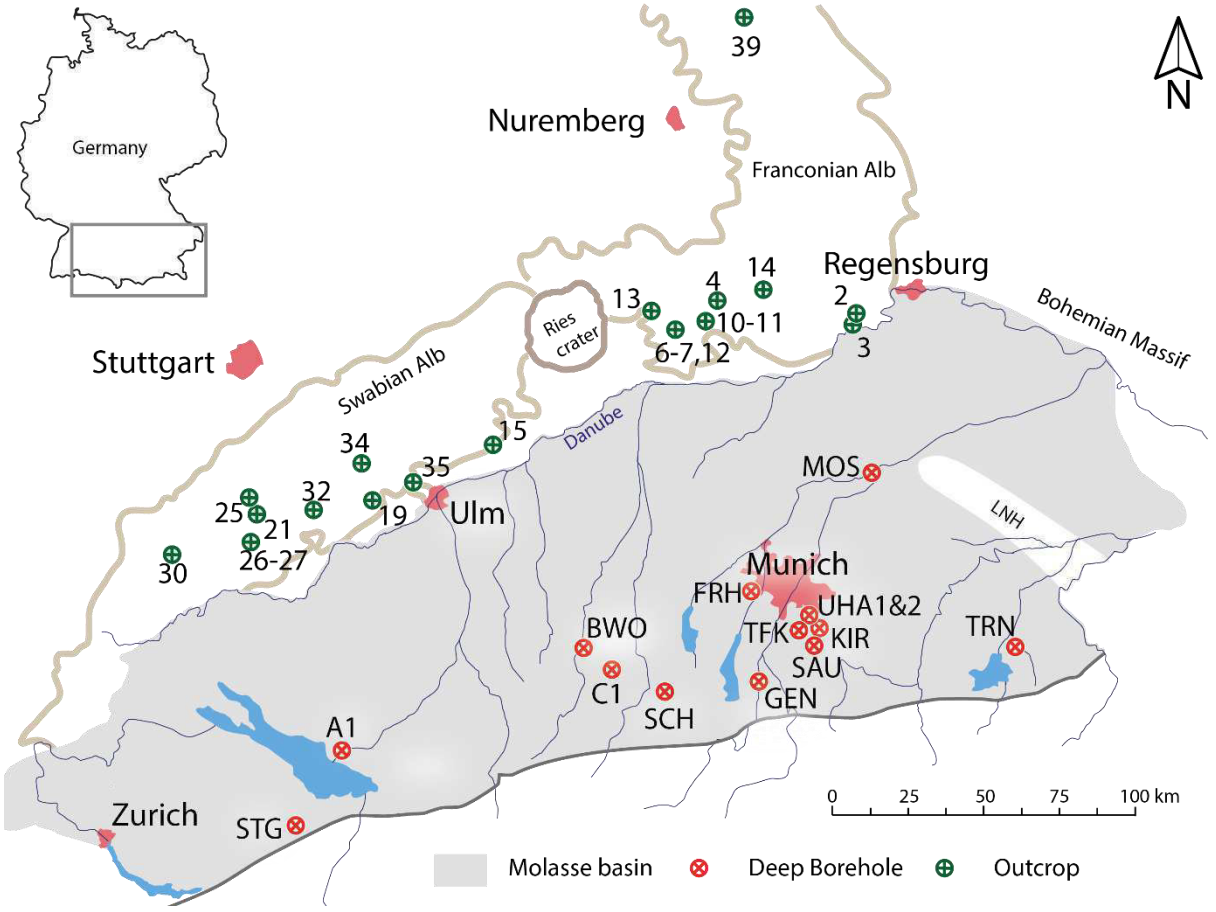


Fig. 17: Overview of the study area in the Molasse Basin, southern Germany and eastern Switzerland. FRH-Freiham, GEN-Geretsried, KIR-Kirchstockach, MOS-Moosburg, SAU-Sauerlach, TFK-Taufkirchen. TRN-Traunreut, UHA-Unterhaching, SCH-Schongau, STG-St. Gallen, BWO-Bad Woerishofen, outcrops according to Tab. 7.

Furthermore, rock samples from 21 outcrops (74 samples) originating from the Franconian Alb and Swabian Alb (Fig. 17) were analyzed. The outcrop samples are carbonate rocks, generally of the Kimmeridgian, and can show dedolomitization and karst phenomena due to the comparable longer surface influences. Drill cutting samples ranging from three main types of limestone, four main types of dolostone, and three types of vein calcite crystals as well as to dedolomite were used for the isotope measurements in this study (Tab. 7). The reddish to brown, but usually white calcite and dedolomite samples were limited to surface outcrops (karst zones). For the microthermometry measurements, we

mainly analyzed fluid inclusions in vein calcite and in planar-e dolostone, which were linked to fracture zones. There was further a hydrocarbon migration, visible by bitumen impregnation, in the Upper Jurassic rocks, which was described and analyzed but not used in this study. The focus of this study was on the deep, down-lifted carbonate Upper Jurassic reservoir (> 1,000 m) in the Molasse Basin. The Upper Jurassic reservoir was sampled over a wide depth range (0-4722 m TVD) to determine possible changes in the fluid composition and temperature with increasing depth.

### 5.2.3 Geology

The evolution of the Upper Jurassic reservoir in the Molasse Basin started with the deposition of carbonate rocks, limestones and dolostones on a carbonate platform in an epicontinental sea (Niebuhr and Pürner, 2014; Meyer and Schmidt-Kaler, 1989). The lithology, stratigraphy, and microfacies of the Upper Jurassic carbonate rocks of the Molasse Basin are further described in detail in Mraz et al. (2018b); Wolfgramm et al. (2017); Beichel et al. (2014); Lüschen et al. (2014); Wolfgramm et al. (2012); Wolfgramm et al. (2011); Reinhold (1996); Liedmann (1992); Geyer and Gwinner (1991); Meyer and Schmidt-Kaler (1989) and others. A strongly simplified evolution from deposition to the recent structure of Upper Jurassic carbonate rocks is given in Fig. 18. The evolution of the Upper Jurassic carbonate rocks started with the deposition of relatively pure limestones of the massive facies and with thin alternating layers of limestone, marlstone, argillaceous marlstone and claystone of the bedded facies. The massive facies was formed during early diagenesis as a light gray to beige carbonate rocks (grainstone to bindstone), and the bedded facies as a gray to brown mostly micritic carbonate rocks (mudstone-wackestone). Small dolomite crystals were formed in the vicinity of small fractures and stylolites in an early diagenetic stage. Overall, dolomite crystals were formed in three phases during the burial of the sediments according to Reinhold (1996). Faults and fractures were filled with calcite crystals during a late phase of burial, as the white and transparent calcite crystals have usually precipitated on the massive dolostones and limestones. Generally, two types of calcite crystals can be distinguished: firstly, transparent calcite crystals formed from ascending meteoric fluids, present in the upper part of the Upper Jurassic, and secondly white calcite crystals in darker limestones and dolostones, which are dominant in the lower part of the Upper Jurassic. In addition, a third type of calcite crystals with white and transparent crystals and red and yellow rims were identified together with dedolomite crystals. The appearance of the third type is limited to the surface outcrops of the Swabian and Franconian Alb.

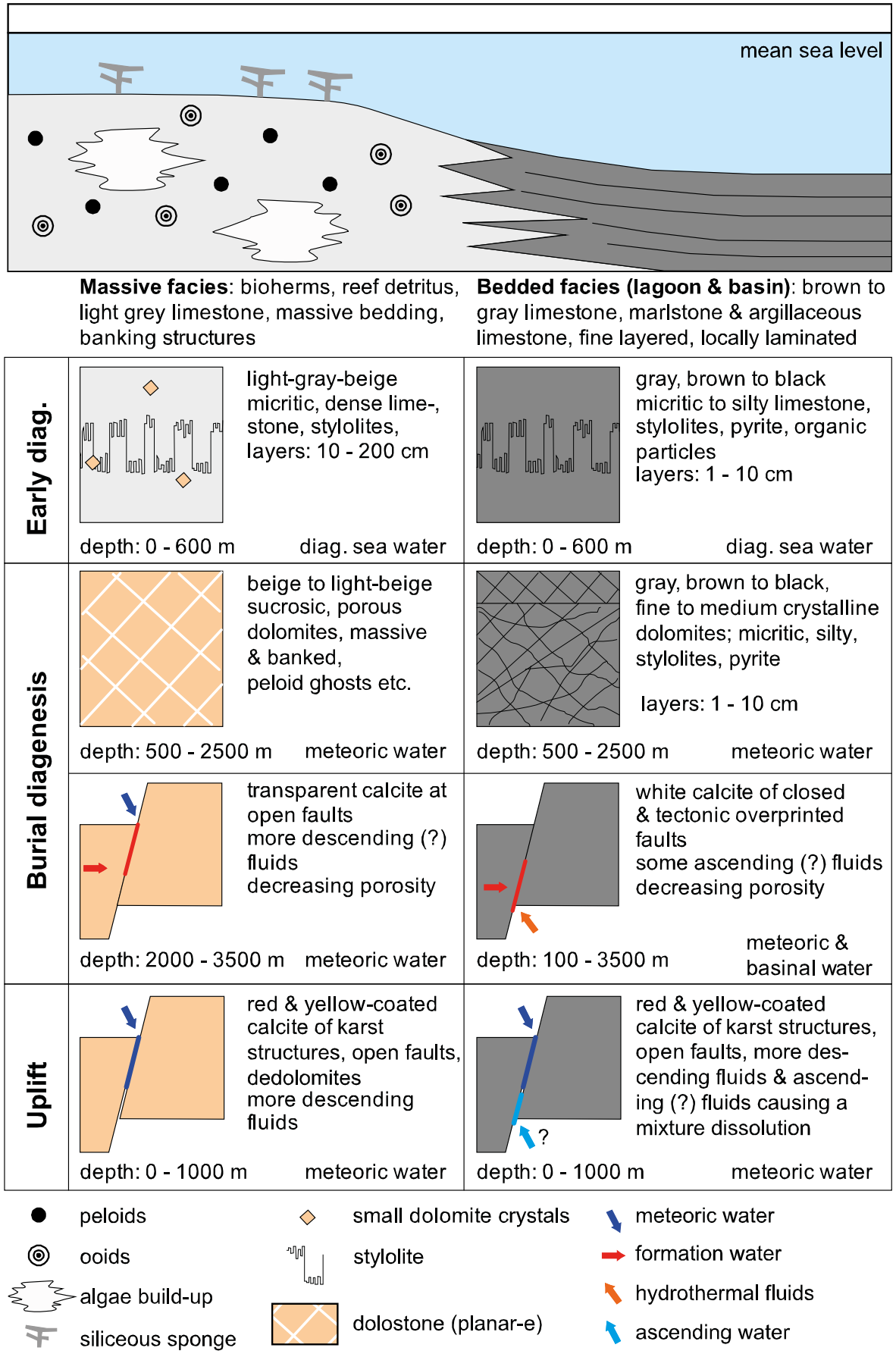


Fig. 18: Schematic burial history of Upper Jurassic carbonates of the Molasse Basin (Reinhold, 1996; Liedmann, 1992).

During the Late Jurassic, the passive Tethys margin was occupied by an extensive carbonate-dominated platform that extended northward, the so-called Franconian platform (Ziegler, 1990). In the late Kimmeridgian to Tithonian, sea level gradually dropped and a sea level low stand was reached at the Jurassic-Cretaceous transition (Ziegler, 1990). The Tethys transgressed and regressed from the south on the platform during the Cretaceous, causing erosional phases of the Upper Jurassic rocks. In the Paleogene, the Central European Alps developed as the Adriatic and European plates collided (Lemcke, 1988), which caused a southward subduction of the Penninic Ocean. This convergence resulted in a northward thrusting of the European passive margin and a downward flexing of the European plate. This entailed the formation of the North Alpine Foreland Basin (Molasse Basin) (Bachmann and Müller, 1996). The subsequent deposition of two regressive cycles of marine and fresh water sediments occurred during the Paleogene (Kuhlemann and Kempf, 2002; Lemcke, 1988). Afterward, Quaternary sediments were deposited on top. The Molasse Basin can be subdivided into a western and an eastern part with the transition zone west of Munich according to the investigated well data.

### 5.2.4 Methodology

Rock samples including hand specimens, drill cores, and drill cuttings from boreholes and outcrops were used in this study to determine the lithology and diagenesis. The thin and thick sections were made from drill core and hand specimens. The drill cutting material was made into thin sections with blue dyed resin. The stable isotopes $\delta^{18}O$ and $\delta^{13}C$ were measured from drill cuttings. For the microthermometry measurements, a new sample approach with cuttings of around 1 mm was developed by using the unprepared and unpolished drill cuttings. In addition, conventional thick sections were measured with microthermometry. At the Geretsried well, drill cuttings and conventional double-side polished thick sections of bore cores were measured using microthermometry to compare the results and confirm the drill cutting measurements. To measure drill cuttings using microthermometry, the drill cuttings are usually embedded in an epoxy resin, polished on both sides, and used as thick sections with the drill cuttings still embedded in the resin. However, the epoxy resin is not stable in the temperature range between -110°C and 200°C, which was necessary for this study. Silicone or Teflon are stable polymers for this temperature range, but they are soft at room temperature, and the cuttings lose their bond to the polymers during polishing and fall off the resin. As a consequence, the cuttings in this study were cleaned with water and measured in the form in which they were produced. In addition, the Upper Jurassic carbonate rocks were classified by microfacies and lithology, which was published in detail by Mraz et al. (2018b). The microthermometry samples of this study mainly consisted of relatively late diagenetic blocky calcite, which precipitated along fractures or veins (Wolfgramm et al., 2016; Reinhold, 1996). Vein calcite crystals, limestones, dolostones, dolomite crystals, dedolomite (calcite) and scales, which are calcite crystals from the geothermal power plants Unterhaching and Kirchstockach, were investigated.

For the stable isotope measurements, the Upper Jurassic carbonate samples were finely ground and examined in line with Hoefs (1997) in the mass spectrometer of the University of Kiel. Approximately 10 mg of a sample was dissolved in pure phosphoric acid. The calcite samples were completely

dissolved after 4 min, the dolomite samples after 18 min. Subsequently, the resulting $CO_2$ was measured at temperatures between 850 - 1000°C under vacuum. The $^{12}C/^{13}C$ ratios were specified in δ notation with reference to the international standard PDB, the measurement error of the double determination was ± 0.5 ‰. The oxygen isotopes were given in accordance with the SMOW (water) or PDB (minerals) standard.

The microthermometry study of fluid inclusions was performed on double-polished thick sections from drill cores as well as on drill cuttings of vein calcites and dolomite crystals. The drill cuttings generally showed a smooth surface at former cleavage planes or at fresh fracture surfaces. However, not every cutting sample showed good visibility and a flat surface, and therefore they could not be measured in this fluid inclusion study. In the heating-freezing stage, the cuttings were always placed with the flat and largest surface on the silver block, and they were measured at very slow heating and cooling rates to prevent a high temperature gradient in the sample to determine the exact temperature. Furthermore, the drill cuttings were directly measured at least 2-3 times to exclude a high temperature gradient in the sample. The microthermometry measurements were performed on a heating-cooling stage, a Linkam stage apparatus mounted on an Olympus microscope with a precision of 0.1 K. For the aqueous one-phase and two-phase fluid inclusions (liquid and vapor), the shape, size, texture, genesis, phase type, host mineral, and phase volume ratio were documented in line with Van den Kerkhof and Hein (2001). When a nucleation of a bubble was not possible in one-phase fluid inclusions at around 4°C, the sample was then further cooled to -110°C to check for possible phase transitions. In contrast, two-phase fluid inclusions were first heated in increasing order to homogenization in the liquid phase and afterward cooled to -110°C to minimize the possibility of inclusion deformation. The homogenization temperature ($T_h$) was measured in small inclusions by temperature cycling. Afterward, the eutectic temperature ($T_e$) and last melting and/or ice melting ($T_m$) temperature were measured. If possible, fluid inclusions in an assemblage (FIA) were investigated. In the present study, data from fluid inclusion assemblages (FIA) were used preferentially before single fluid inclusion measurements. However, when a constant liquid-vapor ratio in comparison to the FIA was given, some single $T_h$ measurements of one- and two-phase fluid inclusions were used in this study. Leakage of a fluid inclusion was sometimes not observable, but it was determined by an increase in $T_m$ and gas bubble size during the measurement. Sometimes, a positive $T_m$ and a change in $T_m$ was observed in small fluid inclusions, which can be caused by metastability or by clathrate melting. The measured positive $T_m$ led us to assume that gases and clathrates are present. To identify the aqueous fluid system and mineral phases, micro-Raman spectroscopy was performed, using a Horiba Jobin Yvon XploRA PLUS confocal Raman microscope. The spectrometer was equipped with a frequency-doubled Nd:YAG laser (532 nm, with a maximum power of 22.5 mW) and an Olympus 100× long working distance objective with a numerical aperture of 0.9. The operation conditions had a confocal hole of 300, a spectral slit of 100, and a grating of 1800 T. However, the high fluorescence of the calcite host mineral in the range of 2500-4000 $cm^{-1}$ led to an insufficient spectrum. Consequently, the aqueous 2-phase fluid inclusions could not be specifically identified using the micro-Raman spectroscopy.

With the $T_m$, the bulk salinity was interpreted using the computer program SoWat (Sodium chloride Water), which is a model of almost equation of state for fluid inclusions in the $H_2O$-NaCl system (Driesner, 2007; Driesner and Heinrich, 2007; Goldstein and Reynolds, 1994). The measured $T_h$ using microthermometry should represent the minimal formation or trapping temperatures of the fluid inclusions (Roedder, 1984). For the fluid and temperature evolution, the formation (entrapment) temperature was calculated with a pressure correction using the assumed depth during crystal growth. For the maximum formation temperature, todays sample depth was used as the input parameter for the pressure correction, because it was assumed that the maximum depth has been reached today.

For the burial history and plot, compaction was not calculated due to a lack of data, and periods of subaerial exposure were used according to literature studies. The stratigraphy is based on two borehole profiles of this study, one in the southeastern and the other in the southwestern Molasse Basin. The eroded strata in the Upper Miocene (Upper Freshwater Molasse) were around 200 m thick (Gusterhuber et al., 2012; Kuhlemann and Kempf, 2002), the Upper Oligocene to Lower Miocene strata around 250 m thick (Kuhlemann and Kempf, 2002; Lemcke, 1988), and the Cretaceous and Upper Jurassic strata were assumed to be around 600 m thick (Mazurek et al., 2006). Up to now, no burial history with fluid and temperature data has been described for the German Molasse Basin. From the burial data of ten investigated deep boreholes, it was assumed that the maximum burial depth has been reached today.

Tab. 7: Overview of the sampled wells and outcrops for the reconstruction of paleo-fluid composition and temperature in the Molasse Basin (Fig. 17). The thick sections were made from drill cores. n: number of measurements. Tithonian – ti, Kimmeridgian – kim. The well abbreviations are the same as in Fig.1.

| Well | Depth [m TVD] | Strati-graphy | Fluid inclusions | | | Stable isotopes | | |
|---|---|---|---|---|---|---|---|---|
| | | | n | Thick section | Cutting sample | n | Thick section | Cutting sample |
| STG | 4350-4440 | ti-kim | 25 | 3 | | 15 | x | x |
| A1 | 2646-2740 | ti-kim | 23 | 2 | | | | |
| MOS | 1288- 1449 | ti-kim | 43 | 2 | | 7 | x | |
| C1 | 3303 | ti-kim | 15 | 1 | | | | |
| SCH | 4375-4378 | ti-kim | 105 | 4 | | | | |
| FRH | 2130-2410 | ti-kim | 18 | | 5 | | | |
| GEN | 4360-4850 | ti-kim | 113 | 2 | 7 | 20 | x | x |
| UHA | 3060-3555 | ti-kim | 40 | | 2 | 59 | | x |
| TRN | 4220-4860 | ti-kim | 19 | | 10 | 11 | | x |
| BWO | 2370-2565 | ti-kim | 10 | | 5 | | | |
| KIR | 3425-4090 | ti-kim | | | | 46 | | x |
| SAU | 4060-5475 | ti-kim | | | | 41 | | x |
| TFK | 3480-3933 | ti-kim | | | | 10 | | x |
| **Outcrop** | | | | | | | | |
| 2 | | ti | | | | 2 | x | |
| 3 | | kim | | | | 1 | x | |
| 4 | | kim | | | | 2 | x | |
| 6 | | kim | 1 | 2 | | 2 | x | |
| 7 | | kim | | | | 2 | x | |
| 10 | | kim | 4 | 4 | | 14 | x | |
| 11 | | ti | 8 | 1 | | 1 | x | |
| 12 | | kim | 4 | 1 | | | x | |
| 13 | | kim | 4 | 1 | | 2 | x | |
| 14 | | kim | 1 | 1 | | | x | |
| 15 | | ti | | | | 2 | x | |
| 19 | | ti | | | | 4 | x | |
| 21 | | kim | 2 | 1 | | | | |
| 25 | | kim | 1 | 1 | | | | |
| 26 | | kim | | | | 2 | x | |
| 27 | | kim | 1 | 1 | | | | |
| 30 | | kim | | | | 2 | x | |
| 32 | | kim | 1 | 2 | | 2 | x | |
| 34 | | kim | 1 | 1 | | 2 | x | |
| 35 | | kim | | | | 2 | x | |
| 39 | | kim | 4 | 1 | | 15 | x | |
| **Sum** | | | **443** | **31** | **29** | **266** | min. 21 | min. 7 |

## 5.2.5 Results

### 5.2.5.1 Types of fluid inclusions

All measured calcite crystals, limestone cements and vein calcite cements were completely transparent or had cloudy areas due to numerous very small inclusions (< 3.0 µm) (Fig. 19), which we were unable to measure. The dolomite crystals were idiomorphic, transparent to light beige, and we were only able to measure them at the Traunreut well. No fluid inclusion measurements could be performed in the matrix of the limestones and dolostones. The crystal size of the calcite and dolomite crystals was around 0.5 mm to 1.0 mm. Overall, the size of the fluid inclusions was very small in the range from 1.2 µm up to 72.0 µm, with the mean value of 8.2 µm measured at 363 inclusions. The measured fluid inclusions were primary, secondary or pseudo-secondary and hosted in vein calcite cements and in planar-e dolostones (vein dolomite). Usually, primary fluid inclusions had a rectangular shape, whereas secondary or pseudo-secondary inclusions were often rounded to drop-shaped (Fig 3). The primary fluid inclusions were between 1.3-72.0 µm (mean value 9.4 µm, n=240) and were always bigger than the secondary or pseudo-secondary fluid inclusions (1.2-39.7 µm, mean value 8.3 µm, n=109). Furthermore, all measured inclusions contained aqueous one-phase and 2-phase fluid inclusions. The one-phase inclusions were hosted in limestone cements and in a few vein calcite cements, and were measured with microthermometry to describe possible a phase transition. However, most one-phase fluid inclusions showed no phase change during ice melting. All measured fluid inclusion assemblages (FIA) were homogenous, with constant liquid-vapor ratios of around 15 %, and showed consistent $T_h$ and had slightly varied sizes. Because of the constant fluid-vapor ratio and similar fluid system, the fluid inclusion measurements could be compared between the investigated wells.

The thick sections and cutting samples of the Geretsried well showed similar and consistent fluid inclusion data, especially the measured $T_h$ in FIA (cuttings: 145°C; thick sections: 143°C), which was not expected as temperature increases at the drill bit during the drilling process.

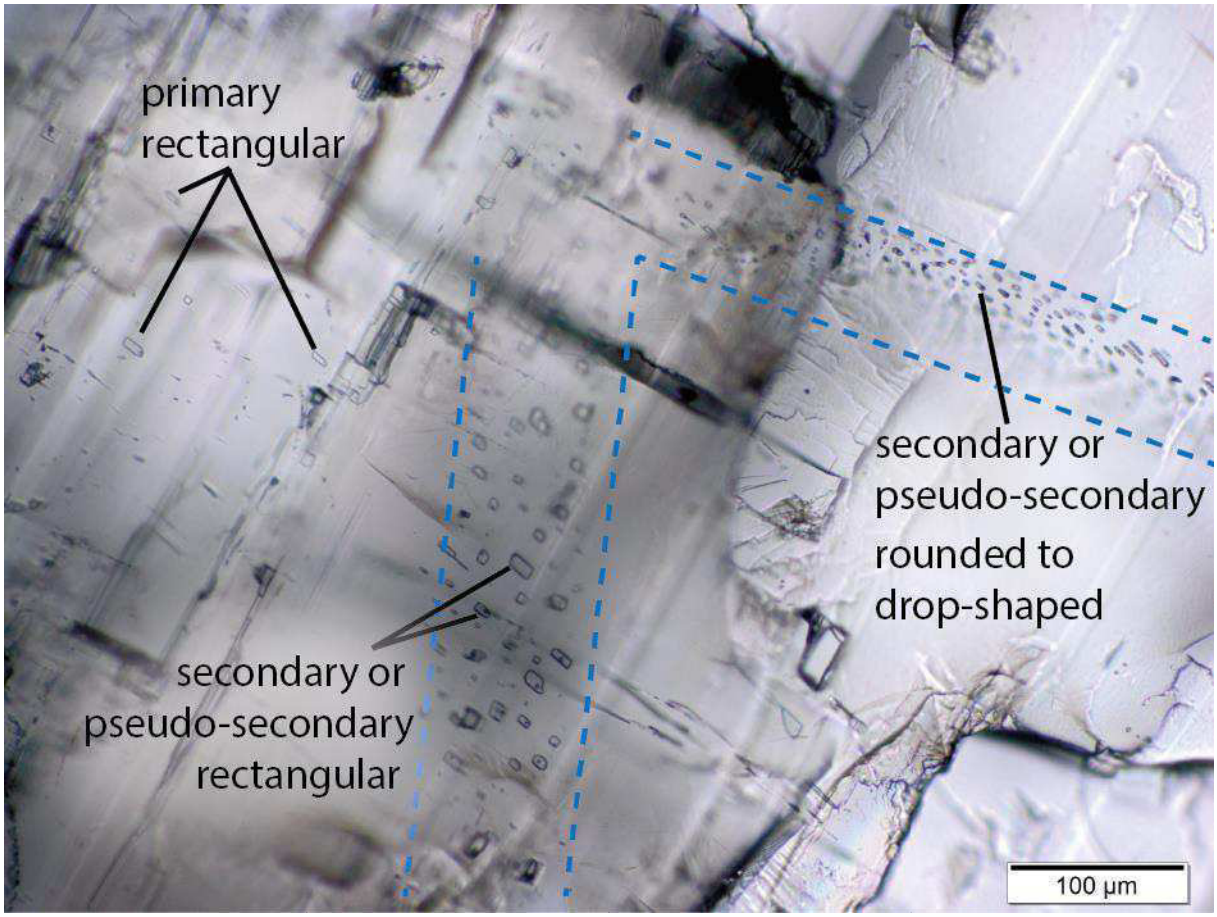


Fig. 19: Fluid inclusion morphology in vein calcite crystals in one focal layer.

Some fluid inclusions had a $T_e$ of -21.6°C (n=30); therefore, a NaCl-system was assumed for all evaluated samples (Goldstein, 2001).

### 5.2.5.2 Fluid inclusion temperature

The $T_h$ for all primary fluid inclusions ranged between 59°C and 190°C, with the mean value of 136°C (n=196) and for secondary or pseudo-secondary fluid inclusions between 100°C and 167°C, with the mean value of 139°C (n=94) (Fig. 20). The $T_h$ of the secondary or pseudo-secondary fluid inclusions were nearly consistent with the primary fluid inclusions. The formation and maximum formation temperatures are given in Tab. 11. The formation temperatures were around 10 K above the $T_h$.

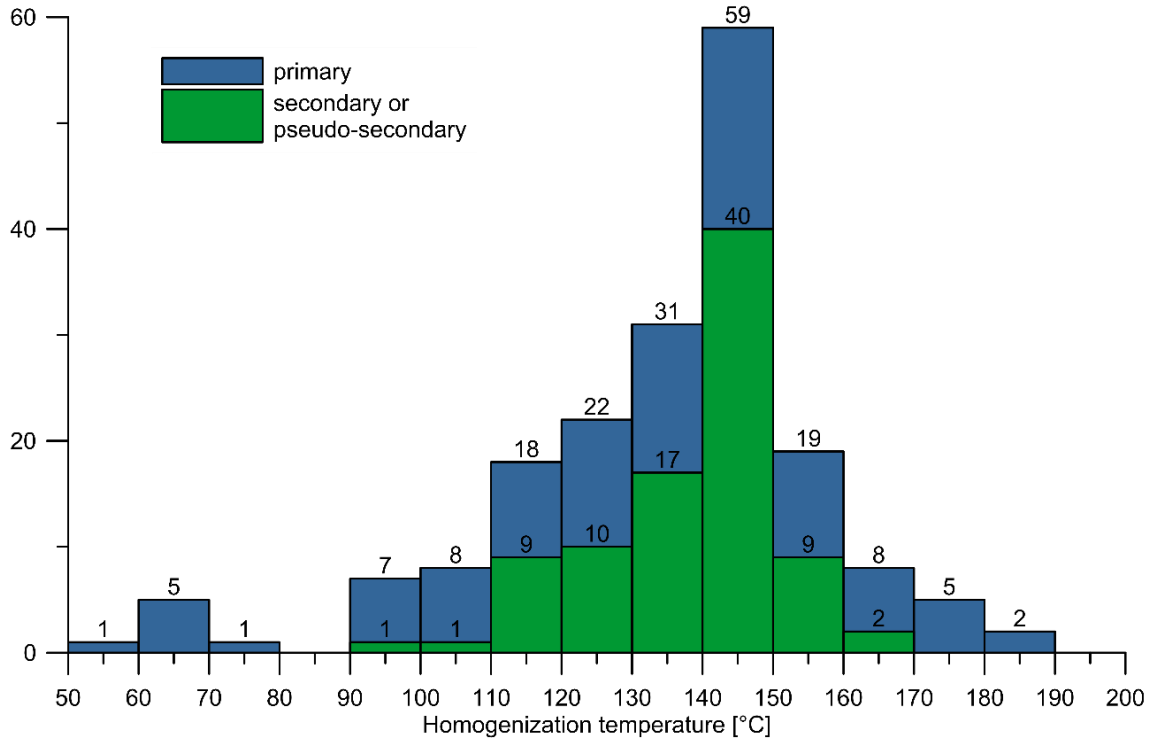


Fig. 20: Histogram of the distribution of homogenization temperature ($T_h$) measured in primary, secondary or pseudo-secondary fluid inclusions in calcite cements linked to fractures and dolostone crystals.

The fluid inclusion $T_h$ was plotted versus sample depth of the wells in Fig. 21. With increasing depth, the $T_h$ increases, but with a different gradient at the different wells. In comparison to the outcrop samples, the well samples showed an increase in $T_h$, but consistent $T_m$. At the Traunreut well, the recent reservoir temperatures and $T_h$ increased with a slightly lower gradient (25 K/km) in comparison to the recent reservoir gradient of around 30 K/km in the Upper Jurassic aquifer in the Munich area (Agemar et al., 2012). At the Moosburg and Freiham wells, a $T_h$ higher than the geothermal gradient of 30 K/km was measured (Fig. 21).

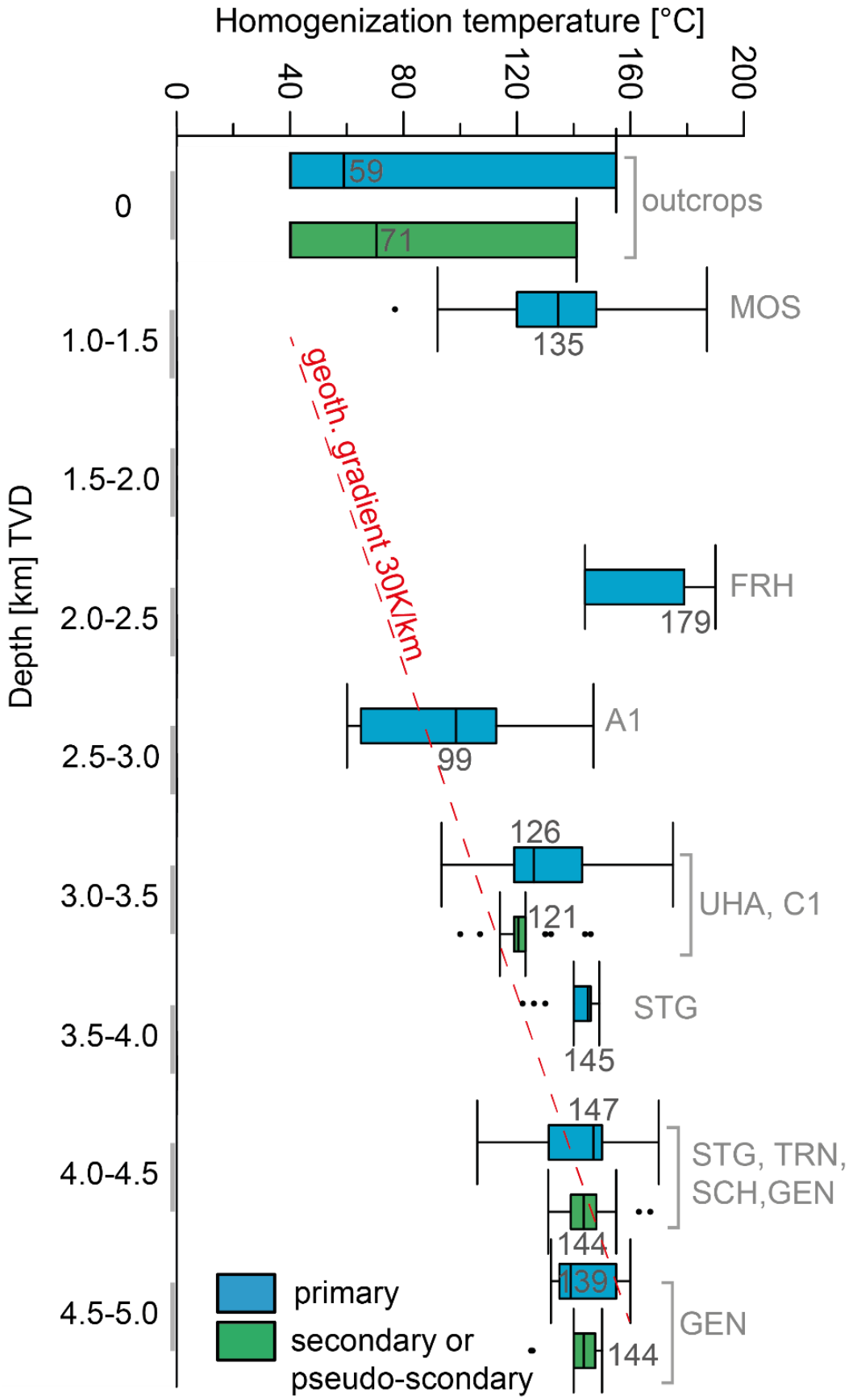


Fig. 21: Boxplot of homogenization temperature versus true vertical depth of the calcite and dolomite 2-phase fluid inclusions from the wells in the Molasse Basin. In addition, the geothermal gradient of 30 K/km is shown. In gray, the sampled wells are named using the same abbreviation as Fig. 17.

$T_m$ ranged from -31.4 to 0.0 C, with the mean value around -1.0°C (Fig. 22). The primary fluid inclusions had a $T_m$ between -31.4°C and 0.0°C with a mean value of -2.3°C (n=143). In contrast, the temperature of secondary or pseudo-secondary fluid inclusions ranged between -4.2°C and -0.2°C, with a mean value at -1.1°C (n=49). There was a temperature increase in the $T_m$ from the primary fluid inclusions to the secondary or pseudo-secondary inclusions from -2.3°C to -1.1°C, indicating decreasing salinity. In a few samples, $T_m$ was positive with a mean value above 0°C (n=56, min. 0.1°C, max. 11.8°C). The positive $T_m$ changed with every heating measurement in the single fluid inclusion of an assemblage and did not stay constant. Those positive temperature measurements were not used for the further calculation and analysis. All vein calcite cements had a maximum $T_m$ around -1.0°C for primary fluid inclusions and around -0.7°C for secondary or pseudo-secondary fluid inclusions. Consequently, the fluid inclusion generations can be grouped according to their salinity, but not by their $T_h$. Some samples from hydrocarbon well A1 showed $T_m$ below -2.0°C to as low as -18.0°C, which results in highly saline fluids during basin evolution. The STG samples showed a slight decrease in $T_m$ with depth, from a mean value of -1.6°C at 3911 m and 4135 m to -2.0°C at 4157 m. The $T_m$ determined for dolomite crystals from the Traunreut well were around -3.0°C, slightly lower than the blocky, vein calcite (-0.7°C to -2.0°C). Two different generations of 2-phase fluid inclusions could be distinguished at the GEN well, with unequal $T_m$ and $T_h$. The primary inclusions had a mean $T_h$ of around 145°C and the mean value of the $T_m$ was -2°C for the GEN samples. Furthermore, the secondary or pseudo-secondary inclusions showed slightly lower $T_h$ of around 140 °C, as well as higher and lower $T_m$, with mean temperatures of -0.7°C and -4.0°C compared to the primary fluid inclusions. Hence, two secondary or pseudo-secondary fluid inclusion generations might exist at GEN, with the same $T_h$ but different salinities.

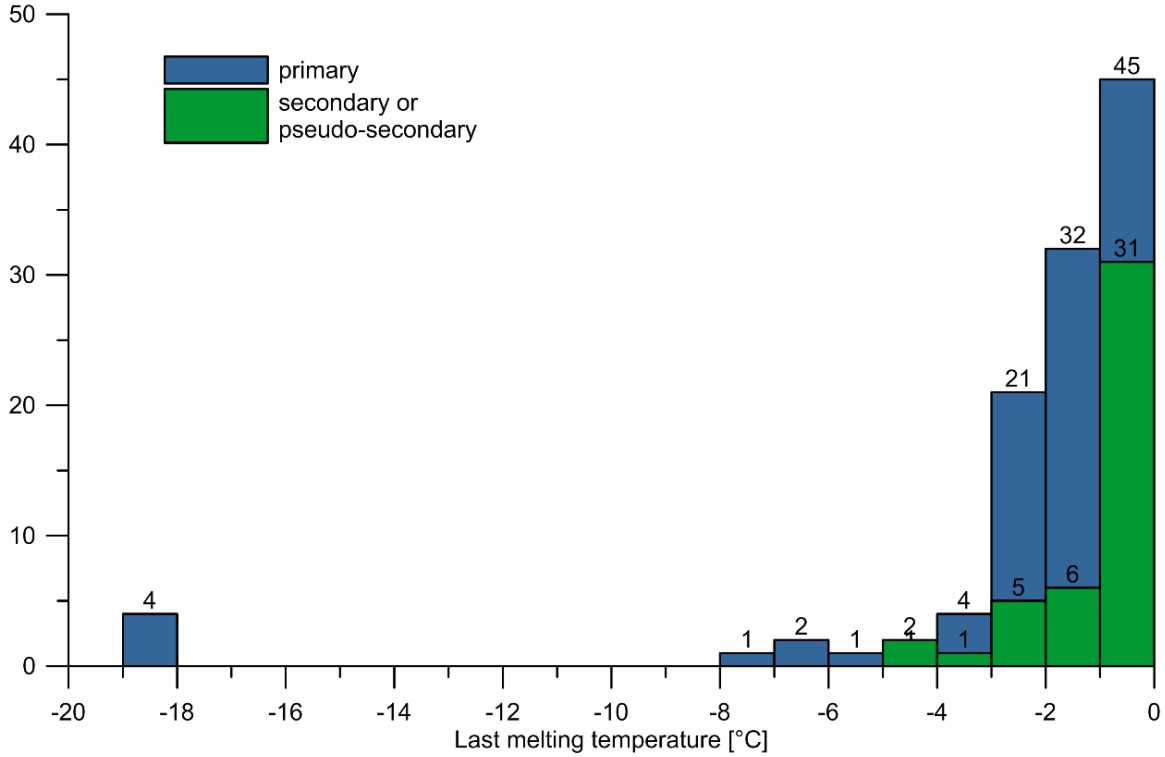


Fig. 22: Histogram of the distribution of the last melting temperature ($T_m$) measured in primary, secondary or pseudo-secondary fluid inclusions in calcite crystals linked to fractures and dolomite crystals.

### 5.2.5.3 Diagenetic fluid composition by stable isotopes

The stable isotopes ($\delta^{18}O$ and $\delta^{13}C$) of Upper Jurassic limestones, dolostones, and calcite cements were measured from the deep well (Fig. 24) and outcrop samples (Fig. 23). A summary of the data is given in Tab. 8. In Fig. 23and Fig. 24, we distinguished between rather brown and dark gray micritic limestones and beige micritic limestones. The dark brown limestones had the highest $\delta^{18}O$ value with -3.4 ‰ PDB (Fig. 24), the gray micritic limestones had an intermediate value, and the lowest $\delta^{18}O$ value of -5.4 ‰ PDB was measured in the light beige micritic limestones. This decrease in $\delta^{18}O$ was caused by a meteoric water influence in the beige micritic limestones. In general, the $\delta^{13}C$ of the limestones decreased from + 2.0 ‰ PDB to + 1.4 ‰ PDB (Fig. 24) with increasing temperature during burial and $CO_2$-degassing. The dolostones had lower $\delta^{18}O$ values than the limestones and showed the same decrease in $\delta^{18}O$ value as the limestones with a lighter rock color. $\delta^{18}O$ value decreased from the dark-brown platy dolomite crystals (-4.5 ‰ PDB), the lower part of the Upper Jurassic, toward the massive dolostone to the sucrosic light-beige dolostones (-7.5 ‰ PDB) (Fig. 24). For the dolostones, $\delta^{18}O$ increased and $\delta^{13}C$ decreased from the dark (+ 2.5 ‰ PDB) to the beige dolomite crystals (+ 2.2 ‰ PDB) and again to the dedolomite crystals (-7.0 ‰ PDB). The isotopic signatures of the outcrop dolostones, plotted in the area of low temperature dolomite or at the transition zone to high thermal dolomite, which correspond to an early stage of dolomite formation (Reinhold, 1996). Within the carbonate rock groups (limestone and dolostone), the trend with decreasing $\delta^{18}O$ values and increasing $\delta^{13}C$ values was visible during the evolution.

The vein calcite crystals of the Upper Jurassic were measured in the deep wells and were classified into the transparent calcite crystals of the upper part and the white calcite crystals of the lower part, associated with the brown and dark matrix dolomite. The white calcite crystals had very low $\delta^{13}C$ values of around -2.7 ‰ PDB and a low $\delta^{18}O$ value of -21.9 ‰ PDB in contrast to the $\delta^{13}C$ value of -2.2 ‰ PDB and the $\delta^{18}O$ value of -15.1 ‰ PDB of the transparent calcite crystals. The lower $\delta^{18}O$ values of the transparent and white vein calcite crystals showed an influence of meteoric water. The white and transparent calcite crystal types precipitated from different fluids and at different diagenetic steps. The white calcite crystals were probably formed during an earlier stage of burial, as the $\delta^{18}O$ values were only slightly higher for the limestones. In the surface outcrops and associated with karstified carbonate rocks, a third calcite crystal generation was observed, which had the lowest $\delta^{13}C$ value of -7.0 ‰ PDB of all measured vein calcite crystals.

Tab. 8: Isotope data of different rock types of the Upper Jurassic from the Molasse Basin; *data from outcrop samples, n = sample count, stratigraphy – origin of samples: ti – Tithonian, kim – Kimmeridgian, ox – Oxfordian.

| Rock type | stratigraphy | Rock color | n | Median | |
|---|---|---|---|---|---|
| | | | | $\delta^{18}O$ [‰ PDB] | $\delta^{13}C$ [‰ PDB] |
| Limestone | ti-ox | Dark-gray, brown | 16 | -3.4 | + 2.0 |
| Limestone | ti-ox | Gray | 15 | -4.3 | + 1.0 |
| Limestone | ti-kim | Beige, light-gray | 61 | -5.4 | + 1.4 |
| Dolostone | ti | Brown, fine crystalline | 10 | -4.5 | + 2.2 |
| Dolostone | kim-ox | Dark-brown, platy, toothed | 13 | -4.8 | + 2.5 |
| Dolostone | ti-ox | Beige, light-gray, massive | 30 | -6.1 | + 2.3 |
| Dolostone | ti-ox | Beige, light-gray, sugar-grained | 27 | -7.5 | + 2.2 |
| Vein-Calcite | kim-ox | White | 14 | -15.1 | -2.7 |
| Vein-Calcite | ti-kim | Transparent | 23 | **-21.9** | -2.2 |
| *De-dolomite | ti-kim | Light-beige | 2 | -5.3 | -4.9 |
| *Vein-Calcite | ti-kim | White, transparent | 16 | -5.8 | -2.1 |
| *Karst-Calcite | ti-kim | Yellow to red-coated crystals | 9 | -7.9 | **-7.0** |

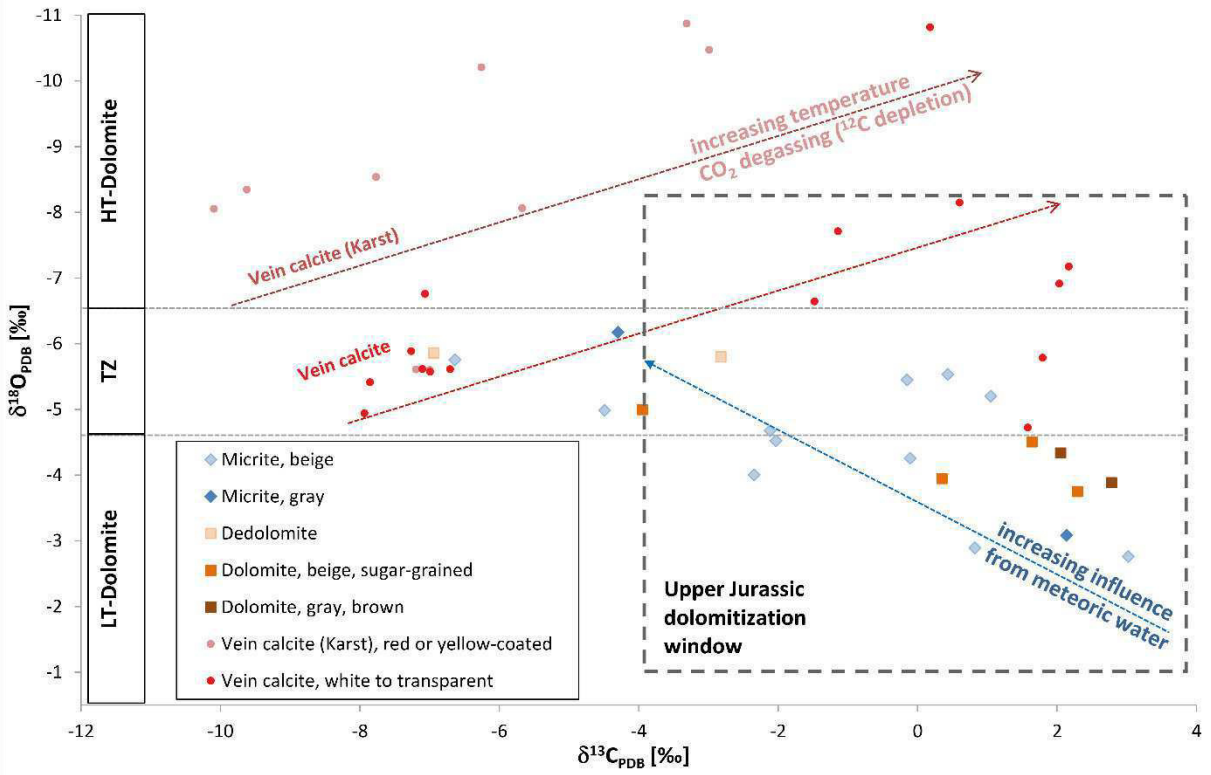


Fig. 23: Oxygen and carbon isotopes of Upper Jurassic carbonate rocks from outcrops of the Franconian and Swabian Alb; Dashed window – Upper Jurassic dolomitization window according to Reinhold (1996); LT-Low temperature dolomites, HT- high temperature dolomites and TZ- transition zone according to Allan and Wiggins (1993); the arrow lines with a trend of increasing meteoric influence according to Liedmann (1992).

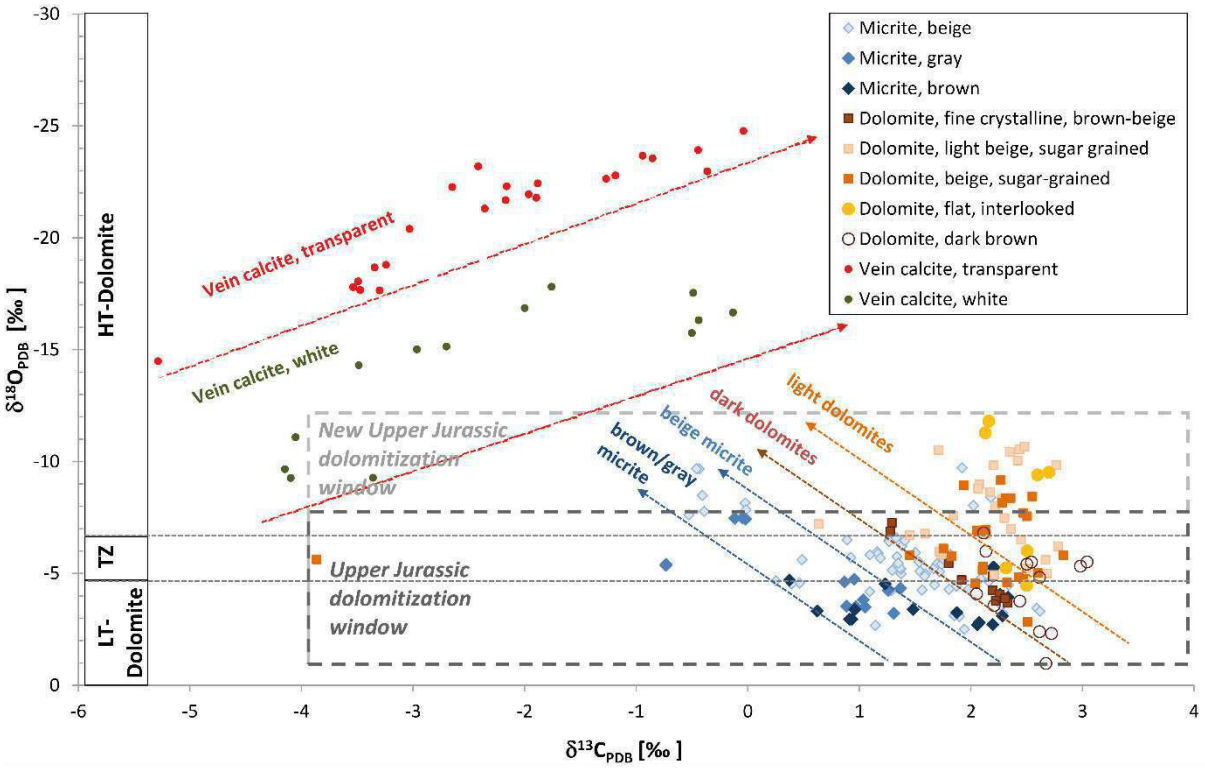


Fig. 24: Oxygen and carbon isotopes of Upper Jurassic carbonates from deep wells of the southern Molasse Basin; Dashed window – Upper Jurassic dolomitization window according to Reinhold (1996); the new interpreted Upper Jurassic dolomitization window, LT-Low temperature dolomites, HT- high temperature dolomites and TZ- transition zone according to Allan and Wiggins (1993); arrows lines with a trend of increasing meteoric influence according to Liedmann (1992).

In general, the isotope values showed the following trends: The $\delta^{18}O$ and $\delta^{13}C$ values of the vein calcite crystals were significantly lower than the matrix calcite and dolomite crystals at comparable depths; the $\delta^{18}O$ values of the vein calcite samples decreased with depth; the $\delta^{13}C$ values of vein calcite crystals increased with depth (one outlier); the $\delta^{18}O$ and $\delta^{13}C$ values of matrix calcite and dolomite crystals decrease with depth (some outliers); a third vein calcite generation with low $\delta^{18}O$ value and the lowest $\delta^{13}C$ value were measured only at the outcrops (karst, dedolomite).

### 5.2.5.4 Temperatures from stable isotopes

For the temperature evolution of the Upper Jurassic reservoir, the temperature was calculated using the isotope ratio for oxygen. In addition to the fluid inclusion and stable isotope measurements of Upper Jurassic carbonates, stable isotopes of recently formed calcite crystals, the so-called scales, as well as reservoir fluids were measured. The scale samples (scalings) were from the well head, filter, production pipe and deep pump from two geothermal power plants (Unterhaching and Kirchstockach) south of Munich. Former researchers have described the $\delta^{18}O$ values of the produced reservoir fluid in the range between -11.9 and -10.4 ‰ VSMOW (Mayrhofer et al., 2014), -12.8 and -10.6 ‰ SMOW (Stichler et al., 1987). Our fluid data in the investigated wells showed a median value of -11.0 ‰ SMOW (-12.1 to -10.6 ‰ SMOW, n=11). The $\delta^{18}O$ values of the scales varied for the first Unterhaching well from -22.3 to -26.7 ‰ PDB (median -25.9 ‰ PDB; production temperature about 122°C) and for the

second Kirchstockach well from -26.2 to -27.3 ‰ PDB (production temperature about 137°C). To determine the formation temperature of the different scale samples, various geothermometers based on the fractionation factor between $^{18}O/^{16}O$ of calcite and $^{18}O/^{16}O$ of the fluid were tested (Kim and O'Neil, 1997; Friedman and O'Neil, 1977). The geothermometer values according to Friedman and O'Neil (1977) showed the best match with our data (Fig. 25). The formation temperature of the scales was calculated to be around 119.1°C for the first Unterhaching well and around 135.8°C for the second Kirchstockach well. Lower temperatures than the reservoir temperature represented a scale formation during downtime periods of the power plant, whereas higher temperatures represented scales in close proximity to the pump (motor temperatures up to 175°C).

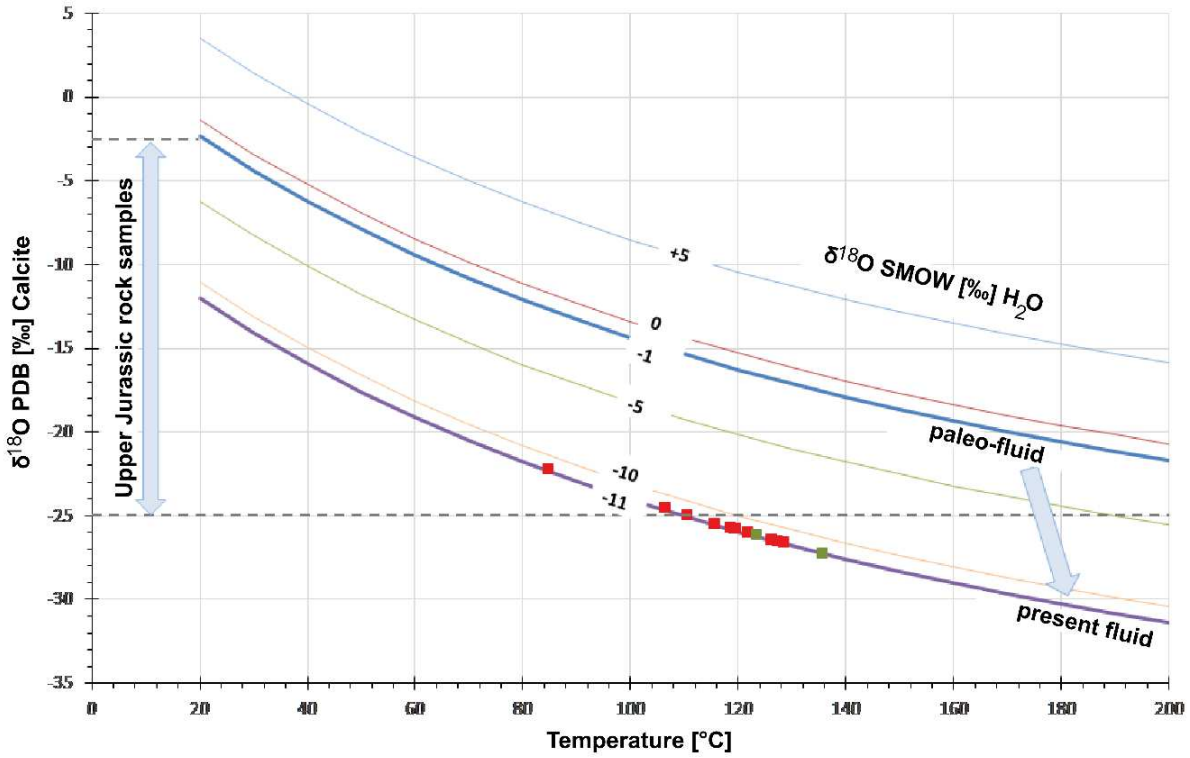


Fig. 25: Isotope composition of water versus calcite crystals according to Friedman and O'Neil (1977); red squares – scaling from the Unterhaching geothermal plant, green squares – scaling from the Kirchstockach geothermal plant.

The paleo-fluid of the Upper Jurassic ocean was around -1.0 ‰ SMOW according to Prestel (1990) and Wallmann (2001). The paleo-temperature of the Upper Jurassic ocean has been determined to be around 18.6 to 24.8°C (Liedmann, 1992; Fritz and Smith, 1970). Saline waters with current $\delta^{18}O$ values of up to + 5.5 ‰ SMOW were observed at one Upper Jurassic well (STG) in the western part of the Molasse Basin. Liedmann (1992) determined two geothermometer equations: (Geo-1) to calculate the paleo-temperature supported by fluid inclusion studies with $\delta^{18}O$ values of calcites and $\delta^{18}O$ values of dolomite crystals of the Upper Jurassic with a maximum temperature of 110°C. Additionally, the paleo-temperatures were calculated using two equations (Geo-2) concerning the fractionation factor between $^{18}O/^{16}O$ of calcite and $^{18}O/^{16}O$ of the fluid for calcite (Friedman and O'Neil, 1977) (Fig. 25) and for dolomite (Fritz and Smith, 1970), which was previously developed in this study to be the best fit with the scaling measurements. The temperature results for calcite crystals which had precipitated from

Jurassic sea water with $\delta^{18}O$ values of -1 ‰ SMOW and -11 ‰ SMOW for the recent fluids are shown in Tab. 9. At -11 ‰ SMOW, the calculated temperatures using the Geo-2 equation for minerals precipitating from paleo-fluids were too low, as this equation could only be applied to recent non-diagenetic fluids. However, at -1 ‰ SMOW (Jurassic sea water), all temperatures from the Geo-2 equation for precipitating minerals from paleo-fluids showed paleo-temperatures comparable to Liedmann (1992) (Geo-1).

Tab. 9: Paleo-temperature from isotopic geothermometers ($\delta^{18}O$ values Tab. 8); Geo-1: $^{18}O$ geothermometers according to Liedmann (1992); Geo-2: $^{18}O$ geothermometer after Friedman and O'Neil (1977) for calcite and Fritz and Smith (1970) for dolomite and for paleo-fluids with an $^{18}O$ value of -1 ‰ SMOW and -11 ‰ SMOW; **bold** – reliable data.

| Mineral | Properties | T [°C] Geo-1 | T [°C] Geo2 [-1‰] | | | T [°C] Geo2 [-11‰] | | |
|---|---|---|---|---|---|---|---|---|
| | | median | min | median | max | min | median | max |
| cc-m1 | Dark-gray, brown | **30.2** | 21.7 | 25.0 | 43.3 | 10.7 | 11.5 | 12.3 |
| cc-m2 | Gray | **35.5** | 22.9 | 30.1 | 31.6 | | 10.6 | 12.0 |
| cc-m3 | Beige, light-gray | **41.7** | 20.7 | 35.8 | 40.1 | | 10.2 | 12.6 |
| dol-1 | Brown, fine crystalline | **54.9** | 53.1 | 57.5 | 247.9 | 7.8 | 11.3 | 117.9 |
| dol-2 | Dark-brown, platy, interlocked | **57.3** | 39.2 | 59.5 | 71.9 | -4.5 | 12.8 | 21.5 |
| dol-3 | Beige, light-gray, massive | **66.0** | 48.5 | 67.1 | 111.0 | 4.0 | 18.2 | 44.7 |
| dol-4 | Beige, light-gray, sucrosic | **76.8** | 60.2 | 76.4 | 101.0 | 13.3 | 24.4 | 39.1 |
| cc-v1 | White | 114.4 | 58.9 | 108.0 | 125.1 | 14.0 | 34.8 | 50.3 |
| cc-v2 | Transparent | 183.2 | 99.6 | 199.9 | 238.9 | 30.7 | 81.6 | 108.3 |
| cc-dd | Light-beige | **41.0** | 35.2 | 35.2 | 35.3 | 10.2 | 10.2 | 10.2 |
| cc-v12 | White, transparent | **43.8** | 29.5 | 37.7 | 43.8 | | 10.2 | 17.3 |
| cc-v3 | Yellow to red coated crystals | **57.4** | 34.2 | 50.1 | 54.0 | 10.3 | 11.7 | 16.5 |

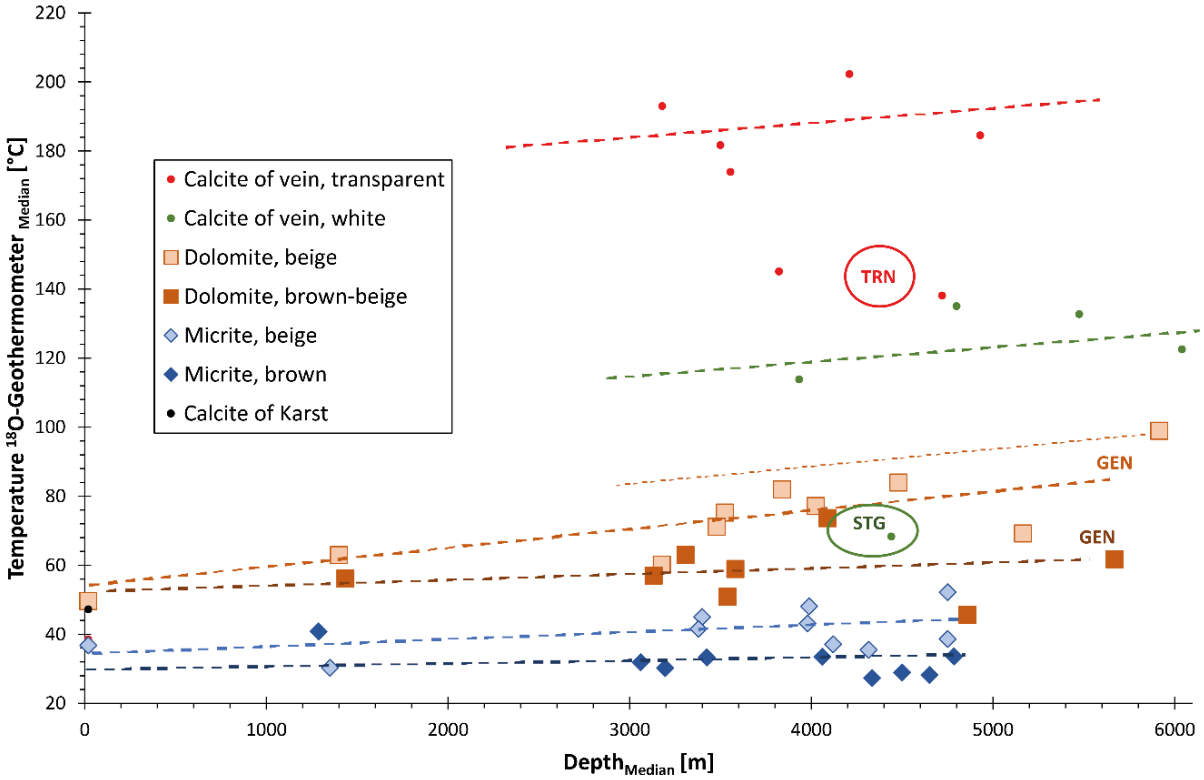


Fig. 26: Temperatures calculated using the $^{18}O$ geothermometer versus the median of depth (Liedmann, 1992).

For the other well samples, the paleo-temperature was calculated using the $^{18}O$ geothermometer in line with Liedmann (1992) with the separation at different mineral phases and depths. The micritic limestones showed (Fig. 26) the lowest median at around 30-40°C. The $^{18}O$ geothermometer temperature increased from the dolostones, 45°C to a maximum of 100°C, to the vein calcites with a temperature range between 100°C and 200°C (Fig. 26). Consequently, the temperature as well as the burial depth increased from the limestone to the dolostone and had their highest values at the vein calcites.

### 5.2.6 Use of cuttings for fluid inclusion analyses

In this study, we used our new approach for the fluid inclusion measurements on drill cuttings in their unprepared and unpolished form. In comparison to the conventional thick sections from bore cores, the measurements of the $T_h$ and $T_m$ of the drill cuttings were confirmed at the Geretsried well. The mean $T_h$ in the drill cuttings was 145°C (n=64) and in thick sections 143°C (n=16), with both samples from a similar depth. Summarizing, fluid inclusion studies of drill cutting samples expanded our study area to sites where no other rock samples were available, with the advantage of still measuring a direct sample from the diagenetic system. To determine the $T_h$ and $T_m$ from drill cuttings, the measurements were conducted 2-3 times on cuttings with a flat and smooth surface, as well as with low heating and cooling rates.

## 5.2.8 Discussion

### 5.2.8.1 Paleo-fluid evolution in the Upper Jurassic reservoir

We analyzed the paleo-fluid evolution of fluids stored in the crystals of the Upper Jurassic reservoir rocks using the isotope data and fluid inclusion measurements. Isotope data (Fig. 23, Fig. 24, Tab. 8) were further used to extend the burial history based on sedimentological and lithological data (Fig. 18). Fluid were divided into four main types based on isotope data: (1) Upper Jurassic seawater, (2) meteoric water (ground water or rainfall) and (3) basinal as well as (4) evaporated or diagenetic fluids with high salinity. The diagenetic evolution was very broadly divided into five steps (Fig. 27): (I) sedimentation, (II) early diagenesis with the first dolomitization, (III) burial diagenesis with a second dolomitization, (IV) late burial diagenesis, dominant in fractures and fault systems, and (V) the present reservoir.

**Phase I - Sedimentation**

In the first diagenetic step (sedimentation), the lime mud and bioclastic components were deposited and became lithified into two different limestones. The light-gray limestones of the reef facies mainly consist of pure carbonate and had a high primary porosity (Wolfgramm et al., 2017) in contrast to the more impure clay-bearing limestones of the lagoon and basin facies. The dark dolostone was possibly formed from dark micritic limestones in lagoons and basins with a potentially high bitumen content. The fluid evolution started with the stored Jurassic seawater, which was afterward influenced by various diagenetic processes and diagenetic fluids, depending on the facies type, mineralogy during burial, and/or differences in permeability. Paleo-fluids during the Upper Jurassic sedimentation had $\delta^{18}O$ values of approximately -1 ‰ SMOW for the ocean water, about -3 ‰ SMOW at a depth of 100 – 200 m and can be expected to be in the range of -4 to -5 ‰ SMOW at a depth of 400 – 500 m (Hoefs, 1997; Marshall, 1992). The one-phase fluid inclusions showed no phase changes during heating and freezing, but have probably been trapped at low temperatures with formation temperatures below 50°C, as suggested by Goldstein (2001). The dense, brown micritic limestones showed isotopic temperatures between 30-40°C, and the porous, beige micritic limestones were between 30-50°C. Therefore, the isotope measurements were consistent with the fluid inclusion data. In this early sedimentation stage, the fluid might become enriched in Mg- and Fe- ions and organic carbon, maybe originating from the clayey sediments, causing the first occurrence of matrix dolomite. We theorize that two different diagenetic fluids were present during sedimentation, first the modified sea water originating from lagoons and basins, and second the modified sea water from reefs of the carbonate platform in the Upper Jurassic. The slight temperature increase from the brown to beige micritic limestone could be caused by our sampling method, as the dolomite crystals (matrix dolomite) in the calcitic matrix (limestone) were not separated. Therefore, the bulk measurements of the beige micritic limestone, which contains matrix dolomite, indicated an increased temperature due to the lower $\delta^{18}O$ values of the dolomite crystals (-5.4 ‰ PDB instead of the -3.4 ‰ PDB for the limestone). The temperatures at the top of the sediment during deposition were approx. at 25°C (Liedmann, 1992). Consequently, the limestone cements and matrix dolomite crystals were formed at a depth of 300 to 650 m.

**Phase II - early diagenesis with the first dolomitization**

Afterward, the early diagenesis with the first dolomitization period occurred in a gradual transition from the sedimentation phase. The early diagenetic stage was characterized by an intense dolomitization of carbonate rocks in contact with meteoric and basinal fluids (Wolfgramm et al., 2012; 2011; Reinhold, 1996; Liedmann, 1992). The formation temperature of the dolomite crystals was between 50°C and 70°C, with lower values for the brown and dark dolostones compared to the beige dolostones. The temperature increased from the limestones to the dolostones, suggesting dolomite formation at greater depths. Due to the higher formation temperatures, the dolostones (-4.5 ‰ to -7.5 ‰ PDB) generally showed lower $\delta^{18}O$ values of around -1.5 ‰ PDB in contrast to the limestones (-3.4 ‰ to -5.4 ‰ PDB). The three parameters increasing influence of meteoric fluids, increasing temperature, and/or fluid-rock interactions in an open system seem to be responsible for the decrease in $\delta^{18}O$ (-3.4 ‰ PDB to -5.4‰ PDB limestones; -4.5 ‰ PDB to -7.5‰ PDB dolostones) with increasing depth and temperature (Fig. 23) (Marshall, 1992; Hudson, 1977). In contrast, evaporation would generally increase $\delta^{18}O$ values, which was not confirmed in this study, but expected due to the evaporitic Purbeck sediments. Due to the higher reservoir temperature in the southern deeper reservoir part, some of the carbonate values from the deep wells did not plot in the 'Upper Jurassic dolomitization window' (Fig. 24) according to Liedmann (1992) and Reinhold (1996), whose samples had a maximum depth (paleo-depth) of 1200 m. Therefore, we had to include higher temperatures and lower $\delta^{18}O$ values of the Upper Jurassic dolomitization window (Fig. 24) in the present study. The carbonate rocks analyzed by Liedmann (1992) and Reinhold (1996) were sampled from around 50 outcrops of the Oxfordian and Kimmeridgian from the Swabian and Franconian Alb, and sampled at eight shallow wells with a maximum depth of 930 m in the western Molasse Basin. The dolomitization and form of dolomite crystals depended strongly on the depositional and diagenetic fabric of the Upper Jurassic rocks, as pure carbonates showed bigger and clearer dolomite crystals than the dark carbonates. Furthermore, we described a diagenetic replacement of limestone by dolomite, so-called matrix or replacive dolomite, which is in line with previous studies (Machel, 2004; Reinhold, 1996; Liedmann, 1992). This dolomite replacement is usually affected by temperature, alkalinity, pH value, concentration of $Mg^{2+}$ and $Ca^{2+}$, $Mg^{2+}$ to $Ca^{2+}$ ratio, fluid, rock ratio, mineralogy of the carbonate replacement, and surface area (Gregg et al., 2015; Machel, 2004). The diagenetic replacement is one of the dolomitization models, which are still being studied focus and have not been solved for the Upper Jurassic in Germany (Hiatt and Pufahl, 2014; Machel, 2004; Warren, 2000). Usually, massive dolomitization, as visible in the investigated Upper Jurassic rocks, is linked to an enormous fluid flow with a high concentration of magnesium. A stratiform dolomitization, as visible in the Purbeckian dolostones, could occur in deposits with accumulated microbial mats under evaporitic pumping (Fookes, 1995) and by normal to moderately evaporated seawater (Gregg et al., 1992). Evaporation of the Purbeckian sediments was described by halite pseudomorphs in the Purbeck sediments (Barthel, 1969). As we found no indicators of an evaporitic fluid and two main dolomitized areas in the reservoir, we assumed a burial diagenetic dolomitization process, probably precipitated in fractures and fault systems. Another possible

dolomitization could have occurred by compaction fluids, with the $Mg^{2+}$ source within clayey sediments of the bedded facies (Warren, 2000). Thereby, the $Mg^{2+}$ becomes mobile due to the differential compaction of the sediment layers and can move to areas with a lower compaction such as the reef facies. Because of this $Mg^{2+}$ migration, the less compacted reef facies was dolomitized. A third dolomitization option for the Upper Jurassic carbonate rocks would be dolomitization linked to faults and fractures (Beaudoin et al., 2014; Swennen et al., 2012; Di Cuia et al., 2011; Baqués et al., 2010; Gasparrini, 2003), with the probable occurrence of a hydrothermal fluid (Ronchi et al., 2012).

**Phase III - burial diagenesis with a second dolomitization**

Thirdly, during the burial diagenesis the second dolomitization period occurred simultaneously with a probable hydrocarbon emplacement. This second phase of dolomitization in combination with bitumen or hydrocarbons and a higher formation temperature has not been described for the Upper Jurassic reservoir before. The formation temperature of dolomite crystals was around 120-136°C at depths of 3050-3100 m TVD at Traunreut, colder than the later vein calcite crystals at the same depths, but hotter than the first phase dolomites. With the recent geothermal gradient of 25 K/km at the Traunreut well, the formation temperature of the dolomite crystals should only be around 75-80°C. In addition, the dolomite crystals showed a higher salinity with 40 g/L NaCl equiv. compared to the later formed blocky, vein calcite crystals, with a salinity of 10 g/L to 20 g/L NaCl equiv. An increase in salinity from core to rim in dolomite crystals have been shown by Liedmann (1992), but could not be confirmed in this study due to a lack of measured dolostone samples. The decrease in $\delta^{13}C$ or lower $\delta^{13}C$ in the limestones (+1.4 to +2.0 ‰ PDB) to the vein calcites (-2.2 to -2.7 ‰ PDB) may result from an increasing influence of meteoric fluids or a higher content of organic carbon (Marshall, 1992). In contrast, the increase in $\delta^{13}C$ from the limestones (+1.4 to +2.0 ‰ PDB) to the dolostones (+2.2 to +2.5 ‰ PDB) may result from $CO_2$-degassing, due to the hydrocarbon emplacement, or an inflow of marine waters (Fig. 23) (Marshall, 1992). The main dolomitization had further occurred during the burial phase and was not synsedimentary or early diagenetic, which is in line with previous studies (Reinhold, 1996; Liedmann, 1992).

**Phase V - late burial diagenesis**

During the Paleogene and foreland basin development, the late burial diagenesis in the Upper Jurassic carbonate rocks happened, which was characterized by faulting, high subsidence rates, and higher temperatures due to increased burial depths. Permeable, porous beige dolostones of the upper part of the Upper Jurassic, were overgrown by transparent calcite crystals. In contrast, in the lower part of the Upper Jurassic, the dark to brown, dense dolostones were overgrown by white vein calcite crystals. The white vein calcite crystals were only found connected with the more impermeable dark to brown dolostones. In addition, the white vein calcite crystals showed a strong fingerprint of basinal water with $\delta^{13}C$ values of -2.1 ‰ PDB and $\delta^{18}O$ values of -5.8‰ PDB. In contrast, the transparent calcite crystals of the upper part of the Upper Jurassic were formed from meteoric fluids during late diagenesis with $\delta^{13}C$ values of -2.2 ‰ PDB and $\delta^{18}O$ values of -21.9‰ PDB. The isotope temperature values for the limestones and dolostones seemed reliable, whereas the isotope temperature results of the vein calcite crystals from the

deep wells were up to 216°C higher than the recent reservoir temperature. However, the geothermometer equation (Geo-1) (Liedmann, 1992) was extended in this study to temperatures above 110°C, due to the application and validation of the equation by Liedmann at higher temperatures (max. 200°C). The fluid salinity of the blocky calcite was below seawater (35 g/L NaCl equiv.) with a $T_m$ of -1.0°C (17 g/L NaCl equiv.) for primary inclusions and -0.7°C (12 g/L NaCl equiv.) for secondary or pseudo-secondary inclusions. This fluid salinity of the late calcite cements was consistent to the data by Liedmann (1992) for the outcrops and shallow boreholes. Furthermore, there were fluids with a higher salinity with $T_m$ between -2.0°C and -18.0°C and salinity between 33-112 g/L NaCl equiv. in the southernmost and westernmost wells such as St. Gallen and A1. At the St. Gallen well, an increase in salinity with increasing depth was measured from 28 g/L to 34 g/L NaCl equiv. This increase in salinity with depth was also described by Liedmann (1992) with $T_m$ between -2.0 and -5.0°C. At the Geretsried well, both an increase and decrease in fluid salinity was measured starting with 34 g/L NaCl equiv. (primary) to 64 g/L NaCl equiv. (secondary 1) and 12 g/L NaCl equiv. (secondary 2) respectively. Those different secondary or pseudo-secondary salinities may have been caused by the influence of two different saline fluids. Beside clathrates, another caused of the positive $T_m$ in small fluid inclusions is metastability, which may have caused the changing, but persistently positive $T_m$ with a fast gas bubble formation. Therefore, no $CO_2$ or $CH_4$ gases were assumed to be contained in the fluid inclusions (Bakker, 1997). This was unexpected, as hydrocarbons are stored in the Upper Jurassic rocks and should be present in the fluid inclusions. The higher saline fluids might have their source in the Upper or Middle Triassic (Reinhold, 1996), the Purbeck or the lower Oligocene sediments (Lemcke, 1988; 1976). The Triassic and the Oligocene salt waters are unlikely sources for the following reasons: a Triassic fluid would have had to migrate against the hydraulic pressure, because the Triassic aquifer is under-pressured; the Oligocene aquifer is under-pressured as well and would need to flow against the higher pressure of the Upper Jurassic aquifer (Lemcke, 1976). Therefore, neither ascending nor descending saline fluids were assumed. The Purbeck sediments are brecciated and micritic limestones, which were deposited under brackish to evaporitic conditions during the late Upper Jurassic and early Lower Cretaceous (Barthel, 1969). Therefore, a potential source area of the salts in the Upper Jurassic reservoir could be the Purbeck rocks.

**Phase IV – the present stage**

The present reservoir has been explored by hydrocarbon and geothermal wells and represents the last diagenetic phase of our study. Downward migrating fluids, probably from rainfall, moving along faults and karst phenomena may have lowered the $\delta^{18}O$ reservoir values to the recently measured -11 ‰ SMOW (-12.1 to -10.6 ‰ SMOW, n=11). Today, the Upper Jurassic reservoir fluid has a mineral concentration below 1 g/L according to Mayrhofer et al. (2014); Stober (2014); Waber et al. (2014); Stober et al. (2013/2014); Birner et al. (2011). Tab. 10 and Tab. 11 show the diagenetic fluid composition from the wells investigated in this study, the calculated diagenetic fluid salinity (equiv. NaCl), the present reservoir data, and reservoir data according to Birner et al. (2011). The diagenetic fluid salinity (equiv. NaCl) in late calcite crystals in veins has a mean value of 32.0 g/L NaCl equiv., which is higher than the present reservoir salinity (mean value: 4.8 g/L). In addition, the salinity of the

reservoir fluid varies depending on the location of the well (Birner et al., 2011). Prestel (1990) reported an increase in the salinity of the fluid reservoir to the south with a salinity of up to 37 g/L at the Opfenbach hydrocarbon well. Today, the reservoir water signature should be characterized by the diluted Upper Jurassic sea water with meteoric water, and by dissolved salts in the western area (Tóth, 1995). In the southwest, the increase in salinity might be caused by a reduced exchange of fluids due to the lower permeability. The relative high $\delta^{18}O$ values of up to + 5.5 ‰ SMOW of the present reservoir water in this area probably results from evaporitic or diagenetic processes. The only possible pathways for fluid flow must then be along fault systems. The hydrochemical data support the theory that the Jurassic sea water was diluted by a meteoric water, as determined by stable isotopes and fluid inclusions (Tab. 11). In this study, the source area of the meteoric fluids was not determined, but previous researchers described the origin in the Swabian and Franconian Alb (Prestel, 1990). Because the ancient Jurassic sea water had a salinity of around 35 g/L (Liedmann, 1992), the reservoir fluid became less saline during the evolution of the foreland basin with a fluid salinity in late vein cements of around 10-20 g/L NaCl equiv., and the present salinity with the lowest salinity of 0.5 g/L. Thereby, the fluid salinity of late vein cements represents an intermediate point in the evolution of the Upper Jurassic reservoir. In addition, the concentration of dissolved ions in the reservoir fluid has decreased with time and location, from east to west. Examples are the westernmost St. Gallen well with the highest salinity and the easternmost Traunreut well with the lowest salinity of the present reservoir fluid. The greater dilution of the former Jurassic seawater in the eastern section of the reservoir could be caused by the high permeability of the carbonate rocks.

Tab. 10: Fluid composition of the geothermal wells in the southern Molasse Basin. Recent well data were provided by Florian Heine, Technical University of Munich (TUM), Chair of Hydrogeology. * Wolfgramm et al. (2015), **Birner et al. (2011), ***Stober et al. (2013/2014).

| **Well** | **Salinity from FI data [g/L]** | **Salinity [g/L] Reservoir in production** |
|---|---|---|
| STG | 33 | *18.0 |
| A1 | 112 | **0.5-10.6 |
| MOS | 12 | ***0.2-2.0 |
| C1 | 9 | **5.0-10.0 |
| SCH | 18 | **5.0-10.0 |
| FRH 1 | 19 | 4.1 |
| GEN | 27 | 1.6 |
| UHA 1 | 18 | 0.6 |
| TRN 1 | 42 | 0.5 |

Tab. 11: Hydrochemical data from the deep wells showing a dilution of the Jurassic sea water from the St. Gallen well (Wolfgramm et al., 2013), Geretsried, Unterhaching, and the most diluted formation water at the Traunreut well. Traunreut data from Florian Heine, TUM Hydrogeology.

| Parameter | Jurassic sea water | | St. Gallen | | Geretsried | | Unterhaching | | Traunreut | |
|---|---|---|---|---|---|---|---|---|---|---|
| | [g/l] | [%] | [g/l] | [%] | [g/l] | [%] | [g/l] | [%] | [g/l] | [%] |
| Sodium | 10.7 | 30.5 | 6 | 30.9 | 0.8 | 26.5 | 0.12 | 17.5 | 0.13 | 23.5 |
| Potassium | 0.4 | 1.1 | 2.2 | 11.3 | 0.08 | 2.6 | 0.02 | 2.9 | 0.02 | 3.6 |
| Magnesium | 1.3 | 3.7 | 0.03 | 0.2 | 0.02 | 0.7 | 0.005 | 0.7 | 0.004 | 0.7 |
| Calcium | 0.4 | 1.1 | 0.12 | 0.6 | 0.1 | 3.3 | 0.03 | 4.4 | 0.03 | 5.4 |
| Chloride | 19.3 | 55.0 | 9.6 | 49.5 | 1.4 | 46.4 | 0.11 | 16.1 | 0.08 | 14.4 |
| Sulphate | 2.7 | 7.7 | 0.15 | 0.8 | 0.08 | 2.6 | 0.02 | 2.9 | 0.01 | 1.8 |
| HCO3- | 0.2 | 0.6 | 1.2 | 6.2 | 0.44 | 14.6 | 0.28 | 40.9 | 0.28 | 50.5 |
| Residual | 0.1 | 0.3 | 0.1 | 0.5 | 0.1 | 3.3 | 0.1 | 14.6 | <0.1 | <18.1 |
| Sum | 35.1 | 100 | 19.4 | 100 | 3.02 | 100 | 0.685 | 100 | 0.554 | 100 |

The determined, calculated and measured temperatures of the Upper Jurassic aquifer are shown in Tab. 12. The $T_h$, trapping, and maximum trapping temperatures measured in the vein calcites using microthermometry were higher than the recent reservoir temperature in nearly every measured well. However, the reservoir temperature was not corrected for the borehole temperature BHT and could have an error of around 20 K. The three following reasons could explain the higher formation temperatures of around 25°K: (1) ascending hotter basement fluids along fractures and fault zones, (2) necking or stretching of the fluid inclusions while heating (re-equilibrium), and/ or (3) a higher or different geothermal gradient. As no cement phase possessed a different chemistry or isotope signature, ascending basement fluids are unlikely. The re-equilibrium of the fluid inclusions means that the maximum temperature stored from re-equilibrium was measured in this study (Barker and Goldstein, 1990; Goldstein, 1986). As large fluid inclusions are more likely to re-equilibrate than small ones (McLimans, 1987), the possibility of the small 2-phase fluid inclusions in the present study was low. Because of the similar $T_h$ and $T_m$ and consistent liquid-vapor ratios in the measured FIA in the vein calcites, we assumed that no re-equilibrium occurred. The higher geothermal gradient seemed to be the most relevant cause of the temperature increase, as a varying geothermal gradient would explain the high temperatures and might not cause a change in fluid chemistry. Moreover, a varying geothermal gradient would be in line with previous studies by the hydrocarbon industry for the Cenozoic sediments in the Molasse Basin (Mazurek et al., 2006; Teichmüller and Teichmüller, 1986). Liedmann (1992) discussed possible paleo-temperature gradients of up to 60 K/km, but this study did not confirm that. In contrast to the average geothermal gradient of the Upper Jurassic reservoir, the Traunreut well has an anomaly with a lower temperature and geothermal gradient today (Agemar et al., 2012; Wrobel et al., 2002).

Tab. 12: Temperature measurements of the recent reservoir temperatures from unpublished borehole reports. UJR: Upper Jurassic reservoir; temperature at top of UJR (Top T), maximum temperature of the UJR (Max. T UJR), homogenization temperature from fluid inclusions ($T_h$), calculated formation temperature ($T_{form}$), maximum formation temperature ($T_{form}$ max.) and temperature data according to Agemar et al. (2014a) (Top T UJR GeotIS). (- : no data available; *Schneider et al. (2012)).

| **Well** | **Top T UJR [°C]** | **Max. T UJR [°C]** | **$T_h$ [°C]** | **$T_{form}$ [°C]** | **$T_{form}$ max [°C]** | **Top T UJR GeotIS [°C]** (Agemar et al., 2014a) |
|---|---|---|---|---|---|---|
| STG | 144 | 150 | 140-156 | 137-177 | 142-184 | - |
| A1 | 104 | 104 | 70-130 | 121-152 | 123-154 | 100 ± 11 |
| MOS | 79* | 87* | 130 | 131-147 | 133-175 | 70 ± 7 |
| C1 | - | - | 123 | 128-134 | 131-137 | 108 ± 11 |
| SCH | 128 | 131 | 122-158 | 124-175 | 130-181 | 133 ± 12 |
| FRH | | 105 | 144-190 | 148-195 | 150-197 | 80 ± 11 |
| GEN | 125 | 150 | 141-148 | 152-174 (ST: 132-167) | 157-178 (ST: 136-171) | 147 ± 14 |
| UHA | 91 | 124 | 123-135 | 123-128 | 127-131 | 118 ± 11 |
| TRN | 106 | 115 | 106-115 | | | 108 ± 11 |

### 5.2.8.2 Subsidence history of the Molasse Basin

The measured formation temperature in the vein calcites and dolomite crystals in combination with the reconstruction of the subsidence history, paleo-fluids and paleo-temperature using stable isotopes, provided evidence of the North Alpine Foreland Basin evolution (Fig. 27, Fig. 28). The evolution started with the Jurassic sea water, which had a temperature of around 25°C during deposition (Liedmann, 1992) at an assumed water depth of 150-200 m (Selg and Wagenplast, 1990). As the suggested formation depth of the sedimentary rocks was between 200-400 m, the temperatures were around 30-40°C during early diagenesis and rock formation. After the limestone cementation, the dolostones were formed by isotope temperatures of around 40-70°C for the brown dolostones and 60-90°C for the beige dolostones. The dolostones showed an increase in temperature compared to the light beige, subhedral-euhedral, pure dolostone. The dolomitization could have increased the porosity during dolomitization in the reefs and on the carbonate platform (Machel, 2004). Due to the temperature and isotope data, the assumed depth of dolomitization is around 1-2 km with a possible inflow from meteoric fluids. In the further subsidence of the rocks to a depth of 1.0-2.5 km, the dolostones with a bitumen coating were formed at temperatures between 70-100°C. This probably happened during a further or second dolomitization phase, which has not been described before, and while a high migration of hydrocarbons was present. In addition, a $T_h$ of around 110°C and a salinity of 40 g/L NaCl equiv. for these idiomorphic dolomite crystals (planar-e dolostones) were measured, but with no indication of hydrocarbons. The sampled dolomite crystals were either vein or fractured dolomite crystals from the Traunreut well at depths of 3086 m TVD. Our study confirmed the data by Liedmann (1992), who assumed a deep burial hydrothermal dolomitization during the Alpine orogeny, and early dolomitization with temperatures of around 40-90°C. Consequently, dolomitization occurred during the burial diagenesis, first at lower (40-90°C) and later at higher (70-100°C) temperatures. In addition, a meteoric influence was present during the diagenesis, as the former

Jurassic seawater was diluted in the southern Upper Jurassic rocks during the Cretaceous and Paleogene (Fig. 28).

The highest $T_h$ in the transparent vein calcites (Fig. 28) was close to the maximum value, and it confirmed the growth of the calcite crystals at a late diagenetic stage with maximum temperatures of up to 190°C, which was also described by Liedmann (1992). As the calcite crystals precipitated in fractures and veins, the formation must have happened during the tectonic phase of the Molasse Basin. The isotope temperature for the white vein calcite crystals was between 110°C and 140°C, excluding St. Gallen with temperatures of 70°C. These temperatures could be higher due to a measuring error, as the salinity of the ascending fluids might be increased from highly saline lagoon and basin fluids, and therefore the geothermometer from Liedmann (1992) (Geo-1) could have calculated lower values. The transparent vein calcite crystals were probably formed in a second tectonically active phase because the isotope temperatures were between 140-200°C, higher than the white vein calcites. Consequently, the white vein calcites were formed at depths of 1-3 km, and the transparent vein calcites precipitated from low saline fluids (10-20 g/L NaCl equiv.) at depths between 1.0 km and 3.5 km. The transparent vein calcites at the Traunreut well showed the lowest isotope temperatures, which confirmed the present low-temperature anomaly (Fig. 28). Furthermore, the Traunreut well has the most diluted reservoir fluid today (Fig. 28), indicating a meteoric influence with decreasing grade to the southwest. Hence, the late meteoric water was present during the growth of the transparent vein calcite, as the fluid inclusions showed the dilution of the former Jurassic sea water as well. However, in some fluid inclusions, positive $T_m$ were measured due to metastability, therefore no hydrocarbons or gases were present during the inclusion trapping in the vein calcites. This is controversial, as the Upper Jurassic carbonate rocks store hydrocarbons, which were explored during the 1960s to 1980s. In summary, our study showed that the early diagenetic fluids and cements might be overprinted by a hotter hydrothermal fluid migration or a higher geothermal gradient, evidenced by the vein calcites in the Upper Jurassic reservoir (Fig. 28). This hot fluid migration, stored in the late vein cements, was probably along fault and fracture systems.

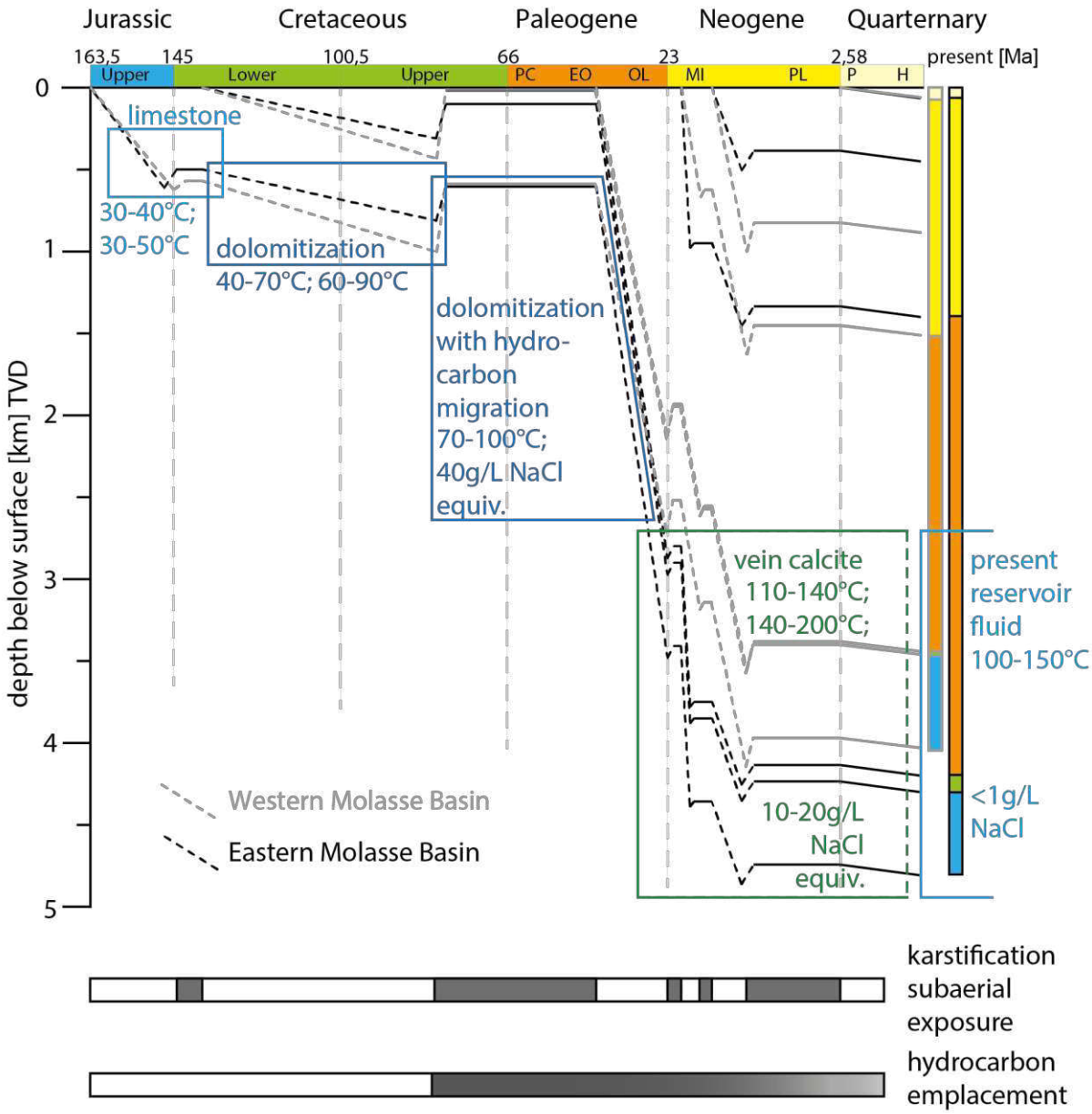


Fig. 27: Subsidence plot for the Upper Jurassic carbonate rocks, divided into the western (gray) and eastern (black) Molasse Basin. The eastern Molasse Basin was down-lifted further than the western Molasse Basin, and both parts have reached the maximum depth today. The sediment thickness was used from the borehole data at Traunreut (eastern Molasse Basin) and Mauerstetten (western Molasse Basin) and was not corrected for compaction. Due to varying geothermal gradients, the relative depths were assumed.

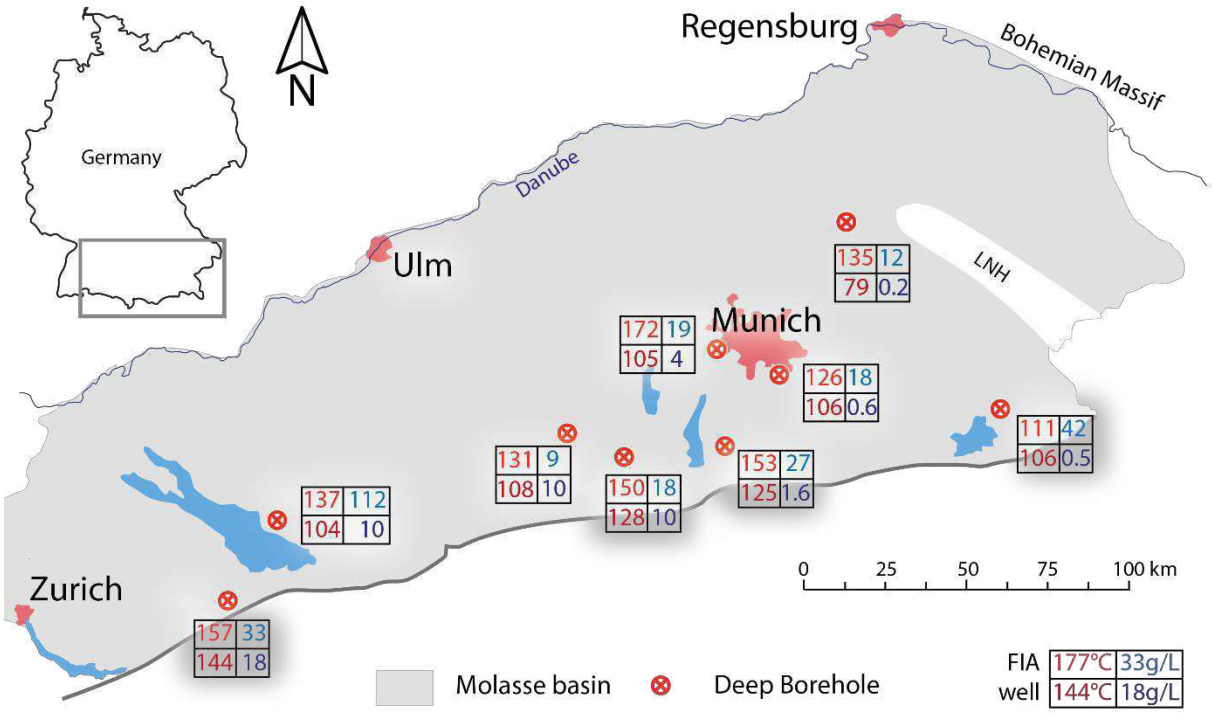


Fig. 28: Overview of the study area in the Molasse Basin, southern Germany and eastern Switzerland. In addition, the measured temperature and salinity values measured in the fluid inclusion assemblage (FIA) and in the present reservoir fluid are provided from Tab. 10 and Tab. 12.

Temperatures above 50°C have been possible since the Eocene, which is characterized by the Paleogene sedimentation (Fig. 27). Surface outcrops might have reached depths of around 600 m due to the low cement formation temperatures, and of up to 4,000 m in the deeper down-lifted Upper Jurassic reservoir in the southern Molasse Basin (Fig. 27). Using the subsidence plots (Fig. 27), higher temperatures were assumed in the eastern part of the Molasse Basin, as the sedimentary rocks are at greater depths. However, the Traunreut well in the eastern part of the Molasse Basin showed relatively low temperatures for the vein calcites compared to the dolomitization temperatures, possibly due to an already existing temperature anomaly (Agemar et al., 2014a; 2012).

### 5.2.9 Conclusion

In our study, the fluid and temperature evolution of the Upper Jurassic reservoir in the North Alpine Foreland Basin was analyzed using fluid inclusion measurements and stable isotopes of different cement phases in the carbonate rocks. In a new approach to measure fluid inclusions in drill cuttings, the study area was extended to boreholes drilled for a geothermal purpose, where drill cuttings were the only available samples. Thereby, old and newly drilled wells could be measured, and a wide area was investigated from the surface to depths of 4500 m. The burial development of the Upper Jurassic rocks could be reconstructed from temperature and fluid composition data. Our results showed an early diagenesis of the limestones, followed by two burial dolomitization phases and a late, tectonically active burial phase, which developed fractures and fault zones (Fig. 27). The main dolomitization phase could have occurred during the Alpine orogeny in the Cretaceous and early Paleogene. This early dolomitization might have developed at a depth of around 1-2 km. A later, second dolomitization is

characterized by idiomorphic dolomite crystals coated with bitumen and temperatures of around 80-100°C. This second, and newly described dolomitization was measured in fluid inclusions hosted in dolomite crystals with formation temperatures of around 110°C and a salinity of 40 g/L NaCl equiv., which is below the values of the Upper Jurassic seawater.

Our hypothesis was that the Jurassic sea water (formation water) was diluted from a subsequent infiltration of karst or meteoric water. The timing of this dilution phase is unclear and might not only have happened during periods of erosion (Fig. 27). At nearly every well, the measured Upper Jurassic reservoir fluids became less saline during basin evolution, however, the southwestern area showed a higher salinity than the Jurassic sea water salinity. The least saline well is Traunreut today, which might be caused by a more permeable reservoir. The source area or formation of the high salinity of the diagenetic fluid in the southwestern part is still unclear, and could not be determined in this study. Another interesting result was that dolomitization occurred in the same temperature range at the Traunreut well as in the Munich area, but afterward the reservoir temperature must have decreased. Therefore, the present low-temperature anomaly around Lake Chiemsee might have existed since the tectonically active phase and the formation of the transparent vein calcites. Further studies should be performed of vein calcite samples from the Traunreut well to understand the fluid evolution, dilution, and change in geothermal gradient in detail. The Geretsried well showed two different types of secondary or pseudo-secondary fluid inclusions with the same trapping temperature but different salinities. In addition, the St. Gallen well indicated an increase in salinity with depth. Those measurements support the theory of a meteoric water influence, migrating from the surface downward. In the outcrop samples, a third calcite cement was found, which probably developed from karstification processes, which can sometimes recrystallize dolomite to dedolomite. For high permeability areas, the influence of the meteoric fluids must be important, which might be along fracture and fault zones in the Molasse Basin. The areas with a high fluid migration on the basis of our results would seem to be the best target areas for a geothermal installation, because they show a high primary porosity, dolomitization, and still open fractures. In the present study, we did not focus on a detailed analysis of the dolomitization process, but it will be addressed in future research.

## 5.3 Dolomitization of Upper Jurassic carbonate platform rocks: A case study from the North Alpine Foreland Basin

### 5.3.1 Introduction

For the characterization of the geothermal, carbonate Upper Jurassic reservoir in the North Alpine Foreland Basin, a basin-wide comparison of the cements, dolomite crystals, and dolomite types was performed. Thereby, important process as recrystallization and/or calcification, and dolomitization were investigated, which might develop high porous and high-permeability areas (Machel, 2004). Furthermore, the relationship between the facies, diagenesis, dolomite types, and porosity was analyzed, as highlighted by Machel (2004). The Upper Jurassic carbonate rocks are studied for facies types (Meyer, 1994; Meyer and Schmidt-Kaler, 1989), hydraulic and hydrochemical properties (Stober, 2014; Birner et al., 2012), diagenesis and dolomitization (Reinhold, 1996; Liedmann, 1992), particularly in outcrops of the Franconian and Swabian Alb. In this study, the Upper Jurassic carbonate rocks, such as limestones and dolostones, were sampled from 13 deep wells (2.5-5.0 km) of the North Alpine Foreland Basin, so-called Molasse Basin. The Upper Jurassic carbonate rocks of the deep wells show differences and variations in dolomite types, amount of dolomite, facies and lithology, and especially in productivity of reservoir fluid (Böhm et al., 2011; Meyer, 1994). In addition, the deep Upper Jurassic reservoir (1-5 km) was compared by the occurring dolomite types and their distribution to the shallow Upper Jurassic reservoir (< 1 km), as well as to previous research. For that reason, 12 outcrops of Upper Jurassic in the Franconian and Swabian Alb were sampled besides the 13 deep wells, which intersect the Upper Jurassic carbonate rocks. For the characterization, the dolomite crystals as well as the carbonate host rock samples were measured using optical and cathodoluminescence (CL) microscopy, scanning electron microscopy (SEM), and X-ray diffraction (XRD). The CL data was compared to fluid inclusion and stable isotope data published by Mraz et al. (2018c), which measured the same samples.

For the further geothermal exploration of the Upper Jurassic reservoir, the dolomite problem needs to be addressed to understand the origin and timing of dolomitization, as well as the size and distribution of the dolomitized carbonate rocks. Especially for the geothermal exploration, the porosity and permeability pattern are important (Birner et al., 2012; Warren, 2000), which depend on pore space generating processes such as dolomitization, dissolution, and karstification. However, this pore space can be cemented by the precipitation of calcite, quartz (silica) or even dolomite crystals contemporaneously (Hiatt and Pufahl, 2014; Machel, 2004). In general, the dolomitization process is still in research focus, as the dolostones occur in many sedimentary and diagenetic settings (Adams et al., 2018; Makhloufi et al., 2018; Richter et al., 2018), with the genetic interpretation differs depending on the geological setting. Furthermore, dolomite is more abundant in older rocks, and well-ordered, stoichiometric dolomite is never produced in nature (Machel, 2004). Dolomitization processes are generally described according to Hiatt and Pufahl (2014) and Machel (2004) to happen under three conditions: (1) seawater in conjunction with evaporative conditions, (2) freshwater mixed with seawater, (3) burial diagenetic environments. Usually, the dolomite crystals replace calcite crystals in a limestone,

so called replacement dolomite or matrix dolomite, which can created an inter-crystalline micro-porosity (Machel, 2004). In the present study, the dolomitization was of special interest, as good target areas are generally found within a dolomitized massive facies of the Upper Jurassic (Birner et al., 2012; Böhm et al., 2011). We assumed that the dolomitization of the deep Upper Jurassic reservoir happened during the burial diagenesis, as it is described for the shallow Upper Jurassic carbonate rocks (Reinhold, 1996), however at higher temperatures due to the higher present reservoir temperatures with 65-150°C at depths of 2.5-5.0 km. Besides, variation in dolomitization depending on the facies, clay and/or unsolved residual content, proximity to fault and fracture zones, and to bedding in the Upper Jurassic reservoir were supposed. Therefore, the following key questions were addressed: (I) What types of dolomite crystals can be distinguished and are they linked to certain settings, (II) Are the dolomite crystals associated with a certain facies or mineral phase, (III) Are there indications of when the dolomite crystals were formed, (IV) Under which conditions were the dolomite crystals formed, (V) how is the distribution of matrix porosity in the carbonate rocks.

### 5.3.2 Study area and geology

This study focused on the characterization of the Upper Jurassic reservoir in the Molasse Basin (Fig. 29), which was exploited for hydrocarbons in the past and is used to generate geothermal energy by producing the warm (65-150°C), low saline reservoir fluid (1-10 g/L) today (Mraz et al., 2018c). Therefore, 13 wells intersecting the Upper Jurassic carbonate rocks were selected in addition to 12 outcrops at the Franconian and Swabian Alb (Tab. 13). Some of the selected wells only reach at the final depth the sediments of the Lower Kimmeridgian (previously called Malm gamma), and therefore do not encounter the complete Upper Jurassic.

The Upper Jurassic carbonate rocks were deposited on a epicontinental marine platform, and can be subdivided by the main and dominating organisms and by the depositional environment into a massive facies and a bedded facies (Meyer and Schmidt-Kaler, 1989). The massive facies, or sometimes so-called reef facies, is composed of siliceous sponges, microbial mats, tubiphytes, ooids, and peloids, which are sometimes reworked (Pawellek and Aigner, 2003; Meyer, 1994). In contrast, the bedded facies was deposited within basins and contains transported bioclasts of the surrounding massive facies in micritic, marly limestones (Meyer, 1994). To the late Upper Jurassic, the carbonate rocks grade into a brackish, evaporitic facies, the so-called Purbeckian facies (Joachimski, 1994; Strasser, 1988; Barthel, 1969).

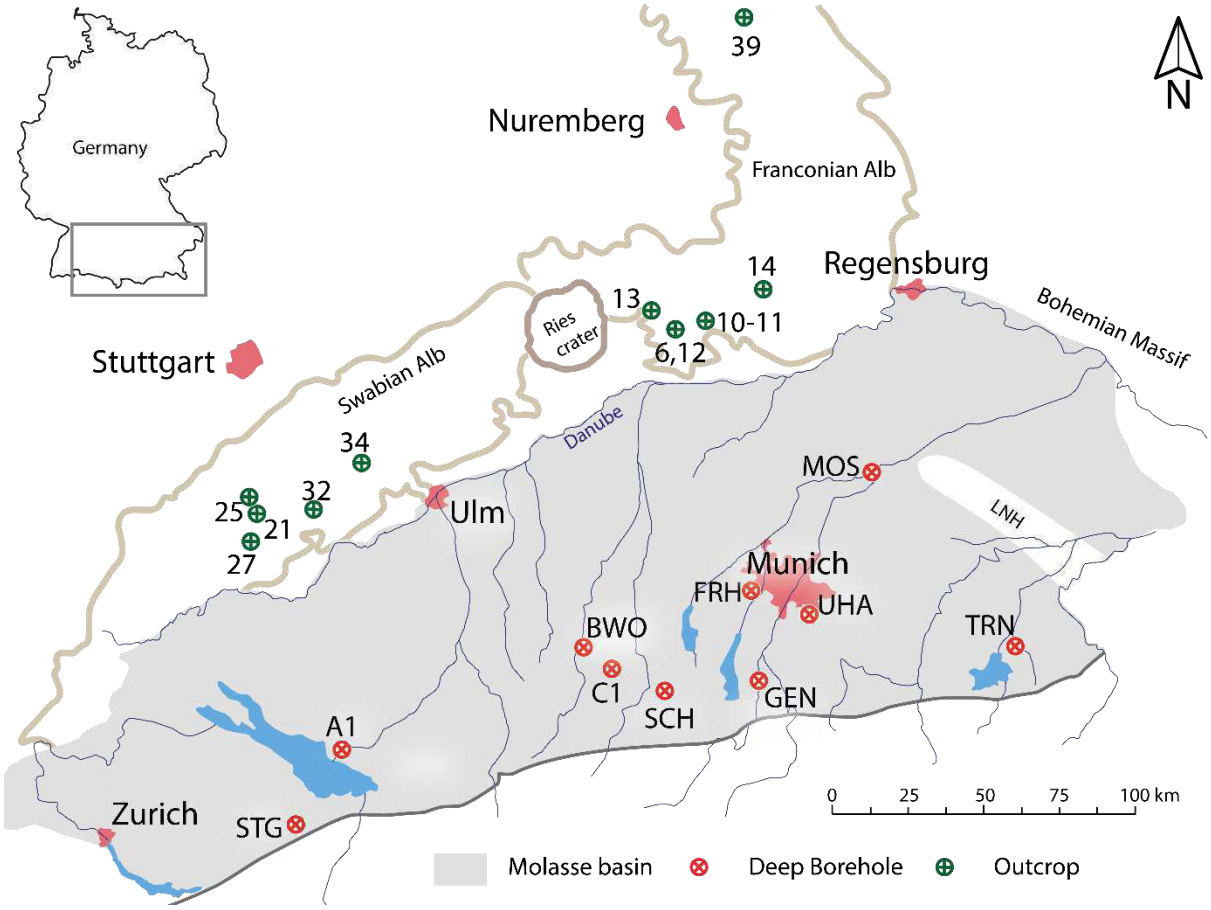


Fig. 29: Overview of the study area in the Molasse Basin, southern Germany and eastern Switzerland. FRH-Freiham, GEN-Geretsried, MOS-Moosburg, TRN-Traunreut, UHA-Unterhaching, SCH-Schongau, STG-St. Gallen, BWO-Bad Woerishofen, outcrops according to Tab. 13.

The Upper Jurassic carbonate reservoir is situated in the North Alpine Foreland Basin, overlaying Middle Jurassic and Permo-Carboniferous sediments, as well as a crystalline basement (Kuhlemann and Kempf, 2002; Bachmann and Müller, 1996). Due to the wedge-shape of the Molasse Basin, the Upper Jurassic sedimentary rocks crop out at the Franconian and Swabian Alb and are situated at around 5 km depth at the Alpine deformation front. The Upper Jurassic carbonate rocks are overlain by Cretaceous and Cenozoic sedimentary rocks. During the diagenesis, the carbonate rocks of the Upper Jurassic were affected by recrystallization and dolomitization processes (Liedmann, 1992), by a hydrocarbon emplacement and migration of silicate rich fluids. Previous researchers (Mraz et al., 2018c; Wolfgramm et al., 2016; Reinhold, 1996; Liedmann, 1992; Prestel, 1990) described the diagenesis using fluid inclusions, geochemical data, and cathodoluminescence (hot cathode) as following: (I) early diagenetic calcite cements precipitated and formed the sedimentary rocks; (II) during the early burial diagenesis, the dolomitization of the former limestones happened, developing in parts massive dolostones. These massive dolostone (planar-e, high porous) are usually distributed within the Kimmeridgian, have developed in the massive facies, and build up the main highly permeable reservoir (Wolfgramm et al., 2011; Böhm et al., 2010). The carbonate rocks of the Tithonian and Purbeckian showed slightly different dolomite types (Liedmann, 1992), which sometimes form a second high-permeability area in the Upper Jurassic reservoir (Wolfgramm et al., 2011; Böhm et al., 2010). As the North Alpine Foreland Basin

evolved, the Upper Jurassic carbonate rocks were deformed and fault and fracture systems developed, especially in the Eocene to Miocene, parallel to the Alps (Mraz et al., 2018a; Budach et al., 2017; Kuhlemann and Kempf, 2002; Lemcke, 1988). (III) In the still continuing burial diagenesis, the carbonate rocks were influenced by hydrocarbons and idiomorphic dolomite crystals precipitated at former fracture zones. (IV) In the late burial diagenesis, calcite cements were precipitated along former fracture zones, hosting 2-phase fluid inclusions (liquid-vapor). Previous researchers described further a hydrothermal dolomitization connected to tectonic structures (Reinhold, 1996; Liedmann, 1992). Due to a high overburden stress, pressure solution and stylolitization happened in all Upper Jurassic carbonate rocks during the burial diagenesis. In periods of subaerial exposure, probable during the Cretaceous, and by the presence of meteoric waters, the Upper Jurassic carbonate rocks were dissolved, became karstified and in parts dedolomitized, especially at the shallow reservoir rocks and at the outcrop areas (Koch, 2011; Reinhold, 1996).

Tab. 13: FI-Fluid inclusions, CL-cathodoluminescence, X-thick section, Y-thin section, Z-cutting sample.

| **Sample** | **Stratigraphy** | **depth** | **Method** | | **Method** | **Sample** | **Meas.** | **Sample** |
|---|---|---|---|---|---|---|---|---|
| **Well** | **Upper Jurassic** | **[m TVD]** | **FI** | **n** | **CL** | **n** | **n** | type |
| A6.1 | dolostone, Treuchtlingen-Fm. | | x | 1 | x | 1 | 1 | X |
| A6.3 | dolostone, Treuchtlingen-Fm. | | | | x | 1 | 4 | X |
| A10.18 | dolostone, Treuchtlingen-Fm. | | x | 2 | x | 1 | 4 | X |
| A10.7 | dolostone, Treuchtlingen-Fm. | | x | 1 | x | 1 | 1 | X |
| A10.9 | dolostone, Treuchtlingen-Fm. | | x | 1 | x | 1 | 2 | X |
| A11.1 | limestone, Altmühltal-Fm. | | x | 8 | x | 1 | 2 | X |
| A12.1 | dedolostone, Treuchtlingen-Fm. | | x | 4 | x | 1 | 3 | X |
| A13.2 | dedolostone, Treuchtlingen-Fm. | | x | 4 | x | 1 | 1 | X |
| A14.1 | limestone, Treuchtlingen-Fm. | | x | 1 | x | 1 | 4 | X |
| A21.4 | dolostone, Treuchtlingen-Fm. | | x | 2 | x | 1 | 5 | X |
| A25.1 | limestone, Treuchtlingen-Fm. | | x | 1 | x | 1 | 2 | X |
| A27.1 | limestone, Treuchtlingen-Fm. | | x | 1 | x | 1 | 6 | X |
| A32.2 | limestone, Arzberg-Fm. | | x | 1 | x | 1 | 2 | X |
| A34.1 | dolostone, Frankenalb-Fm. | | x | 1 | x | 1 | 1 | X |
| A39.1 | dolostone, Frankenalb-Fm. | 400 | x | 4 | | | | X |
| **sum** | | | | **32** | | **14** | **38** | |
| FRH-1 | Kimmeridgian | | x | 17 | x | 12 | 27 | Y, Z |
| GEN-1 | Kimmeridgian | 4365-4722 | x | 73 | | 15 | 8 | Z |

| Sample | Stratigraphy | depth | Method | | Method | Sample | Meas. | Sample |
|---|---|---|---|---|---|---|---|---|
| Well | Upper Jurassic | [m TVD] | FI | n | CL | n | n | type |
| GEN-1ST-A1 | Kimmeridgian | 4602-4722 | x | 29 | x | 1 | 2 | Z |
| C1 | Tithonian | 3303, 2 | x | 15 | x | 1 | 1 | X |
| MOS | Tithonian-Kimmeridgian | 1288-1449 | x | 40 | x | 2 | 4 | X |
| SCH | Tithonian | 4375-4378 | x | 84 | x | 4 | 9 | X |
| STG | Oxfordian-Kimmeridgian | 3910-4156 | x | 28 | x | 3 | 6 | X |
| A1 | Kimmeridgian | 2646-2739 | x | 18 | x | 2 | 2 | X |
| TRN-1 | Tithonian-Kimmeridgian | | x | 24 | x | 49 | 35 | Y, Z |
| TRN-2 | Tithonian-Kimmeridgian | 4336-4509 | x | 9 | x | 30 | 8 | Z |
| UHA-1 | Kimmeridgian | 3067, 5 | x | 28 | x | 2 | 1 | Z |
| UHA-2 | Kimmeridgian | 3289, 5 | x | 12 | x | 2 | 2 | Z |
| BWO | Tithonian-Kimmeridgian | 2370-2565 | x | 12 | x | 5 | 5 | Y, Z |
| **sum** | | | | **389** | | **128** | **110** | |

### 5.3.3 Methodology

The Upper Jurassic samples of the 12 outcrops were 14 hand specimens, whereas the 128 samples of the 13 deep wells were either drill cores or drill cuttings (Fig. 29). The 12 outcrop samples were made into double-sided thick sections. The drill core samples of the Upper Jurassic were made into thin and thick sections, while the drill cuttings were made into thin sections or were measured unprepared as they were produced by drilling. The drill cuttings had generally a size of around 1 mm. Depositional facies and lithology of the veins and carbonate rocks were studied using optical microscopy on alizarin stained thin sections. The lithology and petrography were previous published in detail in (Mraz et al., 2018b). The 443 fluid inclusion studies and 266 stable isotope data ($\delta^{13}C$ and $\delta^{18}O$) was used as published in Mraz et al. (2018c), as the same samples were analyzed. The diagenetic features (compaction, stylolitization, recrystallization), as well as dolomite and calcite crystals were observed in 149 measurements under an optical and cathodoluminescence microscope. Thereby, a cold cathode system from CITL (Cambridge Image Technology Ltd.) coupled to an Olympus microscope and a digital Olympus DP25 camera was used. Operating conditions were in the range of 260-365 µA/mm² and 15-20 keV gun current with a vacuum during the measurement below 0.06 mbar. The camera was adjusted to ISO 200 with a constant exposure time of 5 s for all photos. A problem was that the exposure time of the camera could not be extended to 5s or more, as usually an exposure time of 45s is used. Carbonate rocks with the amount of dolomite crystals above 75 % were called dolostones in the present study. The dolomite crystals and dolostone textures were classified according to Machel (2004) and Sibley and Gregg (1987).

The cathodoluminescence (CL) was measured conventional at thin and thick sections, and in addition at unprepared and unpolished drill cuttings. It was possible to measure drill cuttings in CL, if they had a smooth and flat surface. However, sometimes in contact with the electron beam the cuttings moved outside the visible field. Furthermore, it was necessary to check for a minimal space between the particles to prevent a shadow of the electron beam by neighboring cuttings, due to the thickness of the drill cuttings. In general, CL in carbonate rocks is, especially in calcite and dolomite crystals, due a doping of foreign atoms (impurities) and subordinating by lattice defects (Götze, 2002; Amieux, 1982). Therefore, CL provides information on the growth textures in the crystals, which are indicative of the forming conditions and diagenesis. In addition, the CL color and intensity depends on activators, sensitizers, quenchers in the crystal lattice, and fluctuations in redox-potential, as well as in growth rates, temperature, crystal surface structure, fluid chemistry, and chemical species in solution (Boggs and Krinsley, 2006; Pagel, 2000). The CL in diagenetic carbonate rocks is usually visual detectable by the activator of manganese ($Mn^{2+}$), which can exchange the $Ca^{2+}$ and/or $Mg^{2+}$ position in the crystal lattice and can be further quenched by $Fe^{2+}$, $Co^{2+}$, $Ni^{2+}$ and $Fe^{3+}$ (Richter et al., 2003; Pagel, 2000). The $Mn^{2+}$ activated luminescence in calcite and dolomite crystals, change the CL from the intrinsic blue-violet color to an extrinsic orange-red color (Boggs and Krinsley, 2006). Hence, in this study different cement phases based on CL and fluid inclusion data were characterized. However, using a cold cathode, only qualitative measurements were possible. In the samples, sometime dust particles were visible by a bluish CL on the sample surface. An intrinsic, blue to violet CL was not visible in all executed CL measurements on calcite cements. Furthermore, the CL intensity was increased at uneven fracture surfaces at the drill cutting samples. The CL colors of the Upper Jurassic carbonate rocks were red, non-luminescent, red with non-luminescent concentric zonation, orange, yellow with non-luminescent sector zonation, and dull yellow.

In addition, SEM and energy dispersive X-ray (EDX) analyses were carried out on thin sections and drill cuttings to determine the composition of the cement phases in the limestones and dolostones. XRD measurements were further conducted in line with DIN EN 13925-1, 2, 3; DIN EN 1330-11 on four Upper Jurassic bore core samples, which were selected from dark gray, micritic limestones (2942-4709 m TVD). Both quantitative analyses helped to further investigate the cements, microfabrics, and diagenetic sequence of the Upper Jurassic carbonate rocks.

## 5.3.4 Results

### 5.3.4.1 Limestones and early cements

The first diagenetic phase was represented by limestones, such as mudstones, wackestone, packstone, grainstone, and only in parts by bindstones. Initially, the micritic matrix (mudstone to packstone) showed no CL. However, most investigated limestones and early cements of the deeper basin part were recrystallized by blocky cement (e.g. grainstone), indicated by the missing of different early cement types such as fibrous or palisade cements, which were described by Liedmann (1992) for the shallow reservoir. At the outcrop samples, intrinsic Cl was measured, but not at the well samples. Some of the

recrystallized limestones did show a dull red to slightly orange CL, with a dark red CL at calcite cements within the limestones. Bioclasts and components, such as peloids or ooids had typically no CL, but some recrystallized bioclasts showed a dull orange CL.

Stylolites were found in the outcrops and deep well rock samples. As some silicified areas are limited by stylolites, the stylolites must have formed before the recrystallization of the siliceous sponges and migration of silica happened. Furthermore, the silica of the siliceous sponges has migrated through the Upper Jurassic carbonate rocks and precipitated in form of siliceous concretes above the former siliceous sponge rich layers.

### 5.3.4.2 Dolostones and dolomite crystals

The dolomite types were subdivided into dolostones (>75 % dolomite crystals) and matrix dolomites (replacement dolomite). The matrix dolomite crystals were usually idiomorphic to hypidiomorphic (30-120 µm), but showed heterogeneous distribution depending on the original limestone texture. Usually, the matrix dolomite crystals were beige to light gray, but they can have a dark brown color similar to the micritic limestones. The matrix dolomite has formed in all types of limestones, sometimes starting in the sparite or within the bioclasts, such as ooids. Besides, matrix dolomite can be equally distributed or enriched at stylolites. Some matrix dolomites were zoned, with a cloudy center and a clear rim. The matrix dolomites were separated by their CL in no and red matrix dolomites. In some samples, the non-luminescent matrix dolomites were overgrown by a thin red CL rim. The red CL matrix dolomites (TRN and C1) became sometimes more intense toward the rim and showed a concentric zonation in transmitted light. Furthermore, an overgrowing phase on the dull red luminescent matrix dolomite core was visible, starting with non-luminescence and grading into a red thin zone of luminescence. EDX element analysis showed no zonation or chemical change in these matrix dolomite crystals.

The white to beige dolostones had generally planar-e crystals (200-300 µm) or planar-s crystals (160-230 µm). The massive dolomites, polymodal planar-e to planar-s dolostone, have formed in mudstones to grainstone, few containing peloids as mimetic ‘ghost’ structures. A completely dolomitized ooidal grainstone was visible in SEM by the distribution of different sized dolomite crystals, representing the former texture. Some dolostone with planar-e dolomite crystals were coated by a black thin material, possible bitumen, and showed a visible porosity. In component-rich limestones, polymodal, planar-e to planar-s dolostones were formed. This is probable due to an intense dolomitization of the massive limestones, and because the bigger sparite of the grainstones was not as easily dissolved as the former lime mud. In contrast, the unimodal dolomite planar-e dolostone might have formed from wackestones to packstones, where no bigger bioclasts or particles with sizes of more than 1 cm were found. Planar-a dolostones (120-200 µm crystals size) were developed in the lower Upper Jurassic rocks and were frequently dark beige to light brown. In addition, a bigger size and a higher amount of dolomite crystals is described for the pure, massive limestones, compared to the micritic dark colored limestones. In some southern wells (GEN, MST, TRN), the planar-e to planar-s dolostone graded into a planar-a dolostone, starting at different depths (3500-4700 m TVD).

Most dolomite crystals showed a non-luminescence to blue CL core and sometimes a thin red CL rim. This thin red CL phase was only found in dolostone which were intersected in the deep wells. Some cloudy crystal center showed a dull red luminescent, a non-luminescent intermediated phase, and sometimes a last red or non-luminescent thin phase at the clear, transparent rim. Due to the recrystallization process of the dolomite crystals, caused by a higher temperature and a further supply of Mg-rich fluids, the dolomite crystals might have further grown syntaxial and could have formed the clear, transparent rim. In addition, limestone relicts were probable incorporated in the crystal lattice of the dolostone, which explains that some dolomite crystals centers showing the same red CL color of the limestones. Another possibility is that the first matrix dolomite was recrystallized and therefore show the red dull limestone (Reinhold, 1998). Rarely, the thin red CL phase was not developed and/or developed as a very thin phase, and/or showed a concentric zonation with up to 3 phases. In drill cuttings, the dolomite crystals had a reddish-orange luminescent CL, with the beige dolostone cuttings showing an intensive orange luminescent CL.

Vein dolomites had idiomorphic dolomite crystals and showed a concentric to sector zonation of red and non-luminescent CL. The vein dolomite crystals contained a higher amount of Magnesium in EDX, compared to the dolostones. In the deeper Upper Jurassic reservoir (> 3 km), the vein dolomite crystals were dominating at fault systems and in the massive facies. As a result, the vein dolomite formation is bound to fractures and open cavities (void), as dolomite crystals possibly precipitated from an Mg-rich fluid at surfaces. At some wells, e.g. TRN, the dolomite crystals showed no indications of corrosion or dissolution, as the crystal surfaces were smooth and even under SEM. Furthermore, pyrite crystals were developed as framboidal or spherical aggregates (5-20µm) at a growth zone in the vein dolomite crystals and/or in the matrix of the limestones. In addition, vein dolomites were coated by hydrocarbons in some samples. In some dolostone samples, a blue, intrinsic CL of the dolomite crystals was visible. In some samples, a blueish to greenish CL occurred from the blue dyed epoxy resin.

### 5.3.4.3 Calcite cements

In the outcrops thin section samples, the last cement phase was often yellow in CL. In the samples of the deeper basin part, the late vein cements showed a non-luminescent CL or rarely a yellow CL, similar to the shallow rock samples. The yellow phase was sometimes sector zoned with a non-luminescent CL phase, visible in a few cutting thin sections of the deep wells. In addition to thin and thick section, the unprepared drill cuttings were measured. As most fluid inclusions were hosted in transparent vein calcites, cuttings of transparent vein calcites were measured. The vein calcites were always the last cement phase and showed a sector zonation of non-luminescent and yellow CL, with most fluid inclusions hosted in the non-luminescent CL phase (Mraz et al., 2018c).

Only at outcrop sections and at shallow Upper Jurassic carbonate rocks (< 1 km), a dissolution (karstification) and dedolomitization was visible by orange to light orange-yellow CL calcite cements. These dedolomite cements, pseudomorphs of calcite after dolomite rhombs, showed a sector zonation possible due to oscillating conditions. The dedolomitization typically started in the dolomite crystal

centers, with corroded calcite centers, followed by a transparent dolomitic rim. The dedolomite centers had an orange CL, followed by a yellow and dull orange CL rim. At the SCH well dedolomite was visible, which migrated to the overlaying carbonate rocks to dolomite. Only at TRN quartz was visible with a blue CL color as well as under SEM and EDX at drill cuttings. The XRD measurements (Tab. 14) determined for the dark gray, micritic limestones no clay content, but a high calcite content. Therefore, the dark limestones were all nearly pure limestones.

Tab. 14: XRD measurements of the dark gray, micritic limestone of the deeper Upper Jurassic carbonate rocks.

| Sample | Depth [m] TVD | lithology | Description |
|---|---|---|---|
| GEN-1ST-A1 | 4596 | dark gray bioclastic wackestone with bioturbation | 93,9 % calcite, 5,7 % dolomite, 0,3 % quartz, 0,1 % pyrite |
| GEN-1ST-A1 | 4654 | dark gray mudstone with abundant stylolites and thin calcite veins (~ 1 cm) | 96,8 % calcite, 2,6 % dolomite, 0,7 % quartz |
| GEN-1ST-A1 | 4709 | dark gray, bioclastic packstone to floatstone | 99,5 % calcite, 0,1 % dolomite, 0,3 % quartz |
| Hydrocarbon well A1 | 2942 | dark gray, bioclastic wackestone with stylolites | 91,0 % calcite, 3,7 % dolomite, 3,3 % quartz, 2,0 % muscovite |

In all investigated wells, dolomites were found, however restricted in the western Molasse Basin part to fractures (STG, A1, B1). In the eastern wells (MST, GEN, UHA, TRN), massive dolostones within the Purbeckian (upper Tithonian) and Kimmeridgian carbonate rocks were found. Besides, no saddle dolomites were observed in the investigated wells. In this study, only the relative age and an evolution of the pore cements and vein mineralization was established, therefore the relative age in the diagenetic evolution was described.

## 5.3.5 Discussion

### 5.3.5.1 Diagenetic evolution

Due to the in CL visible cement phases, some indications about the geochemical evolution were gained. By CL, SEM (EDX), and XRD studies, a diagenetic evolution of the carbonate reservoir was detected, which is illustrated in Fig. 30. Because of the massive dolostone distribution, the diagenetic dolomite sequence is only valid for the eastern part of the Upper Jurassic reservoir.

The diagenetic evolution of the Upper Jurassic carbonate rocks was subdivided into seven phases: (1) early diagenetic limestone formation, (2) formation of matrix dolomite, (3) formation of dolostone, (4) recrystallization of dolostone, (5) vein dolomite formation, (6) vein calcite precipitation, (7) dedolomitization (Fig. 30). Moreover, the dolomitization was included in the diagenetic evolution of the Upper Jurassic carbonate rocks, which is illustrated in the subsidence plot in Fig. 31.

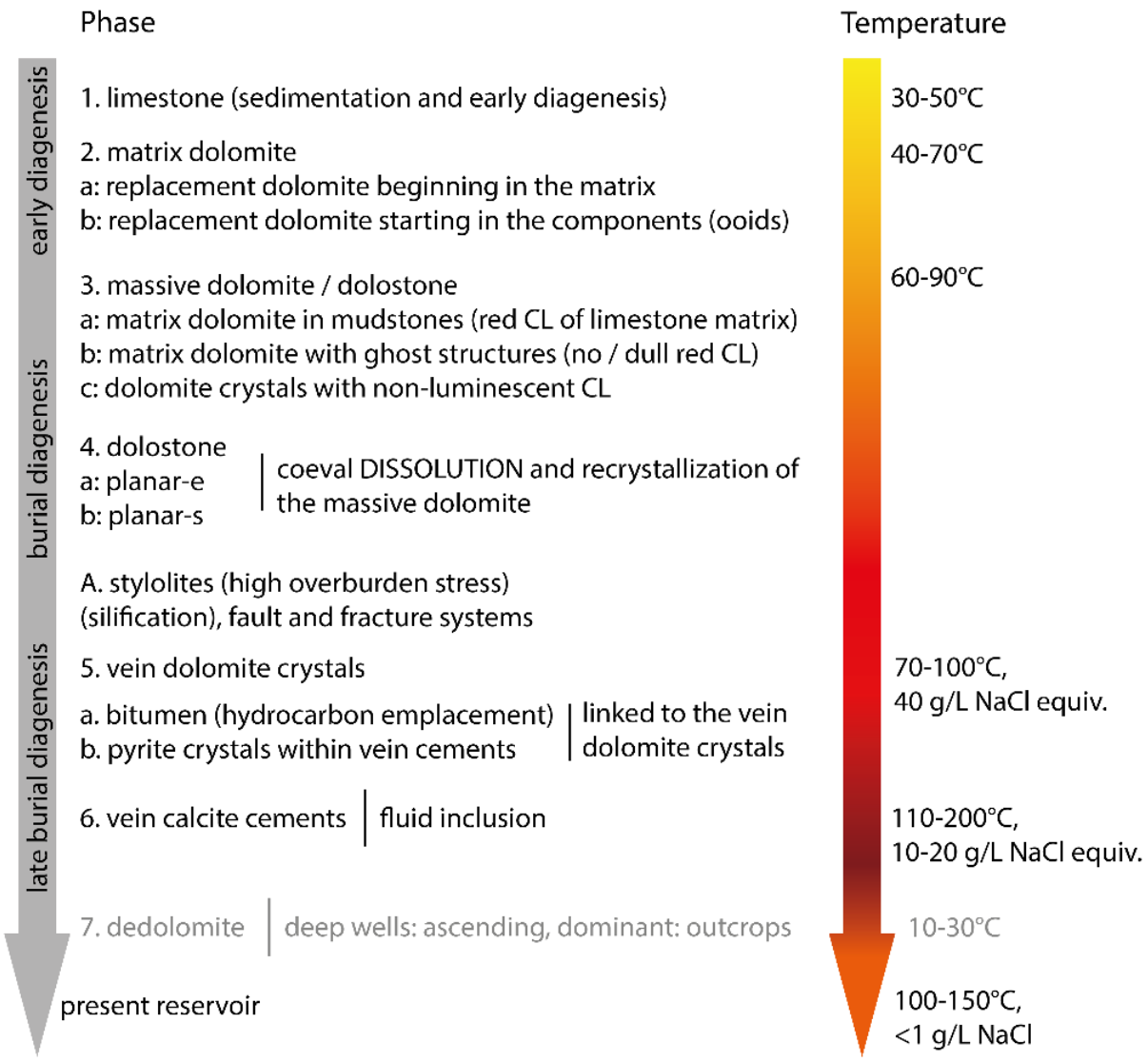


Fig. 30: Diagenetic evolution of the Upper Jurassic cement phases. The temperature and salinity were determined in fluid inclusions studies and by stable isotopes.

**1. Phase - early diagenetic limestone formation**

In our study, most components did show non-luminescent CL (Fig. 32), and only if they were recrystallized a dull red-orange CL. This is confirmed by previous researchers (Wolfgramm et al., 2016; Reinhold, 1996; Liedmann, 1992), which showed that the components such as peloids, ooids and intraclasts showed a dull to bright orange CL with non-luminescing areas in the limestones. Unclear is the development of early cement phases in the wells, which were previously described by Liedmann (1992) and Reinhold (1996) for the outcrop and shallow Upper Jurassic strata. In this study, an intrinsic CL was determined at the outcrop samples which is in line with Liedmann (1992) and Reinhold (1996). The early cements are recrystallized during diagenesis in the southern Molasse Basin and only show blocky cements. Hence, no intrinsic CL was observed at the recrystallized early calcite cements from the wells. The recrystallization of the early cements was first described in the present study for the Upper

Jurassic carbonate rocks in the southern part of the Molasse Basin. Therefore, the early diagenetic cements and phases were influenced and overprinted by the late burial diagenetic phases.

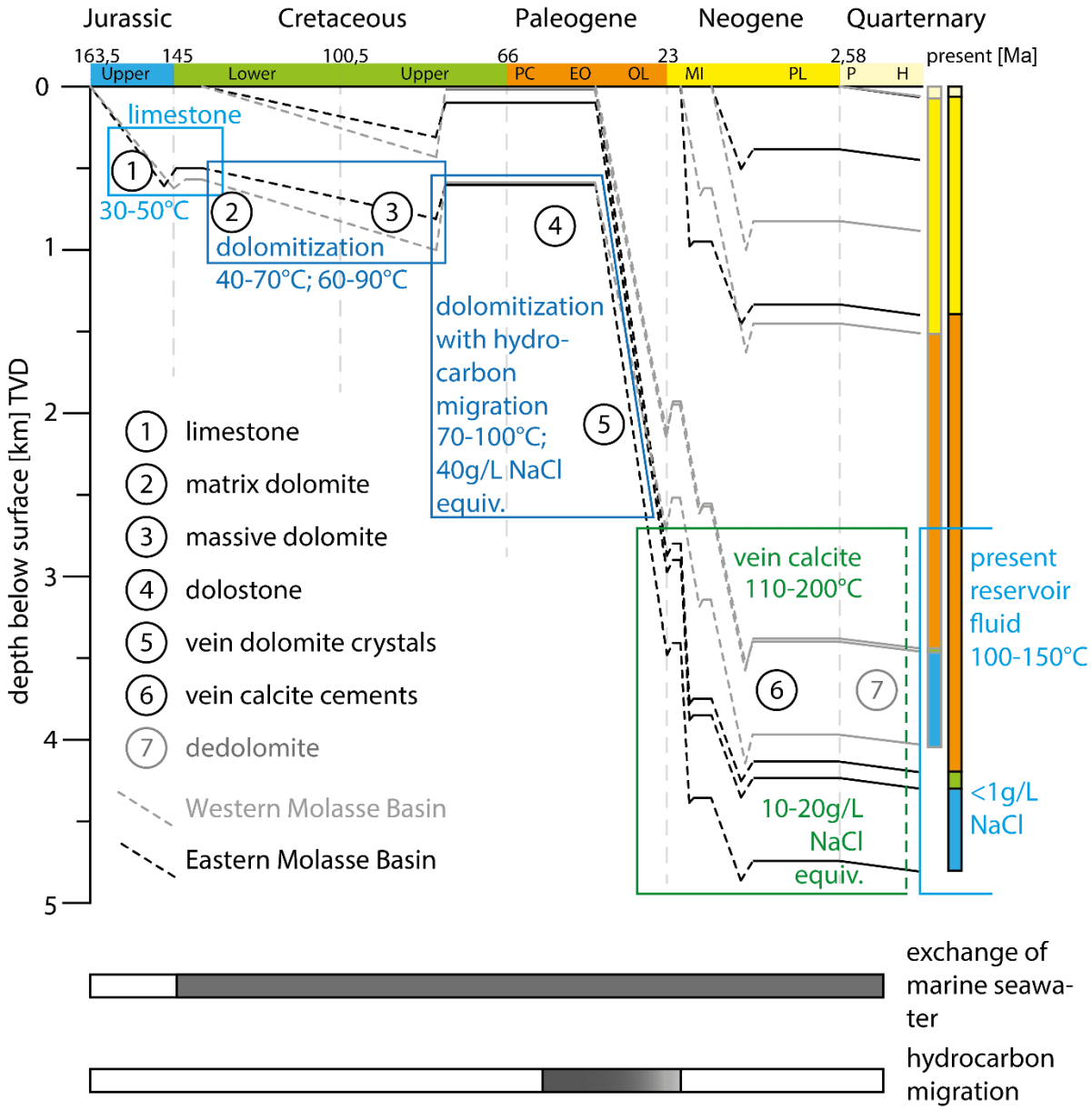


Fig. 31: Subsidence plot with diagenetic evolution for the Upper Jurassic carbonate rocks, divided into the western (gray) and eastern (black) Molasse Basin. The temperature and salinity were determined in fluid inclusions studies and by stable isotope measurements. Due to varying geothermal gradients and no absolute age measurements, the relative depths were assumed.

**2. Phase – formation of matrix dolomite (early burial diagenesis)**

In the second phase, matrix dolomite was formed within the Kimmeridgian and upper Tithonian limestones (Purbeckian). At the matrix dolomites, the geochemistry measurements determined no change in Ca-Mg ratio and no CL zonation, only one phase for the matrix dolomitization was assumed. In all Upper Jurassic carbonate rocks, the matrix dolomite (Fig. 32) was formed as a replacement dolomite either starting in the matrix and cements of the limestones, or in the components such as ooids. Another possible location of the matrix dolomite formation was along stylolites. However, there are no

indications of the genesis of the matrix dolomites at the stylolites. They could either be formed at the dissolution seams, or could be the undissolved remaining rest (Huber, 1987). For the dolomitization a high amount of Mg-rich fluid is necessary (Machel, 2004), which might has preferentially migrated along fractures, or through a high permeable limestone (grainstone) faster than through a dense, micritic Upper Jurassic limestone (Lucia, 2007; Budd and Vacher, 2004). As the Purbeck sediments showed evaporitic to brackish sediments and no significant burial and stylolitization, a shallow marine diagenesis with a reflux model dolomitization in line with Machel (2004) and Adams et al. (2018) has possible caused the stratiform dolomite crystals in the late Upper Jurassic rocks. Therefore, the dolomitization of the Purbeck and Tithonian limestones by matrix dolomite (replacement dolomite) happened probable early diagenetic after the Upper Jurassic deposition. Still unclear is the origin of the Mg-rich fluid and the flow pathways for the Kimmeridgian strata. Previous researchers discussed a Mg-source in the burial compaction fluid (Reinhold, 1996). This compaction fluid migrated from the basinal shale-limestones (bedded facies) to the massive Upper Jurassic carbonate rocks in southern Germany during burial diagenesis (Reinhold, 1998). Furthermore, at the Upper Jurassic reservoir, the Kimmeridgian and Purbeckian carbonate rocks contain the highest amount of matrix dolomite (Beichel et al., 2014; Böhm et al., 2010). Therefore, the Upper Jurassic dolomite formation and dolomite distribution was controlled by the depositional and diagenetic fabric, as it is described for other dolomite geobodies (Makhloufi et al., 2018; Di Cuia et al., 2011; Baqués et al., 2010; Dawans and Swart, 1988). However, the dolomitization of matrix dolomite does not increase the porosity of the dolomitized limestone, as generally a slight decrease in porosity is observed with up to 50 % matrix dolomite (Murray, 1960). Accordingly, matrix dolomite has a minor influence on matrix permeability.

**3. Phase – formation of dolostone (early burial diagenesis)**

As the dolomite crystal centers were cloudy and overgrown by a transparent thin rim at the dolostones (Fig. 32), we suggested that some matrix dolomite crystals might have grown further and formed the massive dolostones. As a result, the formation of massive dolomites and dolostones occurred after the matrix dolomitization in the Upper Jurassic carbonate rocks. Some mimetic dolostones indicate in optical and CL microscopy a former micritic limestone such as a peloidal packstone (Fig. 32), which was unexpected. Usually, dolostones form in limestones, which contain a low amount of trace elements and insoluble residue (Koch et al., 2010; Koch, 2000; Bausch, 1994). In addition, a higher amount of bigger dolomite crystals was found in the pure, massive limestones compared to the micritic, dark limestones, which was also previous described for the Upper Jurassic carbonate rocks by Böhm et al. (2010) and Koch et al. (2010). For this reason, the white to beige planar-e and planar-s dolostones of this study indicate particle-rich limestones, which relate after Böhm et al. (2010) to mud losses during drilling and to high-permeability areas. Besides, some dolostones were probable formed under reducing conditions, as pyrite crystals are preserved in dolomite crystals and in the limestone matrix. Those dolostone, associated with a pyritic limestone are described in other studies to be Fe-rich (Wolfgramm et al., 2016; Reinhold, 1996; Liedmann, 1992).

**4. Phase – recrystallization of dolostone (early burial diagenesis)**

After the first massive dolomites and dolostones were formed, the dolomitization process was probable interrupted by a dissolution phase and recrystallization of the calcite and dolomite crystals. This could have occurred by a change in fluid migration. Due to the still continuing burial diagenesis, the fluid flow in the Upper Jurassic reservoir could have interact with ascending basement fluids or descending meteoric fluid along fractures and faults, as described by fluid inclusion data (Mraz et al., 2018c). By this change in fluid migration, the micritic matrix of some dolomitized mudstone to packstone limestones was probable dissolved, as the fine-grained micritic matrix (former lime mud) possess a higher reactive surface than the dolomites. This dissolution process is known to occur at matrix dolomites in micritic limestones (Machel, 2004). Due to the dolomitization in the micritic limestones, a migration of fluids might have existed, which was reused by the further migration of corrosive fluids. Consequently, the dolomite crystals remained as relicts and formed the porous planar-e dolostones. Our hypothesis is that dolostones showing a dull red CL in the center can be former matrix dolomites, which have incorporated the limestone matrix within the crystal lattice or be mimetic dolomite. This recrystallization process of massive dolostones is in line with previous study by Reinhold (1998). There could also be a further precipitation and crystal growth of dolomite (dolomite cementation) (Machel, 2004), which could have increased the amount of dolomite crystals and could decline the pore space and thereby the porosity. This dolostones showed a blue CL core, and is in line with Reinhold (1996).

Unexpected was the occurrence of planar-e and planar-s dolostone in the Upper Jurassic reservoir (Fig. 32), which has a temperature of around 100-150°C today. Studies have shown that dolomite crystals recrystallized above the critical roughening temperature at around 50-60°C to a nonplanar (planar-a) dolomite texture (Machel, 2004; Warren, 2000; Sibley and Gregg, 1987). The fluid study by Mraz et al. (2018c) showed a dolomite formation temperature in the range of 40-90°C in the Upper Jurassic carbonate rocks, which is below and above the critical roughening temperature. However, the assumed recrystallization of the planar-e or planar-s dolostones of the Upper Jurassic was not visible, as the process might be very slow or has not started so far. The planar-e dolostone were further coated by bitumen, indicating a high-permeability for hydrocarbons during the burial diagenesis. At high productive wells (e.g. TRN), planar-e to planar-s dolostones are still preserved, which can control the high-permeability in the Upper Jurassic reservoir.

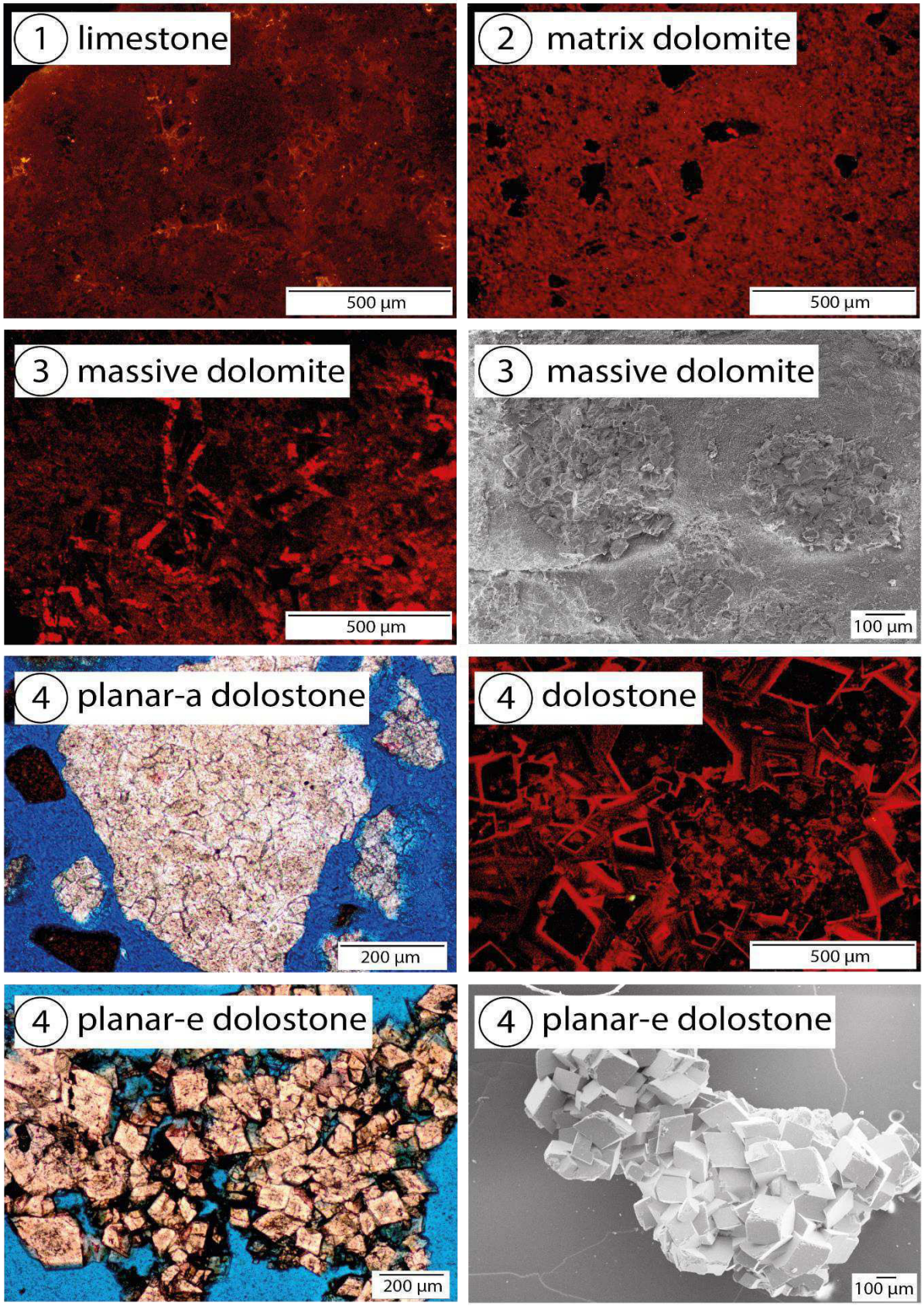


Fig. 32: Cathodoluminescence (CL), transmitted light and scanning-electron microscope images (SEM) of the Upper Jurassic carbonate rocks divided into the diagenetic phases (Fig. 31). (1) Limestone in CL with a red to dull red luminescent matrix. (2) Matrix dolomite with no CL. (3) Massive dolomite with a dark center and a thin red luminescent rim, showing in parts mimetic textures (SEM). (4) Recrystallized dolostones, with planar-e and planar-a dolostone in transmitted, CL and SEM.

**5. Phase – vein dolomite formation (late burial diagenesis)**

During the burial diagenesis and the Alpine orogenesis, faults and fracture systems developed, as well as stylolitization due to overburden stress of the overlying strata. The nearly idiomorphic, coarse-grained, Mg-rich dolomite crystals (vein dolomite) (Fig. 33) indicated high permeable pathways at former surfaces and open-space, and therefore a fracture-controlled fluid flow. The fluid inclusion data (Mraz et al., 2018c) show temperatures of 70-100 °C, which indicate that a hydrocarbon emplacement was possible contemporaneously in the southern Molasse Basin. During that time, the Upper Jurassic aquifer contained still a saline fluid, liquid and/or gaseous hydrocarbons, and pyrite minerals in the carbonate rocks. The occurrence of pyrite crystals indicates that reducing conditions were present in the carbonate aquifer during the late burial diagenesis. In contact to meteoric fluids, the Upper Jurassic aquifer might have become oxidized. Hence, the stability of the Fe-ions, which were incorporated in the dolomite crystal lattice, varied between the $Fe^{2+}$- (no CL) and $Fe^{3+}$ ions (red CL). A study by Hiatt and Pufahl (2014) showed that pyrite formation removes Fe from the pore water, whereas the pore water becomes $Mn^{2+}$ enriched. By this process, the cathodoluminescence intensity increase of the formed cement phase because of the $Mn^{2+}$ enrichment. The vein dolomite crystals showed a concentric to sector zonation in CL and might have formed under changing conditions, which could be explained by the Fe stability variation. For the dolomitization of the vein dolomite crystals, a burial seawater dolomitization was assumed, as the fluid inclusions in the vein dolomite crystals showed a salinity of around 40 g/L at temperature between 70-100°C (Mraz et al., 2018c). The dolomitization fluids were probable interacting between compaction, thermal convection and fluid flow along fractures zones in the Upper Jurassic reservoir. At two wells, where a bigger fault zone was encountered, the dolostones were composed of a dolomite breccia. The dolomite breccia consisted of transparent to slight beige dolostone clast (non-luminescent) within a dark gray or beige fine-crystalline, dull red CL dolomite matrix (Fig. 33). Because the dolostone clasts showed a thin red CL rim, the fourth phase of dolomitization was developed (Fig. 31) and the brecciation must have happened afterward. Therefore, this dolomite breccia could have possibly formed by fast ascending fluids along the high permeable fracture areas. The occurrence of dolomite breccia for the Upper Jurassic reservoir was described by Reinhold (1998) and slightly similar for the Latemar platform by Jacquemyn et al. (2014). In all dolomite rock samples no saddle dolomite was found, which was expected as in other geological conditions saddle dolomites are described with formation temperature above 100°C e.g. (Sirat et al., 2016; Di Cuia et al., 2011; Machel, 2004).

**6. Phase – vein calcite precipitation (late burial diagenesis)**

A possibility is that the last yellow CL phase (Fig. 33) is influenced by meteoric water, as the fluid inclusions hosted the least saline fluids (Mraz et al., 2018c) due to a dilution process. Non-luminescing fracture calcites were described within the shallow boreholes of the Molasse Basin (BLZ2) (Liedmann, 1992). A light yellow to light orange CL was visible at late vein calcite cements, which contained fluid inclusions with modified marine formation waters at shallow Upper Jurassic rock samples (Liedmann, 1992). Consequently, the vein calcite cements were found at the shallow and deep Upper Jurassic aquifer and hence are consistent within the Molasse Basin. The vein calcite cements are predominantly found

at thin former fractures (< 1 mm aperture), resulting in a loss of pore space. Consequently, the vein calcite cements decrease the porosity of the Upper Jurassic carbonate rocks.

**7. Phase – dedolomitization (late burial diagenesis)**

The concentric zonation of dedolomite cements (Fig. 33) is due to oscillating conditions, which is in line with previous studies (Koch, 2011; Liedmann, 1992). The shallow Upper Jurassic carbonate rocks (< 1.0 km) were affected by meteoric and near-surface waters for a longer period than the deeper Upper Jurassic reservoir, which enhanced the process of dedolomitization and the precipitation of late calcite cements within the former pore space (Reinhold, 1996; Liedmann, 1992; Meder, 1987; Bausch et al., 1986). Therefore, it was assumed in this study that no dedolomitization should be found in the deep basin part (> 2 km). However, in one investigated well (SCH), dedolomite was found, which graded into dolomite crystals at the top of the Upper Jurassic reservoir. Consequently, we assumed that an ascending corrosive fluid flow occurred, causing the dedolomitization in this part of the deeper reservoir.

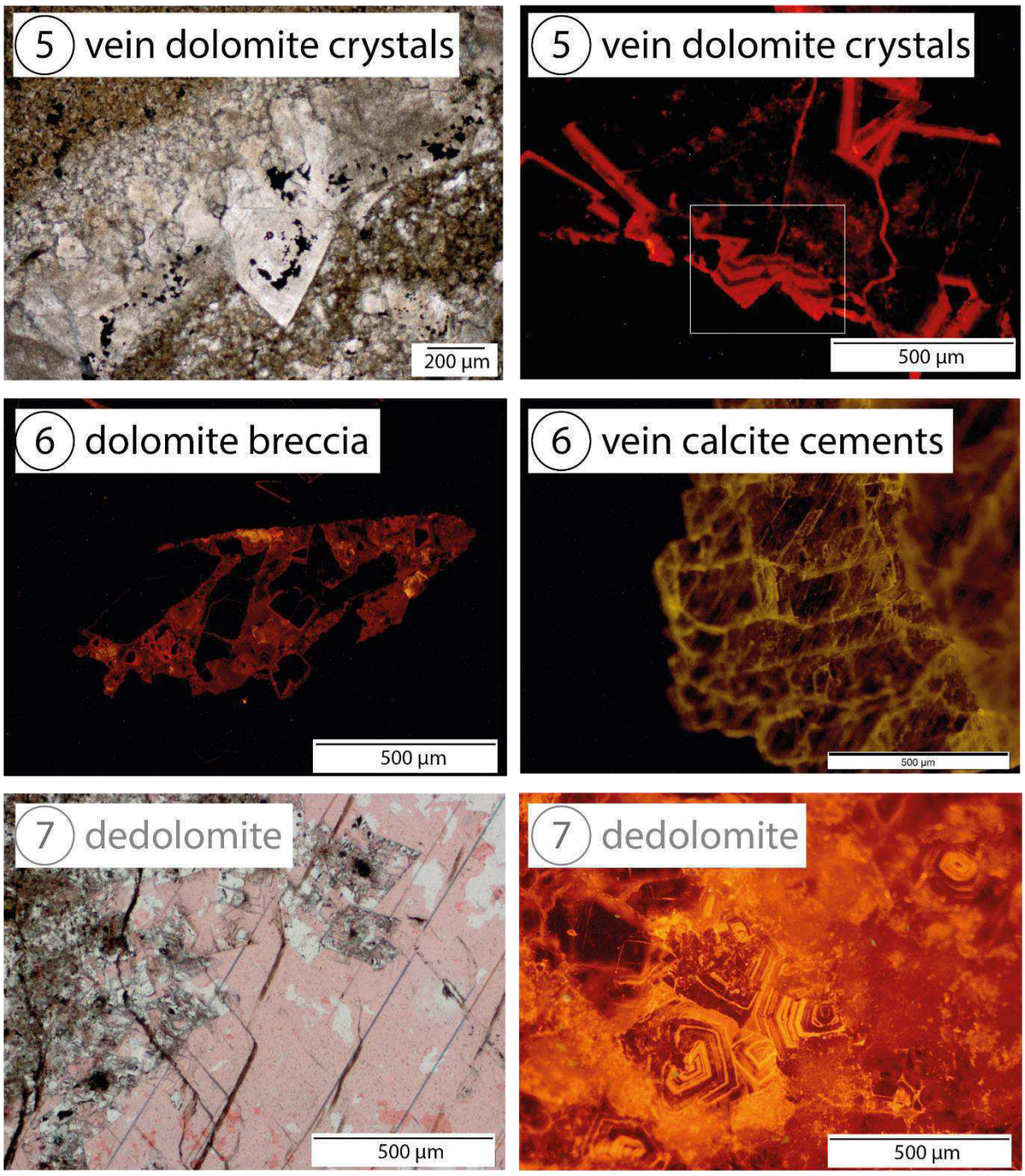


Fig. 33: Cathodoluminescence (CL), transmitted light and scanning-electron microscope images (SEM) of the Upper Jurassic carbonate rocks divided into the diagenetic phases (Fig. 31). (5) Vein dolomite in transmitted light with pyrite (black) at a growth zone, in CL displaying a sector zoned red luminescence. (6) CL image of the dolomite breccia; vein calcite cements hosting the 2-phase fluid inclusions with a yellow CL, in parts sector zoned. (7) Transmitted light image of an alizarin stained dedolostone, with the recrystallized dolomite rhombs; CL image of a dedolostone showing a concentric zoning of the calcite crystals and the former cloudy dolomite rhombs.

### 5.3.5.2 Porosity and Permeability

The porosity and permeability reduction of the Upper Jurassic carbonate rocks by diagenesis can be caused by (i) compaction, (ii) recrystallization, (iii) replacement, and (iv) cementation, which is in line with global carbonate studies (Ahr, 2008). In this study, indications of compaction in the bedded facies (limestones) and dolostones were found, and a recrystallization of the dolomite crystals in the fourth phase (Fig. 33) and from the planar-e to planar-a dolostones was visible. Besides, vein cements of dolomite and calcite were found, as well as dedolomite. As a result, the interaction between these discussed processes can cause a decline in porosity in the Upper Jurassic carbonate rocks from the southern part of the Molasse Basin.

The planar-e to planar-s dolostones showed a high porosity in this study, and usually provide a high intercrystal porosity and a positive correlation between porosity and permeability (Woody et al., 1996). This was further confirmed at the Scherstetten wells in the Upper Jurassic carbonate rocks (Koch et al., 2010). In contrast, planar-a dolostones with small crystals sizes have a low-permeability in the Upper Jurassic strata (Koch et al., 2010). Moreover, the dark beige to light brown dolostone were probable formed above the critical roughening temperature of 50-60°C (Warren, 2000), as they contain planar-a dolomite and the formation temperature range between 40-90°C (Mraz et al., 2018c). According to Woody et al. (1996) the dolomite permeability is not directly related to the total porosity or crystals size, but depends on the connectivity of the pores via pore throats. These pore throats are in turn based on the number and size of the pore throats (Woody et al., 1996), which were described for the massive Upper Jurassic carbonate rocks with maximums at 0.5 µm, 8.0 µm and 25 µm (Koch et al., 2010). The effective porosity of the dolomitized massive facies is around 10-30 % in intercrystalline pores in southern Germany (Beichel et al., 2014; Böhm et al., 2010; Koch et al., 2010; Koch and Sobott, 2005). Consequently, planar-e to planar-s dolostones cause a high-permeability of the matrix with 3 x $10^{-18}$ m² to 6 x$10^{-14}$ m² (Birner, 2013; Koch and Clauser, 2006; Bertleff et al., 1988), however fractures show a permeability between 6.7 x $10^{-13}$ and 6.7 x $10^{-11}$ m² (Bertleff et al., 1988) in the Upper Jurassic carbonate rocks. Planar-e to planar-s dolostones show flow pathways along intercrystal pores with a permeability of 1.9 x $10^{-17}$ m² to 3.6 x $10^{-13}$ m² (porosity 7.9-16.8 %) in carbonate rocks from North America (Bennion and Bachu, 2010). Thus, planar-e to planar-s dolostone have a high-permeability and can provide a reservoir for fluids.

In general, according to (Pagel, 2000) it is unlikely that carbonate cements form with identical composition and simultaneous over several tens of kilometers in aquifers, especially when there are preferential flow pathways. However, this study showed that the main cement phases, the dolomites and vein calcites, can be found within the Upper Jurassic in the eastern Molasse Basin in Bavarian. This could indicate that processes were very slow, or fracture systems and fault zones channeled the fluids to distribute nearly equally within the Upper Jurassic reservoir of the Molasse Basin. A challenge was at the investigated boreholes, that usual a highly dolomitized facies and a fault zone were encountered. Therefore, the dolomitization either facies-controlled or fracture-controlled could not be distinguished. But what was found is that the planar-e to planar-s dolostones provide the main matrix permeability in

the Upper Jurassic reservoir today and dominate in the Kimmeridgian and Purbeckian rocks. In contrast, limestones and planar-a dolostone only have an insignificant porosity. The dark rock color of the Upper Jurassic limestones occurs probable due to a high organic content, as the XRD measurements found no clay minerals. Therefore, the higher amount of insoluble residue is only minor for the Upper Jurassic carbonate rocks. In this study, as the planar-e dolostones showed mimetic structures of peloids and ooids, we assumed that the planar-e dolostones are former matrix dolostones, where the limestone matrix was dissolved during the fourth diagenetic phase.

However unclear was, if the high-permeability areas of the Upper Jurassic reservoir were highly dolomitized or if the dolomitization (overdolomitization) was stopped by the descending meteoric or ascending fluids preserving the pore space. At high productive wells (e.g. TRN), the planar-e dolomite crystal surfaces were smooth under the SEM, and hence indicate a dolomite stability in the present reservoir fluid. Besides, the hydrocarbon coating of the planar-e dolostones, which was found in high- and low-permeability wells today, indicate previously similar flow pathways for hydrocarbons. Therefore, the development of the low-permeability was probable after the hydrocarbon emplacement. We assume by the distribution of the lowly permeable planar-a dolostone and formation temperature above 50-60°C, that the deeper Upper Jurassic carbonate rocks only developed planar-a dolostones. In consequence, there is no overdolomitization, but maybe a further influence from compaction. In the high-permeability areas, due to a higher influence of possibly cold meteoric waters, the recrystallization of planar-e dolostone to planar-a dolostone was probably prevented. In addition, these areas have a low saline reservoir fluid and low temperature today. At the low-permeability areas, the reservoir temperatures are relatively high, indicating no strong interaction with fluids. Therefore, the recrystallization is and was favored at those sites.

### 5.3.6 Conclusion

On the basis of our results, the Upper Jurassic carbonate rocks of the North Alpine Foreland Basin encompass four different dolomite types: (1) matrix dolomite (replacement dolomite), (2) planar-e dolostone, (3) planar-s dolostone, (4) planar-a dolostone. The matrix dolomites were formed in the matrix or cements of limestones or in components, such as ooids. The dolostones were preferentially formed in massive limestones, grainstones to bindstones, and are distributed within the Kimmeridgian and Tithonian carbonate rocks. Thereby, the dolostones dominantly grew in the upper Kimmeridgian and upper Tithonian (Purbeckian). The matrix dolomites rarely formed at stylolites or were concentrated at stylolites during the dissolution process of stylolitization. Due to recrystallization processes and still visible diagenetic features, such as the planar-e dolostones and CL zonation, it was assumed that the dolomites of the Upper Jurassic have formed after the sediments of the Upper Jurassic have been deposited. The dolomites of the Purbeckian (late Tithonian) were probable formed by an evaporitic reflux dolomitization and the Kimmeridgian carbonate rocks were dolomitized by a burial modified seawater. Due to a dissolution and recrystallization phase in the dolomitized limestones (matrix dolomite) during the early Paleogene, porous planar-e to planar-s dolostones were formed, which provide areas with the highest matrix permeability of the Upper Jurassic carbonate rocks. Moreover, in

the North Alpine Foreland Basin development, stylolitization happened and fractures were formed. These fractures are in parts cemented by calcites, which decrease the porosity of the carbonate rocks. Today, planar-e dolostones dominate at less saline, high-permeability areas of the Upper Jurassic reservoir, mainly in the Molasse Basin in eastern Bavarian. The planar-a dolostones do not provide necessary flow pathways and usually dominate at greater depths. The established diagenetic sequence through petrographic, microscopic and geochemical analysis is applicable, with exceptions of the dolostones, to the complete Upper Jurassic, either at the outcrop area or in the covered southern part of the Molasse Basin. In addition, this study first describes the occurrence of planar-e dolostone formation and their location at high-permeability areas. In contrast, planar-a dolostones were observed at low-permeability areas and at greater reservoir depths. Unclear remains the interaction of the fault systems with high-permeability facies zones, which were usually encountered in the wells. Therefore, the overlapping processes could not be detailed analyzed such as facies-controlled dolomitization vs. fracture-controlled dolomitization, and massive facies vs. bedded facies. Future studies of the Upper Jurassic carbonate rocks should analyze the different cement generations in detail by geochemical studies to test the aforementioned diagenetic evolution. In addition, wells should be selected for investigation which either truncate a fault zone or a highly permeable facies to characterize differences in dolomitization. This study showed that for the geothermal reservoir exploration it is necessary to understand the formation of the high-permeability, planar-e dolostones to find high productive areas. Based on our results, this development might depend on meteoric, diagenetic fluids, which were so far not classified and described in detail.

# 6 Synoptic Discussion

Several authors have attributed the low-permeability of the Upper Jurassic reservoir in the past to the dense, micritic Helvetian facies, and/or a lower degree in karstification, and due to higher temperatures and pressures during diagenesis in the south. Unclear was, what effects the higher temperature and pressure, through overburden load and tectonic stresses, had on the Upper Jurassic reservoir rock mass. Seismic exploration helped to better identify karst structures and fault patterns through 3D imaging (Hartmann et al., 2016), however seismic survey data are not applicable to image, to explain and to understand the permeability distribution related to microfacies and diagenesis, as these geological controls are below the seismic resolution.

This detailed study identified two possible reasons which caused the decrease in permeability of the Upper Jurassic reservoir toward the south of the Molasse Basin: (I) a change in depositional facies, and (II) differences in diagenesis and a higher compaction of the carbonate rocks. In the following section both reasons are discussed in detail.

## 6.1 Change in depositional facies

Porosity and permeability studies of the hydrocarbon industry described that a micritic, dense limestone (mudstone to wackestone) has low to no porosity and thereby no permeability (Lucia, 2007; Budd and Vacher, 2004). In southern Germany, the micritic, dense Helvetian facies was assumed to dominate the facies realm of the southern Molasse Basin causing a decline in well productivity (Birner, 2013; Meyer and Schmidt-Kaler, 1989; Schneider, 1962). This study contradicts this assumption and reveals the occurrence of a transition zone facies in the southern part of the Molasse Basin, which can explain the decrease in well productivity to a certain degree, and that the Helvetian facies is not developed in the southern part of the Molasse Basin.

This study showed that dark, micritic limestones with pyritized, planktonic organisms and a high organic content occur in the investigated wells in the lower Upper Jurassic (Fig. 34). The overlying carbonate rocks are gray to light gray and by their microfacies similar to the massive facies of the Franconian and Swabian facies (Fig. 35). In the area around Munich, these dark, micritic limestones are not found and the carbonate rocks were classified into the Franconian facies (Beichel et al., 2014; Wolfgramm et al., 2011; Böhm et al., 2010; Koch et al., 2010). In addition, the Kimmeridgian and Tithonian carbonate rocks of the Franconian facies provide sufficient flow rates for a geothermal application for example at the sites Unterhaching (Beichel et al., 2014) and Kirchstockach (Wolfgramm et al., 2011) in the Munich area (Wolfgramm et al., 2012).

In Switzerland, the Helvetian facies is characterized by dark, micritic limestones with a high abundance of tintinnids (calpionellids) in the late Upper Jurassic (Mohr and Funk, 1995; Mohr, 1992). As dark, micritic limestones are present with abundant planktonic organisms but no calpionellids in the lower Upper Jurassic in the southern part of the Molasse Basin, and as the Purbeck facies is developed at every

investigated well, this study suggests that the Helvetian facies is not present in the southern Molasse Basin. Instead, a change in depositional environment at the beginning of the Upper Jurassic is suggested with the development of the transitional facies, which migrated into a depositional environment similar to the Franconian and Swabian massive facies in the Kimmeridgian and Tithonian at the investigated boreholes. This development of the lower Upper Jurassic is newly called transition zone facies, which contains planktonic organisms like radiolaria, foraminifera and crinoids (*Saccocoma* sp.) in a dense, dark gray, organic-rich, pyrite-containing, micritic mudstones to wackestones. Consequently, this development of the depositional environment reflects a transition zone facies in the lower Upper Jurassic on the deeper part of the Franconian platform and not the Helvetian facies. In addition, at every investigated well, a similar sea level trend is assumed as the Upper Jurassic strata overlies a calcareous, glauconitic sandstone with abundant chamosite- or Fe-ooids of the Middle Jurassic, and the Upper Jurassic strata ends with the brackish to evaporitic Purbeckian facies. Therefore, the Franconian and Swabian platform rim and the beginning of the Helvetian shelf must be situated further south, possibly below todays Alpine orogenic belt, as a basin-wide regression-transgression-regression trend was found.

A tectonic activity was described to be present during the Upper Jurassic deposition (Mraz et al., 2018a), which was indicated by the varying thickness of the Upper Jurassic strata in this study. In the investigated wells where the carbonate rocks are developed in the massive facies, a similar water depth and sediment thickness was suggested. Hence, the thickness increases from the area around Lake Constance (400 m) to the south of Munich (600 m) and decrease to eastern Bavaria (400 m) might be influenced by syn-tectonics. Alternatively, the paleo-surface of the epicontinental Tethys could have caused these thickness variations and further tectono-stratigraphic studies are needed to explain these differences in the Upper Jurassic sediment thickness.

Even though the transition zone facies is developed instead of the Helvetian facies, and the massive carbonate rocks of the Franconian facies are intersected in the southern investigated wells, the carbonate rocks have low to no matrix porosity in the Kimmeridgian and Tithonian section. Nearly every primary pore space is either filled with cements or with solid hydrocarbons. As a result, the carbonate rocks show no porosity and well productivity. Moreover, at the GEN well the bedded facies is developed probably during the late Kimmeridgian (Fig. 35), which is underlying and overlying the massive facies. Hence, it is assumed that the bedded facies was deposited in small basins between massive structures (e.g. algae-build ups), which existed for a short period. This development of small basins between massive structures has been described in seismic interpretation for the Munich area (Fritzer et al., 2012), but not for the southern part of the Molasse Basin. However, the development of these dense, bedded carbonate rocks can further decrease the permeability.

As a consequence, low porosity and permeability can be expected in these carbonate rocks of the southern part of the Molasse Basin. The results of the GEN well showed a low well productivity and a high well injectivity (Wolfgramm and Thiem, 2018). Moreover, the observed total mud losses during drilling operation and the brecciated core from the fault zone in addition to the hydraulic well tests, a hydraulically fractured rock of very low porosity was indicated. This reservoir rock is characteristic for

petrothermal systems and the GEN well could be developed with petrothermal technologies, i.e. smaller diameters for lower flow rates. The overall results indicate a new play type in the Upper Jurassic reservoir, especially the transition zone facies, which formed the tight reservoir rock, which might be suitable for petrothermal technologies When faults in the transitions zone, and in the dense, southern massive facies are accessed, the high hydraulic conductivity of these faults can establish a natural heat exchanger, and probably hydraulic stimulation can be avoided. Unclear remains the black rock color of the transition zone facies, as no detailed study of the organic content was made. The XRD measurements indicate a low clay content, which confirmed the assumption of a high organic content.

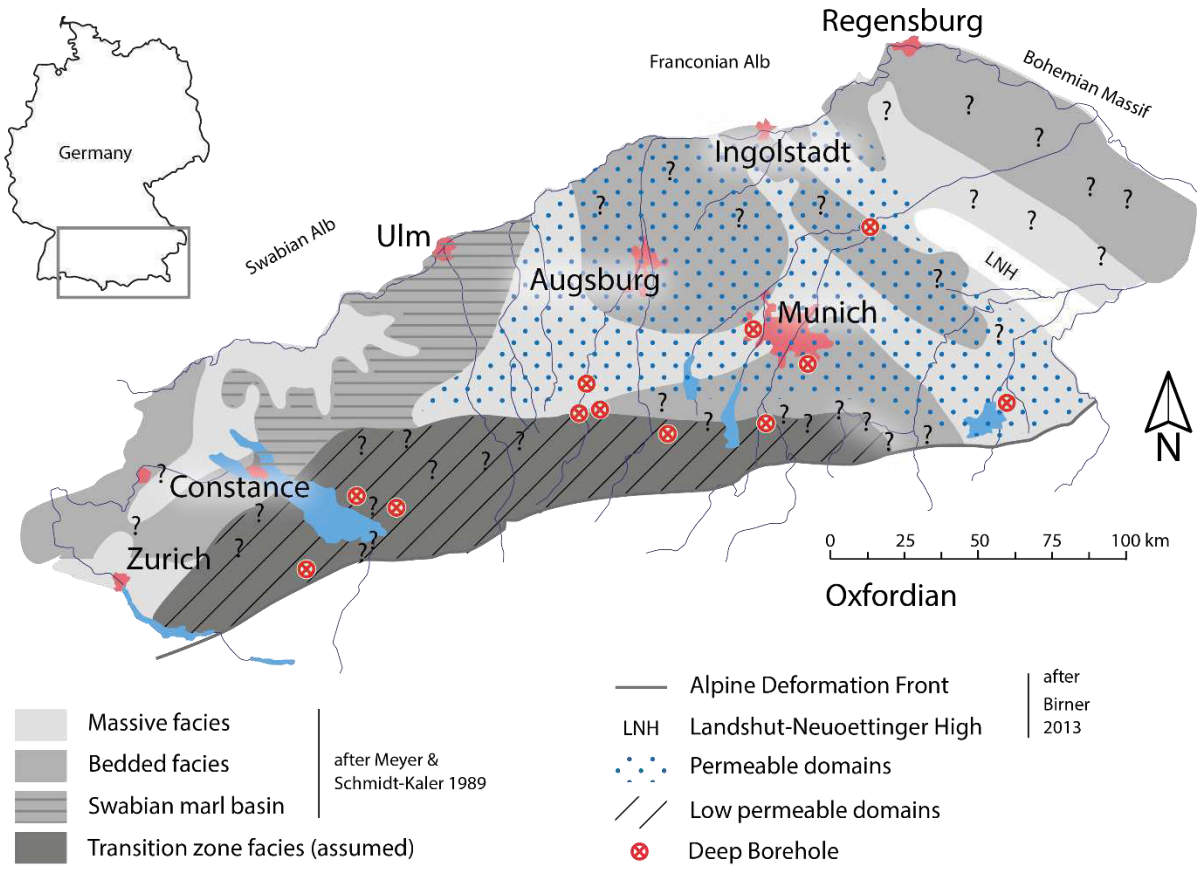


Fig. 34: Assumed distribution of the depositional environment and permeable domains for the Upper Jurassic during the Oxfordian based on the evaluated data. The bedded and massive facies, as well as the Swabian marl basin are after Meyer and Schmidt-Kaler (1989), with the new described transition zone facies.

Another hypothesis for the permeability decrease was the lower degree of karstification, which might have affected the southwestern part for a shorter period (Koschel, 1991; Strasser, 1988; Villinger, 1988). The first possible phase for subaerial exposure and erosion was at the end of the Upper Jurassic sedimentation (Purbeckian) and the beginning of the Lower Cretaceous. In the middle and eastern investigated wells, the first Cretaceous sediments are of Hauterivian age, thus the minimum subaerial exposure was for around 13 Ma. In contrast, at the westernmost wells (STG and A1) the overlying sediments are Oligocene, implying a longer period for karstification. In the two investigated wells, A1 and MST, calcareous, glauconitic quartz sandstones were intersected within the Upper Jurassic strata,

which indicates karst structures filled with Lower Cretaceous rock within the Upper Jurassic carbonate rocks. Accordingly, the Upper Jurassic rocks were karstified with an increase in karstification to the southwest, and in some areas these karst structures are filled with Lower Cretaceous sediments. For this reason, the lower degree in karstification has not been confirmed in this study. Instead, a longer karstification was determined causing no increase in well productivity in the western part of the Molasse Basin. This is probably due to the cemented and filled karst structures.

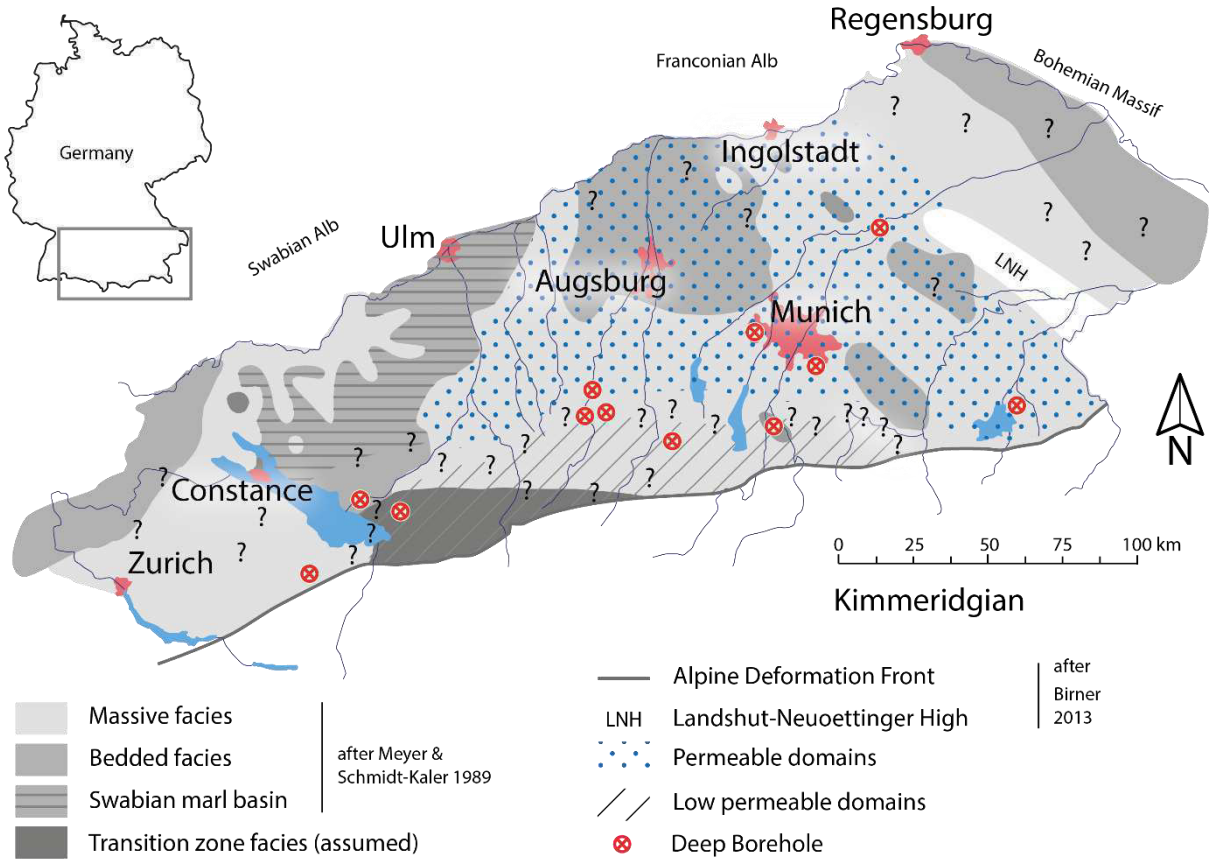


Fig. 35: Assumed distribution of the depositional environment and permeable domains for the Upper Jurassic during the Kimmeridgian based on the evaluated data. The bedded and massive facies, as well as the Swabian marl basin are after Meyer and Schmidt-Kaler (1989), with the new described transition zone facies in the southern part of the Molasse Basin.

## 6.2 Diagenesis

Because fluid inclusions and stable isotopes are affected during diagenesis, the isotopic ratio and fluid inclusions stored in the carbonate rocks document the fluid evolution and diagenesis of the Upper Jurassic rocks in the Molasse Basin. In this study, four main types of paleo-fluid were distinguished:

(1) Upper Jurassic seawater,

(2) meteoric water,

(3) basinal water, and

(4) evaporated or diagenetic fluids with a high salinity.

Thereby the diagenetic evolution was divided into five main phases:

(I) sedimentation,

(II) early diagenesis and first dolomitization,

(III) burial diagenesis and second dolomitization,

(IV) late burial diagenesis (at fracture and fault systems), and

(V) the present reservoir.

This diagenetic evolution was previously described by Liedmann (1992) and Reinhold (1996) at the shallow Upper Jurassic reservoir and outcrops in the Franconian and Swabian Alb. The diagenetic evolution was extended in this study to the south and by the new (III) burial phase with second dolomitization. As previous studies focused on the shallow Upper Jurassic reservoir and outcrops, this study extended the diagenetic evolution to higher temperatures and pressures with up to 200°C. In addition, by the stable isotopes and fluid inclusion data the dolomitization window by Reinhold (1996) was expanded to higher temperature and to lower $\delta^{18}O$ values, as well as the Geo-1 equation (stable isotope geothermometer) by Liedmann (1992) to temperature above 110°C. In the present study, the diagenesis started with the limestones formation in phase (I) and (II) at depths between 200-400 m ($\delta^{18}O$ values -3.4 to -5.4 ‰ PDB) and temperature in a range of 40-50°C in the basin-wide Upper Jurassic strata. The first dolomitization appeared with matrix dolomite (replacement dolomite) and massive dolomitization by meteoric and basinal fluids at 50-70°C ($\delta^{18}O$ values -4.5 to -7.5 ‰ PDB) during early and burial dolomitization (phase II and III). Subsequently, the second dolomitization (phase III) occurred at 70-100°C, precipitating nearly idiomorphic vein dolomite cements, probably followed by a hydrocarbon emplacement with temperatures between 120-136°C. The salinity of the second dolomitizing fluid is with 40 g/L slightly increased compared to the Upper Jurassic seawater with 35 g/L (Liedmann, 1992). The hydrocarbon emplacement was further indicated by a decrease in $\delta^{13}C$ values and might be in addition influenced by meteoric fluids. During the late burial diagenesis (phase IV), first white (110-140°C) and afterward transparent (140-200°C) calcite veins were precipitated, indicating a first basinal and a second meteoric influence. These two vein calcites are usually less saline (12-17 g/L) compared to the Upper Jurassic seawater but show in the southwestern area an increase in salinity with up to 112 g/L. Due to the high $\delta^{18}O$ values with +5.5 ‰ SMOW, the salt source might be evaporitic brines. In contrast, the present reservoir has the least saline reservoir water with < 1 g/L, and indicate an increase in salinity to the southwestern part of the basin with up to 18 g/L. Moreover, in the outcrop samples a calcite cement phase was determined which was influenced by karstification and dedolomitization. The diagenetic evolution as described in chapter 5.3 was confirmed in all investigated wells, and slightly modified in the outcrop areas. There, the late burial diagenesis is more developed caused by uplift and exposure as indicated by karstification and dedolomitization at the Franconian and Swabian Alb. A possible salt source for the high saline fluids in the Upper Jurassic was assumed to be the Purbeck, Oligocene (Lemcke, 1988; 1976) or Upper or Middle Triassic sediments (Reinhold, 1996), but this study supposes the salt source in the brackish to evaporitic Purbeck sediments.

The investigated diagenetic evolution, especially of the dolomites, was divided into seven phases by CL, SEM (EDX), XRD:

(1) early diagenetic limestone formation,

(2) formation of matrix dolomite,

(3) formation of massive dolostone,

(4) recrystallization of dolostone,

(5) vein dolomite formation,

(6) vein calcite precipitation, and

(7) dedolomitization.

A similar dolomitization was described by Reinhold (1996) for the shallow reservoir, but the (5) vein dolomite formation was first described in this study. The recrystallization of dolostone (phase 4) was similar to the previous study by Reinhold (1998). EDX measurements showed only slight changes in Ca-Mg ratio of the dolomite crystals (matrix dolomite, unimodal/polymodal planar-e, -s, -a dolostone), with the vein dolomites having the highest Mg-content. However, still unclear is the Mg-source for the Upper Jurassic dolomitization. A possible Mg-source could be clay minerals of the bedded facies (dark, micritic limestones) which migrated with compaction fluids into the massive facies. Another Mg-source might be the Upper Jurassic seawater (Machel, 2004) which is stored in the carbonate rocks as formation water, and was measured in fluid inclusion studies (35-40 g/L). Flow pathways for the massive dolomitization might be in the porous massive facies and along discontinuities such as bedding, fractures and fault zones, which were not characterized in detail in this study.

Several studies have described saddle dolomites for temperature above 100°C (Sirat et al., 2016; Di Cuia et al., 2011; Machel, 2004) and for dolostones a critical roughening temperature at 50-60°C (Warren, 2000). Unexpected was the lack of saddle dolomite and recrystallization in the investigated samples, as the dolostones are planar-s and planar-e at depths between 3500-4700 m today (chapter 5.3). Liedmann (1992) and Reinhold (1996) investigated the early diagenetic cements, which were not observed in this study possibly due to recrystallization. Moreover, the high organic content and pyrite in the Upper Jurassic in the southern part of the basin suggest anoxic conditions, which are contradicting to a meteoric inflow with possible oxic conditions and to previous studies (Liedmann, 1992). As the shallow Upper Jurassic reservoir was in the previously research focus, the extensive dark rocks and anoxic conditions were first observed in this study for the deeper reservoir part (> 3 km).

In the Upper Jurassic carbonate rocks, a dolomite breccia was newly described for the GEN and TRN wells. This dolomite breccia is a dense dolostone and is composed of light beige dolostone clasts in a dark or light beige dolomitic matrix. In this study, it was suggested that the dolomite breccia was formed after the dolostones were recrystallized and precipitated, as in CL the dolomite crystals of the dolostone clasts reveal the same zonation as the unbrecciated dolostones. A similar brecciation of a dolostone was described by Reinhold (1998) and slightly similar for the Latemar platform by Jacquemyn et al. (2014).

Still unclear is the genesis of the dolomite breccias, and a genesis by fast ascending fluids along high permeable fractures was suggested.

Dolomitization models for the Upper Jurassic carbonate rocks were burial diagenetic or based on hydrothermal fluids (Reinhold, 1996; Liedmann, 1992). The dolomitization in the investigated wells began with the diagenetic limestone replacement for matrix dolomite. In pure, light limestones, the dolomite crystals are bigger than in clay-bearing limestones. Furthermore, beige dolostones are mainly planar-s to planar-e, whereas dark dolostones are planar-a. Hence, this study confirmed that dolomitization in pure and light limestones is more effective than in dark, clay-bearing limestones (Böhm et al., 2010). For the investigated Purbeck sediments, a stratiform dolomitization by a normally to moderately evaporated seawater (evaporitic pumping) and for the massive Kimmeridgian dolostone a burial diagenetic seawater dolomitization (35-40 g/L) is assumed. The massive dolomitization is possibly further influenced by compaction fluids of the bedded facies and hydrothermal fluids along fractures and fault zones. For the massive dolomitization (300-400 m thickness of dolostones) an enormous fluid flow is necessary (Machel, 2004), which might be provided by the stored Upper Jurassic seawater. This seawater could have migrated during burial diagenesis, due to the measured salinity of 40 g/L in dolomite crystals. Consequently, a massive dolomitization should exist along fault zones and in the highly porous massive facies, which was confirmed at the investigated wells. Nevertheless, the texture of the dolostones indicated a dolomitization which is controlled by depositional and diagenetic fabric in the Upper Jurassic strata but could not be clearly characterized as most investigated wells intersect a porous facies and a fault zone.

The salinity evolution and stable isotopes showed that the Upper Jurassic seawater was gradually diluted by a meteoric water to values below 1 g/L. The Upper Jurassic seawater has probably been retained in the southwestern part of the basin (STG, A1; salinity 18 g/L), however not in the deeper part of the basin which is situated in the eastern part of the Molasse Basin (TRN; salinity 0.5 g/L). This dilution process might indicate high permeability areas due to the less saline reservoir fluid in the high productive areas. The salinity increase, in contrast, probably suggest a low permeability area and an influence of evaporation during the late Tithonian or early Lower Cretaceous, which is located in the southwest of the Molasse Basin.

Numerous studies described a change in geothermal gradient in the Molasse Basin, either by hydrocarbon (Wehner and Kuckelkorn, 1995) or by fluid inclusion studies (Liedmann, 1992) or by borehole measurements (Agemar et al., 2013; Agemar et al., 2012). An important trend was demonstrated by the temperature evolution during the Upper Jurassic diagenesis, as an increase above the recent reservoir temperature could be measured in vein calcites by microthermometry. This temperature increase could be explained by either (1) ascending hotter basement fluids, and/or (2) necking or stretching of the fluid inclusions, and/or (3) change in geothermal gradient. As no different chemistry, and no necking was observed, the change in geothermal gradient is the most probable reason for the increase in temperature, followed by a decrease in temperature. The low temperature anomaly at the region of Lake Chiemsee (Agemar et al., 2012) was investigated, as higher temperatures due to the

increased depth of the Upper Jurassic carbonate rocks compared to the Munich area were assumed. But as the deeper, eastern part was more extensively flushed by meteoric fluids, the reservoir could possibly be cooled by this process or by a lower thermal conductive heat flow. Both processes would explain the low geothermal gradient today. Another aspect is that the dilution process might be faster than the temperature change and might indicate that the reservoir will cool down in the surrounding areas as well. Another interesting fact is that no hydrocarbons were found within the vein calcites and vein dolomites, but hydrocarbons are found as coating within pore spaces of planar-e dolostones. Hence, no hydrocarbons were probably present during the formation of the vein calcite cements.

The genesis of the high permeability areas in the Upper Jurassic reservoir remains unclear, as they are highly dolomitized and not cemented by dolomite crystals. A high fluid flow could have stopped a dolomite cementation, but no corrosion of the mineral surfaces was visible. The late burial vein calcite precipitation could have cemented the remaining pore space, which is only visible at low productive wells (e.g. GEN). Furthermore, the cementation of the pore space in different phases might be intersected by phases of dissolution, or a coating of bitumen/hydrocarbons prevented a precipitation of calcite cements. Therefore, the pore space was preserved and not cemented by vein dolomite or vein calcite crystals. However, dolomites and vein calcites were found in all investigated wells and outcrops and could reflect a basin-wide diagenetic phase, with an unknown flow pathway network in the varying permeable carbonate rocks of the Upper Jurassic reservoir. Besides, the southward reservoir temperature increase did not cause a completely different diagenesis, but the higher pressure and overburden stresses did cause a higher compaction and loss in pore space. At the southern investigated wells, an increase in stylolitization with stylobedding and stylobreccia was observed which directly link to a higher compaction (Huber, 1987; Logan and Semeniuk, 1976). At the deepest wells GEN (4.3 km) and TRN (4.2 km) the development of stylolites, dolostones, and well productivity is quite different. At GEN, the stylolites are very abundant in mudstones to packstone, showing even stylobedding and stylobreccias, whereas at TRN only few stylolites are visible. Furthermore, beige, planar-e dolostones are massively developed at TRN resulting in a high well productivity, but dark gray, planar-s to planar-a dolostones with a low well productivity are present at GEN. Because of this, a certain depth where the compaction is dominating was not defined, as the differential compaction is controlled by the amount of bedded and massive facies. At the TRN well the massive facies caused an early cementation, which resulted in low compaction. While at GEN, the bedded facies is developed with only a small amount of massive facies resulting in a higher compaction and probable low number of dolomites. This lower amount of dolostones could be caused by a lower amount of Mg, which migrated to the massive facies during differential compaction, as described above.

Consequently, the differences in diagenesis are minor between the Munich area and the southern Molasse Basin, as the diagenetic phases as well as the pore space evolution are similar in the middle and eastern investigated wells. Only the missing of the massive dolomitization is different in the western part. At the outcrops in Franconian and Swabian Alb further differences in diagenesis are described, as the carbonate rocks contain dedolomite and karstification. There, the karstification and dedolomitization

have developed due to the subaerial exposure since the foreland basin development for a long period. Arising out of these aspects, the influence of the facies and transition zone facies on well productivity to the south of the basin are minor, as well as general diagenetic processes. Despite this, the dolomitization did not developed massive porous dolostones, and the greater depths caused in the south a higher compaction resulting in a loss of pore space. Therefore, the interaction of facies, diagenesis, and compaction can result in an increase or decrease in well productivity of the Upper Jurassic reservoir.

# 7 Conclusion

In the Upper Jurassic limestones and dolostones of the Molasse Basin, an overlapping of multiple processes such as facies, diagenesis and burial depth are responsible for the southward decrease in reservoir productivity. Optical observations of 839 thin and thick sections from cores and drill cuttings reveal a new transition zone facies on the Franconian and Swabian platform during the lower Upper Jurassic. By cathodoluminescence microscopy, fluid inclusion studies, geochemical measurements, and stable isotopes of over 650 rock samples, five main phases of diagenesis with seven dolomite phases were used to reconstruct the evolution of the Upper Jurassic carbonate rocks.

The Upper Jurassic limestones and dolostones of southern German formed within an extensive shallow dipping (1-5°) carbonate platform along the northern epicontinental margin of the Tethys. The strata record multiple sea level fluctuations, along with a stratigraphically upward increase in aridity and evaporative to brackish textures. During the Oxfordian, a new transition zone facies was discovered in the southern part of the Molasse Basin, which developed on the Franconian and Swabian platform. The carbonate rocks of the transition zone facies contain dense, dark mudstones to wackestones with abundant planktonic organisms such as radiolaria, foraminifera, crinoids (*Saccocoma* sp.). During the Kimmeridgian and Tithonian, the usual Franconian facies, as it is described for the Munich area, is developed on top of the transition zone facies. Cretaceous terrigenous to shallow marine sediments, which lie directly above the Upper Jurassic strata further indicate an erosional phase with karstification of the Upper Jurassic carbonate rocks. However, the karstification happened for a longer period than previously assumed but did not increase the reservoir porosity in the southwestern area. In this study, the dedolomitization and karstification was not only documented at outcrops but also in the southern parts of the foreland basin that were affected by subaerial exposure during the Cretaceous and early Paleogene.

Through the coupling of multiple petrographic (microfacies), geochemical, and isotope signatures, the diagenetic evolution of the Upper Jurassic carbonate rocks, especially of the Upper Jurassic dolomites, has been constructed in detail. In the southern Molasse Basin, previous studies are still valid, however some new phases were described in this study. New is the phase of second dolomitization accompanied by hydrocarbons, the higher temperatures with up to 200°C, an expansion of the dolomitization window (Reinhold, 1996) and the Geo-1 equation (Liedmann, 1992) to higher temperatures. Moreover, the recrystallization of the early diagenetic calcite cements for the southern part of the Molasse Basin was

determined. Petrographic, geochemical and spatial evidence suggest that the massive dolomitization occurred due to a burial seawater dolomitization in the Kimmeridgian rocks, and might be affected by compaction and hydrothermal fluids. In contrast, the Purbeck carbonate rocks were suggested to be stratiform dolomitized with normally to moderately evaporated seawater by evaporitic reflux dolomitization. The most likely Mg source for the dolomitization is the stored Upper Jurassic seawater and possible compaction fluids of the bedded facies. As bigger dolomite crystals formed in pure, light limestones, the massive facies is more suitable for massive dolomitization and can increase the reservoir porosity. The porous, highly permeable planar-e dolostones are preserved at greater depths in some areas of the Molasse Basin, therefore no recrystallization of the porous dolostones (planar-e to –s) above the critical roughening temperatures was found. Unclear remains the occurrence and genesis of dolomite breccia, which was observed in some wells in the deeper Upper Jurassic section. As a minor decrease in pore space and porosity was observed in the massive facies, the massive facies was less compacted due to differential compaction than the bedded facies at a similar depth. Therefore, the occurrence of highly permeable planar-e dolostone results in a higher matrix permeability of the light grey to white massive facies, which is usually the main target area for a geothermal application.

Moreover, the fluid evolution by salinity and temperature, as well as by the geothermal gradient was described the first time in the Upper Jurassic carbonate rocks in the southern part of the Molasse Basin. The salinity of the paleo-fluid showed a continuous dilution of the former Upper Jurassic seawater (35 g/L) by a meteoric fluid, which could not be further classified in this study. However, in the southwestern part of the Molasse Basin an increase in fluid salinity was measured, above the Upper Jurassic seawater, with the possible salt source in the Purbeckian sediments. Today, the salinity of the reservoir fluid is less saline, and increase from around 1 g/L in the east to up to 18 g/L the southwest of the Molasse Basin. Besides, at highly productive wells, the reservoir fluid is less saline than at low productive wells today. By the temperature data, a change in geothermal gradient and/or a possible influence of hydrothermal fluids was demonstrated during diagenesis, which could explain the lower temperature anomaly of the aquifer in the area around Lake Chiemsee today.

So far, only hypothesis about possible reasons causing a decline in well productivity in the Upper Jurassic reservoir were known. But this study showed that interaction between facies (bedded vs massive facies), diagenesis (planar-e or planar-a dolomites) and differential compaction can result in a lower reservoir porosity. However, detailed studies and models are necessary which should prove the characterized processes of this study.

# 8 Outlook

Future studies of the Upper Jurassic in the wider Molasse Basin should examine for the numerous aforementioned trends, in order to establish the occurring depositional environments and the diagenesis (dolomitization history) over the entire basin. It needs to be investigated whether this diagenetic sequence formed similar dolomites or if these trends are unique for the Upper Jurassic strata in the

Molasse Basin. By the evaluation of new wells and the further re-evaluation of existing wells, the lithostratigraphy of the Upper Jurassic strata in the Molasse Basin might be conducted, as well as a more detailed interpretation of the depositional environments, e.g. the distribution of the bedded facies.

Measurements and further studies should be made on the relevance and occurrence of pyrite in the Upper Jurassic carbonate rocks, especially at the vein dolomites. As the black to dark gray rock color was no focus of this research, future studies could concern the hydrocarbon migration and development to determine the source of the hydrocarbons. In addition, the missing of hydrocarbons in the vein calcite fluid inclusions might be solved. By a reconstruction of seismic profiles based on truncated borehole data and lithology, possibly indications of the lithology on the seismic data can be found. Besides, new stable isotope data of the present reservoir fluid and Sr-isotope measurements will confirm or update the interpretation of this study.

This study evidenced a tight reservoir rock as a result of the newly discovered transition zone facies in the southern part of the Franconian facies, and showed that compaction, diagenesis, and depth are important factors for reservoir productivity. Beside future geological studies to better understand the basin subsidence, uplift and its effects on reservoir porosity and permeability, applied research should also emphasize on the technological part to develop this new geothermal play type in the Molasse Basin play province. Since the geothermal play transition zone facies reflects petrothermal characteristics with hydraulically conductive fault zones, new technologies should be developed to utilize this new play type for the “Wärmewende” in Bavaria.

In this respect, this study may be an initial part of an envisioned holistic approach in geothermal development, where surface technology is flexibly adopted to the existing, appropriately investigated subsurface conditions.

# References


ADAMS, A., DIAMOND, L.W. AND ASCHWANDEN, L. (2018) Dolomitization by hypersaline reflux into dense groundwaters as revealed by vertical trends in strontium and oxygen isotopes: Upper Muschelkalk, Switzerland. *Sedimentology*.

AGEMAR, T., ALTEN, J.-A., GANZ, B., KUDER, J., KÜHNE, K., SCHUMACHER, S. AND SCHULZ, R. (2014a) The Geothermal Information System for Germany–GeotIS. *Z. Dtsch. Ges. Geowiss.*, **165,** 129-144.

AGEMAR, T., BRUNKEN, J., JODOCY, M., SCHELLSCHMIDT, R., SCHULZ, R. AND STOBER, I. (2013) Untergrundtemperaturen in Baden-Württemberg. *Z. Dtsch. Ges. Geowiss.*, **164,** 49-62.

AGEMAR, T., SCHELLSCHMIDT, R. AND SCHULZ, R. (2012) Subsurface temperature distribution in Germany. *Geothermics*, **44,** 65-77.

AGEMAR, T., WEBER, J. AND SCHULZ, R. (2014b) Deep geothermal energy production in Germany. *Energies*, **7,** 4397-4416.

AHR, W.M. (2008) *Geology of carbonate reservoirs: the identification, description and characterization of hydrocarbon reservoirs in carbonate rocks*. John Wiley & Sons.

ALDINGER, H. (1968) Die Paläogeographie des schwäbischen Jurabeckens. *Eclogae Geol. Helv.*, **61,** 167-182.

ALLAN, J.R. AND WIGGINS, W. (1993) *Dolomite reservoirs: Geochemical techniques for evaluating origin and distribution*. AAPG.

ALLENBACH, R.P. (2001) Synsedimentary tectonics in an epicontinental sea: A new interpretation of the Oxfordian basins of northern Switzerland. *Eclogae Geol. Helv.*, **94,** 265-287.

AMIEUX, P. (1982) La cathodoluminescence: méthode d'étude sédimentologique des carbonates. *Bull. Cent. Rech. Explor.-Prod. Elf-Aquitaine*, **6,** 437-483.

ANONYMOUS 1957. Schichtenverzeichnis der Aufschlußbohrung A, EXXON Mobil Productions Deutschland.

ANONYMOUS 1958. Schichtenverzeichnis der Aufschlussbohrung C, EXXON Mobil Productions Deutschland.

ANONYMOUS 1960. Schichtenverzeichnis der Aufschlussbohrung B, EXXON Mobil Productions Deutschland.

BACHMANN, G.H., MÜLLER, M. AND WEGGEN, K. (1987) Evolution of the Molasse Basin (Germany, Switzerland). *Tectonophysics*, **137,** 77-92.

BACHMANN, H. AND MÜLLER, M. (1996) Die Entwicklung des süddeutschen Molassebeckens seit dem Variszikum: Eine Einführung. *Z. geol. Wiss.*, **24,** 3-20.

BAKKER, R.J. (1997) Clathrates: computer programs to calculate fluid inclusion V-X properties using clathrate melting temperatures. *Comput. Geosci.*, **23,** 1-18.

BAQUÉS, V., TRAVÉ, A., BENEDICTO, A., LABAUME, P. AND CANTARERO, I. (2010) Relationships between carbonate fault rocks and fluid flow regime during propagation of the Neogene extensional faults of the Penedès basin (Catalan Coastal Ranges, NE Spain). *Journal of Geochemical Exploration*, **106,** 24-33.

BARKER, C.E. AND GOLDSTEIN, R.H. (1990) Fluid-inclusion technique for determining maximum temperature in calcite and its comparison to the vitrinite reflectance geothermometer. *Geology*, **18,** 1003-1006.

BARTHEL, K.W. (1969) Die obertithonische, regressive Flachwasser-Phase der Neuburger Folge in Bayern. *Abhandlungen*, **142,** 172.

BAUER, M., FREEDEN, W., JACOBI, H. AND NEU, T. (2014) *Handbuch Tiefe Geothermie*. Springer.

BAUSCH, W. (1994) *Geochemische Analyse von Karbonatgesteins-Sequenzen*, Wien.

BAUSCH, W.M., ECKSTEIN, G.-O. AND HOEFS, J. (1986) Zur Genese der 'Braunkalke'des fränkischen Malms. *Geologica Bavarica*, **89,** 189-207.

BEAUDOIN, N., BELLAHSEN, N., LACOMBE, O., EMMANUEL, L. AND PIRONON, J. (2014) Crustal-scale fluid flow during the tectonic evolution of the Bighorn Basin (Wyoming, USA). *Basin Research*, **26,** 403-435.

BEICHEL, K., KOCH, R. AND WOLFGRAMM, M. (2014) Die Analyse von Spülproben zur Lokalisierung von Zuflusszonen in Geothermiebohrungen. Beispiel der Bohrungen Gt Unterhaching 1/1a und 2.(Süddeutschland, Molassebecken, Malm). *Geol. Bl. NO-Bayern*, **64,** 43-65.

BENNION, D.B. AND BACHU, S. (2010) Drainage and imbibition CO2/brine relative permeability curves at reservoir conditions for high-permeability carbonate rocks. In: *SPE Annual Technical Conference and Exhibition*. Society of Petroleum Engineers.

BENSE, V., GLEESON, T., LOVELESS, S., BOUR, O. AND SCIBEK, J. (2013) Fault zone hydrogeology. *Earth-Science Reviews*, **127,** 171-192.

BERNOULLI, D. AND JENKYNS, H.C. (2009) Ancient oceans and continental margins of the Alpine-Mediterranean Tethys: deciphering clues from Mesozoic pelagic sediments and ophiolites. *Sedimentology*, **56,** 149-190.

BERTANI, R. (2016) Geothermal power generation in the world 2010–2014 update report. *Geothermics*, **60,** 31-43.

BERTLEFF, B., JOACHIM, H., KOZIOROWSKI, G., LEIBER, J., OHMERT, W., PRESTEL, R., STOBER, I., STRAYLE, G., VILLINGER, E. AND WERNER, J. (1988) Ergebnisse der Hydrogeothermiebohrungen in Baden-Württemberg. *Abhandlungen des Geologischen Landesamtes Baden-Württemberg, LGRB, Freiburg*, **30,** 27-116.

BILLI, A., SALVINI, F. AND STORTI, F. (2003) The damage zone-fault core transition in carbonate rocks: implications for fault growth, structure and permeability. *Journal of Structural geology*, **25,** 1779-1794.

BIRNER, J. (2013) *Hydrogeologisches Modell des Malmaquifers im Süddeutschen Molassebecken*, Berlin, Freie Universität Berlin, 86 pp.

BIRNER, J., FRITZER, T., JODOCY, M., SAVVATIS, A., SCHNEIDER, M. AND STOBER, I. (2012) Hydraulische Eigenschaften des Malmaquifers im Süddeutschen Molassebecken und ihre Bedeutung für die geothermische Erschließung. *Z. geol. Wiss.*, **40,** 133-156.

BIRNER, J., MAYR, C., THOMAS, L., SCHNEIDER, M., BAUMANN, T. AND WINKLER, A. (2011) Hydrochemie und Genese der tiefen Grundwässer des Malmaquifers im bayerischen Teil des süddeutschen Molassebeckens [Hydrochemistry and evolution of deep groundwaters in the Malm aquifer in the Bavarian part of the South German Molasse Basin]. *Z. geol. Wiss.*, **39,** 291-308.

BÖGEL, H. AND SCHMIDT, K. (1976) *Kleine Geologie der Ostalpen: allgemein verständliche Einführung in den Bau der Ostalpen unter Berücksichtigung der angrenzenden Südalpen*. Ott Verlag, Thun.

BOGGS, S. AND KRINSLEY, D. (2006) *Application of Cathodoluminescence Imaging to the Study of Sedimentary Rocks*. Cambridge University Press, 165 pp.

BÖHM, F., BIRNER, J., STEINER, U., KOCH, R., SOBOTT, R., SCHNEIDER, M. AND WANG, A. (2011) Tafelbankiger Dolomit in der Kernbohrung Moosburg SC4: Ein Schlüssel zum Verständnis der Zuflussraten in Geothermiebohrungen des Malmaquifers (Östliches Molasse-Becken, Malm Süddeutschland). *Z. geol. Wiss.*, **39,** 117-157.

BÖHM, F., KOCH, R., HÖFERLE, R. AND BAASCH, R. (2010) Der Malm in der Geothermiebohrung Pullach Th2–Faziesanalyse aus Spülproben (München, S-Deutschland). *Geol. Bl. NO-Bayern*, **60,** 17-49.

BRÖNNIMANN, P. (1976) Revision of the lectotype of Favreina salevensis (Paréjas) (Crustacea, Decapoda) and description of favreine form-species from the Jurassic and Cretaceous of Scotland, Portugal, Yugoslavia and Pakistan. *Paläontologische Zeitschrift*, **50,** 40-56.

BÜCHI, U., LEMCKE, K., WIENER, G. AND ZIMDARS, J. (1965) Geologische Ergebnisse der Erdölexploration auf das Mesozoikum im Untergrund des schweizerischen Molassebeckens. *Bulletin der Schweizerischen Vereinigung von Petroleum-Geologen und-Ingenieuren*, **15,** 7-38.

BUDACH, I., MOECK, I., LÜSCHEN, E. AND WOLFGRAMM, M. (2017) Temporal evolution of fault systems in the Upper Jurassic of the Central German Molasse Basin: case study Unterhaching. *Int. J. Earth Sci.*

BUDD, D.A. AND VACHER, H. (2004) Matrix permeability of the confined Floridan Aquifer, Florida, USA. *Hydrogeology Journal*, **12,** 531-549.

BURRUSS, R.C., CERCONE, K.R. AND HARRIS, P.M. (1985) Timing of hydrocarbon migration: evidenced from fluid inclusions in calcite cements, tectonics and burial history. *SEPM Special Publication*, **36**.

CACACE, M., BLÖCHER, G., WATANABE, N., MOECK, I., BÖRSING, N., SCHECK-WENDEROTH, M., KOLDITZ, O. AND HUENGES, E. (2013) Modelling of fractured carbonate reservoirs: outline of a novel technique via a case study from the Molasse Basin, southern Bavaria, Germany. *Environ. Earth Sci.*, **70,** 3585-3602.

CH, S. (2017) Lithostratigraphic Lexicon of Switzerland. Swiss Committee on Stratigraphy (SCS) and the Swiss Geological Survey.

CHOQUETTE, P.W. AND PRAY, L.C. (1970) Geologic nomenclature and classification of porosity in sedimentary carbonates. *AAPG bulletin*, **54,** 207-250.

COLINS, E., NIEDERBACHER, P. AND SAUER, R. (1989) Kohlenwasserstoffexploration in Vorarlberg-Ergebnisse der Bohrung Vorarlberg-Au 1. *Mitteilungen der Österreichischen Geologischen Gesellschaft*, **82,** 91-104.

DAWANS, J.M. AND SWART, P.K. (1988) Textural and geochemical alternations in Late Cenozoic Bahamian dolomites. *Sedimentology*, **35,** 385-403.

DI CUIA, R., RIVA, A., SCIFONI, A., MORETTI, A., SPÖTL, C. AND CALINE, B. (2011) Dolomite characteristics and diagenetic model of the Calcari Grigi Group (Asiago Plateau, Southern Alps – Italy): an example of multiphase dolomitization. *Sedimentology*, **58,** 1347-1369.

DRIESNER, T. (2007) The system H 2 O–NaCl. Part II: Correlations for molar volume, enthalpy, and isobaric heat capacity from 0 to 1000° C, 1 to 5000bar, and 0 to 1 X NaCl. *Geochim. Cosmochim. Acta*, **71,** 4902-4919.

DRIESNER, T. AND HEINRICH, C.A. (2007) The system H 2 O–NaCl. Part I: Correlation formulae for phase relations in temperature–pressure–composition space from 0 to 1000° C, 0 to 5000bar, and 0 to 1 X NaCl. *Geochim. Cosmochim. Acta*, **71,** 4880-4901.

DUNHAM, R.J. (1962) Classification of carbonate rocks according to depositional texture. In: *Classification of Carbonate Rocks - A Symposium* (Ed W.E. Ham), *AAPG Memoir*, **1**, pp. 108-121. American Association of Petroleum Geologists, Tulsa, Oklahoma.

FALTLHAUSER, M. AND GEIß, A. 2018. Zahlen und Fakten zur Stromversorgung in Deutschland, Wirtschaftsbeirat der Union e.V.

FEELY, M., COSTANZO, A., HUNT, J., WILTON, D. AND CARTER, J. (2016) Oil Exploration and its Relationship to the World of Trapped Micron Scale Fluids: A Review of the Applications of Fluid Inclusion Microscopy to the Study of Aqueous and Hydrocarbon Fluid Dynamics in Sedimentary Basins. In: *Arctic Technology Conference*. Offshore Technology Conference, St. John's, Newfoundland and Labrador, Canada.

FELBER, P. AND WYSSLING, G. (1979) Zur Stratigraphie und Tektonik des Südhelvetikums im Bregenzerwald (Vorarlberg). *Eclogae Geol. Helv.*, **72,** 673-714.

FISCH, H., UHDE, J., BEMS, C., LANG, P. AND BARTELS, J. (2015a) Hydraulic Testing and Reservoir Characterization of the Taufkirchen Site in the Bavarian Molasse Basin, Germany. In: *World Geothermal Congress 2015*, pp. 1-14, Melbourne, Australia.

FISCH, H., UHDE, J., BEMS, C., LANG, P. AND BARTELS, J. (2015b) Hydraulic Testing and Reservoir Characterization of the Taufkirchen Site in the Bavarian Molasse Basin, Germany. *Proceedings of the World Geothermal Congress***,** 1-14.

FLÜGEL, E. (1978) *Mikrofazielle Untersuchungsmethoden von Kalken* Springer, Berlin [u.a.], 454 pp.

FLÜGEL, E. (1982) *Microfacies analysis of limestones*. Springer, Berlin, 633 pp.

FLÜGEL, E. (2010) *Microfacies of Carbonate Rocks: Analysis, Interpretation and Application*. Springer, Berlin, 984 pp.

FOLK, R.L. (1959) Practical petrographic classification of limestones. *AAPG Bulletin*, **43,** 1-38.

FOLK, R.L. (1962) Spectral subdivision of limestone types. In: *Classification of Carbonate Rocks - A Symposium* (Ed W.E. Ham), *AAPG Memoir*, **1**, pp. 62-84. American Association of Petroleum Geologists, Tulsa, Oklahoma.

FOOKES, E. (1995) Development and eustatic control of an Upper Jurassic reef complex (Saint Germain-de-Joux, Eastern France). *Facies*, **33,** 129.

FRIEDMAN, I. AND O'NEIL, J.R. (1977) *Data of geochemistry: Compilation of stable isotope fractionation factors of geochemical interest*. US Government Printing Office.

FRITZ, P. AND SMITH, D. (1970) The isotopic composition of secondary dolomites. *Geochim. Cosmochim. Acta*, **34,** 1161-1173.

FRITZER, T., PAMER, R., SCHULZ, U. AND SIEBLITZ, S. 2012. Geothermische Charakterisierung von Karst-Kluft-Aquiferen im Großraum München, Bayerisches Landesamt für Umwelt.

GASPARRINI, M. (2003) *Large-scale hydrothermal dolomitisation in the southwestern Cantabrian Zone (NW Spain): Causes and controls of the process and origin of the dolomitising fluids*, Ruprecht-Karls-Universität Heidelberg, Heidelberg.

GEOTECCONSULT 2014. Geothermiebohrung Sankt Gallen GT1 Faziesanalyse - Bericht zur Mikrofaziesanalyse an Cuttingproben aus der Bohrung Sankt Gallen GT1 im Bereich von 3.750 m - Endteufe, Geotec Consult - Ingenieurbüro Uhlig und Partner.

GEYER, O.F. AND GWINNER, M.P. (1991) *Geologie von Baden-Württemberg*. Schweizerbart, Stuttgart, 482 pp.

GOLDSTEIN, R.H. (1986) Reequilibration of fluid inclusions in low-temperature calcium-carbonate cement. *Geology*, **14,** 792-795.

GOLDSTEIN, R.H. (2001) Fluid inclusions in sedimentary and diagenetic systems. *Lithos*, **55,** 159-193.

GOLDSTEIN, R.H. AND REYNOLDS, T.J. (1994) *Systematics of fluid inclusions in diagenetic minerals*.

GÖTZE, J. (2002) Potential of cathodoluminescence (CL) microscopy and spectroscopy for the analysis of minerals and materials. *Anal. Bioanal. Chem.*, **374,** 703-708.

GREGG, J.M., BISH, D.L., KACZMAREK, S.E. AND MACHEL, H.G. (2015) Mineralogy, nucleation and growth of dolomite in the laboratory and sedimentary environment: A review. *Sedimentology*, **62,** 1749-1769.

GREGG, J.M., HOWARD, S.A. AND MAZZULLO, S.J. (1992) Early diagenetic recrystallization of Holocene (<3000 years old) peritidal dolomites, Ambergris Cay, Belize. *Sedimentology*, **39,** 143-160.

GRESSLY, A. (1864) Rapport géologique sur les terrains parcourus par les lignes du réseau des chemins de fer jurassiens par le Jura bernois. In: *Rapports concernant le réseau des chemins de fer du Jura bernois: Annexe 3*, **3**, Bern.

GROSS, D., SACHSENHOFER, R., BECHTEL, A., GRATZER, R., GRUNDTNER, M.L., LINZER, H.G., MISCH, D., PYTLAK, L. AND SCHEUCHER, L. (2018) Petroleum systems in the Austrian sector of the North Alpine Foreland Basin: an overview. *Journal of Petroleum Geology*, **41,** 299-317.

GUSTERHUBER, J., DUNKL, I., HINSCH, R., LINZER, H.-G. AND SACHSENHOFER, R. (2012) Neogene uplift and erosion in the Alpine foreland basin (upper Austria and Salzburg). *Geologica Carpathica*, **63,** 295-305.

GYGI, R.A. (1992) Structure, pattern of distribution and paleobathymetry of Late Jurassic microbialites (stromatolites and oncoids) in northern Switzerland. *Eclogae Geol. Helv.*, **85,** 799-824.

GYGI, R.A. (2012) *Quantitative geology of Late Jurassic epicontinental sediments in the Jura Mountains of Switzerland*. Springer Science & Business Media.

GYGI, R.A. (2013) *Integrated stratigraphy of the Oxfordian and Kimmeridgian (Late Jurassic) in northern Switzerland and adjacent southern Germany*. Birkhäuser.

HARDENBOL, J., THIERRY, J., FARLEY, M.B., JACQUIN, T., DE GRACIANSKY, P.-C. AND VAIL, P.R. (1998) Mesozoic and Cenozoic sequence chronostratigraphic framework of European basins. In: *Mesozoic and Cenozoic Sequence Stratigraphy of European Basins* (Eds P.-C. de Graciansky, J. Hardenbol, T. Jacquin and P.R. Vail), **60**, pp. 3-13. SEPM special publications, Tulsa.

HARTMANN, H.V., TANNER, D.C. AND SCHUMACHER, S. (2016) Initiation and development of normal faults within the German alpine foreland basin: The inconspicuous role of basement structures. *Tectonics*, **35,** 1560-1574.

HEIM, A. (1919) *Molasseland und Juragebirge*. Tauchnitz, Leipzig, 704 pp.

HIATT, E. AND PUFAHL, P. (2014) Cathodoluminescence petrography of carbonate rocks: a review of applications for understanding diagenesis, reservoir quality and pore system evolution. *Mineralogical Association of Canada Short Course*, **45,** 75-96.

HILTMANN, W., KUCKELKORN, K. AND WEHNER, H. (1999) Das Inkohlungsprofil der Bohrung Grambach 1 - erster Hinweis auf eine Olküche im Molassebecken. *Erdöl, Erdgas, Kohle*, **115,** 294-297.

HOEFS, J. (1997) *Stable Isotope Geochemistry*. Springer-Verlag Berlin Heidelberg, 203 pp.

HUBER, S. (1987) Drucklösungserscheinungen in Karbonaten des Oxford 1 und Kimmeridge 1 der Bohrung TB-3 Saulgau (Oberschwaben). *Facies*, **17,** 109-119.

HUDSON, J.D. (1977) Stable isotopes and limestone lithification. *Journal of the Geological Society*, **133,** 637-660.

JACOB, H. AND KUCKELKORN, K. (1977) Das Inkohlungsprofil der Bohrung Miesbach 1 und seine erdölgeologische Interpretation. *Erdöl-Erdgas Z.*, **93,** 115-124.

JACQUEMYN, C., EL DESOUKY, H., HUNT, D., CASINI, G. AND SWENNEN, R. (2014) Dolomitization of the Latemar platform: Fluid flow and dolomite evolution. *Marine and Petroleum Geology*, **55,** 43-67.

JEANNET, A. (1951) Stratigraphie und Paläontologie des oolithischen Eisenerzlagers von Herznach und seiner Umgebung. *Beiträge zur Geologie der Schweiz, Geotechnische Serie*, **13,** 1-240.

JOACHIMSKI, M.M. (1994) Subaerial exposure and deposition of shallowing upward sequences: evidence from stable isotopes of Purbeckian peritidal carbonates (basal Cretaceous), Swiss and French Jura Mountains. *Sedimentology*, **41,** 805-824.

KEUPP, H. AND MATYSZKIEWICZ, J. (1997) Zur Faziesrelevanz von Saccocoma-Resten (Schwebcrinoiden) in Oberjura-Kalken des nördlichen Tethys-Schelfs. *Geol. Bl. NO-Bayern*, **47,** 53-70.

KIM, S.-T. AND O'NEIL, J.R. (1997) Equilibrium and nonequilibrium oxygen isotope effects in synthetic carbonates. *Geochim. Cosmochim. Acta*, **61,** 3461-3475.

KLIMCHOUK, A., PALMER, A.N., DE WAELE, J., AULER, A.S. AND AUDRA, P. (2017) *Hypogene Karst regions and caves of the world*. Springer.

KNOTT, S.D., BEACH, A., BROCKBANK, P.J., BROWN, J.L., MCCALLUM, J.E. AND WELBON, A.I. (1996) Spatial and mechanical controls on normal fault populations. *Journal of Structural Geology*, **18,** 359-372.

KOCH, A. AND CLAUSER, C. 2006. Erstellung statistisch abgesicherter thermischer und hydraulischer Gesteinseigenschaften für den flachen und tiefen Untergrund in Deutschland: Phase 1 – Westliche Molasse und nördlich angrenzendes Süddeutsches Schichtstufenland: Abschlussbericht 01.01.2005-31.10.2006, E. ON ERC.

KOCH, A. AND CLAUSER, C. 2011. Erstellung statistisch abgesicherter thermischer und hydraulischer Gesteinseigenschaften für den flachen und tiefen Untergrund in Deutschland: Phase 2-Westliches Nordrhein-Westfalen und bayerisches Molassebecken: Abschlussbericht 01.09.2006-31.05.2009, E. ON ERC.

KOCH, R. (1991) Faziesanalyse aus Spülproben. *Zbl. Geol. Paläont. I*, **8,** 1029-1043.

KOCH, R. (2000) Die neue Interpretation der Massenkalke des Süddeutschen Malm und ihr Einfluß auf die Qualität von Kalksteinen für technische Anwendungen (Beispiele aus der Fränkischen Alb). *Archaeopteryx*, **18,** 43-65.

KOCH, R. (2011) Dolomit und Dolomit-Zerfall im Malm Süddeutschlands – Verbreitung, Bildungsmodelle, Dolomit-Karst. *Laichinger Höhlenfreund*, **46,** 75-92.

KOCH, R., BACHMANN, G.H. AND MÜLLER, M. (2010) Fazies des Oberen Jura (Malm) der Bohrungen Scherstetten 1 und 2 (Molasse-Becken, Süddeutschland) und Ihre Bedeutung für die Geothermische Exploration. *Z. geol. Wiss*, **38,** 327-351.

KOCH, R., SENOWBARI-DARYAN, B. AND STRAUSS, H. (1994) The Late Jurassic 'Massenkalk Fazies' of southern Germany: calcareous sand piles rather than organic reefs. *Facies*, **31,** 179-208.

KOCH, R. AND SOBOTT, R. (2005) Porosität in Karbonatgesteinen–Genese, Morphologie und Einfluss auf Verwitterung und Konservierungsmaßnahmen. *Zeitschrift der Deutschen Gesellschaft für Geowissenschaften*, **156,** 33-50.

KOSCHEL, G. 1991. Geologischer Überblick–Hydrogeologische Randbedingungen, München, Freiburg i. Br.

KUHLEMANN, J. AND KEMPF, O. (2002) Post-Eocene evolution of the North Alpine Foreland Basin and its response to Alpine tectonics. *Sediment. Geol.*, **152,** 45-78.

LANDESAMT FÜR BERGBAU, E.U.G.-R.E.E.U.E. 2018. Erdöl und Erdgas in der Bundesrepublik Deutschland 2017, Hannover.

LEMCKE, K. (1976) Übertiefe Grundwässer im süddeutschen Alpenvorland. *Bulletin der Schweizerischen Vereinigung von Petroleum-Geologen und-Ingenieuren*, **42,** 9-18.

LEMCKE, K. (1988) *Das Bayerische Alpenvorland vor der Eiszeit: Erdgeschichte, Bau, Bodenschätze. Geologie von Bayern I*. Schweizerbart, Stuttgart, 175 pp.

LIEDMANN, W. (1992) *Diagenetische Entwicklung Süddeutscher Malmkarbonate - unter Berücksichtigung lumineszenzpetrographischer, fluid inclusions und geochemischer Untersuchungsmethoden*. Dissertation Universität Heidelberg, Heidelberg, 307 pp.

LOGAN, B.W. AND SEMENIUK, V. (1976) *Dynamic metamorphism: processes and products in Devonian carbonate rocks, Canning Basin, Western Australia*. Geological Society of Australia.

LUCIA, F.J. (2007) *Carbonate reservoir characterization: An integrated approach*. Springer Science & Business Media, 336 pp.

LUPU, M. (1972) Mikrofazielle Untersuchung eines Quintnerkalk-Profils der Mittagsfluh in Vorarlberg. *Verh. Geol. B.-A*, **1972,** 281-287.

LÜSCHEN, E., WOLFGRAMM, M., FRITZER, T., DUSSEL, M., THOMAS, R. AND SCHULZ, R. (2014) 3D seismic survey explores geothermal targets for reservoir characterization at Unterhaching, Munich, Germany. *Geothermics*, **50,** 167-179.

MACHEL, H.G. (2004) Concepts and models of dolomitization: a critical reappraisal. In: *The Geometry and Petrogenesis of Dolomite Hydrocarbon Reservoirs* (Eds C.J.R. Braithwaite, G. Rizzi and G. Darke), *Special Publications*, **235**, pp. 7-63. Geological Society, London.

MAKHLOUFI, Y., RUSILLON, E., BRENTINI, M., MOSCARIELLO, A., MEYER, M. AND SAMANKASSOU, E. (2018) Dolomitization of the Upper Jurassic carbonate rocks in the Geneva Basin, Switzerland and France. *Swiss J. Geosci.*

MARCOU, J. (1848) Recherches géologiques sur le Jura salinois. Première partie *Mémoires de la Société géologique de France, sér. 2*, **3,** 1-151.

MARSHALL, J.D. (1992) Climatic and oceanographic isotopic signals from the carbonate rock record and their preservation. *Geological Magazine*, **129,** 143-160.

MAYRHOFER, C., NIESSNER, R. AND BAUMANN, T. (2014) Hydrochemistry and hydrogen sulfide generating processes in the Malm aquifer, Bavarian Molasse Basin, Germany. *Hydrogeology Journal*, **22,** 151-162.

MAZUREK, M., HURFORD, A.J. AND LEU, W. (2006) Unravelling the multi-stage burial history of the Swiss Molasse Basin: integration of apatite fission track, vitrinite reflectance and biomarker isomerisation analysis. *Basin Research*, **18,** 27-50.

MCLIMANS, R.K. (1987) The application of fluid inclusions to migration of oil and diagenesis in petroleum reservoirs. *Appl. Geochem.*, **2,** 585-603.

MEDER, K. (1987) Dedolomitisierung in oberjurassischen Karbonatsedimenten der Bohrung TB-3 Saulgau (W-Molasse, SW-Deutschland). *Facies*, **17,** 189-196.

MENNING, M. AND HENDRICH, A. (2016) *Stratigraphic Table of Germany 2016*. German Research Centre for Geosciences, Potsdam.

MEYER, R.K.F. (1994) „Moosburg 4 ", die erste Kernbohrung durch den Malm unter der bayerischen Molasse. *Erlanger Geologische Abhandlungen*, **123,** 51-81.

MEYER, R.K.F. AND SCHMIDT-KALER, H. (1989) *Paläogeographischer Atlas des süddeutschen Oberjura (Malm)*. Schweizerbart, Stuttgart, 77 pp.

MEYER, R.K.F. AND SCHMIDT-KALER, H. (1993) Schwarze Kalke im Weißen Jura (Über die Bitumenfazies im Malm der Südlichen Frankenalb). *Geologica Bavaria*, **97,** 155-166.

MOECK, I. AND ZIMMER, R. (2014) Tiefe Geothermie in Bayern: Installierte Leistung, Erlaubnis-/Bewilligungsfelder und Erkundung. In: *Proceedings - Der Geothermiekongress DGK 2014*, Essen.

MOECK, I.S. (2014) Catalog of geothermal play types based on geologic controls. *Renewable and Sustainable Energy Reviews*, **37,** 867-882.

MOHR, H. (1992) Die Entwicklung der Calpionellen an der Jura-Kreide Grenze im Helvetikum der Ostschweiz. Rückschlüsse auf die Biostratigraphie und Sedimentationsgeschichte. *Eclogae Geol. Helv.*, **85,** 1-21.

MOHR, H. AND FUNK, H. (1995) Die Entwicklung der helvetischen Karbonatplattform in der Ostschweiz (Tithonian-Berriasian): Eine sequenzstratigraphische Annäherung. *Eclogae Geol. Helv.*, **88,** 281-320.

MRAZ, E., MOECK, I., BISSMANN, S. AND HILD, S. (2018a) Multiphase fossil normal faults as geothermal exploration targets in the Western Bavarian Molasse Basin: Case study Mauerstetten. *Z. Dtsch. Geo. Geowiss.*, **169,** 389–411.

MRAZ, E., MOECK, I., WOLFGRAMM, M. AND THURO, K. (2018b) Microfacies Analysis in Upper Jurassic Carbonates with Implications for Reservoir Quality in the Molasse Basin. *Facies*, **submitted,** 30.

MRAZ, E., WOLFGRAMM, M., MOECK, I. AND THURO, K. (2018c) A Reconstruction of the Paleo-Fluid Evolution in the North Alpine Foreland Basin. *Geofluids*, **submitted**.

MULLIS, J., MÄHLMANN, R.F. AND WOLF, M. (2017) Fluid inclusion microthermometry to calibrate vitrinite reflectance (between 50 and 270°C), illite Kübler-Index data and the diagenesis/anchizone boundary in the external part of the Central Alps. *Applied Clay Science*, **143,** 307-319.

MURRAY, R.C. (1960) Origin of porosity in carbonate rocks. *Journal of Sedimentary Research*, **30,** 59-84.

NIEBUHR, B. (2014) Lithostratigraphie der mittel-bis oberjurassischen Reliktvorkommen zwischen Straubing und Passau (Niederbayern). *SDGGT***,** 73-82.

NIEBUHR, B. AND PÜRNER, T. (2014) Plattenkalk und Frankendolomit–Lithostratigraphie der Weißjura-Gruppe der Frankenalb (außeralpiner Oberjura, Bayern). *SDGGT***,** 5-72.

OPPEL, A. (1858) *Die Juraformation Englands, Frankreichs und des südwestlichen Deutschlands*. Ebner & Seubert, Stuttgart, 857 pp.

PAGEL, M. (2000) *Cathodoluminescence in geosciences*. Springer, Berlin, 514 pp.

PARNELL, J. (2010) Potential of palaeofluid analysis for understanding oil charge history. *Geofluids*, **10,** 73-82.

PAWELLEK, T. AND AIGNER, T. (2003) Apparently homogenous "reef"-limestones built by high-frequency cycles: Upper Jurassic, SW-Germany. *Sedimentary Geology*, **160,** 259-284.

PIEŃKOWSKI, G., SCHUDACK, M.E., BOSÁK, P., ENAY, R., FELDMAN-OLSZEWSKA, A., GOLONKA, J., GUTOWSKI, J., HERNGREEN, G.F.W., JORDAN, P., KROBICKI, M., LATHUILIERE, B., LEINFELDER, R.R., MICHALIK, J., MÖNNIG, E., NOE-NYGAARD, N., PÁLFY, J., PINT, A., RASSER, M.W., REISDORF, A.G., SCHMID, D.U., SCHWEIGERT, G., SURLYK, F., WETZEL, A. AND WONG, T.E. (2008) Jurassic. In: *The Geology of Central Europe Volume 2: Mesozoic and Cenozoic* (Ed T. McCann), **2**, pp. 823-922. The Geological Society, London.

POMONI-PAPAIOANNOU, F., FLÜGEL, E. AND KOCH, R. (1989) Depositional environments and diagenesis of Upper Jurassic subsurface sponge- and tubiphytes reef limestones: Altensteig 1 well, western Molasse Basin, Southern Germany. *Facies*, **21,** 263-283.

PRESTEL, R. 1988. Hydrochemische Untersuchungen im süddeutschen Molassebecken, Bayerisches Landesamt für Wasserwirtschaft, München, Geologisches Landesamt Baden-Württemberg, Freiburg i.Br.

PRESTEL, R. (1990) *Untersuchungen zur Diagenese von Malm-Karbonatgesteinen und Entwicklung des Malm-Grundwassers im süddeutschen Molassebecken*, Stuttgart, Stuttgart.

PRESTEL, R., WOLF, M., EICHINGER, L. AND SALVAMOSER, J. 1991. Gaszusammensetzung von Ölfeldwässern und Grundwässern im Malm des süddeutschen Molassebeckens, München, Freiburg i. Br.

PYTLAK, L., GROSS, D., SACHSENHOFER, R.F., BECHTEL, A. AND LINZER, H.-G. (2017) Gas accumulations in Oligocene–Miocene reservoirs in the Alpine Foreland Basin (Austria): evidence for gas mixing and gas degradation. *Int. J. Earth Sci.*, **106,** 2171-2188.

QUENSTEDT, F.A. (1858) *Der Jura*. H. Laupp, Tübingen, 842 pp.

REINHOLD, C. (1996) *Prozesse, Steuerung und Produkte komplexer Diagenese-Sequenzen in süddeutschen Malm-Karbonaten - Die oberjurassische Massenkalk- und Bankkalkfazies bei Geislingen/Steige (Oxford/Kimmeridge, östliche Schwäbische Alb)*, Technische Universität Berlin, Berlin, 255 pp.

REINHOLD, C. (1998) Multiple episodes of dolomitization and dolomite recrystallization during shallow burial in Upper Jurassic shelf carbonates: eastern Swabian Alb, southern Germany. *Sediment. Geol.*, **121,** 71-95.

RICHTER, D.K., GILLHAUS, A. AND NEUSER, R.D. (2018) The alteration and disintegration of dolostones with stoichiometric dolomite crystals to dolomite sand: new insights from the Franconian Alb (Upper Jurassic, SE Germany). *Z. Dtsch. Geo. Geowiss.* , **169,** 27-46.

RICHTER, D.K., GÖTTE, T., GÖTZE, J. AND NEUSER, R.D. (2003) Progress in application of cathodoluminescence (CL) in sedimentary petrology. *Mineral. Petrol.*, **79,** 127-166.

ROEDDER, E. (1984) *Fluid inclusions*. Mineralogical Society of America.

ROLL, A. (1952) Der Unmittelbare Nachweis des Vindelizischen Rückens unter der Süddeutschen Molasse. *Geologische Rundschau*, **40,** 243-248.

RÖLZ, P. (1966) *Schichtenfolge und Faltenstruktur im Helvetikum des Bregenzer Waldes zwischen Mörzenbach und Mellau (Vorarlberg)*. Technische Universität München, München.

RONCHI, P., MASETTI, D., TASSAN, S. AND CAMOCINO, D. (2012) Hydrothermal dolomitization in platform and basin carbonate successions during thrusting: A hydrocarbon reservoir analogue (Mesozoic of Venetian Southern Alps, Italy). *Mar. Pet. Geol.*, **29,** 68-89.

RUF, M., LINK, E., PROSS, J. AND AIGNER, T. (2005) Integrated sequence stratigraphy: Facies, stable isotope and palynofacies analysis in a deeper epicontinental carbonate ramp (Late Jurassic, SW Germany). *Sediment. Geol.*, **175,** 391-414.

SCHEGG, R. (1992) Thermal maturity of the Swiss Molasse Basin: indications for paleogeothermal anomalies? *Eclogae Geol. Helv.*, **85,** 745-764.

SCHLEGELMILCH, R. (2012) *Die Ammoniten des süddeutschen Malms: Ein Bestimmungsbuch für Fossiliensammler und Geologen*. Springer Spektrum, Berlin ; Heidelberg.

SCHMIDT-KALER, H. (1962) Stratigraphische und tektonische Untersuchungen im Malm des nordöstlichen Ries-Rahmens: Nebst Parallelisierung des Malm Alpha bis Delta der südlichen Frankenalb über das Riesgebiet mit der schwäbischen Ostalb. *Erlanger Geologische Abhandlungen*, **44,** 51.

SCHNEIDER, J. (1958) Der Jura in Erdölbohrungen des westlichen Molassetroges. *Z. Dtsch. Ges. Geowiss.*, **110,** 1-16.

SCHNEIDER, J. (1962) Der Jura in Erdölbohrungen des westlichen Molassetroges. *Hermann-Aldinger-Festschrift***,** 163-172.

SCHNEIDER, M., THOMAS, L., BIRNER, J., STEINER, U., BÖHM, F., SAVVATIS, A., BAUMANN, T., MAYRHOFER, C. AND NIESSNER, R. 2012. Wissenschaftliche und technische Grundlagen zur strukturgeologischen und hydrogeologischen Charakterisierung tiefer geothermisch genutzter Grundwasserleiter am Beispiel des süddeutschen Molassebeckens.

SCHULZ, R., AGEMAR, T., ALTEN, A., KÜHNE, K., MAUL, A., PESTER, S. AND WIRTH, W. (2007) Aufbau eines geothermischen Informationssystems für Deutschland. *Erdöl Erdgas Kohle*, **123,** 76-81.

SCHWEIGERT, G. (2015) Ammonoid Biostratigraphy in the Jurassic. In: *Ammonoid Paleobiology: From macroevolution to paleogeography* (Eds C. Klug, D. Korn, K. De Baets, I. Kruta and R.H. Mapes), pp. 389-402. Springer Netherlands, Dordrecht.

SCHWERD, K. AND HUBER, K. (1995) Das Geologische Profil der Tiefbohrung Hindelang 1 (Allgäuer Alpen). *Geologica Bavarica*, **100,** 23-54.

SELG, M. AND WAGENPLAST, P. (1990) Beckenarchitektur im süddeutschen Weißen Jura und die Bildung der Schwammriffe. *Jh. geol. Landesamt Baden-Württemberg*, **32,** 171-206.

SIBLEY, D.F. AND GREGG, J.M. (1987) Classification of dolomite rock textures. *Journal of Sedimentary Research*, **57**.

SIRAT, M., AL-AASM, I., MORAD, S., ALDAHAN, A., AL-JALLAD, O., CERIANI, A., MORAD, D., MANSURBEG, H. AND AL-SUWAIDI, A. (2016) Saddle dolomite and calcite cements as records of fluid flow during basin evolution: Paleogene carbonates, United Arab Emirates. *Mar. Pet. Geol.*, **74,** 71-91.

STEIGER, T.H., UHLIG, S. AND MOECK, I.S. (2015) Thin Section Based Cutting Analysis as a New Approach in Rock Type Determination While Drilling Deep Geothermal Wells. In: *Proceedings - World Geothermal Congress 2015*, pp. 1-8, Melbourne, Australia.

STICHLER, W., RAUERT, W., WEISE, S., WOLF, M., KOSCHEL, G., STIER, P., PRESTEL, R., HEDIN, K. AND BERTLEFF, B. (1987) Isotopenhydrologische und hydrochemische Untersuchungen zur Erkundung des Fließsystems im Malmkarstaquifer des süddeutschen Alpenvorlandes. *Z. Dtsch. Geo. Geowiss.* , **138,** 387-398.

STOBER, I. (2014) Hydrochemical properties of deep carbonate aquifers in the SW German Molasse basin. *Geothermal Energy*, **2,** 1.

STOBER, I. AND BUCHER, K. (2012) *Geothermie*. Springer, 302 pp.

STOBER, I., WOLFGRAMM, M. AND BIRNER, J. (2013/2014) Hydrochemie der Tiefenwässer in Deutschland. *Z. geol. Wiss.*, **41/42,** 339-380.

STRASSER, A. (1988) Shallowing-upward sequences in Purbeckian peritidal carbonates (lowermost Cretaceous, Swiss and French Jura Mountains). *Sedimentology*, **35,** 369-383.

SUCHI, E., DITTMANN, J., KNOPF, S., MÜLLER, C. AND SCHULZ, R. (2013) Untersuchungswürdige Gebiete für eine CO2-Einlagerung und nachgewiesene hydrothermische Potenziale (unmittelbar verfügbar) für Tiefe und Mitteltiefe Geothermie. In: *Geothermieatlas zur Darstellung möglicher Nutzungskonkurrenzen zwischen CCS und Tiefer Geothermie*. Leibniz-Institut für Angewandte Geophysik, Bundesanstalt für Geowissenschaften und Rohstoffe.

SWENNEN, R., DEWIT, J., FIERENS, E.L.S., MUCHEZ, P., SHAH, M., NADER, F. AND HUNT, D. (2012) Multiple dolomitization events along the Pozalagua Fault (Pozalagua Quarry, Basque–Cantabrian Basin, Northern Spain). *Sedimentology*, **59,** 1345-1374.

TEICHMÜLLER, R. AND TEICHMÜLLER, M. (1986) Relations between coalification and palaeogeothermics in Variscan and Alpidic foredeeps of western Europe. In: *Paleogeothermics: Evaluation of Geothermal Conditions in the Geological Past* (Eds G. Buntebarth and L. Stegena), pp. 53-78. Springer Berlin Heidelberg, Berlin, Heidelberg.

TÓTH, J. (1995) Hydraulic Continuity In Large Sedimentary Basins. *Hydrogeology Journal*, **3,** 4-16.

TRÜMPY, R. (1952) Der Nordrand der Liasischen Tethys in den Schweizer Alpen. *Geol. Rundsch.*, **40,** 239-242.

VAN DEN KERKHOF, A.M. AND HEIN, U.F. (2001) Fluid inclusion petrography. *Lithos*, **55,** 27-47.

VERBRAUCHERSCHUTZ, B.F.J.U.F. (2018) Gesetz für den Ausbau erneuerbarer Energien (Erneuerbare-Energien-Gesetz - EEG 2017), **2018**.

VÉRON, J. (2005) The Alpine Molasse Basin: Review of petroleum geology and remaining potential. *Bull. für Angew. Geol*, **10**.

VILLINGER, E. (1988) Bemerkungen zur Verkarstung des Malms unter dem westlichen süddentschen Molassebecken. *Bulletin der Schweizerischen Vereinigung von Petroleum-Geologen und-Ingenieuren*, **54,** 41-59.

VOLLMAYR, T. (1983) Temperaturmessungen in Erdölbohrungen der Schweiz. *Bulletin der schweizerischen Vereinigung von Petroleum-Geologen und-Ingenieure*, **49,** 15-27.

VON FREYBERG, B. (1966) *Der Faziesverband im unteren Malm Frankens: Ergebnisse der Stromatometrie*. Universität, Geolog. Inst., 112 pp.

VON HARTMANN, H., TANNER, D.C. AND DUSSEL, M. (2018) The relevance of tectonic structures for karst development in the Upper Jurassic carbonates of the German Molasse Basin. In: *EGU General Assembly Conference Abstracts*, **20**, pp. 14822.

WABER, H., HEIDINGER, M., LORENZ, G. AND TRABER, D. 2014. Hydrochemie und Isotopenhydrogeologie von Tiefengrundwässern in der Nordschweiz und im angrenzenden Süddeutschland, Nationale Genossenschaft für die Lagerung radioaktiver Abfälle.

WALLMANN, K. (2001) The geological water cycle and the evolution of marine δ18O values. *Geochim. Cosmochim. Acta*, **65,** 2469-2485.

WARREN, J. (2000) Dolomite: occurrence, evolution and economically important associations. *Earth-Sci. Rev.*, **52,** 1-81.

WEBER, J. AND MOECK, I. (2018) *Wärmewende mit Geothermie – Möglichkeiten und Chancen in Deutschland*. Leibniz-Institut für Angewandte Geophysik.

WEHNER, H. AND KUCKELKORN, K. (1995) Zur Herkunft der Erdöle im nördlichen Alpen-/Karpatenvorland. *Erdöl, Erdgas, Kohle*, **111,** 508-514.

WEISE, S., WOLF, M., FRITZ, P., RAUERT, W., STICHLER, W., PRESTEL, R., BERTLEFF, B. AND STUTE, M. 1991. Isotopenhydrogeologische Untersuchungen im Süddeutschen Molassebecken, Bayerisches Landesamt für Wasserwirtschaft, München, Geologisches Landesamt Baden-Württemberg, Freiburg i.Br.

WILDI, W., FUNK, H., LOUP, B.F.R., AMATO, E. AND HUGGENBERGER, P. (1989) Mesozoic subsidence history of the European marginal shelves of the alpine Tethys (Helvetic realm, Swiss Plateau and Jura). *Eclogae Geol. Helv.*, **82,** 817-840.

WOLFGRAMM, M., BARTELS, J., RINKE, M. AND JAHRFELD, T. (2011) Der Einfluss von Stratigraphie, Fazies und Diagenese auf die Produktivität im Projekt Kirchstockach. In: *Proceedings - Der Geothermiekongress*, pp. 14, Karlsruhe (Germany).

WOLFGRAMM, M., BIRNER, J., BUDACH, I., THIEM, S., THORWART, K., NOWAK, K., LENZ, G., SEIBT, P., ZIMMERMANN, J. AND BUSE, C. 2016. Verbundprojekt MAFA: Parametrisierung von Fazies, Diagenese, Struktur- und Spannungsfeld sowie Optimierung der Testabläufe im Malm zur Verringerung des Erfolgsrisikos, Teilprojekt A: Sedimentologisch-fazielle Analyse, Testplanung : Forschungsvorhaben 0325673A.

WOLFGRAMM, M., BLOCH, T., BARTELS, J., HEUBERGER, S., KUHN, P., NAEF, H., VOIGT, H., SEIBT, P., SONDEREGGER, M., STEIGER, T. AND UHLIG, S. (2015) Reservoir-geological characterization of a fractured limestone: Results obtained from the geothermal well St. Gallen GT-1 (Switzerland). In: *Proceedings of the World Geothermal Congress*.

WOLFGRAMM, M., BUSE, C., MRAZ, E. AND THIEM, S. (2017) Analyse von Bohrklein: Methode sowie Cuttingatlas für Karbonate des Oberjura im Molassebecken. In: *German Geothermal Congress*, Munich.

WOLFGRAMM, M., DUSSEL, M., LÜSCHEN, E., SCHULZ, R., THOMAS, R. AND KOCH, R. (2012) Zuflusszonen im Malm—Untersuchungen des geothermischen Hauptgrundwasserleiters im süddeutschen Molassebecken. *BBR - Sonderheft Geothermie***,** 75-82.

WOLFGRAMM, M. AND THIEM, S. 2018. Geretsried 1 Sidetrack (GEN-1ST-A1) - Feldtestbericht, Gutachten, Geothermie Neubrandenburg GmbH.

WOLFGRAMM, M., VOIGT, H.-D. AND BARTELS, J. 2013. Geothermieprojekt St. Gallen, Test und Stimulation, GTN-Abschlussbericht.

WONG, T.-F. AND BAUD, P. (2012) The brittle-ductile transition in porous rock: A review. *Journal of Structural Geology*, **44,** 25-53.

WOODY, R.E., GREGG, J.M. AND KOEDERITZ, L.F. (1996) Effect of texture on petrophysical properties of dolomite: evidence from the Cambrian-Ordovician of southeastern Missouri. *AAPG bulletin*, **80,** 119-131.

WROBEL, J.-P., FRITZER, T., MIKULLA, C., SCHULDES, D. AND SUCKOW, A. (2002) Forschungsbohrung Altdorf bei Landshut/Niederbayern–Erkundung einer geothermischen Anomalie im Bereich des Landshut-Neuöttinger-Hochs. *Grundwasser*, **7,** 14-24.

WYSSLING, G. (1985) Palinspastische Abwicklung der helvetischen Decken von Vorarlberg und Allgäu. *Jahrbuch der Geologischen Bundesanstalt*, **127,** 701-706.

ZERLAUTH, M., BERTRAND, A., RANTITSCH, G., GROß, D., ORTNER, H., POMELLA, H. AND FÜGENSCHUH, B. (2016) Thermal history of the westernmost Eastern Alps (Penninic Rhenodanubian Flysch nappes, Helvetic nappes, and Subalpine Molasse thrust sheets). *Int. J. Earth Sci.*, **105,** 1525-1547.

ZIEGLER, P.A. (1990) *Geological Atlas of Western and Central Europe*. Shell Internationale Petroleum Mij. and Geol. Soc. of London.

# Appendix

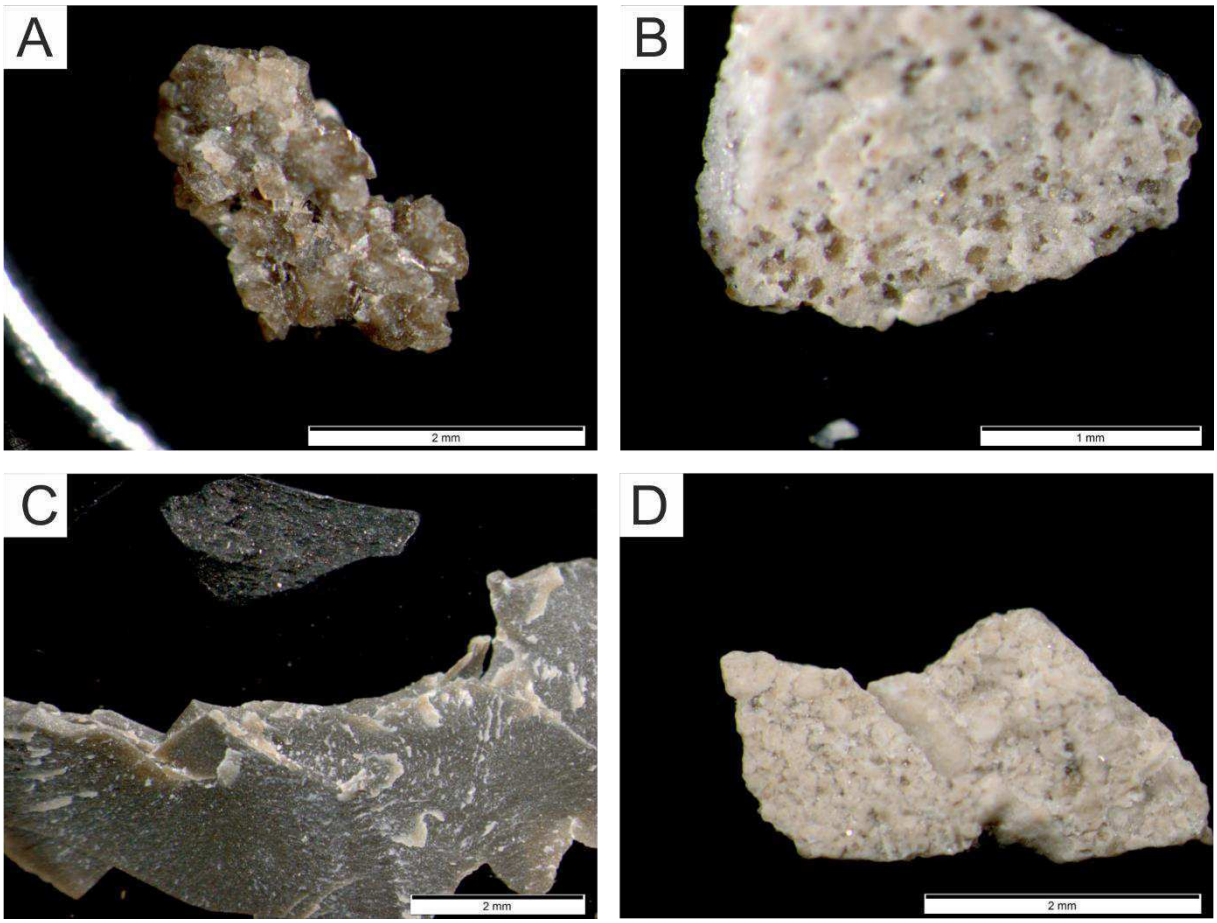


Table 1: Drill cuttings of the Upper Jurassic carbonate rocks from one well in the Molasse basin. (A) dark beige planar-e dolostone, (B) light gray limestone with beige matrix dolomite rhombs, (C) dark gray micritic limestone, (D) light gray to white bioclastic limestone with bigger bioclasts.

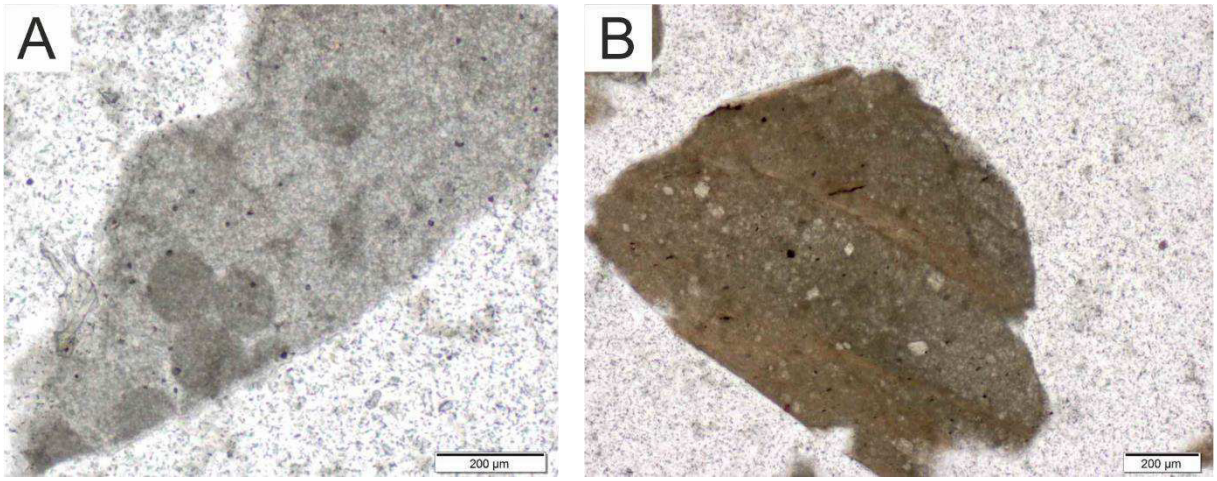


Table 2: Thin section photos of the Purbeckian carbonate rocks (drill cuttings) in transmitted light. (A) 'black pebbles' within a gray limestone, (B) worm hole tube (*Terebella* sp.) in a brown limestone with light gray matrix dolomite rhombs.

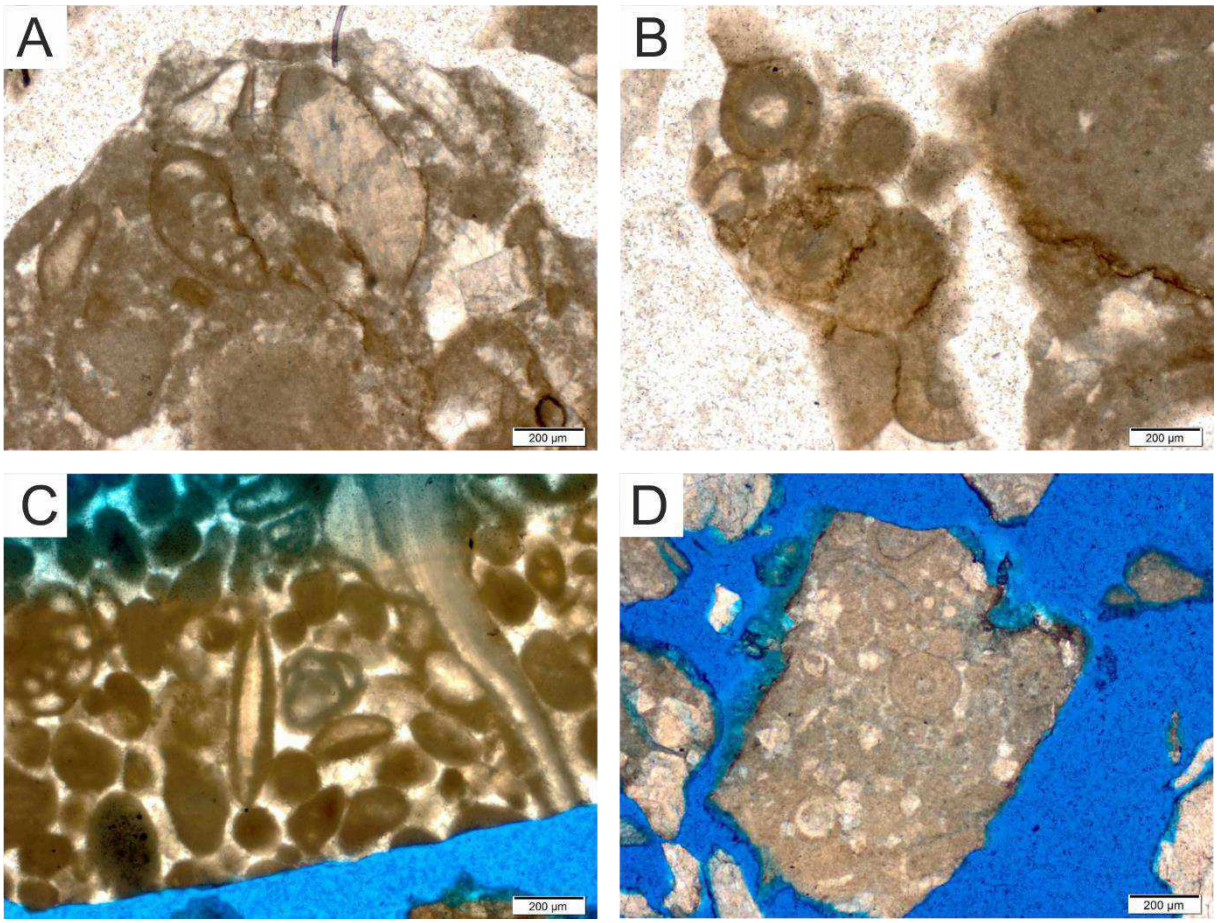


Table 3: Thin section photos of Upper Jurassic drill cuttings in transmitted light with typical organisms. (A) bioclastic packstone with foraminifera and bioclasts, (B) ooids with pressure solution and stylolites, (C) grainstone with peloids, oncoids and foraminifera, (D) bioclastic packstone with matrix dolomite rhombs in light gray and *Tubiphytes* sp.

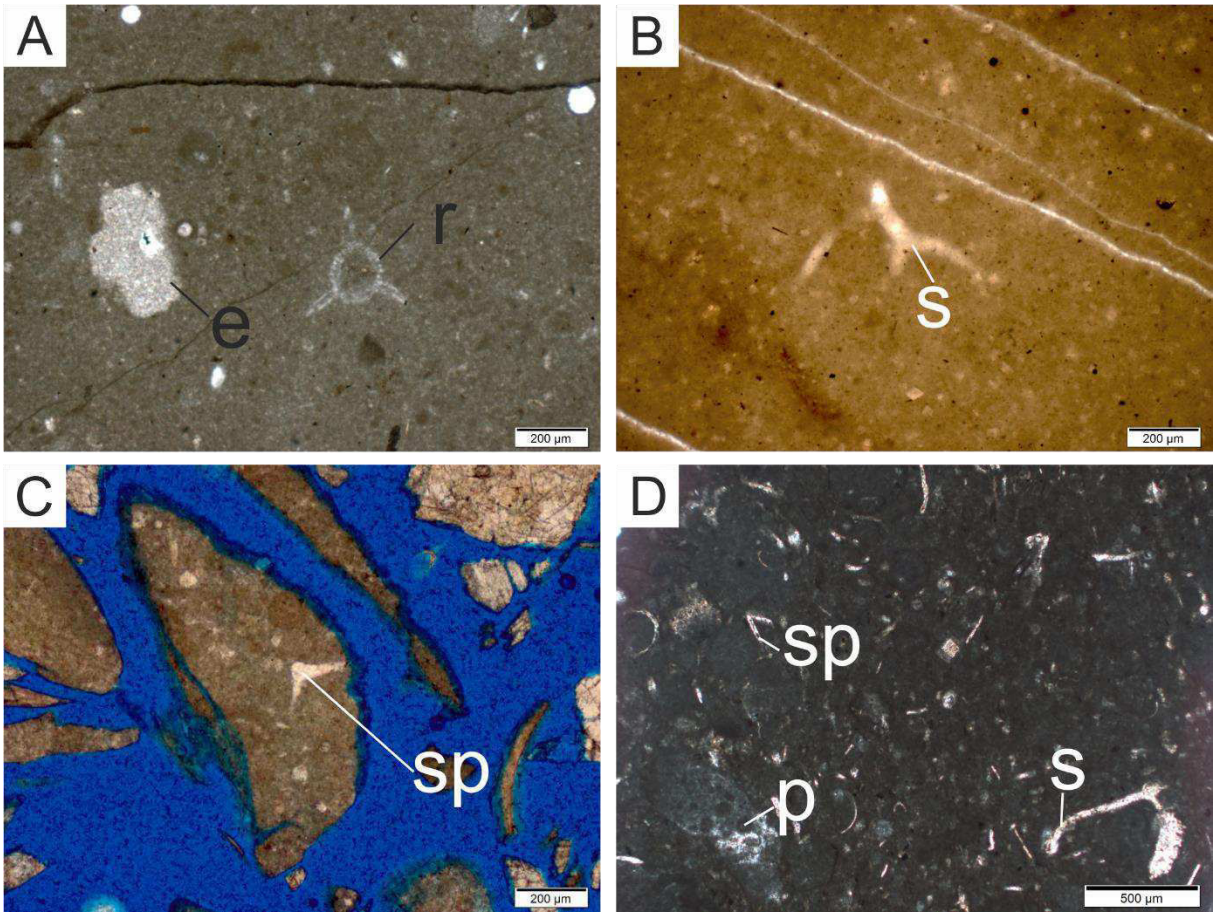


Table 4: Thin section photos of Upper Jurassic transition zone facies drill cuttings in transmitted light. (A) bioclastic wackestone with echinoderms (e) and radiolaria (r), (B) bioclastic wackestone with small matrix dolomite rhombs and planktonic echinoderms (s) (*Saccocoma* sp.), (C) bioclastic wackestone with calcified sponge spiculae (sp), (D) dark gray bioclastic wackestone with planktonic crinoids (s), sponge spiculae (sp.), and peloids (p).

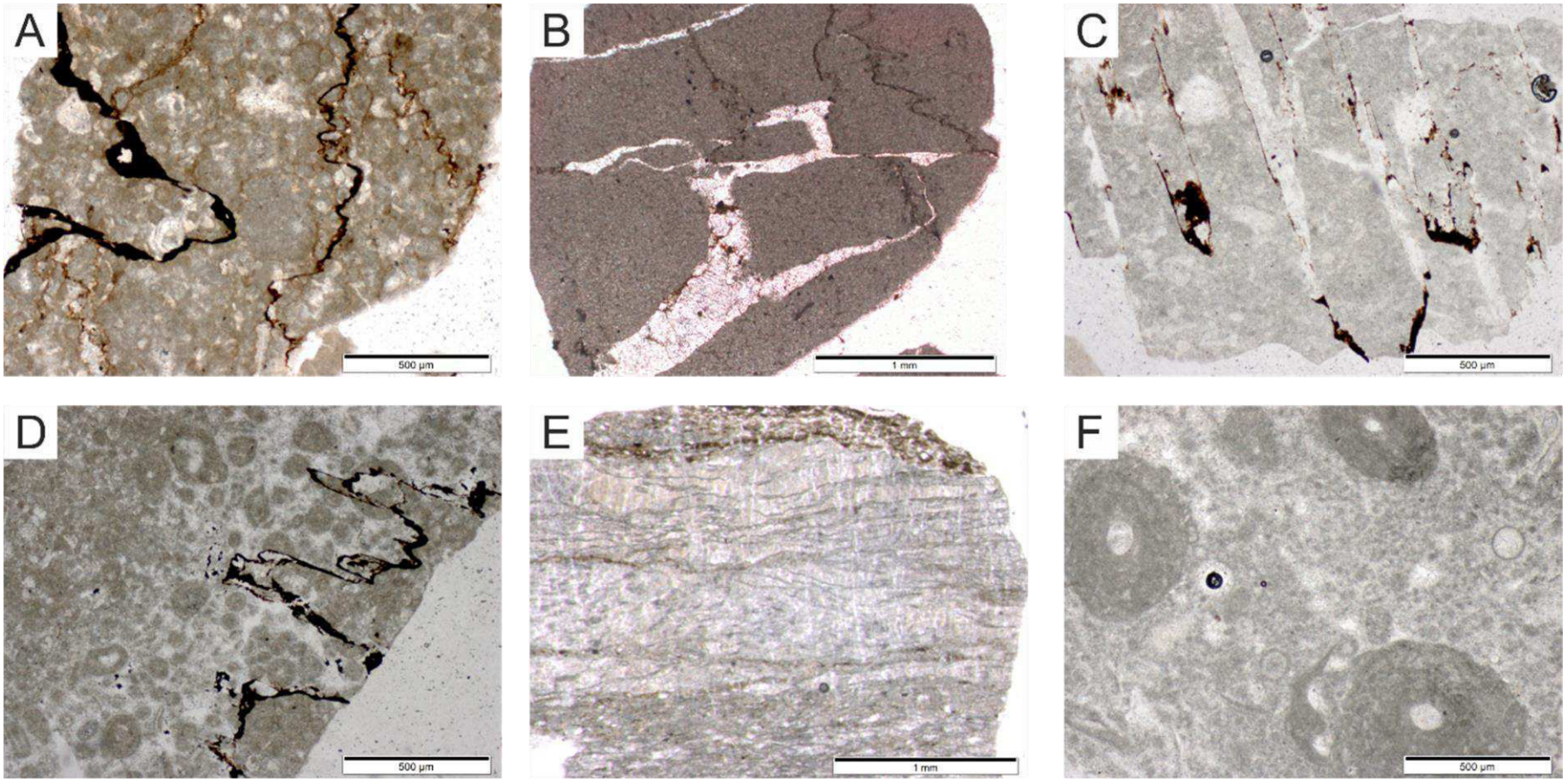


Table 5: Thin section photos of the Upper Jurassic drill cuttings from the MST well in transmitted light. (A) packstone with stylolites, (B) gray limestone with stylolites and vein calcite cements, (C) light gray limestone with stylolites, (D) light gray peloidal grainstone with stylolites, (E) bindstone, (F) gray floatstone with tubiphytes.

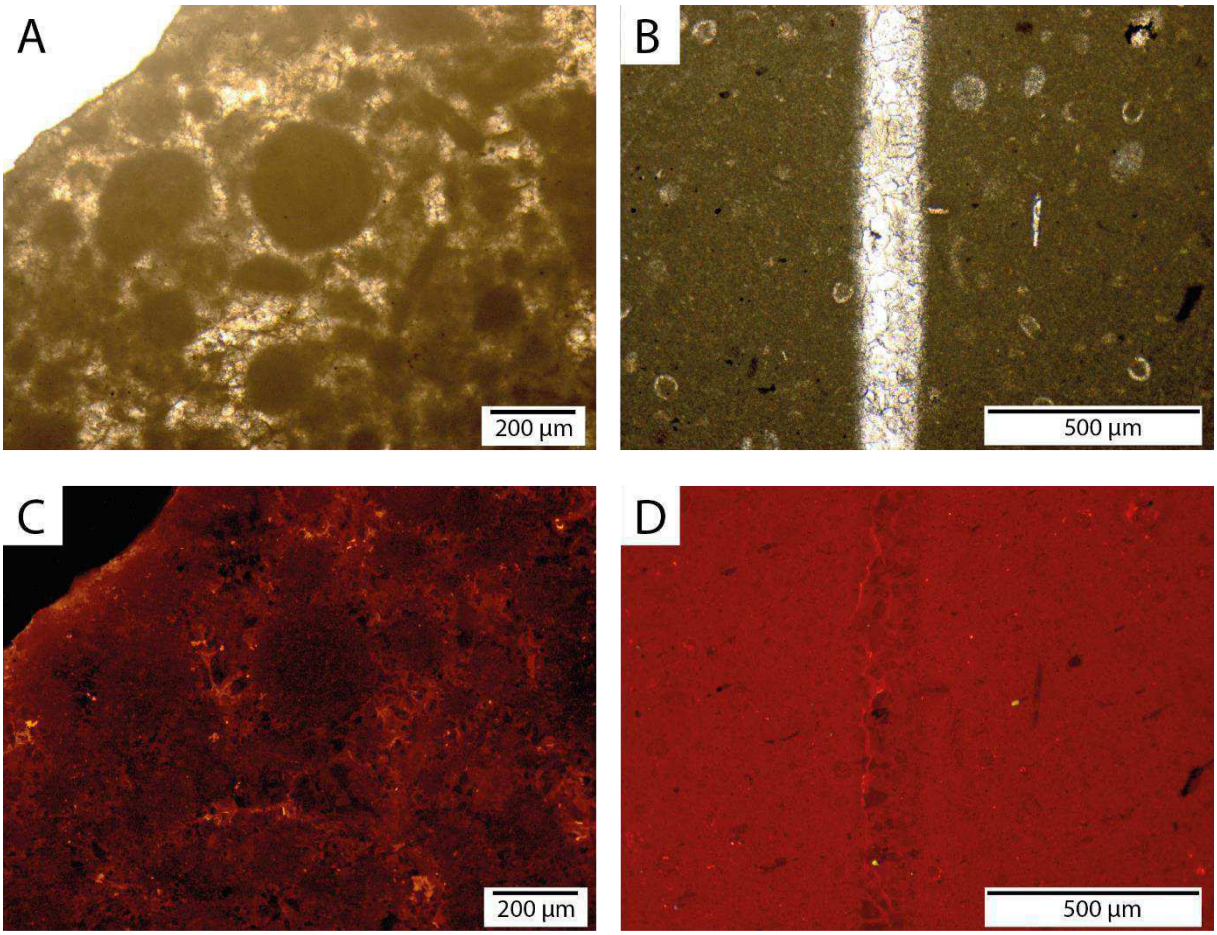


Table 6: Thin sections of drill cuttings in transmitted light (A, B) and under CL (C, D). (A) bioclastic peloidal grainstone, with dull red luminescing components and a red CL matrix (C), (B) bioclastic wackestone with vein calcite cement (A) and a red CL matrix (D).

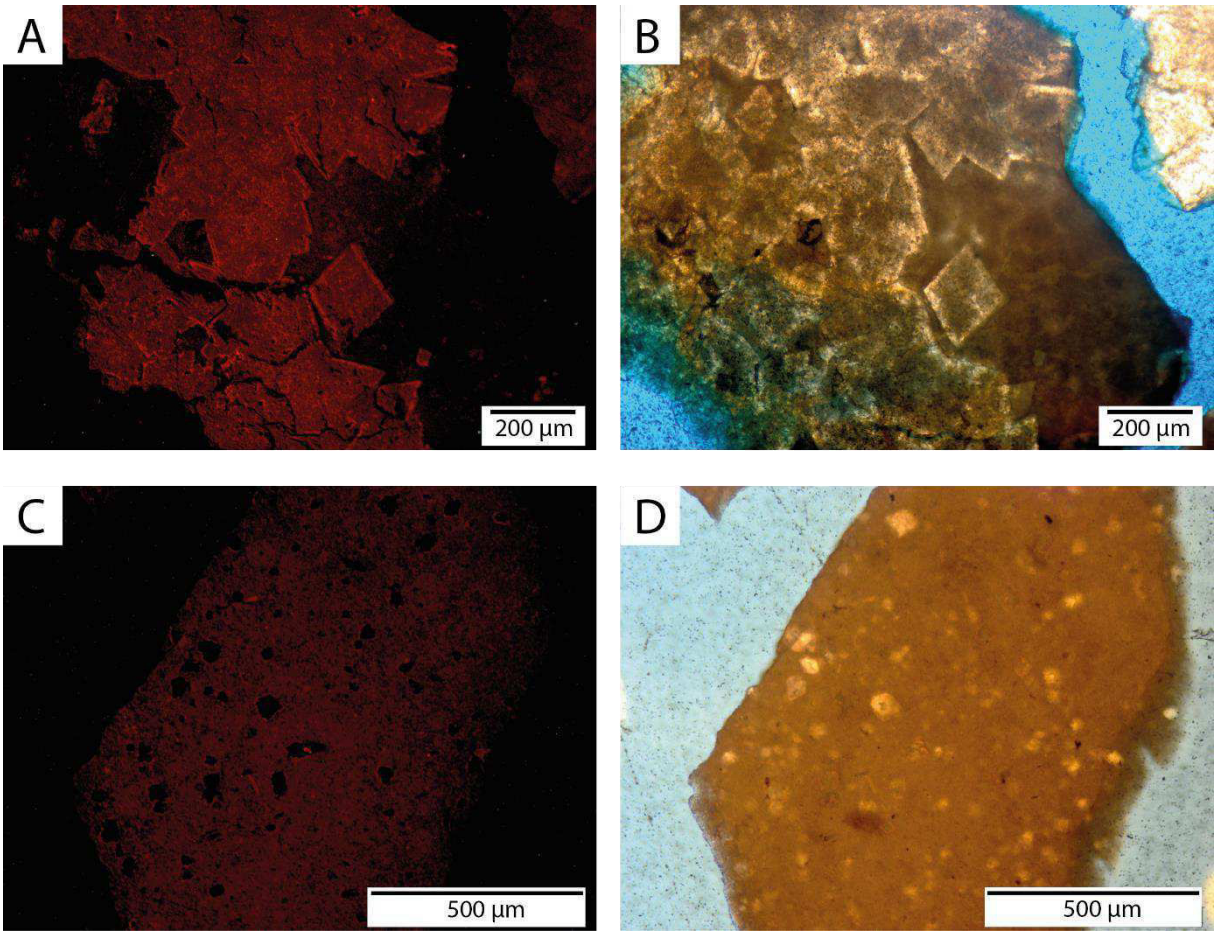


Table 7: Thin sections of drill cuttings in transmitted light (B, D) and under CL (A, C). (B) mudstone to wackestone with red luminescent matrix dolomite rhombs (A) with a thin red intense Cl rim, (D) mudstone to wackestone with non-luminescent matrix dolomite rhombs and a red CL matrix (C).

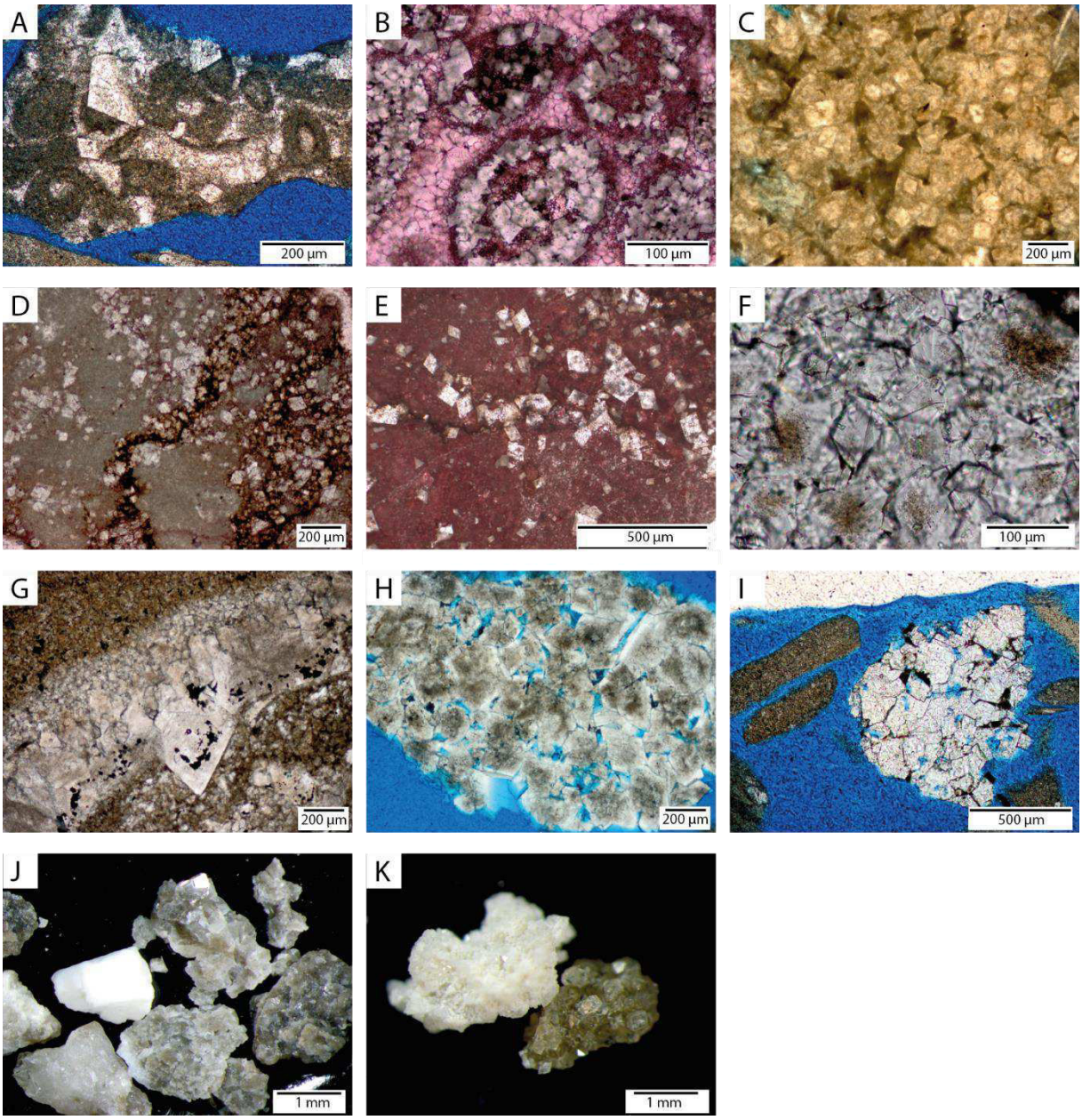


Table 8: Drill cutting in thin sections under transmitted light (A-I) and reflected light (J, K). (A) peloidal grainstone with matrix dolomite rhombs in the matrix, (B) peloidal, ooidal grainstone, stained with alizarin-red and matrix dolomite rhombs within the components, (D) concentric zoned matrix dolomite rhombs, (D) matrix dolomite rhombs and stylolites in a wackestone, (E) matrix dolomite rhombs along a stylolite, stained with alizarin-red, (F) planar-a dolostone, with brownish cloudy centers, (G) dolostone with growth zone of idiomorph dolomite rhombs and a growth zone with pyrite (black), (H) blue dyed, porose planar-e dolostone with concentric zonation with a clear rim, (I) planar-e to planar-s dolostone with a black coating in the former pore space, (J) light gray to gray dolostones, (K) white and beige planar-e dolostone.

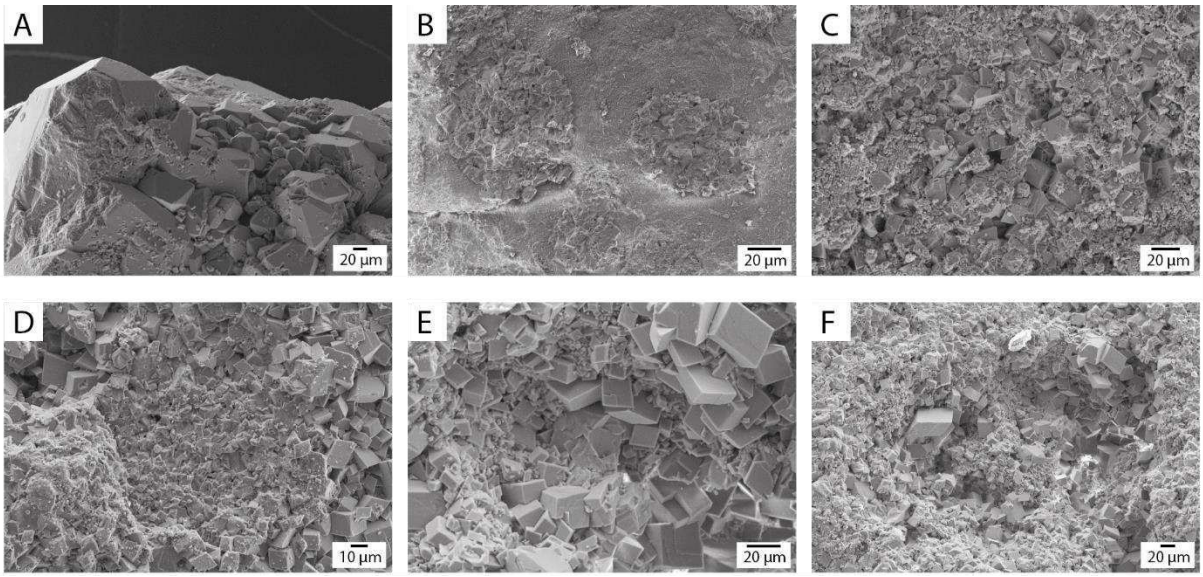


Table 9: Drill cuttings under the scanning electron microscope (SEM) in back-scatter image. (A) vein quartz crystals, (B) etched dolostone with mimetic structure of a peloidal grainstone, (C) planar-e dolostone, (D) planar-e dolostone with fine- and coarse-grained dolomite rhombs, (E) planar-e dolostone, (F) planar-e dolosoten with polympodal dolomite crystals.

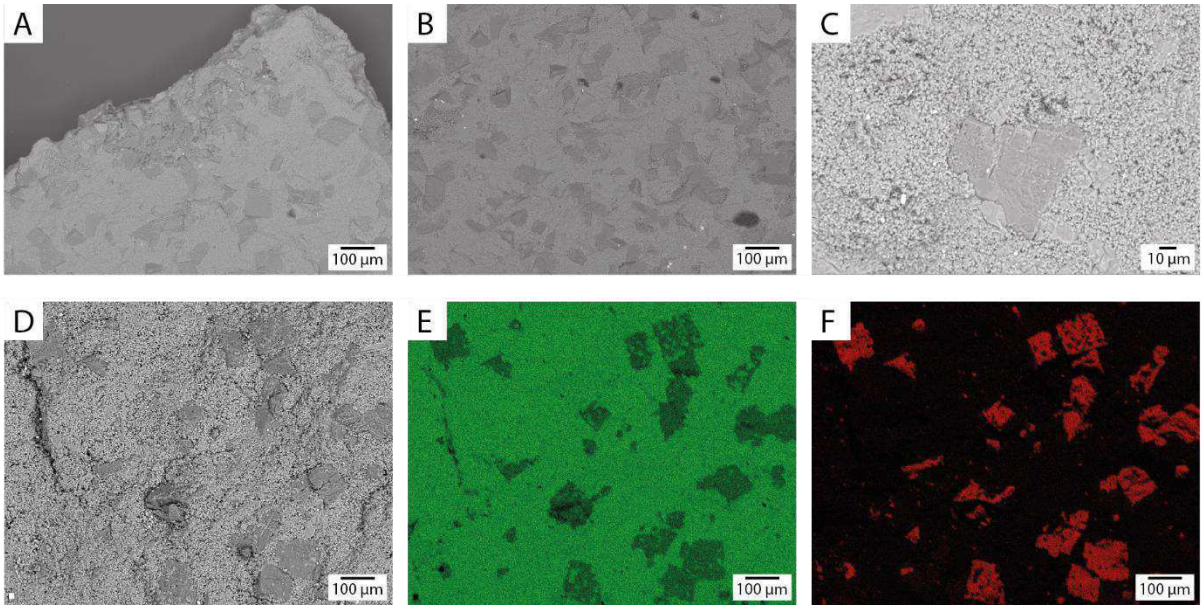


Table 10: Drill cuttings under SEM in back-scatter image. (A, B, C, D) matrix dolomite rhombs in a calcitic matrix with darker gray dolomite rhombs, (E, F) EDX map of (D) with green Ca (E), and red Mg (F).

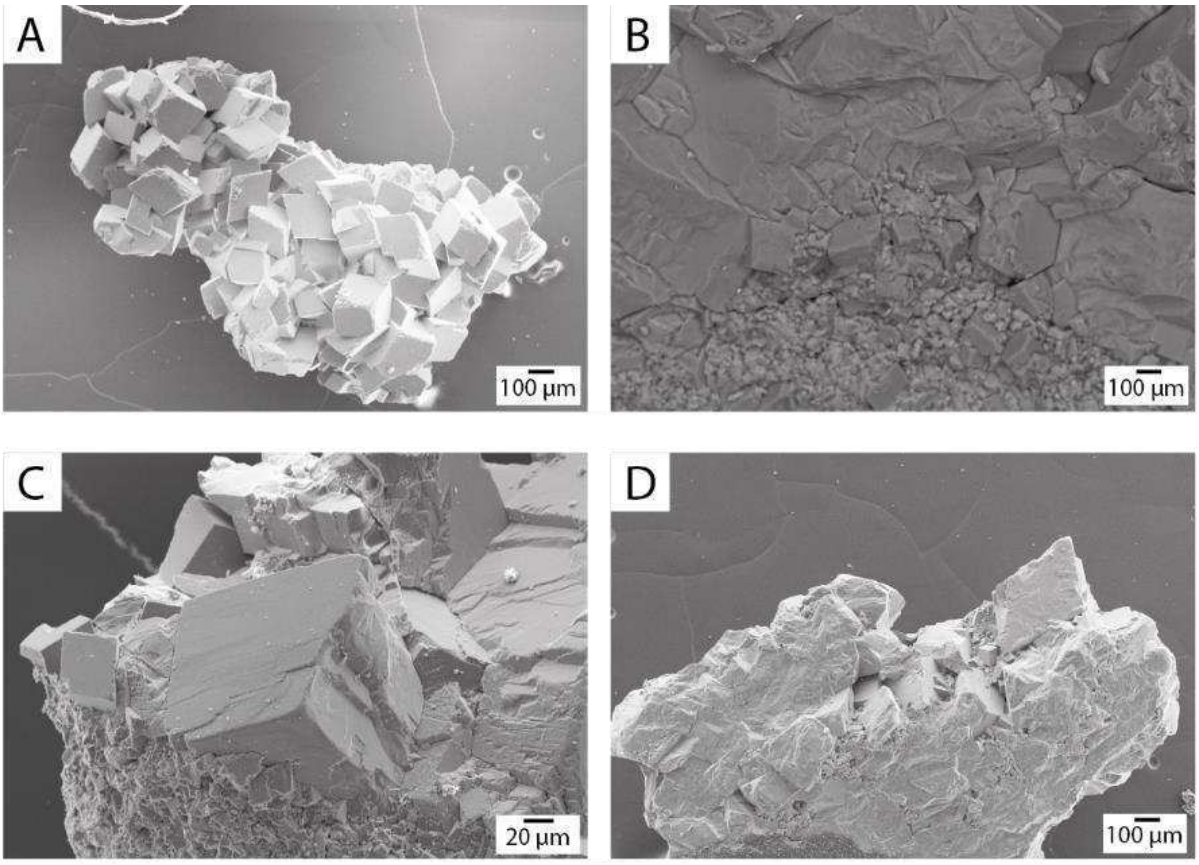


Table 11: Drill cuttings under SEM in back-scatter image. (A) planar-e dolostone, (B) contact between matrix dolomite and vein calcite cement, (C) vein dolomite cement, (D) planar-s to planar-e dolostone.

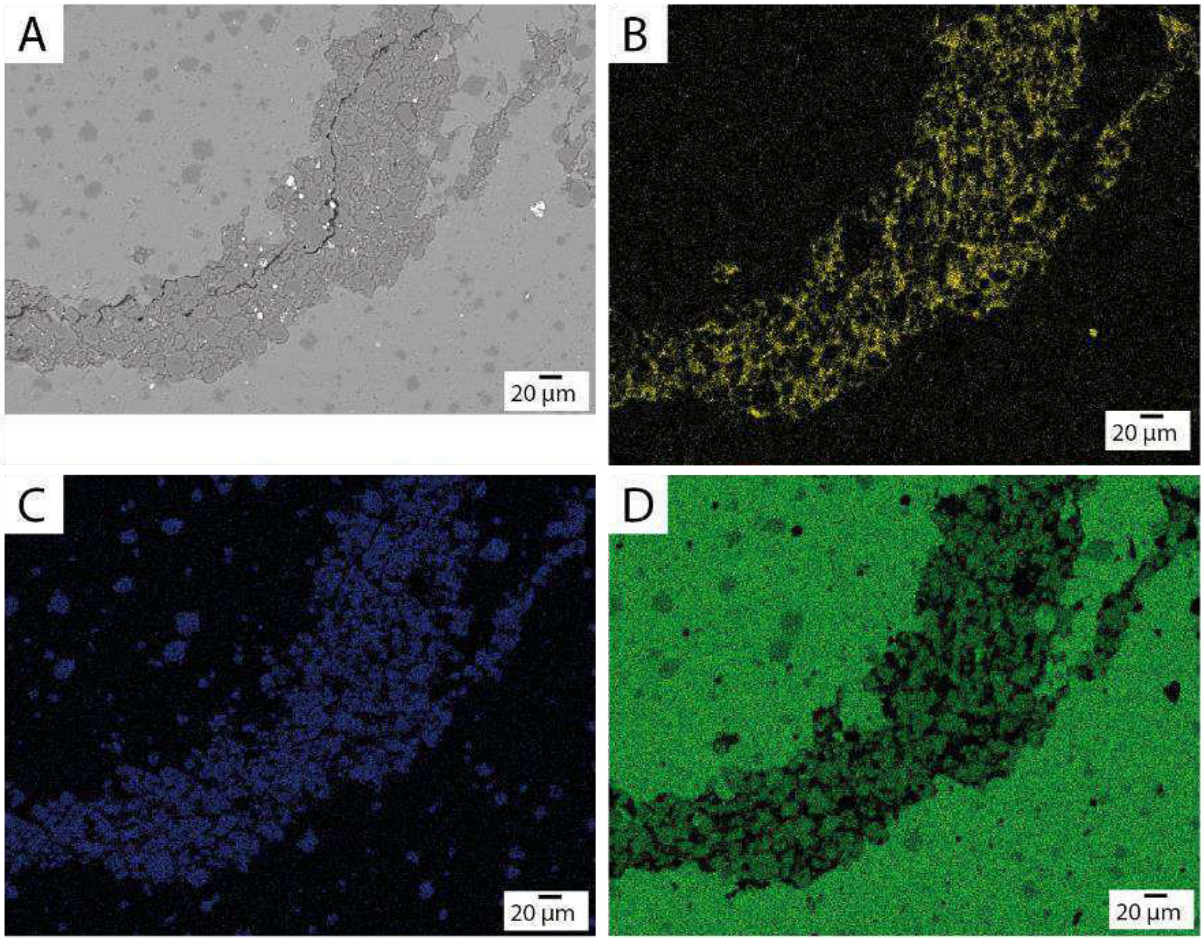


Table 12: Thin section with a stylolite under SEM in back-scatter (A), (B-D) same detail as in (A). EDX map of aluminum (Al) (B), of magnesium (Mg) (C), of calcium (Ca) (D).

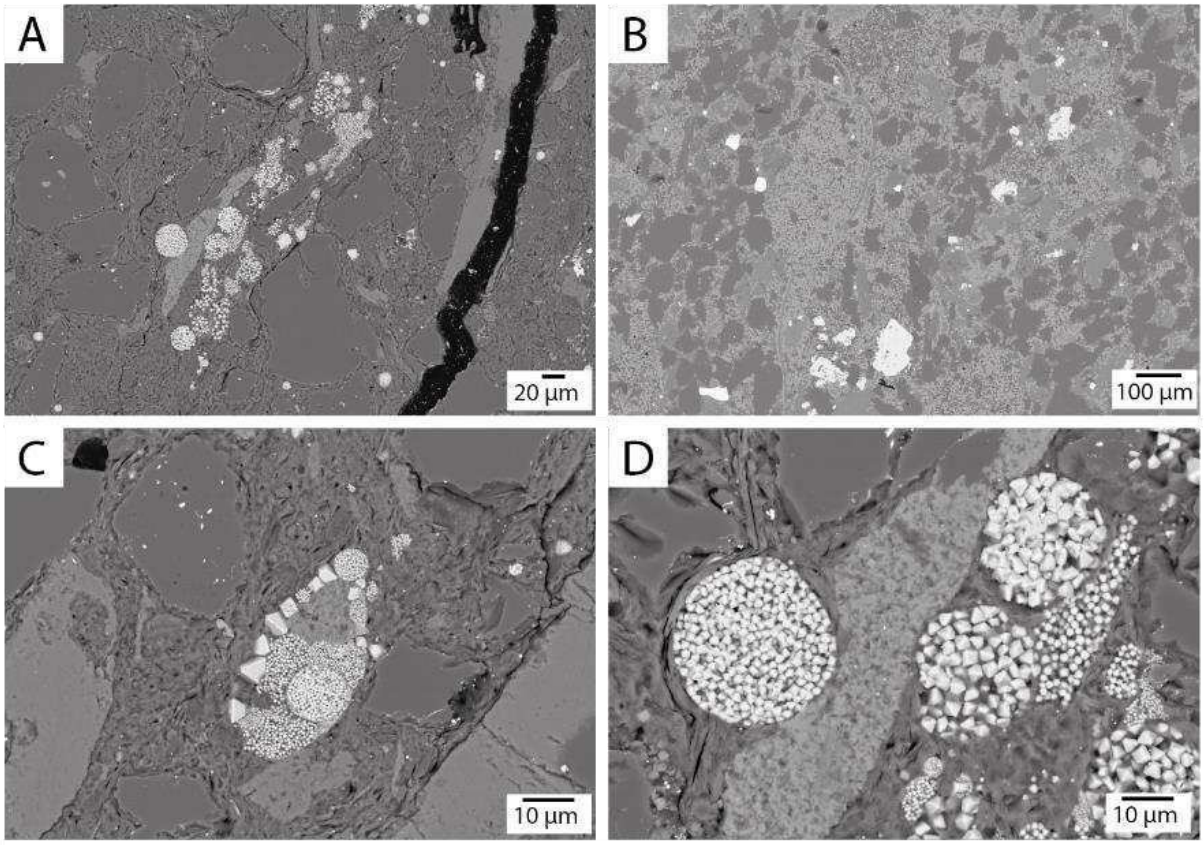


Table 13: Thin section under SEM in back-scatter. (A) limestone with stylo-bedding and white pyrite crystals, (B) marlstone with white pyrite crystals, light gray iron-oxides, grey quartz, (C) recrystallized bioclasts by pyrite, (D) magnified image of (A) with pyrite octahedral crystals in some parts.

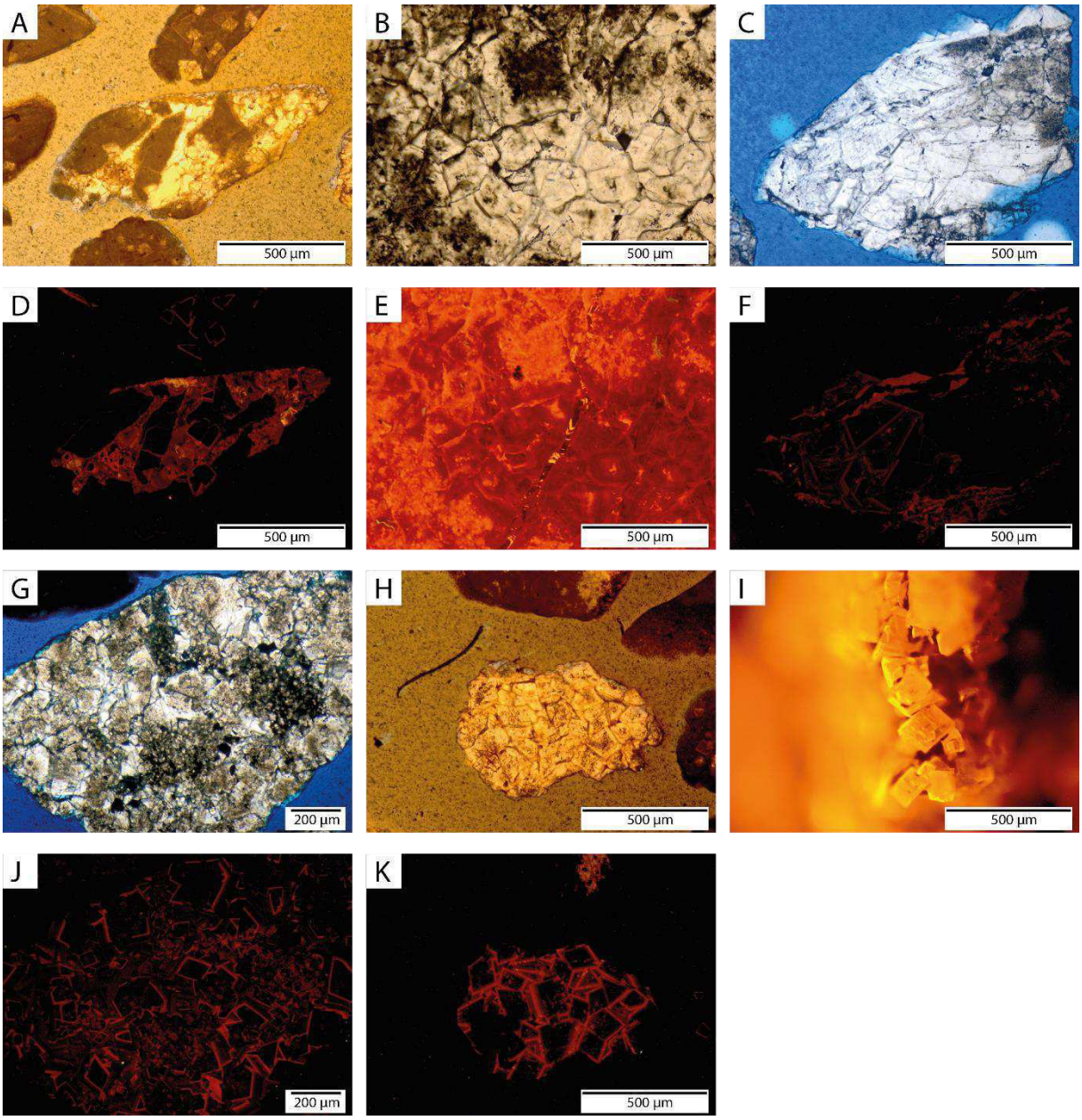


Table 14: Thin sections of drill cuttings under transmitted light (A-C, G, H) and CL (D-F, I-K). (A, D) dolomite breccia, with a thin red rim around the dolostone clasts and a dull red matrix, (B, E) zonec planar-s to planar-a dolostone with light red CL cores and red rim, (C, F) vein dolomite cements with asector and concentric zonation, (G, J) planar-s to planar-a dolostone with a concentric zonation, (H, K) planar-a dolostone with a concentric zonation of idiomorph dolomite rhombs in CL, (I) planar-e dolostone cutings with orange CL.

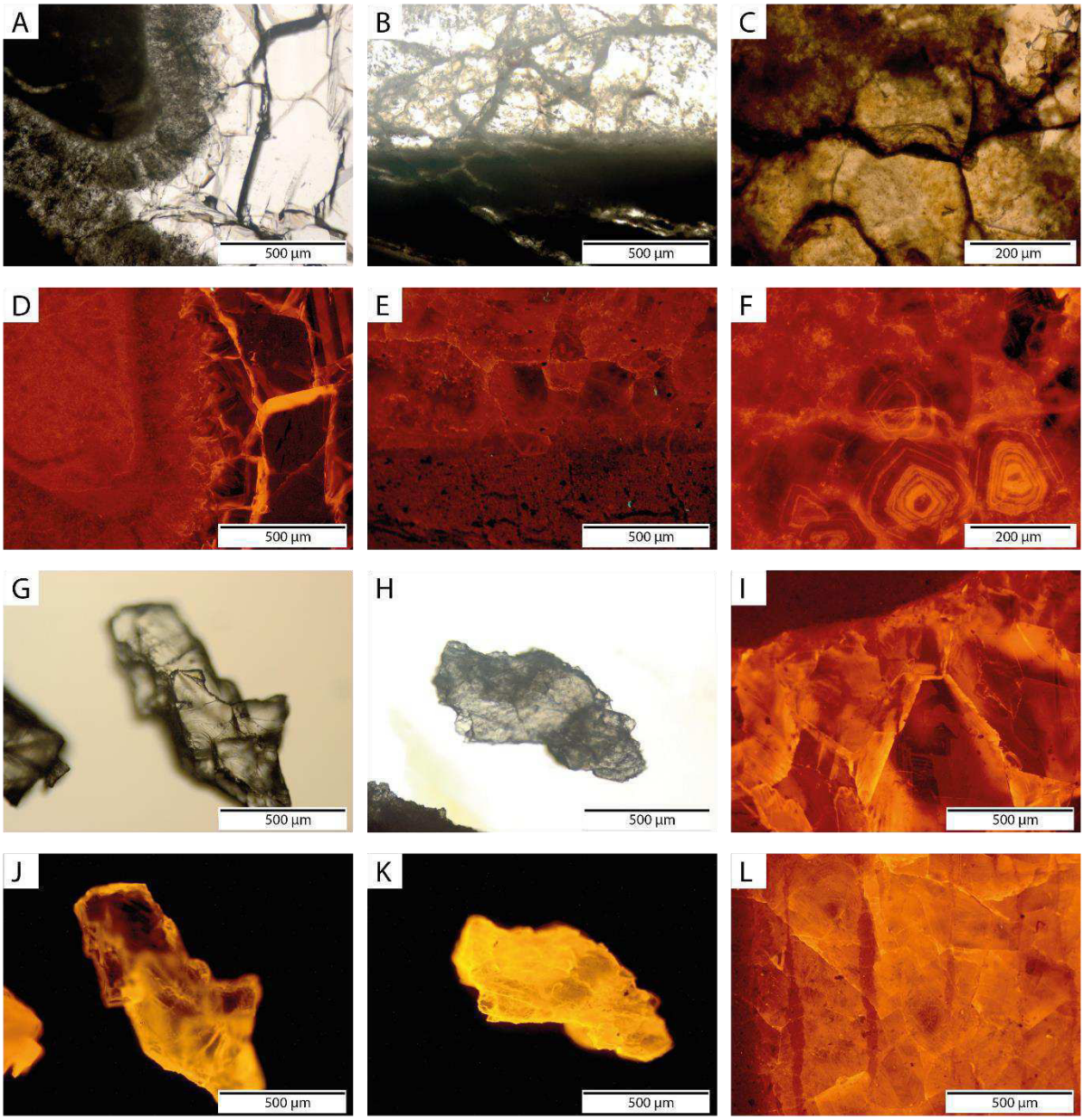


Table 15: Thin sections of drill cuttings under transmitted light (A-C, G, H) and CL (D-F, I-L). (A, D) peloidal grainstone with sector zone calcite cement, hosting fluid inclusions, (B, E) clacite cements with a dull red CL, (C, F) calcite cement with concentric zoned calcite crystals, (G, J; H, K) vein calcite cement with yellow CL, (I, L) sectoral zonation of calcite cements with fluid inclusions.

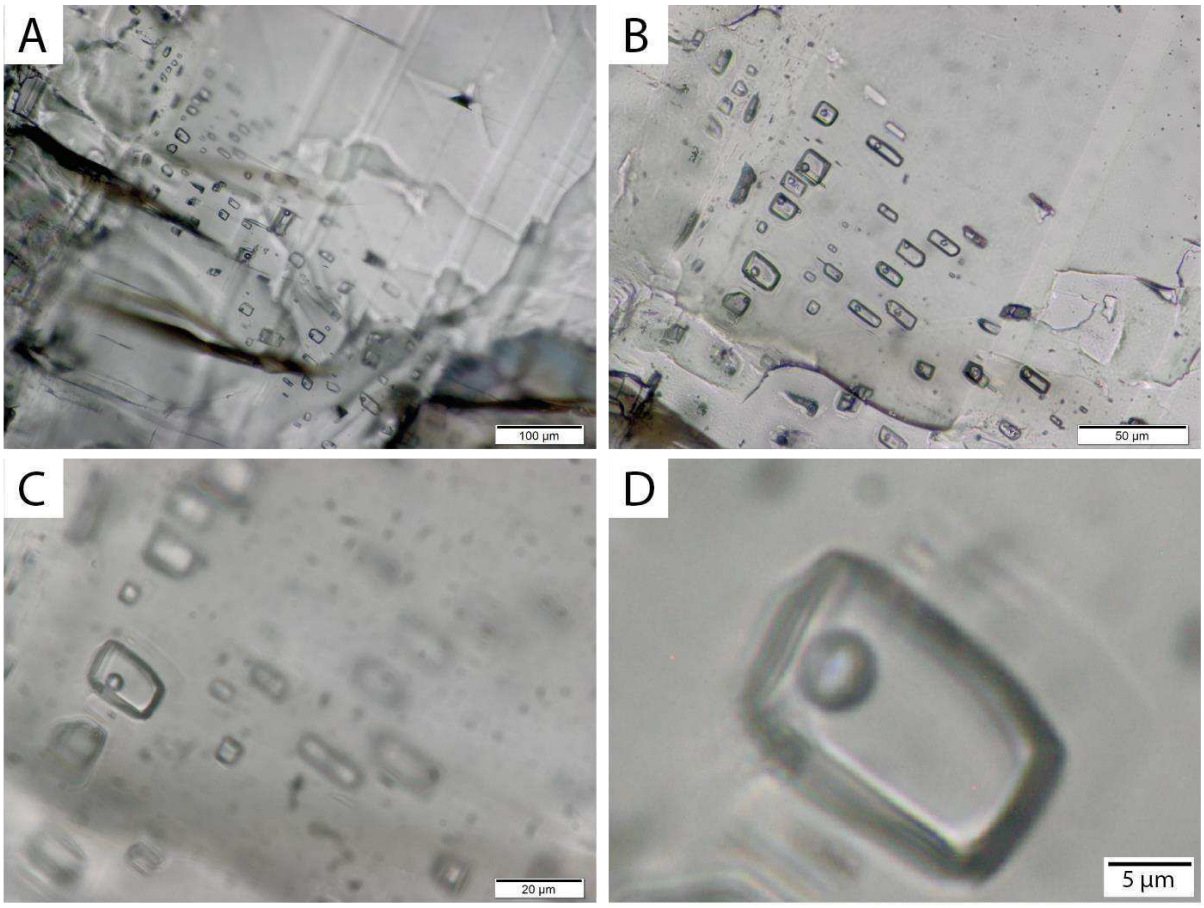


Table 16: Vein calcite cement drill cuttings under transmitted light with 2-phase fluid inclusions in different magnifications.

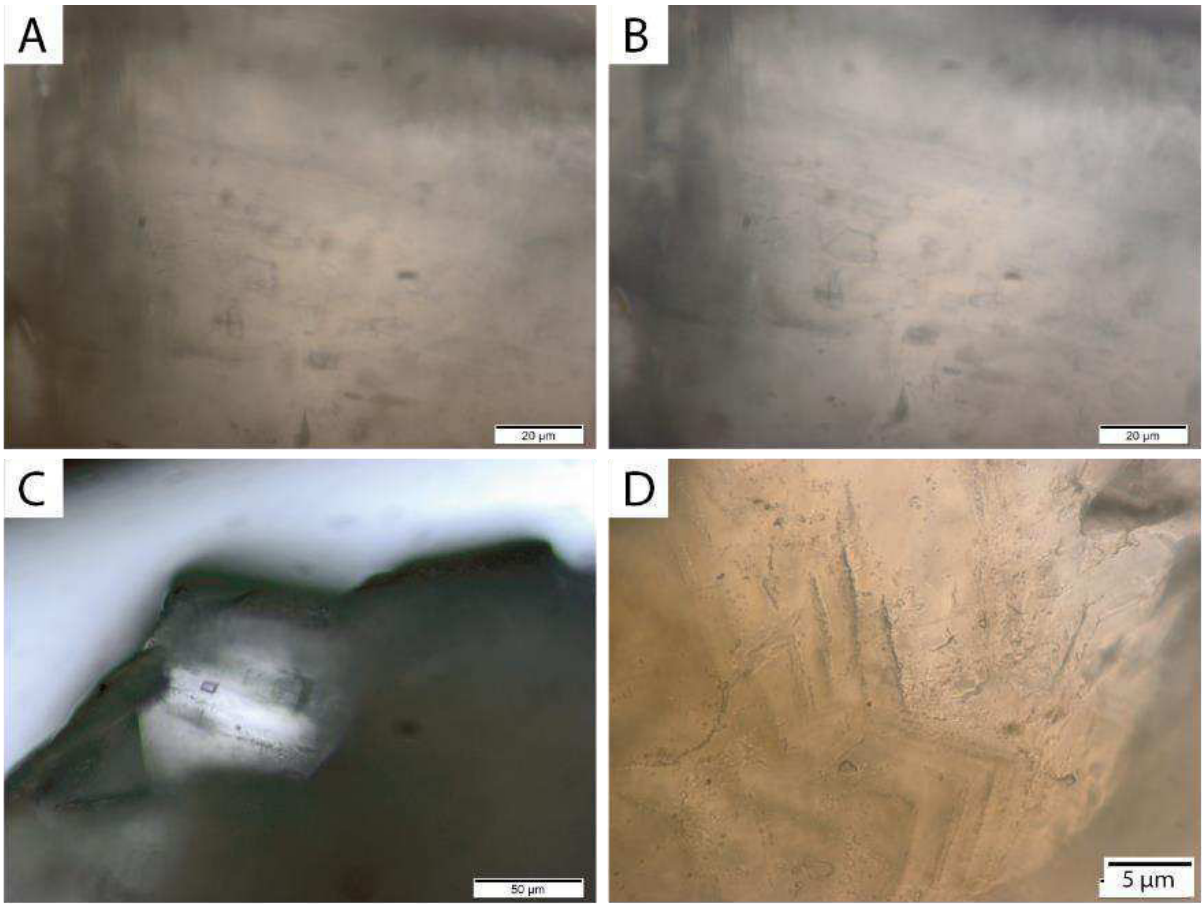


Table 17: Vein dolomite cement drill cutting in transmitted light. (A, B) 2-phase fluid inclusions in the dolostone, (C) fluid inclusion in the dolomite crystal, (D) growth zone within a dolomite crystal.

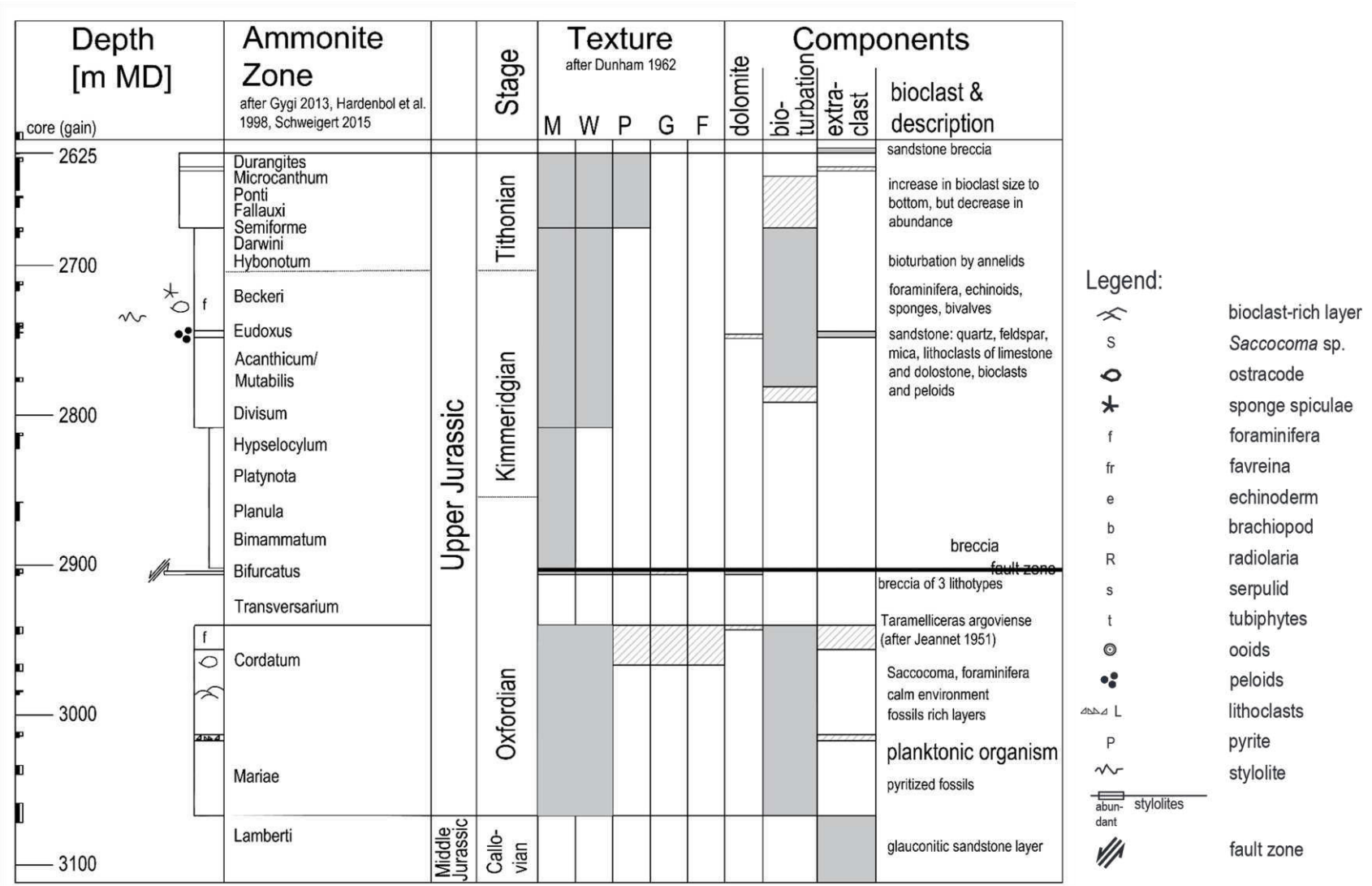


Fig. 1: Schematic profile of the A1 well. Legend for all schematic borehole profiles.

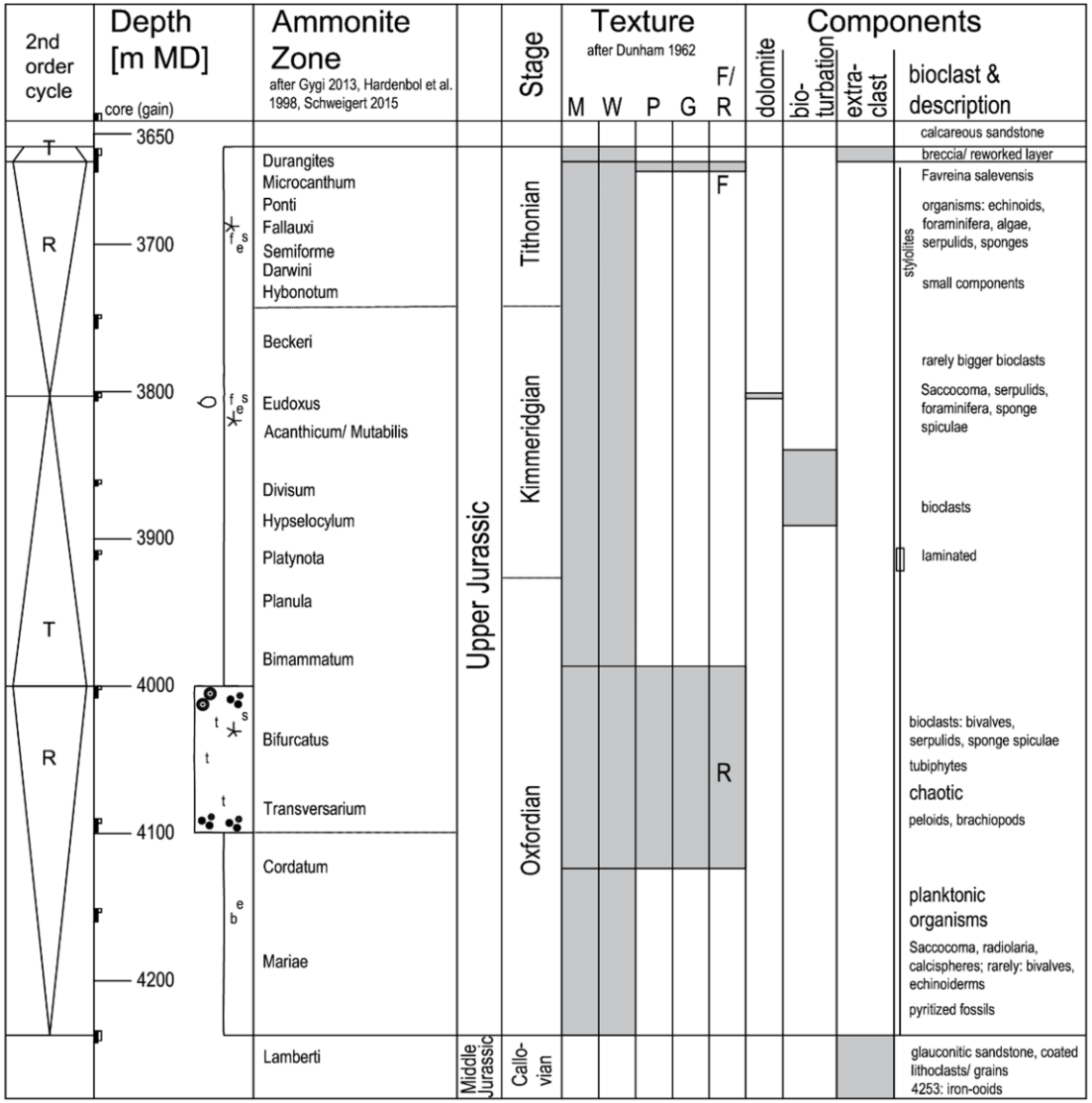


Fig. 2: Schematic profile of the B1 well. Legend as Fig. 1.

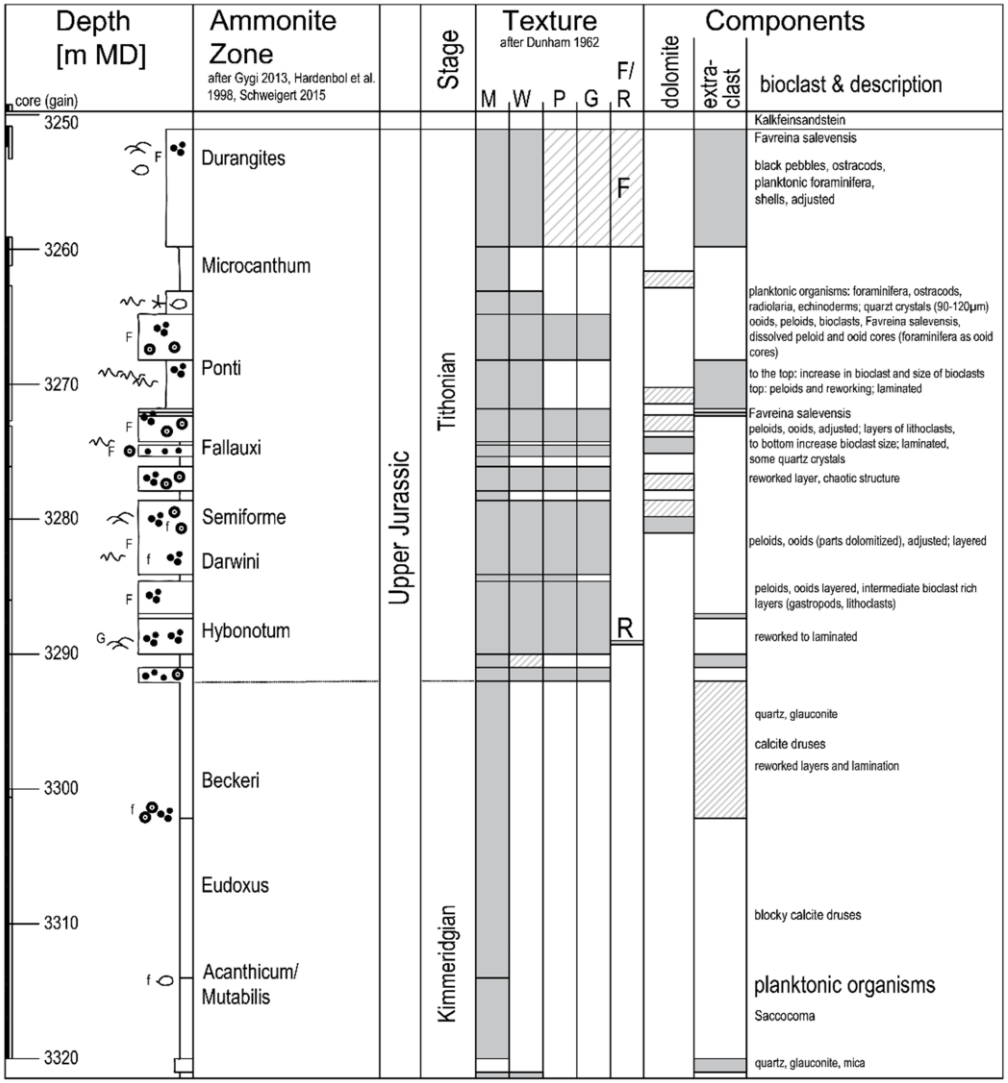


Fig. 3: Schematic profile of the C1 well. Legend as Fig. 1.

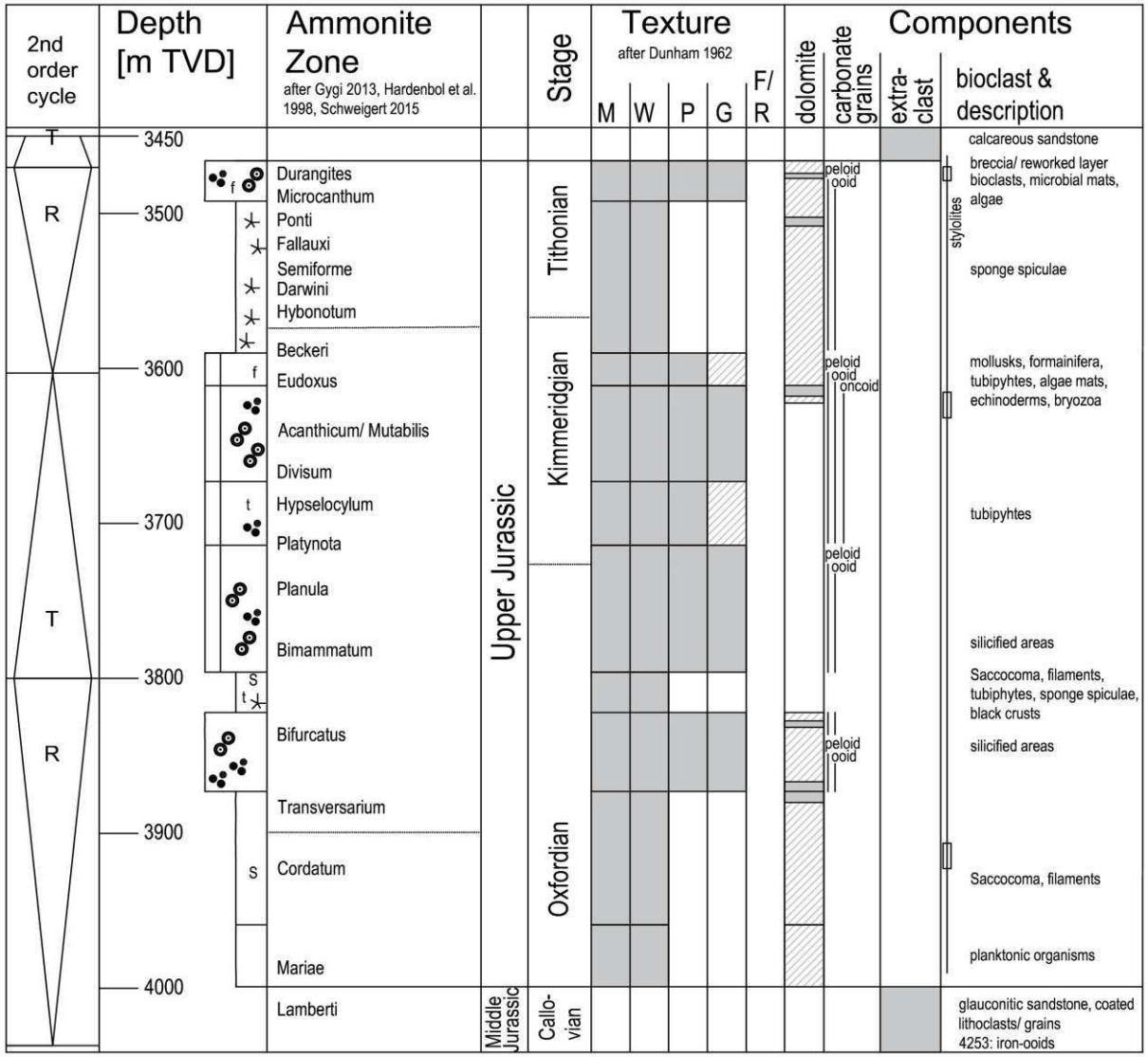


Fig. 4: Schematic profile of the MST well. Legend as Fig. 1.

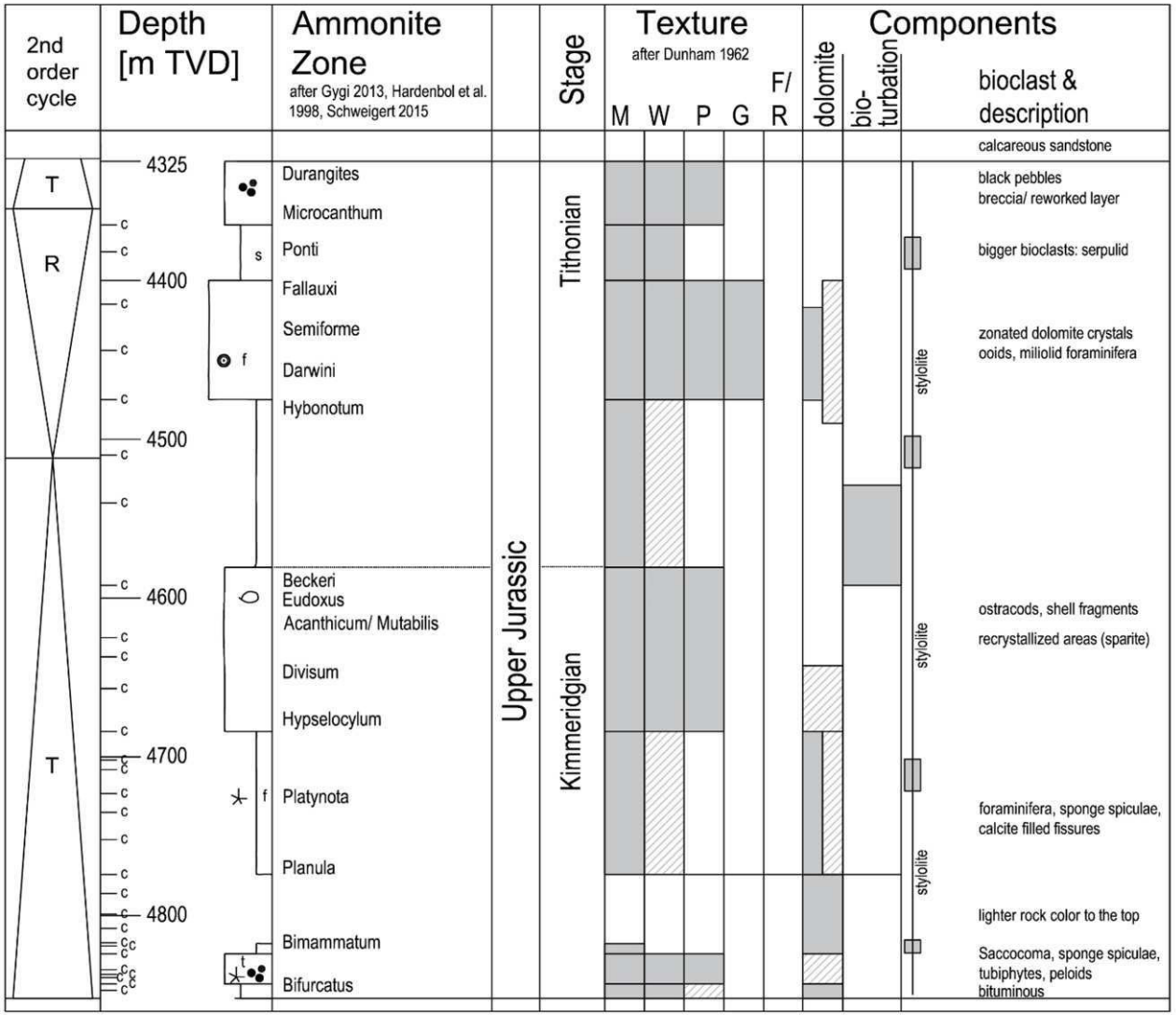


Fig. 5: Schematic profile of the GEN well. Legend as Fig. 1.

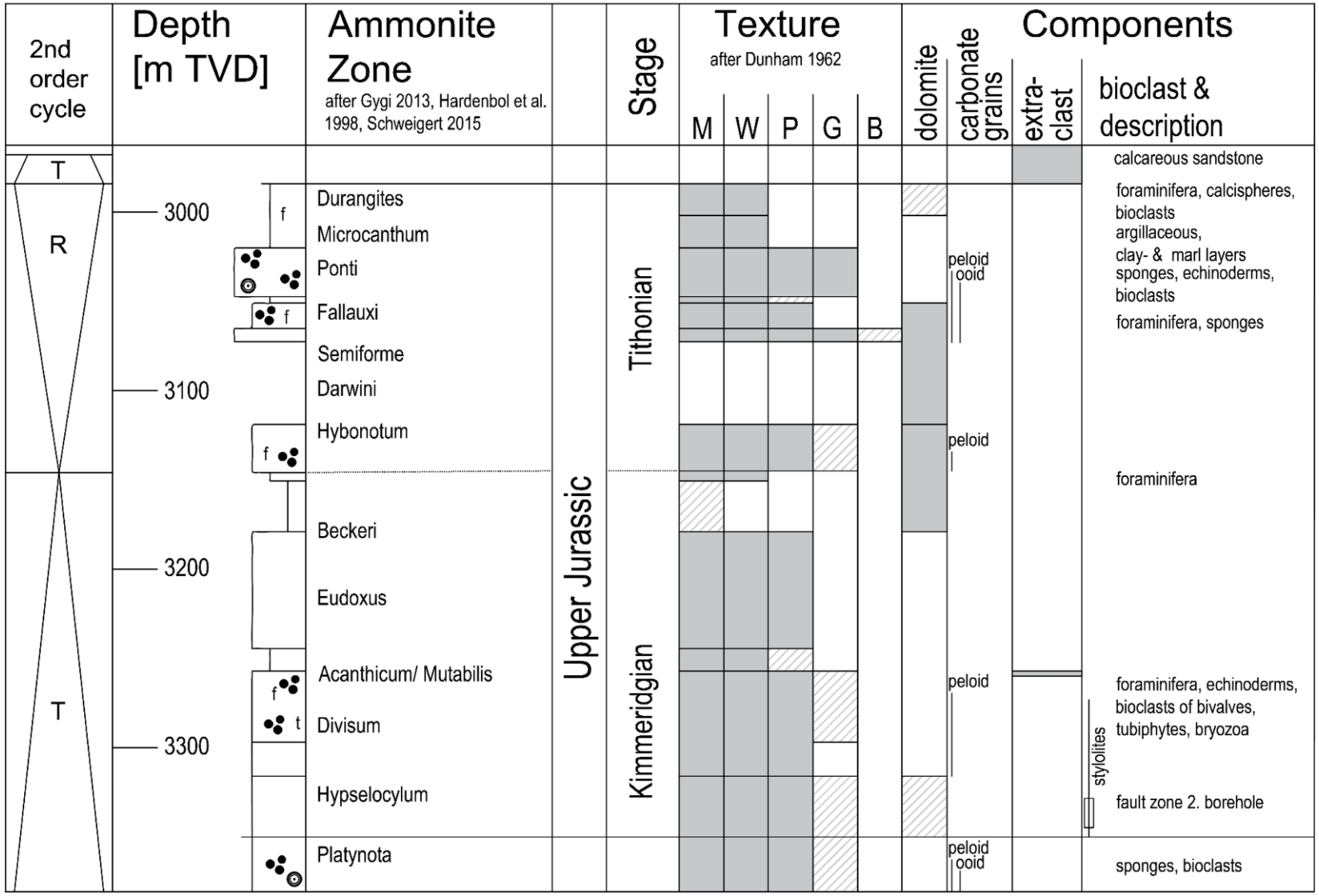


Fig. 6: Schematic profile of the UHA well. Legend as Fig. 1.